The Institute of Paper Chemistry

Appleton, Wisconsin

Doctor's Dissertation

A Comparison of Adsorptive Potential Energies for Argon and Nitrogen Adsorption on the Surface of Cellulose Fibers

Wayne H. Deitrich

June, 1970

A COMPARISON OF ADSORPTIVE POTENTIAL ENERGIES FOR ARGON AND NITROGEN ADSORPTION ON THE SURFACE OF CELLULOSE FIBERS

A thesis submitted by

Wayne H. Deitrich

B.S. 1965, Lehigh University
M.S. 1967, Lawrence University

in partial fulfillment of the requirements
of The Institute of Paper Chemistry
for the degree of Doctor of Philosophy
from Lawrence University,
Appleton, Wisconsin

June, 1970

TABLE OF CONTENTS

SUMMARY

Gas adsorption methods are used to investigate and to characterize solid surfaces. The objective of the present study was to investigate and compare the physical adsorption of argon and nitrogen by cellulose. Adsorption of argon or nitrogen involves nonpolar, dispersion forces. In addition, inductive adsorption forces are important if the cellulose electrostatic field induces a significant dipole moment in the adsorbed molecules. This inductive effect would be greater for nitrogen than for argon adsorption. An estimate of the surface electric field of cellulose was calculated from the results of a heat of wetting study. The electrostatic field strength was small (0.13×10^5 esu/cm.^{2}); induced dipole moments were negligible, and the inductive adsorption forces were insignificant.

The Ross-Olivier adsorption theory was used to study the adsorption systems. The assumptions upon which the theory is based provide a realistic description of the cellulose substrate and an adsorbed film. The surface area, adsorptive potential, and the distribution of adsorptive potentials were investigated for each adsorption system. Good agreement was obtained between experimental and Ross-Olivier model isotherms. A comparison of experimental and theoretical isosteric heats of adsorption and a comparison of mean adsorptive potentials were used to verify the agreement between isotherms.

For argon and nitrogen adsorption the cellulose surface was characterized by a low mean adsorptive potential and a broad distribution of potentials. Nitrogen was more strongly adsorbed, and the adsorbed nitrogen film was a mixture of molecules freely rotating and molecules lying flat on the surface. Argon surface areas were greater; however, the ratio of the surface area by argon adsorption to the surface area by nitrogen decreased as the surface area by argon adsorption increased.

A marked difference between BET and Ross-Olivier estimates of surface area was found. The discrepancy between these values increased with a decrease in the substrate mean adsorptive potential. Multilayer adsorption occurred before completion of the monolayer, and the BET estimate was shown to be a good approximation of the surface area covered by adsorbate before multilayer build-up occurred. The Ross-Olivier estimate was a more realistic approximation of the total surface area accessible to the adsorbate molecule.

INTRODUCTION

At ordinary temperatures a solid differs from other phases in that the molecules at an interface are not easily rearranged to achieve an equipotential surface of minimum free energy. The presence of structural and chemical arrangements create variations in energy across the surface. Characterization of the cellulose surface with respect to energy, chemical and structural arrangements, accessible surface area, etc., would be important in the investigation and the understanding of any surface phenomena – adsorption, adhesion-retention, wetting, catalysis, interfiber bonding.

BACKGROUND OF THE PROBLEM

A BRIEF REVIEW OF EARLY TREATMENTS OF PHYSICAL ADSORPTION DATA

Many theoretical treatments have been generated which enable one to characterize solid substrates or to quantitatively describe adsorption from the experimental data. A broadly accepted adsorption theory usually is based on a model which is thought to be an adequate description of the real surface, of the adsorbed molecules and of the adsorption mechanism. Excellent histories of the development of adsorption theories are given by Ross (1) and Young and Crowell (2).

One of the first quantitative theories of adsorption was proposed by Langmuir (3). The model was based on the simplified assumptions of a uniform substrate with equivalent adsorption sites; the adsorbed film was localized and was restricted to a monolayer, and the adsorbate – adsorbate interactions were neglected. The basis of the Langmuir adsorption theory has been questioned. Opposition arose to the primary assumption of an energetically uniform solid substrate. In addition, experimental investigations have shown that an adsorbed layer can be extremely mobile.

Polanyi (4) proposed a potential theory of adsorption which did not postulate an explicit adsorption – isotherm equation. The potential theory included fewer assumptions about the adsorption mechanism than the Langmuir theory. With this theory, one can predict isotherms at other temperatures from a characteristic curve. The characteristic curve is calculated from one experimental isotherm covering an entire range of adsorption potentials, ε (the work

A list of nomenclature is presented (pp. 82-84).

done by the adsorption forces in bringing a molecule from the gas phase to a point in the adsorbed film).

The BET theory of multilayer adsorption (5) has extended the Langmuir model to one of multilayer adsorption. Because a constant heat of adsorption is assumed in the first layer, it may be claimed that nothing needs to be assumed about the uniformity of the surface or about the presence or absence of horizontal adsorbate interactions. However, without a specific model of molecular structure, intermolecular forces, etc., the BET theory loses much of its significance. A molecular model assuming an energetically uniform surface with negligible adsorbate – adsorbate interactions in the adsorbed film has been used by Hill (6, 7) to derive the BET equation. The use of BET theory and equations for solid surface area determinations is broadly accepted.

A new theoretical approach developed by deBoer (8) assumed the adsorbate to be a nonideal, two-dimensional gas that could be described by the van der Waals' adsorption equation. The deBoer model of monomolecular adsorption supposed an energetically uniform substrate as did the Langmuir model, but a mobile adsorbed film and adsorbate – adsorbate interactions were assumed also. The validity of this theory was suggested by experimental results obtained from specially selected adsorbents which approach an energetically uniform substrate.

THE CONCEPT OF AN ENERGETICALLY NONUNIFORM SUBSTRATE

Recently, the heterogeneity of adsorption energy has been incorporated into adsorption theories. Any general theory of adsorption must recognize energy nonuniformity due to chemical structure and surface and crystal imperfections.

The general isotherm equation is

$$\Theta(P,T) = \int_0^\infty \psi(P,T,U_o)\phi(U_o)dU_o \qquad (1)$$

An adsorption model is presented generally as a function of experimental quantities $\underline{P}$, $\underline{T}$, and $\underline{U}_o$. This function, $\psi(\underline{P},\underline{T},\underline{U}_o)$ represents the local adsorption isotherm function, and $\phi(\underline{U}_o)$ represents the energy of adsorption distribution function. The function $\Theta(\underline{P},\underline{T})$ is the experimentally observed adsorption function. In the above equation,

$\underline{P}$ = pressure

$\underline{T}$ = temperature

$\underline{U}_o$ = adsorptive potential — the difference in potential energy of a molecule in the lowest energy state as a gas and the zero point vibrational level of the adsorbed phase on the surface.

ANALYTICAL SOLUTIONS

Several analytical solutions of Equation (1) have been made, but in these solutions undesirable simplifications were imposed to reduce the integral. For an analytical solution, the local adsorption function, $\psi(\underline{P},\underline{T},\underline{U}_o)$, must be an explicit expression for the local adsorption equilibrium in terms of $\underline{P}$, $\underline{T}$, and $\underline{U}_o$. Because of this restriction, the Langmuir model was used as the local adsorption function in most analytical solutions.

Halsey and Taylor (9) used the Langmuir model and selected an exponential distribution of regions as given by the function

$$f = Ce(-V_o/V'_o), \qquad (2)$$

where $\underline{V}_o$ is the energy difference between the lowest energy state of the gas and lowest energy of the adsorption complex, and $\underline{V'}_o$ is the mean of this difference.

Sips (10) proposed an alternative method for the analytical solution of Equation (1). An empirical equation was assumed for the experimentally observed function, $\Theta(\underline{P},\underline{T})$, and the Langmuir equation represented the local isotherm function $\psi(\underline{P},\underline{T},\underline{U}_o)$. A unique solution nearly equivalent to a Gaussian distribution was found for $\phi(\underline{U}_o)$.

Drain and Morrison (11) avoided the Langmuir equation by differentiating Equation (1) to obtain

$$\phi(U_o) = \frac{1}{\psi}\frac{d\Theta}{dU_o} \tag{3}$$

At a temperature of absolute zero, Equation (3) becomes

$$\phi(U_o) = \frac{d\Theta}{dU_o} \tag{4}$$

The unknown local isotherm function is eliminated at absolute zero temperature since the molecules have no thermal kinetic energy; therefore, no adsorption equilibrium exists between sites of different potential. Beginning at the site of greatest potential, the adsorption sites are filled serially. Each site is either filled or empty depending upon the adsorptive potential of the site and the number of molecules adsorbed by the total surface. Ross (12) summarized this method and the rigorous experimental conditions that are required. Heats of adsorption and the heat capacity of the adsorbed film as a function of surface coverage are measured at low temperatures; the zero degree heats of adsorption are determined by extrapolation. The one time the method was used, Morrison,

et al. (13) obtained the differential heat of adsorption rather than the adsorptive potential.

$$q^{diff} = U_o + aP^{ia} \qquad (5)$$

The term, aP^{ia}, which accounts for lateral attractions among adsorbed molecules, is difficult to determine and was ignored. Also, Equation (4) has been used under improper conditions where temperatures were significantly above absolute zero [cf. Ross (1), Chessick and Zettlemoyer (14), and Young and Healey (15)].

Harkins and Stearns (16) attempted to overcome the restrictions of the Langmuir model. They derived an adsorption isotherm for a mobile adsorbed film with lateral interactions on a surface of nonuniform adsorptive potentials. The thermodynamic and statistical development followed the methods of Hill (7), Tompkins (17), and Everett (18). However, the simplifications made by Harkins and Stearns in deriving the explicit local isotherm function, $\psi(P,T,U_o)$, destroyed the physical basis of their model.

The opinion of Ross and Olivier (19) is that an analytical solution of Equation (1) probably cannot be made based on the model of a mobile adsorbed film with lateral interactions and surface heterogeneity. Only a few attempts have been made to obtain a nonanalytical solution of Equation (1).

NONANALYTICAL SOLUTIONS

Adamson and Ling (20) proposed a graphical method whereby the site-energy distribution function, $\phi(U_o)$, is obtained from the experimental adsorption isotherm, $\theta(P,T)$, and an assumed local isotherm function, ψ. It is not necessary to represent the functions $\theta(P,T)$ and $\psi(P,T,U_o)$ analytically. In applying this method, Adamson and Ling used the Langmuir equation and the Fowler-Guggenheim

equation (the Langmuir equation with a lateral interaction term) for local isotherm functions. Site-energy distributions for the adsorption of butane, oxygen, and nitrogen on rutile and graphon were reported. The adsorption data were from Honig and Reyerson (21), and Joyner and Emmett (22).

The adsorption of argon on carbon black (MT-3100) was analyzed by Hsieh (23) using the Adamson and Ling method. The site-energy distribution obtained was Gaussian-like. Hsieh concluded that the Adamson and Ling method was insensitive to the local isotherm function selected for $\psi(\underline{P},\underline{T},\underline{U}_o)$ and that any local isotherm function may be used without yielding a different site-energy distribution curve.

Hobson modified the Polanyi potential theory to permit the determination of site-energy distributions from adsorption isotherms. This method has been reviewed in detail, and it is commended for making new approximations of the local adsorption – isotherm equation which are a more accurate description of the local isotherm than a step-function (1). Since the step-function approximation was avoided, the assumption that the substrate adsorbs molecules in the serial order of the energies of its adsorption sites was avoided also. The method assumed nothing about the form of the distribution. The primary weakness of the method was the arbitrary adsorption potential parameter. The relationship of the thermodynamic heat of adsorption to this parameter was not defined, and the temperature dependencies for the adsorption cannot be predicted.

Ross and Olivier (12) have proposed a monolayer adsorption theory in agreement with the findings of Ross and coworkers (25-27) that an adsorbed film is a mobile, two-dimensional, nonideal type film. The Hill-deBoer adsorption equation [Equation (6)] is used as the local isotherm function, $\psi(\underline{P},\underline{T},\underline{U}_o)$, and a

Gaussian distribution of adsorptive energies is assumed for $\phi(U_o)$. The Hill-deBoer equation is the mathematical expression of the deBoer adsorption model.

An intractable integral results when the Hill-deBoer equation is used as the local isotherm function in Equation (1). With the aid of a computer, Ross and Olivier obtained theoretical isotherms for different values of all the parameters by summing over the integral limits. The site-energy distribution is determined by comparing the computed theoretical isotherms with experimental isotherms. The distributions obtained are temperature invariant, and the model correctly predicts the adsorption behavior for a number of adsorption systems. The method provides a determination of the monolayer capacity.

The Ross-Olivier model has been criticized for assuming a normal distribution of adsorptive potentials [cf. Adamson and Ling (20) and Hobson (24)]. However, the theory was reviewed favorably by Gregg and Sing (28), although they questioned the divergence of BET and Ross-Olivier surface area estimates for substrates of low adsorptive potential.

APPROACH TO THE THESIS PROBLEM

THE PROBLEM

The Ross-Olivier theory has been applied to the argon-cellulose adsorption system by Barber (29). He observed that the cellulose surface area was characterized by a low mean adsorptive potential, $\underline{U'}_o$, and a wide distribution of adsorptive potentials; that for variously treated cellulose fibers of different surface areas the dependence of $\underline{U'}_o$ on the surface area was minor; that a marked difference exists between the monolayer capacities as determined by the Ross-Olivier theory, $\underline{V}_\beta$, and the BET theory, $\underline{V}_m$; and that the ratio $\underline{V}_\beta/\underline{V}_m$ was dependent upon the mean adsorptive potential of the substrate. Barber supported the hypothesis of Ross and Olivier (30) that for a surface of low adsorptive potential the specific surface area, as determined by the BET method, is grossly in error, and that:

> ...the part of the surface having an adsorptive potential less than that of the liquid adsorbate remains sparsely occupied, even as multilayers build up over the more energetic patches of the surface; this effect combined with that produced by a low value of γ, leads to a value of $\underline{V}_m$ by the BET method that is about one third of the value of $\underline{V}_\beta$ (30).

The argon-cellulose interaction primarily involves dispersion forces. The charge distribution of the argon atom is spherically symmetrical; therefore, the atom possesses no permanent dipole, and it has no external field. However, the atom does have instantaneous dipole and multipole moments. These instantaneous moments induce resonant moments in any neighboring atom. Thus, there is a force of attraction between the atoms due to interaction of the electron clouds. The electron cloud of argon is spherical and is not easily polarized. One would expect a slight dipole to be induced in argon only in the presence of a strong electric field. Barber assumed that induction forces were not a significant part of the adsorption forces for the argon – cellulose system. If this assumption is

correct, the adsorption parameters $\underline{U}'_o$ and γ as determined by Barber characterize the argon-cellulose adsorption system where dispersion forces are the only significant force of attraction.

The next logical study would be an investigation of the interaction of cellulose with an adsorbate which might involve more than just dispersion forces as the attractive forces. The action of the various attraction forces would be reflected in the adsorption parameters for this particular cellulose-adsorbate system. The most convenient adsorbate for this type of study would be nitrogen. The nitrogen molecule is linear, and the polarizability along the common axis of the two atoms is about 1.5 times as great as the polarizability of argon (12).

An estimate of the order of magnitude of the cellulose surface electric field effect on adsorbate molecules having induced polarity and/or permanent dipolar character is necessary. This estimate must be known before these systems can be investigated and analyzed. The thesis was directed toward assessing the effect of the surface electric field of cellulose as one goal.

When polarization and orientation of the adsorbate are insignificant, the ideal value of the two-dimensional van der Waals' constant α is used in the calculation of $2\alpha/\underline{RT}\beta$ (the value of $2\alpha/\underline{RT}\beta$ determines the shape of the calculated model adsorption isotherms). The real value of α is less than the ideal value if a surface electric field induces a dipole moment in the adsorbed molecules (cf. pages 41-3). When isotherm matches are made with a decreased value of $2\alpha/\underline{RT}\beta$, a higher value of the heterogeneity parameter γ is obtained (γ is related to the standard deviation of the distribution of the adsorptive potentials, cf. page 15). Therefore, the effect of an electric field at the surface can be confused with the effect of surface heterogeneity [cf. reference (31)]. Thus, the surface electric field strength must be determined so that its effect on the adsorbate can be distinguished.

In the cellulose-nitrogen system one expects the effect of a surface electric field to be important if significant upright orientation of the nitrogen molecule occurs. When the strength of this field is known, the validity of Barber's assumption of insignificant induction adsorption forces for the cellulose-argon system can be determined.

For this investigation, an estimate of the average surface electric field of the cellulose substrate will be calculated from heat of wetting determinations by the method of Chessick, et al. (32). A homologous series of wetting liquids of various dipole moments is used. The slope of the heat of wetting versus dipole moment curve provides an estimate of the surface electric field strength.

SELECTION OF THE ROSS-OLIVIER MODEL

One expects adsorbate – adsorbate interactions to occur whenever adsorbate molecules are close enough to experience van der Waals' forces of attraction or electronic forces of repulsion. Any reasonable description of physical adsorption must account for these interactions.

The Ross-Olivier theory for monolayer adsorption (12) is the most reasonable description of cellulose – gas physical adsorption systems. The Ross-Olivier adsorption model assumes a mobile adsorbed film with lateral adsorbate interactions. In addition, the model assumes a distribution of site-energies or adsorption potentials; that is, the substrate surface is considered to be energetically heterogeneous. The energy sites are located randomly, and the probability of occurrence for a particular adsorptive potential can be calculated from the Gaussian function.

The assumption of a mobile adsorbed film is compatible with experimental evidence. Ross and coworkers (25-27) have shown that argon or nitrogen adsorbed

films on a variety of substrates are described best as two-dimensional mobile films. The same conclusion was made by Cochrane, et al. (33) for xenon adsorption on graphitized carbon blacks. Theoretical calculations by Hill (7) indicate that the transition from localized to mobile adsorption occurs at very low temperatures for potential barriers of 1000 cal./mole and less.

The results of the field-emission microscope studies of argon, krypton, and xenon adsorption on the tungsten tip of the microscope indicated that physically adsorbed molecules are mobile at low temperatures (2-70°K). These studies also present direct visual evidence for the heterogeneity of surfaces. A summary of these results from the field-emission microscope studies of Gomer (34) and Ehrlich, et al. (35) is given by Hobson (36).

An important aspect of the Ross-Olivier theory is the energy heterogeneity of the substrate. A consideration of the configuration of the cellulose polymer, of the presence of crystallinelike regions, and of the irregular fiber surface suggests an energetically heterogeneous cellulose substrate.

The Ross-Olivier theory is complete thermodynamically, unlike other methods which also account for the heterogeneity of the substrate [cf. Hobson (24) and Adamson and Ling (20)]. An estimate of the monolayer capacity and a distribution of adsorptive potentials are provided; the temperature invariants of these parameters is a requirement of the theory. The Ross-Olivier theory has been applied to the argon – cellulose system by Barber (29).

THE ROSS-OLIVIER THEORY FOR MONOLAYER ADSORPTION AND THE METHOD OF APPLICATION

The Ross-Olivier form of Equation (1), with the Hill-deBoer adsorption equation substituted for $\psi(\underline{P},\underline{T},\underline{U}_o)$ and with the Gaussian probability function

substituted for $\phi(U_o)$, yields an intractable integral. To obtain a solution, the integral is replaced by a sum of i elements. Each element of the sum represents the adsorption on sites of the same adsorptive potential, U_{oi}. These adsorption-sites are called elemental homotattic patches by Ross and Olivier. Each homotattic patch behaves as a uniform and energetically homogeneous region upon which the adsorption is described by the Hill-deBoer equation,

$$p = K_i \left(\frac{\theta_i}{1-\theta_i}\right) \exp\left(\frac{\theta_i}{1-\theta_i} - \frac{2\alpha\theta_i}{RT\beta}\right) \tag{6}$$

where P = equilibrium pressure

K_i = a constant related to U_o of each patch

θ_i = fraction of monolayer completion for patch i

R = gas constant

T = absolute temperature

α,β = two-dimensional van der Waals' constants, corresponding to a and b, respectively.

The frequency of occurrence of a homotattic patch with the particular adsorptive potential, U_{oi}, is given by the Gaussian probability function,

$$f_i = \frac{d\delta_i}{dU} = \phi(U_o) \tag{7}$$

The term $d\delta_i$ represents the fraction of the surface having an adsorptive potential between U_{oi} and $U_{oi} + dU_o$. It is a necessary condition that the summation of $d\delta_i$ over the permitted values of U_o be equal to unity,

$$\int_{U_o \text{ initial}}^{U_o \text{ final}} \phi(U_o)dU_o = 1 \tag{8}$$

Ross and Olivier confine the adsorptive potentials to a range of 5.0 kcal./mole. The terms $\underline{U}_{o\ \text{initial}}$ and $\underline{U}_{o\ \text{final}}$ represent the values of the adsorptive potential at which the frequency of occurrence is $\underline{f}_i = 0.001$. This approximation is imposed without significantly altering the area under the distribution curve. The Gaussian probability function is used in the form

$$f_i = \phi(U_o) = \frac{1}{n} \exp(-\gamma\ (U_{oi} - U'_o)^2) \tag{9}$$

where $\underline{U'}_o$ = the mean adsorptive potential of the total surface and is taken to be 2.5 kcal./mole for the generation of model values.

γ = the heterogeneity parameter and is related to the standard deviation, σ, of the distribution by

$$\gamma = \frac{1}{2\sigma^2} \tag{10}$$

$\underline{n}$ = the normalizing factor as given by

$$n = \int_o^5 \exp\ (-\gamma\ (U_o - U'_o)^2) dU_o \tag{11}$$

For each distribution curve which corresponds to a particular value of γ (refer to Fig. 1), the range of adsorptive potentials between $\underline{U}_{o\ \text{initial}}$ and $\underline{U}_{o\ \text{final}}$ is divided into fifty parts. This procedure effectively divides the surface into fifty finite patches, each of which is defined as that fraction, $\Delta\underline{\delta}_i$, of the total surface having an adsorptive energy between $\underline{U}_{oi}$ and $\underline{U}_{oi} + \Delta\underline{U}_o$, where $\Delta\underline{U}_o = (\underline{U}_{o\ \text{final}} - \underline{U}_{o\ \text{initial}})/50$. The term $\underline{U}_{oi}$ is the midpoint value for the $\underline{i}^{th}$ patch (i.e., $\underline{U}_{oi} = \underline{U}_{o\ \text{initial}} + 1/2\Delta\underline{U}_o$; $\underline{U}_{oi} = \underline{U}_{oi-1} + \Delta\underline{U}_o$).

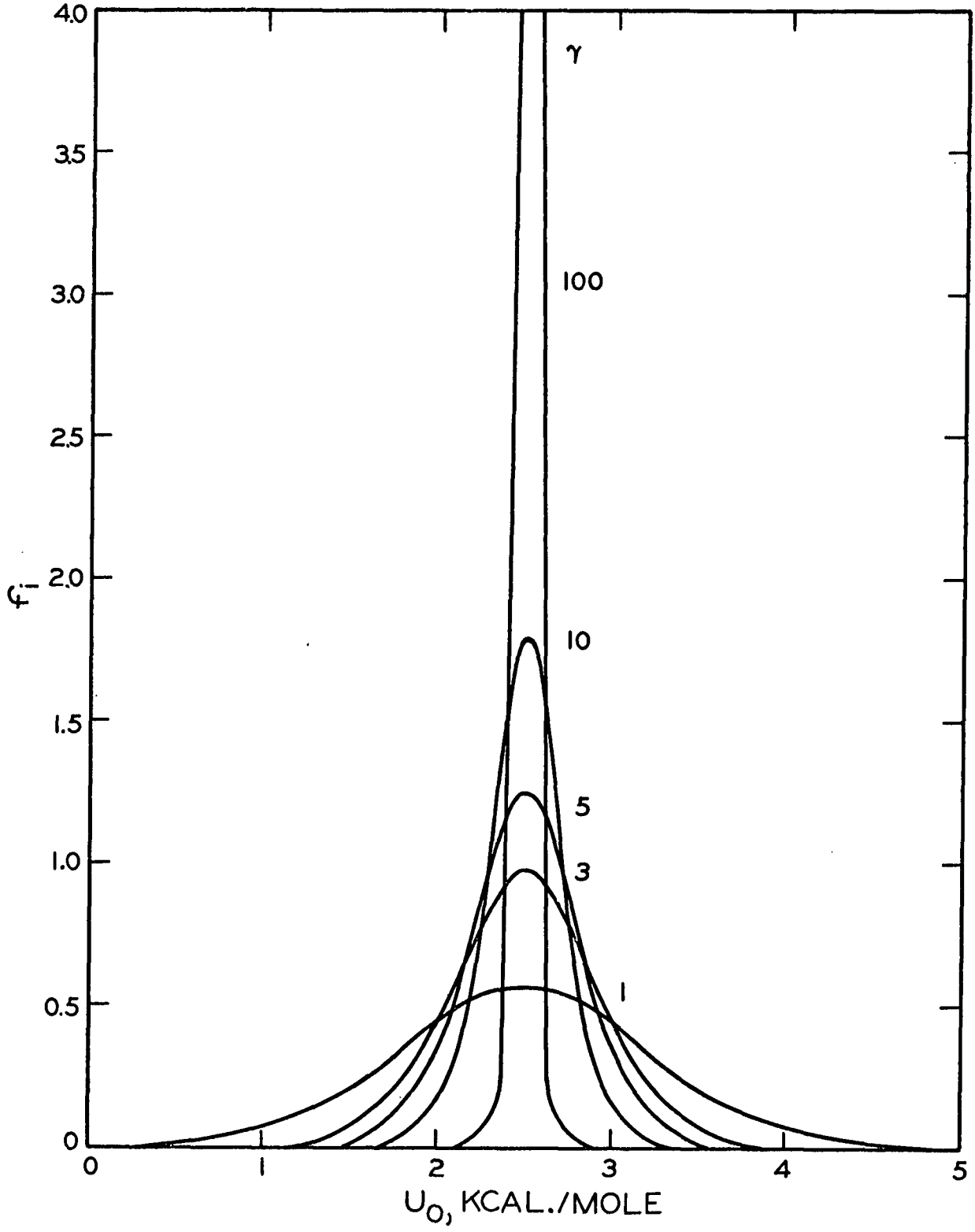

Figure 1. Gaussian Distributions of Adsorptive Potential Energies for Various Values of γ in Equation (8) [After Ross and Olivier (12)]

$$\Delta\delta_i = \int_{U_{oi}}^{U_{oi} + \Delta U_o} \qquad d\delta_i = \int_{U_{oi}}^{U_{oi} + \Delta U_o} f_i dU_o \tag{12}$$

A subdivision of fifty is used by Ross and Olivier in the generation of model isotherms. A greater subdivision, of one hundred for instance, results in more uniform model isotherm curves. For use in the computer, integrations are replaced by sums and differential quantities are replaced by step values.

The constant, $\underline{K}_i$, of Equation (6) is related to the adsorptive energy by

$$K_i = A^o \exp(-U_{oi}/RT) \tag{13}$$

It is possible to calculate $\underline{A}^o$ from thermodynamic considerations of the model. However, for model isotherm generation $\underline{A}^o$ is arbitrarily chosen so that in Equation (13) $\underline{K}_i = 1$ when $\underline{U}_{oi} = \underline{U'}_o = 2.5$ kcal./mole and $\underline{T} = 77.5°K$.

For a particular set of two-dimensional van der Waals' constants, α and β, and for an arbitrarily chosen equilibrium pressure, the Hill-deBoer equation [Equation (6)] is solved by trial and error for the θ_i of each patch of adsorptive potential $\underline{U}_{oi}$. As the adsorptive potential of the patches is increased, $\underline{K}_i$ decreases, and the fraction of coverage, θ_i, increases. The type of adsorbate gas which is used experimentally determines the values of α and β to be used in Equation (6).

The overall monolayer coverage, Θ, for each equilibrium pressure is the average of the fraction of patch coverage weighted by the fraction of total surface represented by that patch of adsorptive potential $\underline{U}_{oi}$.

$$\Theta = \sum_i \Delta\delta_i \theta_i \tag{14}$$

In order to complete the model isotherms, this procedure is repeated for several assumed equilibrium pressure values. A model isotherm for a particular value of γ (the value of γ determines the values of $\underline{U}_{o\ \text{initial}}$ and $\underline{U}_{o\ \text{final}}$ and, consequently, the values of $\Delta\underline{\delta}_i$, $\underline{U}_{oi}$, and $\underline{K}_i$) is obtained in the form Θ versus $\underline{P}$. A series of model isotherms which have been converted to the form ln Θ versus ln $\underline{P}/\underline{K}'$ is presented in Fig. 2.

In order to interpret experimental data in terms of the Ross-Olivier theory (12), it is necessary to compare the experimental isotherm with a series of model isotherms of various values of γ. The series of isotherms is selected for that particular value of $2\alpha/\underline{R}\underline{T}\beta$ needed to describe the adsorbate gas. The experimental isotherm in the form ln$\underline{V}$ (volume adsorbed) versus ln$\underline{P}$ (equilibrium pressure) is superimposed on the model isotherm. The experimental isotherm is positioned so that a best fit with one model isotherm is obtained. The scale of the axes of the two plots must be identical. After a match is obtained, the displacements of the axes yield the parameters $\underline{V}_\beta$ and $\underline{U}'_o$. The vertical axis displacement is ln$\underline{V}_\beta$, and the horizontal axis displacement is ln$\underline{K}'$ [which is related to $\underline{U}'_o$ through Equation (13)]. The value of γ is characteristic of the particular model isotherm that was used for the match. The matching procedure is illustrated in Fig. 2. The parameters that are obtained through this matching procedure characterize the surface as to monolayer capacity, mean adsorptive potential, and the range of adsorptive potentials.

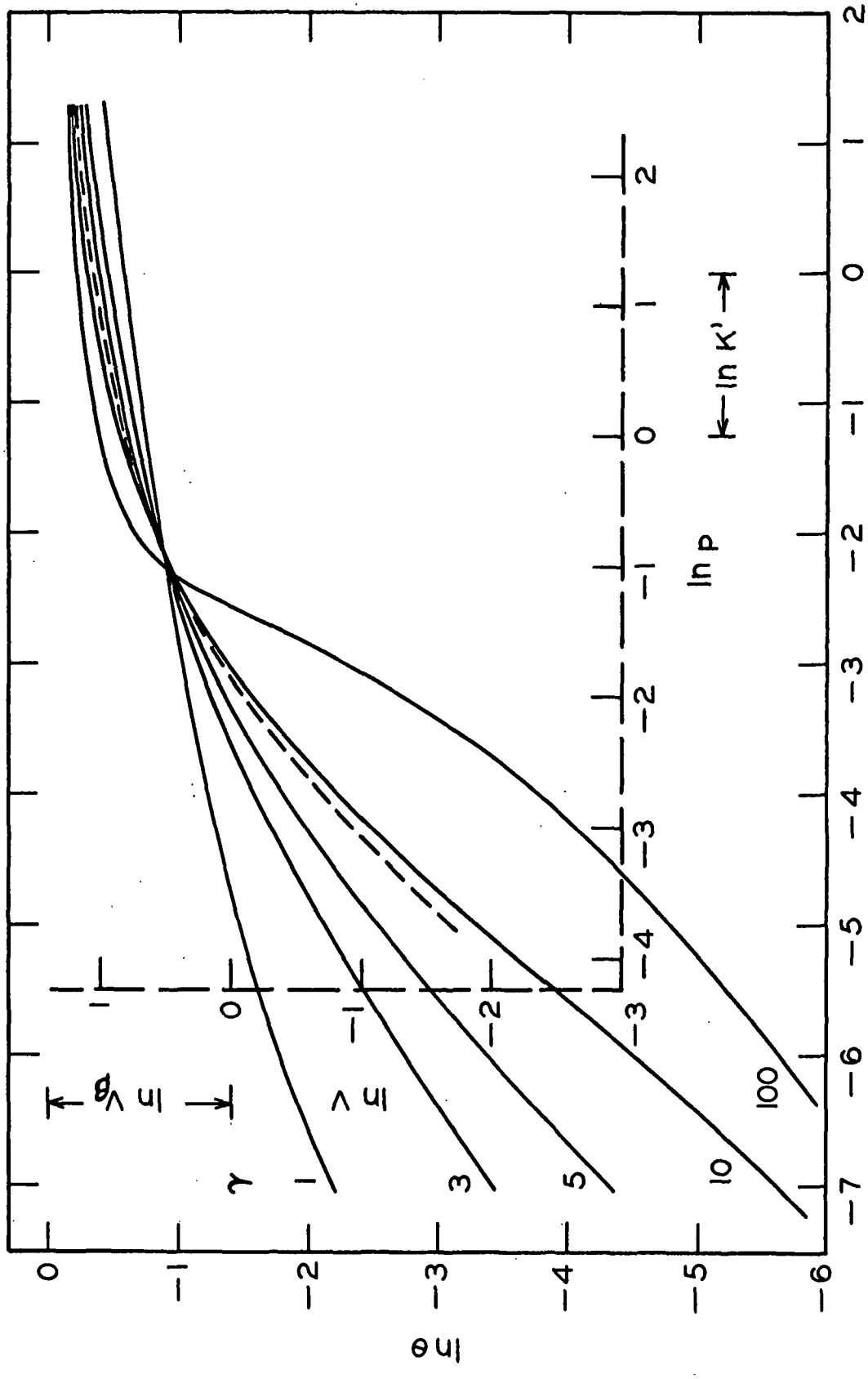

Figure 2. Model Isotherms (Solid Lines) and a Superimposed Experimental Isotherm (Dashed Line) in its Proper Interpolated Position [After Ross and Olivier (12)]

GENERAL EXPERIMENTAL PROCEDURES

SAMPLE PREPARATION

Purified Stoneville-2B cotton was selected as the cellulosic substrate. The impurities in cotton – waxes and pectic substances – can be removed with a mild chemical treatment. The cotton used in this study was of the same origin as that used by Sommers (37) and by Barber (29).

PURIFICATION OF COTTON

The cotton was purified using Sommers' modification (37) of the method of Conrad (38). The purification procedure consisted of a sorting operation, followed by extraction with 95% ethanol, 1.0% boiling caustic, boiling water, and 0.5% acetic acid. Appendix I contains a detailed description of this purification procedure.

SOLVENT EXCHANGE AND DRYING

The solvent-exchange apparatus of Barber (29) was used to remove imbibed water from the fibers. The apparatus was modified to accomodate three samples simultaneously. A schematic diagram of the apparatus is shown in Fig. 3.

Sample bulbs were fabricated from pyrex test tubes and were filled with purified cotton using the technique of Sommers (37). Water was replaced by organic solvents in the sequence methanol – dried methanol – n-pentane – dried n-pentane. The solvent-exchanged samples were dried with nitrogen which had been passed through a drying train of phosphorous pentoxide. Dry methanol was prepared by the method of Lund and Bjerrum (39); n-pentane was dried by refluxing over an extruded ribbon of sodium. Reagent-grade methanol, Phillips 66 pure grade n-pentane and prepurified nitrogen were used in these operations.

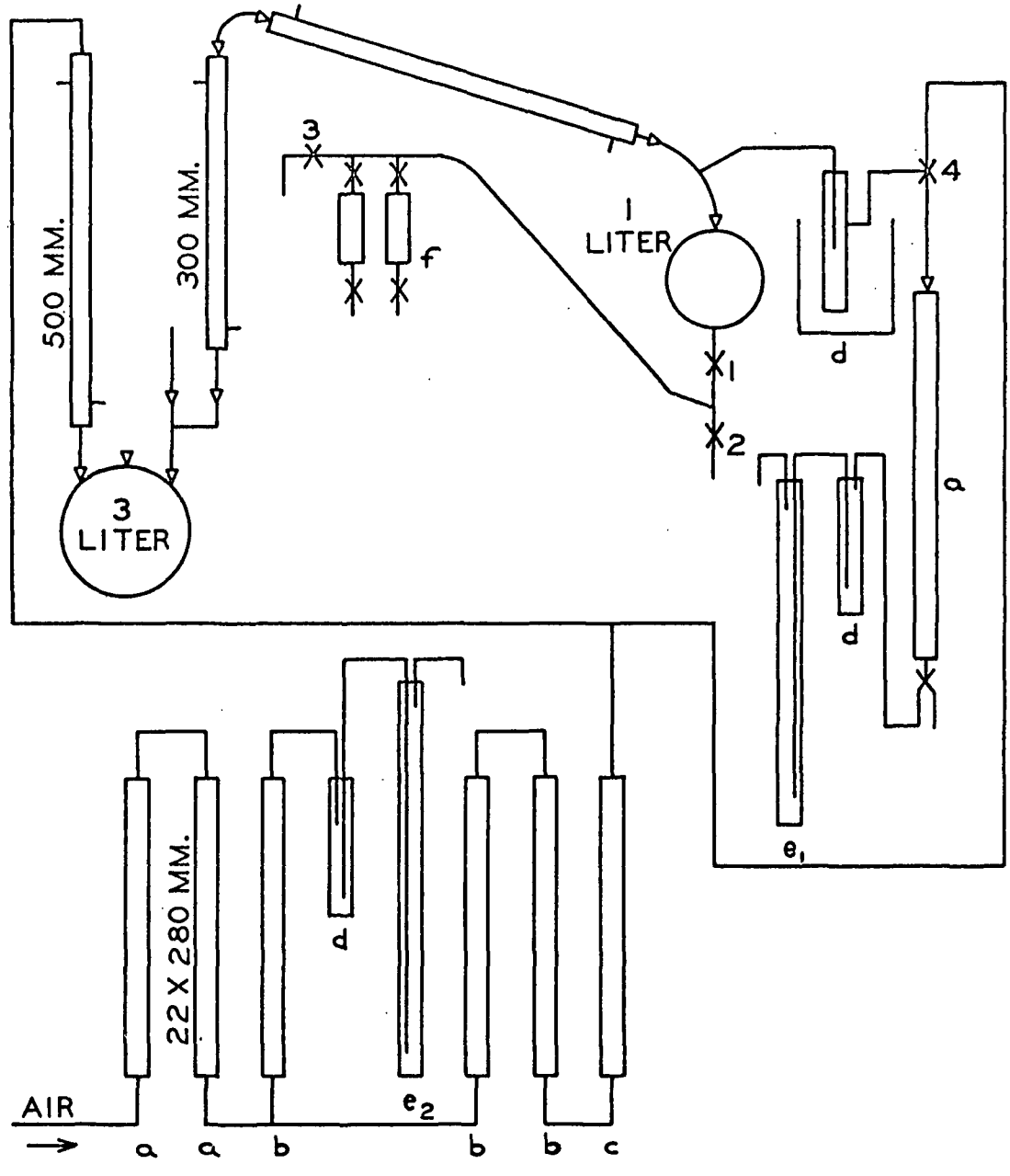

▷ GROUND GLASS JOINT
a DRIERITE
b ANHYDRONE
c PHOSPHORUS PENTOXIDE
d TRAP
e BUBBLER
f SAMPLE BULBS
X STOPCOCKS

Figure 3. Apparatus for the Solvent Exchange and Drying of Samples

The number of exchanges and the contact times varied somewhat for different samples. The purpose of the solvent exchanges was to develop more surface area than would be developed in fibers dried from water. Development of similar surface areas for all samples was not intended. However, an exchange-time schedule was followed as closely as possible. This schedule is given in Appendix I.

MEASUREMENT OF ADSORPTION ISOTHERMS

APPARATUS

The apparatus used for this adsorption study was that of Haselton (40) with modifications made by Merchant (41). A complete description of the design and the method of operation of the adsorption apparatus has been presented by them. With this equipment, adsorption isotherms are determined volumetrically. The apparatus is shown schematically in Fig. 4.

METHOD OF OPERATION

Solvent-exchanged samples were outgassed for about fifteen hours at a temperature within the range of 50-60°C. A pressure of less than 2.0×10^{-6} mm. Hg could be maintained during adsorption runs. A series of adsorption isotherms for one sample could be completed in six days. Equilibrium pressures less than 0.35-0.40 times the adsorbate saturation vapor pressures were investigated.

Sample deadspace determinations were made with prepurified helium at each isotherm temperature. Results of the deadspace determinations are presented with the adsorption data in Appendix III.

The operational procedure for the adsorption apparatus was a combination of the constant volume method and the constant mass method, and it was the same

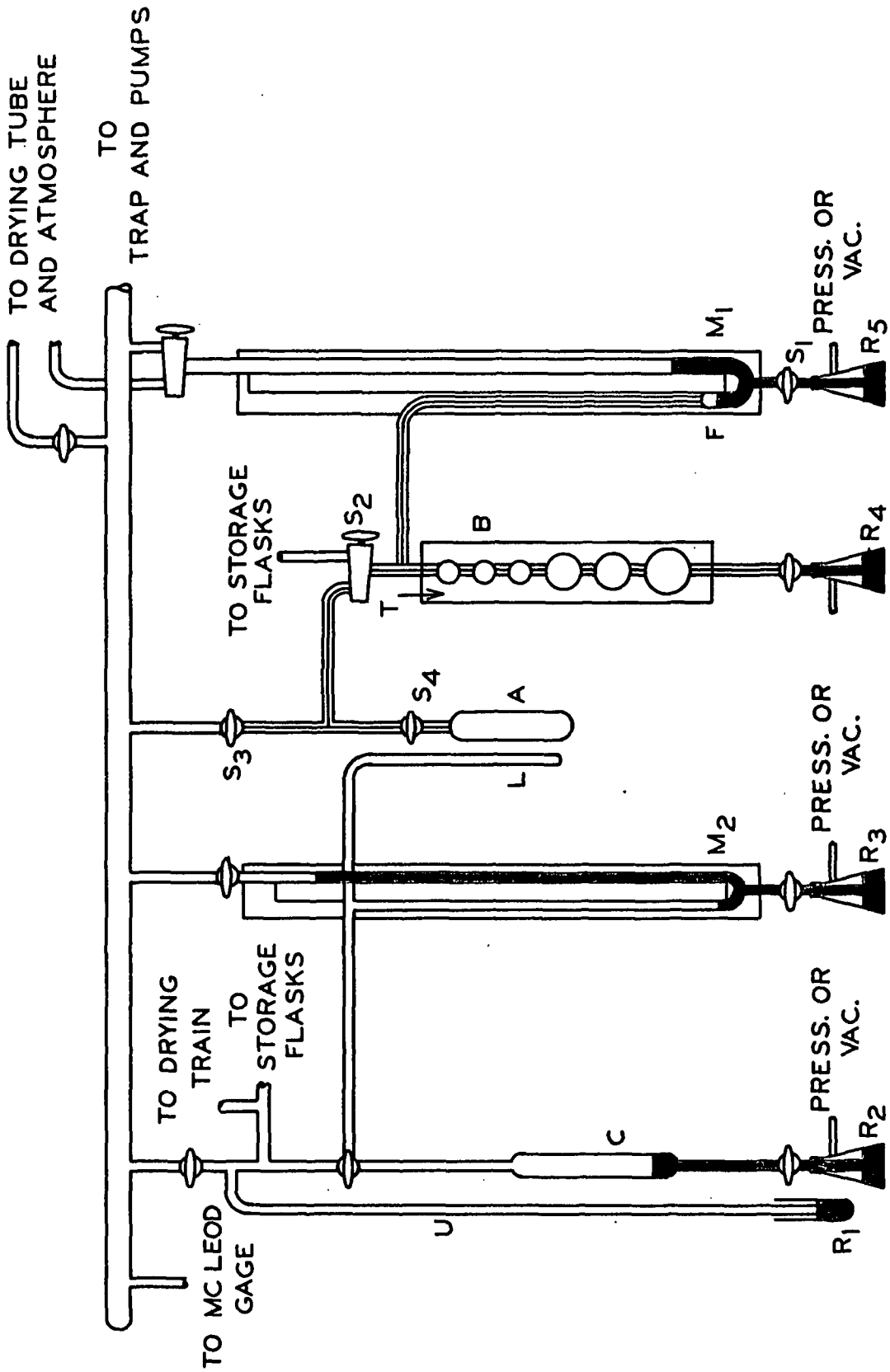

Figure 4. Apparatus for Determination of Adsorption Isotherms

procedure used by Barber (29). The gas buret, B, and a manometer, M, were used to measure the volume of gas added and the equilibrium pressure and volume. Stopcock S_2 was used to add gas to the buret and to expose the sample to the gas. The mercury level was lowered to the bottom of the gas buret before stopcock S_2 was opened to the sample. The upper bulbs were used to add small volumes of gas and to attain more sensitive pressure readings in the low pressure range. The advantages of this method are that large or small volumes of adsorbate gas can be added, that low equilibrium pressures can be measured with greater accuracy, and that duplicate volume-pressure readings can be made by raising or lowering the mercury level to different bulbs in the buret.

Either liquid oxygen or liquid nitrogen was used in a constant temperature bath on the sample during the deadspace determinations and the adsorption data collection. Saturation pressures of the adsorbate gas were determined manometrically with M_2 when possible. When saturation pressures were too large for this type of determination, an oxygen gas thermometer was used to determine an accurate bath temperature. Saturation pressures were deduced from the known bath temperatures.

THE HEAT OF WETTING DETERMINATIONS

SELECTION AND PREPARATION OF THE WETTING LIQUIDS

The heat of wetting of cellulose was determined by the method of Chessick, et al. (32). It is important that the surface available for gas adsorption be maintained during the heat of wetting study. Thus, a prerequisite in the selection of the wetting liquids was that no significant swelling of the fibers should occur during wetting. If no swelling occurred, or if swelling was small so that the heat generated by the swelling was negligible, the heat of

immersion of the cellulose in the wetting liquid would be equal to the heat of wetting plus the heat of bulb breaking.

A series of benzene and substituted benzene liquids was used – benzene, chlorobenzene, nitrobenzene. Robertson (42) in a study of the swelling effects of various liquids on cellulose found that liquids with a molar volume greater than 100 cc. produced insignificant swelling in cellulose. In Robertson's work the fibers were immersed in organic liquids, solvent-exchanged to benzene, and the accessibility of the cellulose to thallous ethylate was measured in benzene. The accessibility was considered to reflect the swelling of the cellulose in the initial organic liquid. Although the molar volume of benzene is less than 100 cc., the swelling effect was found to be small. The molar volumes of chlorobenzene and nitrobenzene are greater than 100 cc.

The wetting liquids must be relatively free of water since water probably would be adsorbed preferentially. The measured heat of immersion would be primarily the heat of sorption of water and the heat of swelling of the cellulose fibers. It was determined that the effects of 1-2 p.p.m. of water could not be detected in the calorimetric determination of the heat of wetting. After purification, the wetting liquids were placed in contact with 4 A molecular sieve, followed by treatment with calcium hydride. After treatment, the water content of the liquids was found to be less than 2 p.p.m. The water determinations were made with a gas chromatograph equipped with a thermal conductivity sensor and a Por-Pak Q column for liquid separation. The liquids were stored over calcium hydride in a sealed glass container.

Detailed procedures for the purification of the liquids and for the water determination are presented in Appendix II.

APPARATUS

The heats of immersion for cellulose in wetting liquids of various dipole moments were determined in a differential calorimeter. A linear quartz thermometer was used to measure changes of temperature during the determinations. The calorimeter design was basically that of Kraus (43) and Berghausen (44) with several modifications for the purpose of decreasing the heat capacity and increasing the response of the system to temperature changes. The calorimeter was constructed by P. Brown (45); the accuracy is 0.05 calorie.

Quartz Thermometer

The thermometer was a Hewlett-Packard, linear quartz thermometer, model HP2801A. Temperature is given as a six-place direct digital display with resolution of 0.01, 0.001, or 0.0001°C. The quartz thermometer is an integrating device, providing an average value of the probe temperature over a fixed reading time. Reading times are related to the resolution selected; sample periods are 0.1, 1.0, and 10 seconds for resolutions of 0.01, 0.001, and 0.0001°C., respectively.

A more detailed description of the thermometer and the quartz crystal as a temperature sensor is given in Appendix II.

Calorimeter

The calorimeter and peripheral equipment are shown in Fig. 5-7. The calorimeter was a twin chamber arrangement insulated by a dead-air space from above and by a silvered dewar surrounded by polyurethane foam. In Fig. 5-7, Vessel 1 has been replaced with a demonstration jacket.

Each chamber contains an immersion heater, a temperature probe, a stirrer, and a platform arrangement for supporting the sample bulb. The supporting rod was made of capillary tubing, and it accomodated a silver metal rod

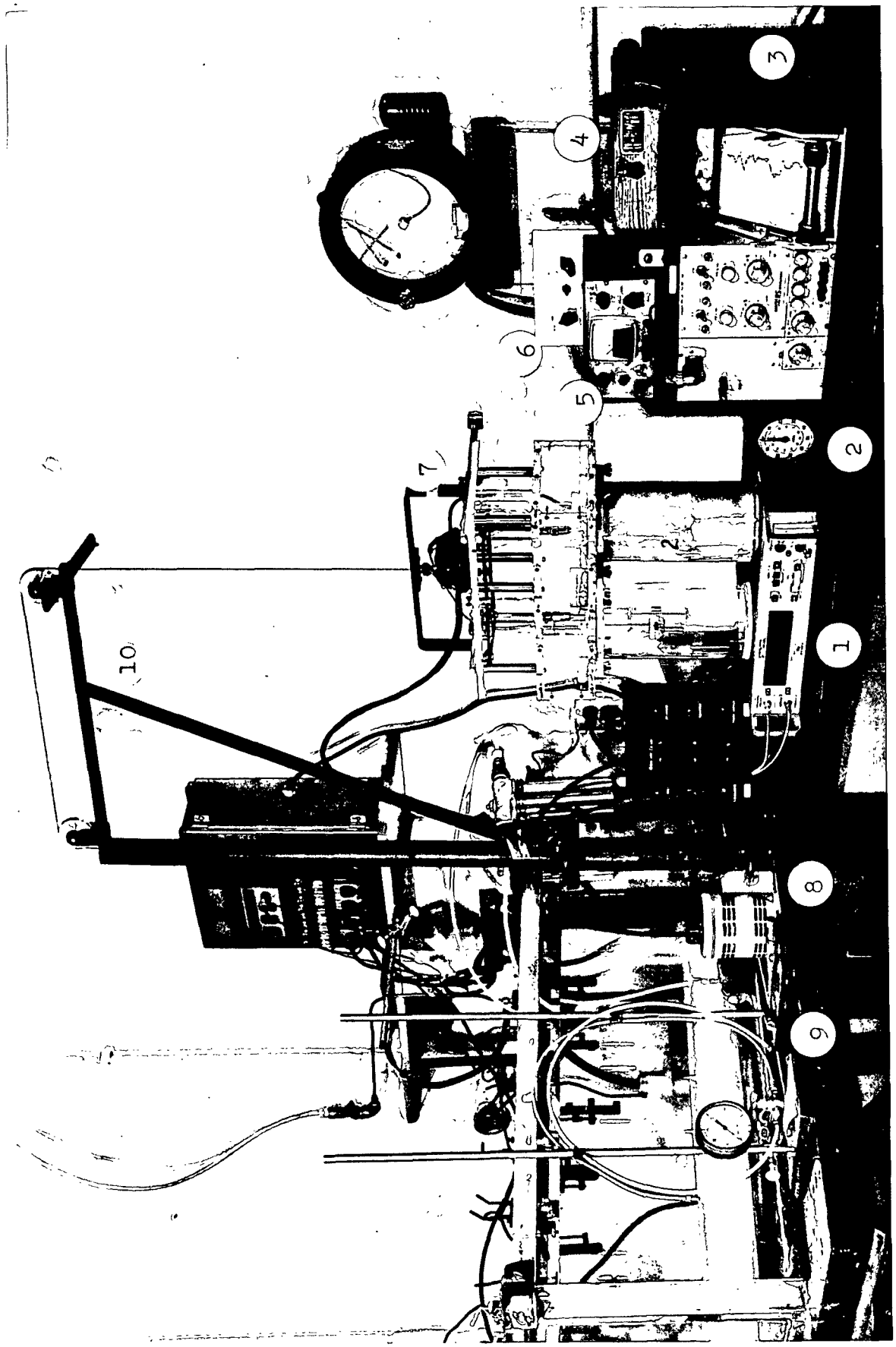

Figure 5. Calorimeter and Peripheral Equipment Used in the Heat of Wetting Determinations: 1) Hewlett-Packard Quartz Thermometer 2) Electric Timer 3) Recorder 4) Milliammeter 5) Kepco Power Supply 6) Switching Box 7) Calorimeter 8) Variac Transformer 9) Vacuum System for Admission of Dried Nitrogen 10) Crane

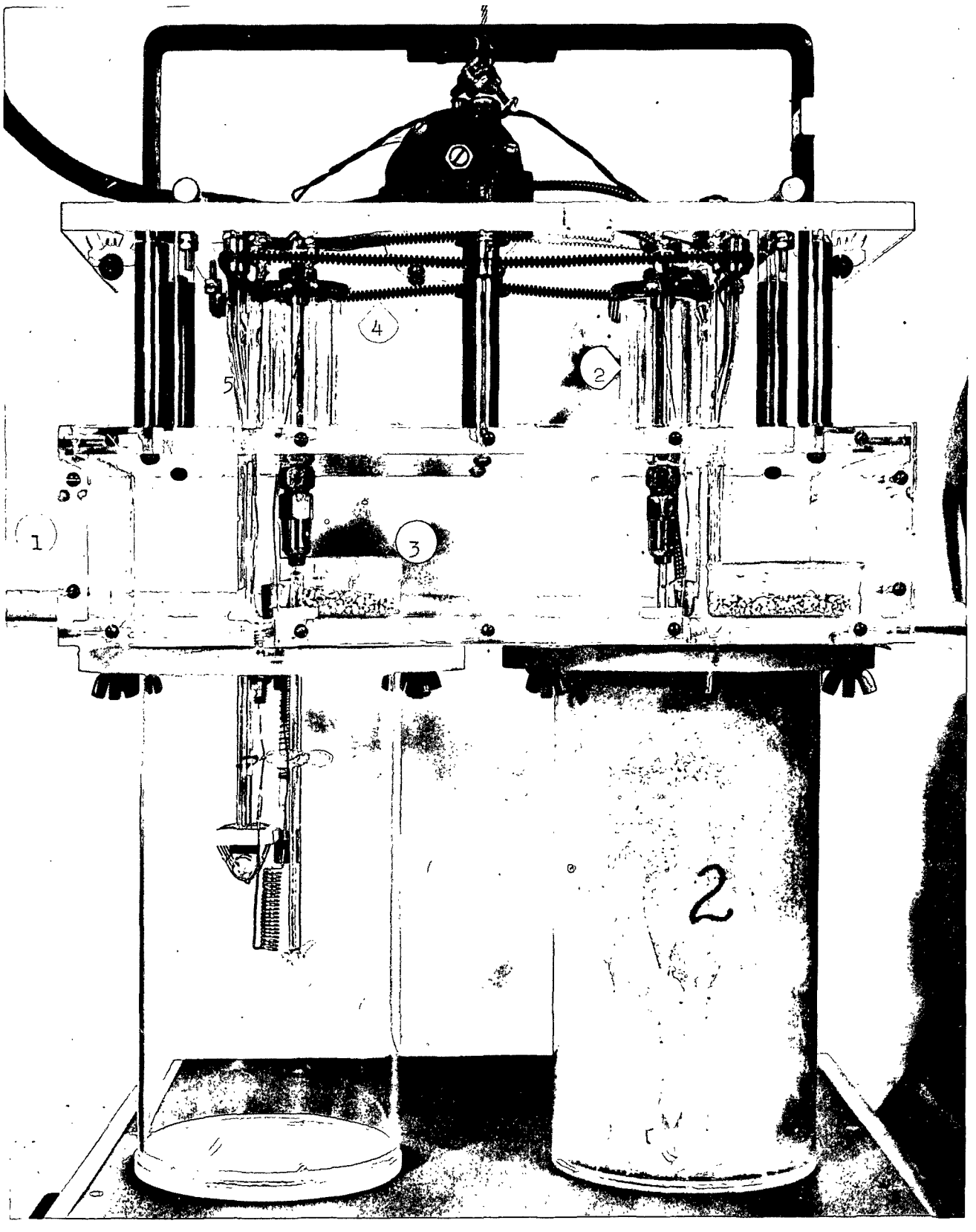

Figure 6. Differential Calorimeter for Heat of Wetting Determinations: 1) Submarine Jacket 2) Dam 3) Indicating Drierite 4) Stirring-Rod-Drive Cable 5) Inlet Tube

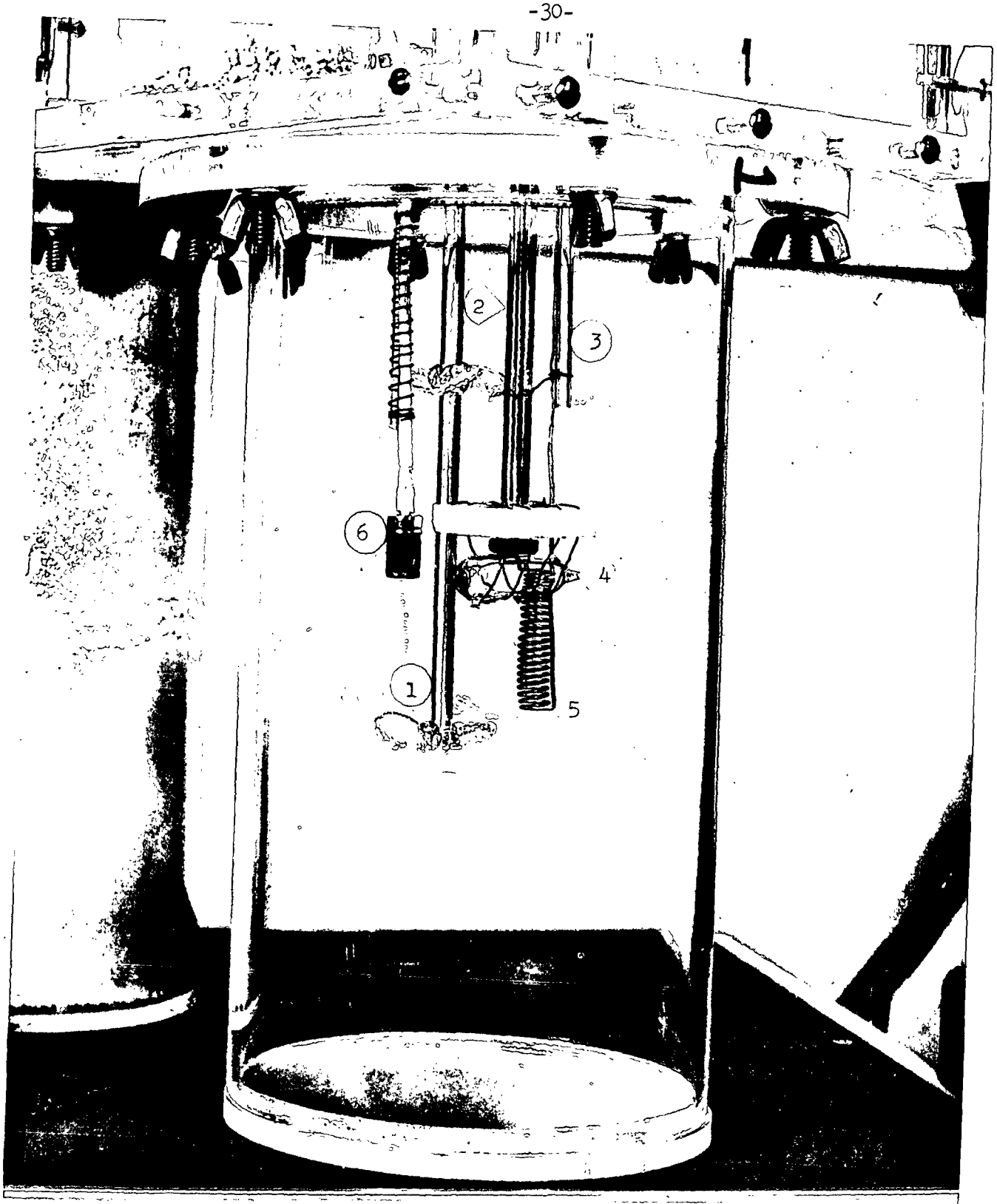

Figure 7. Reaction Chamber for the Differential Calorimeter: 1) Stirring Rod 2) Support Rod 3) Vacuum Line for Admission of Dried Nitrogen 4) Sample Bulb 5) Immersion Heater 6) Thermometer Probe

with a plastic spacer. The stirrers were made from pyrex glass rod. The impeller blades were pitched so that the wetting liquid was forced down from the top and up from the bottom toward the sample. The stirrers were powered by a synchronous motor and timing belt drive to assure uniform and constant stirring rates in each chamber. Internal immersion heaters were made from 18 gage nichrome wire. The heaters were operated from a 6-volt storage battery. The circuit included a timer, milliameter, and a switch for selecting the combination of heaters desired. A connection to a.c. line power for bringing the chambers to some temperatures before initiation of a determination was provided in the circuit also. The 6-volt storage battery was always used to determine the heat capacity of the system.

Among the peripheral equipment shown in Fig. 5 is a water bath maintained at 30.00 $\pm$ 0.01°C. and a swivel support for moving the calorimeter to and from the bath.

A hollow plug which fits into the dewar and seals the chamber is not shown in Fig. 5-7 since it would obscure the details of the sample bulb support, etc. Design details of the plug, calorimeter, and electrical circuit are presented in Appendix II.

Method of Operation

In preparing the calorimeter for a determination, the dewar vessels were washed with acetone, washed with sulfuric acid saturated with dichromate, rinsed thoroughly with distilled water, rinsed with absolute ethanol and placed on the calorimeter. An ethanol-azeotrope was formed, and the chambers were dried by evaporation of the azeotrope. Nitrogen gas was passed through a liquid nitrogen trap to remove any moisture and admitted to the chamber via the connecting line (Fig. 5 – no. 9) and inlet tube (Fig. 7 – no. 3). The gas and evaporated ethanol

escaped the chamber by a second inlet tube (Fig. 6 – no. 5). Several hours were required to dry the chamber in this manner.

The dried wetting liquid was transferred to a separatory funnel. The transfer was made in a dry-box and the liquid was stored in the funnel over calcium hydride until it could be transferred to the calorimeter. The top of the second inlet tube into the chamber (Fig. 6 – no. 5) was a female ground-glass joint. The separatory funnel was fitted with the male counterpart so that a good connection could be made. A nitrogen gas line was connected to the top of the funnel and the wetting liquid was forced into the calorimeter chamber. Calcium hydride was added to the chamber to remove any water sorbed by the wetting liquid during transfer. After removal of the funnel, the inlet tube was plugged with a serum cap. The wetting liquid and the water in the reference chamber were brought to approximately 30.0°C. with the immersion heaters. Thermal equilibrium of the calorimeter required 12-18 hours. After the temperature in the two vessels had stabilized, a determination was started. A temperature base line was established over a period of several minutes; the sample bulb was broken and again a base line was established after the temperature had stabilized. The heat capacity of the system was determined by adding a known amount of energy to the immersion heater and observing the temperature change within the vessel.

A typical plot of temperature versus time for a heat of wetting determination is shown in Fig. 8. The heat of wetting is calculated from the following equations:

$$H_I = R\, I^2 t(\Delta t_A/\Delta t_B) \tag{15}$$

$$H = H_I - H_{BB} \tag{16}$$

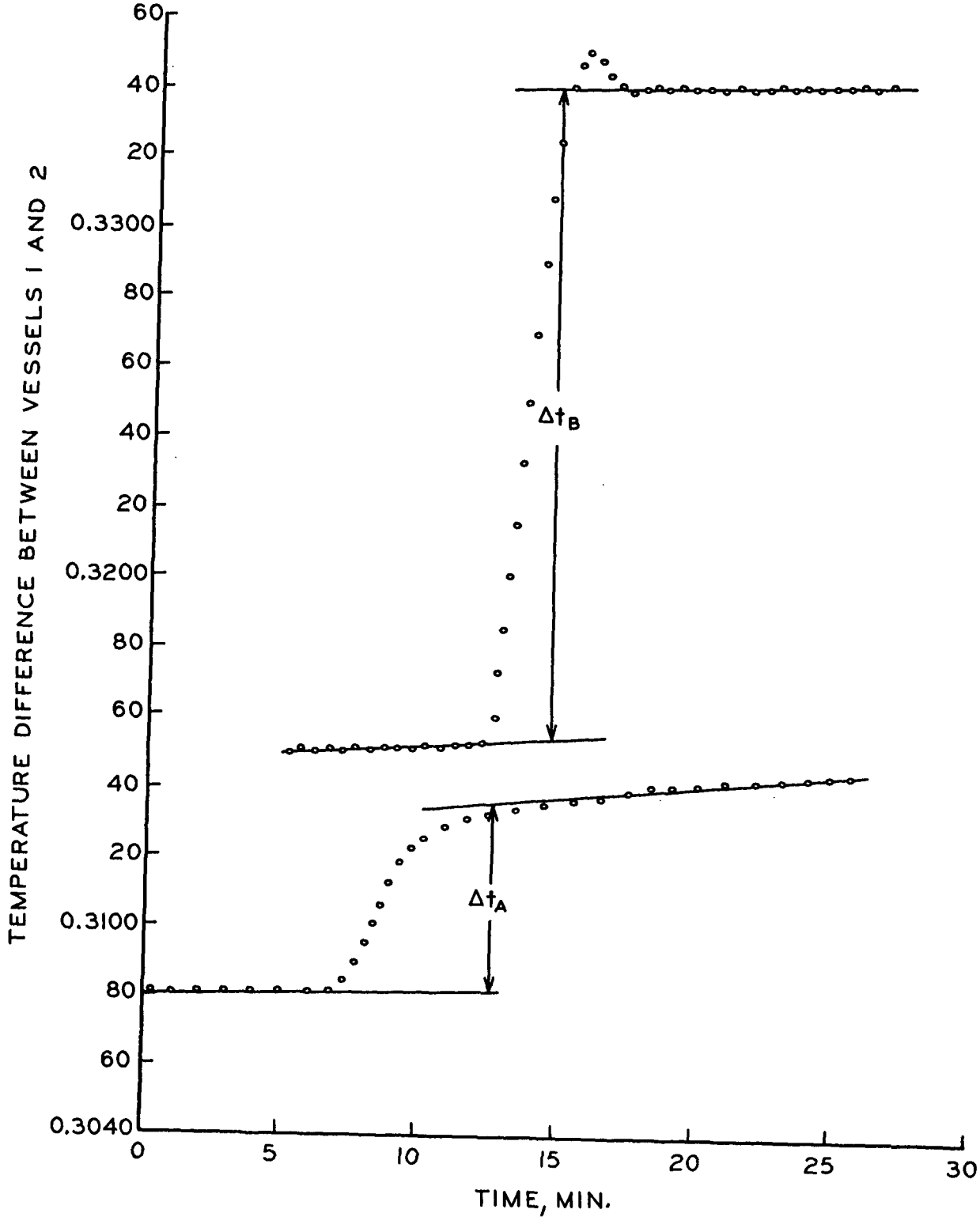

Figure 8. Temperature-Time Curves for a Heat of Wetting Determination (Run Number 9/14-I)

where

H_I = heat of immersion

H = heat of wetting

H_{BB} = heat of bulb breaking

R = resistance of immersion heater

I = current to immersion heater

t = time

Δt_A = temperature increase after bulb breaking

Δt_B = temperature increase during heating with immersion heater

The heat of bulb breaking, H_{BB}, was determined by the breaking of an empty sample bulb during a mock heat of wetting determination. The heat generated in breaking the sample bulb was calculated by Equation (15).

EXPERIMENTAL RESULTS AND DISCUSSION

CAPILLARY CONDENSATION

This adsorption study was carried out at low relative pressures ($P/P_o < 0.4$) where capillary condensation is not significant. No hysteresis occurs in the isotherms for adsorption on cellulose at low relative pressures (37, 46). Entrapment of adsorbate within the pores was not expected to present a problem.

SURFACE AREA STABILITY

Several of the adsorption isotherms were repeated after samples had been exposed to a vacuum for as long as sixteen days. Since isotherms could be duplicated, it was evident that the surface area of the samples was constant during adsorption runs.

The cellulose fibers were solvent-exchanged from water and dried. It was intended that this process should develop more fiber surface area than would have been developed in drying the fibers directly from water. No attempt was made to develop the same surface area in all samples.

SOLVENT ENTRAPMENT

Merchant (41) suggested that the solvent-exchange procedure leaves residual liquid mechanically entrapped and sealed in the pores in the fiber structure. Merchant demonstrated that entrapped liquids were released during moistening of a solvent exchange, dried sample. Barber (29) showed that any entrapped solvent accessible to adsorbate molecules was removed during heating and outgassing of his samples at a low pressure ($< 10^{-6}$ mm. Hg). Barber noted

no significant change in $\underline{U'}_o$ and γ for a solvent exchange, dried sample after humidification and redrying. Gas molecules are adsorbed onto the fiber surface, not on a film of residual solvent.

HEAT OF WETTING DETERMINATIONS

The heat of wetting was calculated by Equations (15)-(16) from the calorimetric data presented in Table I. The heat of wetting in various liquids vs. the dipole moment of the wetting liquid is shown in Fig. 9. The slope of the best straight line through the data is an estimate of the surface electric field of the fibers. Linear regression analysis was used to determine the slope of this line. Confidence limits were established so that a range of solutions was possible; any line outside this range is treated as a nonsolution. The degree of confidence that a line outside the range is not a solution is 95%. The average surface electric field calculated from the slope of the line of best fit and from the maximum slope of all possible solutions was too weak to induce a significant dipole moment in the adsorbed molecules. These calculations are presented in Appendix III. An estimate of the average electrostatic field strength of the cotton-cellulose was found to be 0.13×10^5 esu/cm.^{2}.

The surface electric field strength of several substrates was determined by Chessick, et al. (32) with the heat of wetting method. The validity of the method of Chessick, et al. is based on the approximation that the heat effect due to the adsorption of a monolayer is given by

$$(h_{I(SL)} - h_L)$$

where

$\underline{h}_{\underline{I}(\underline{SL})}$ = the heat of immersion of the clean solid surface per unit area

$\underline{h}_{\underline{L}}$ = the heat of immersing a unit area of the liquid surface.

TABLE I

HEAT OF WETTING DATA AND RESULTS

Run Number	Solvent	Current I_C, amp.	Time, t, sec.	Temperature Deflections Δt_A	Δt_B	Heat of Immersion, $-H_I$, joules	Heat of Wetting, $-H_I+H_{BB}$	Sample Weight, W, g.	Monolayer Capacity, V_β, cc./g.	Heat of Wetting per Area, $-H/\Sigma W$, ergs/cm.^{2}
9/12-I 7HW	Ø-Cl	0.489	120.04	0.0107	0.0207	10.282	9.724	2.266	16.89	69.1
9/14-I 8HW	Ø-H	0.495	120.07	0.0053	0.0190	5.687	5.129	2.236	9.97	62.6
9/17-I 10HW	Ø-H	0.500	119.99	0.0097	0.0218	9.250	8.692	2.608	14.88	61.2
9/19-I 13HW	Ø-Cl	0.498	120.78	0.0120	0.0216	11.532	10.794	2.331	18.65	68.9
9/21-I 9HW	Ø-NO_2	0.496	120.08	0.0130	0.0180	11.715	11.157	2.688	14.73	77.1
9/23-I 12HW	Ø-NO_2	0.480	120.02	0.0098	0.0193	9.731	9.173	2.555	12.45	78.6
10/1 -I 11HW	Ø-Cl	0.500	120.66	0.0223	0.0223	11.155	10.697	2.856	15.01	67.8

NOTE: Σ(m.^{2}/g.) = 0.269 βV_β (cc./g.)

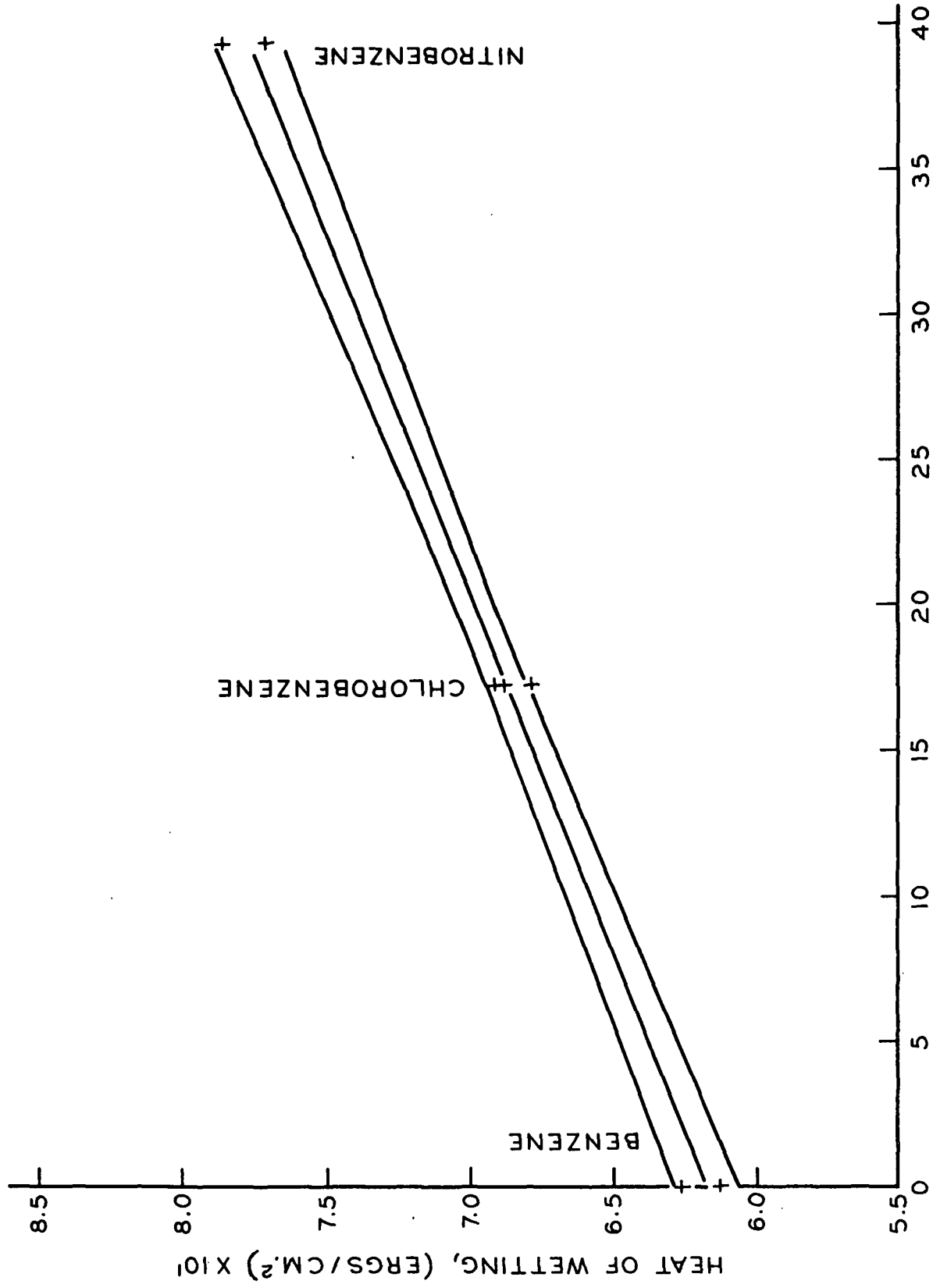

Figure 9. Heat of Wetting vs. Dipole Moment of the Wetting Liquid Stoneville 2B, Solvent-Exchanged Fibers (30.0°C.)

The heat effect is related directly to the net energy of adsorption, $(\underline{E}_A - \underline{E}_L)$, by

$$h_I(SL) - h_L = N_A(E_A - E_L) \tag{17}$$

where

$\underline{N}_A$ = the number of molecules adsorbed per unit area in the monolayer

$(\underline{E}_A - \underline{E}_L)$ = the net integral energy of adsorption for a molecule in the monolayer.

The quantity $(\underline{E}_A - \underline{E}_L)$ represents the energy involved in removing a molecule from the bulk liquid and adsorbing it onto the surface; thus, $(\underline{E}_A - \underline{E}_L)$ represents the interaction between the surface and an adsorbed molecule and does not include interactions between adsorbed molecules and themselves.

Assuming that interactions in the adsorbed state are the same as in the liquid state,

$$E_A - E_L = E_W + E_\mu + E_\alpha \tag{18}$$

where

$\underline{E}_W$ = the contribution from nonpolar van der Waals' forces

$\underline{E}_\mu$ = the contribution arising from the permanent dipole of the adsorbate and the substrate surface electric field

$\underline{E}_\alpha$ = the contribution due to the induction of a dipole in the adsorbate

It is assumed that the differences in the total adsorption energy in various wetting liquids within a homologous series of liquids arise primarily from $\underline{E}_\mu$, thus

$$E_A - E_L \cong E_\mu = -\mu(F) + \Delta \qquad (19)$$

the intercept $\Delta = E_\alpha + E_W$

The slope of a plot of the heat of wetting ($E_L - E_A$) vs. the dipole moment of the wetting liquid, μ, is a measure of the average electrostatic field strength, F. The intercept gives an average value for the dispersion energy, E_W, since E_α is usually small.

The results obtained for cotton fibers are compared with the results for other solids in Fig. 10 and Table II. The heat of wetting studies by Chessick, et al. (32) were carried out in a series of n-butyl derivatives. Therefore, a direct comparison of the dispersion energy for these solids and for cellulose is not valid. Two different sets of data are presented in Table II and Fig. 10.

TABLE II

ELECTROSTATIC FIELD STRENGTHS F AND DISPERSION ENERGIES E_W[a]

Solid	BET Area, $m.^2/g.$	F, esu/$cm.^2$ x 10^{-5}	E_W, $ergs/cm.^2$	Reference
Rutile	6.4	2.0	125[b]	(48)
Rutile (Al_2O_3-SiO_2-coated)	11.2	3.2	135[b]	(48)
Al_2O_3	0.4	1.9	335[b]	(49)
SiO_2 (Aerosil)	120	1.1	75[b]	(50)
Graphon	95	0	80[b]	(51)
Teflon	9.0	0	25[b]	(52)
Cotton cellulose (Stoneville-2B)	--	0.13	62[c]	

[a] All data except cotton cellulose is from Reference (47).
[b] Determination made in straight-chain hydrocarbon.
[c] Determination made in benzene.

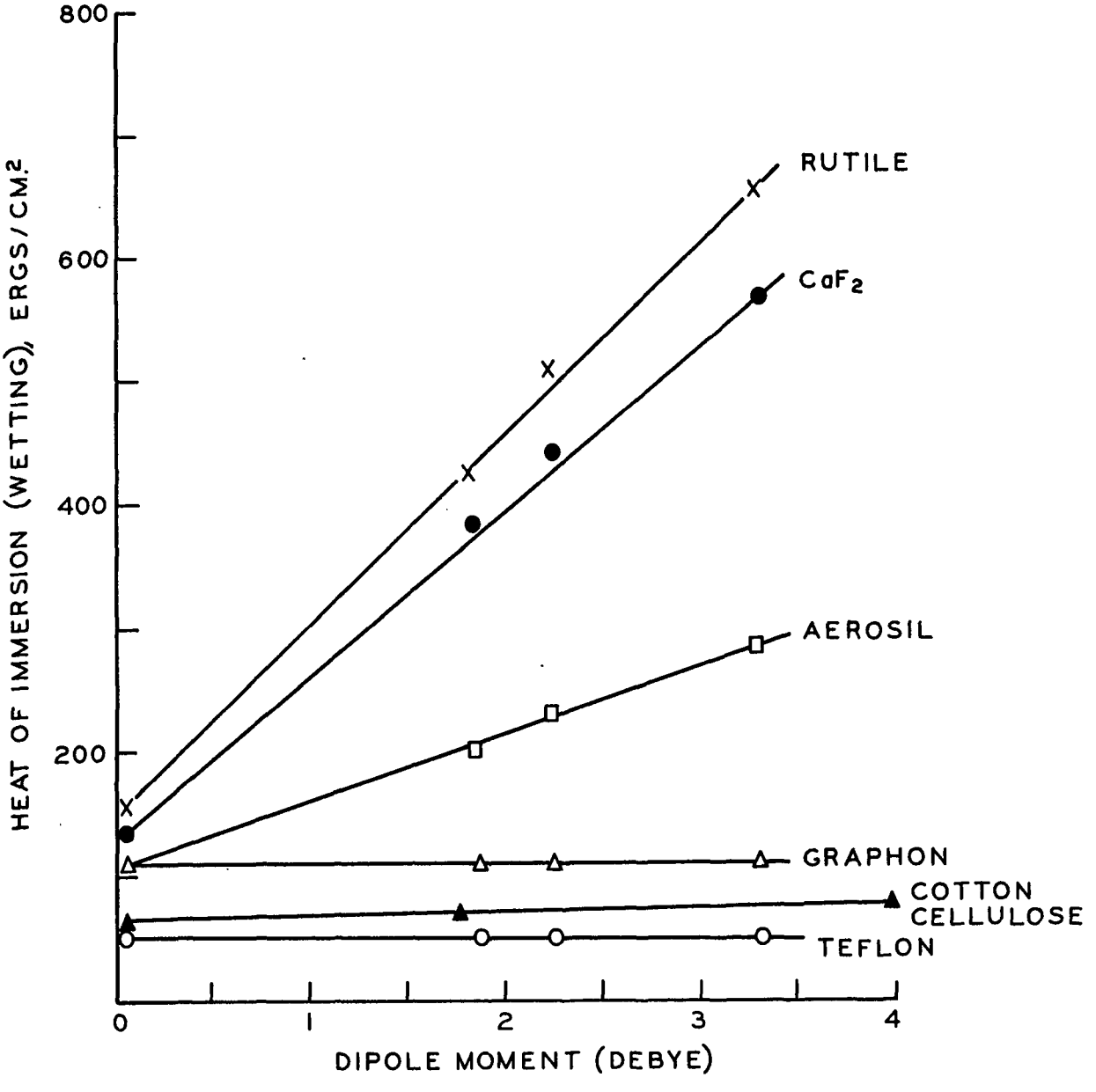

Figure 10. Determination of the Polarity of Solid Surfaces. The Slope of the Straight Line Gives the Average Electrostatic Field Strength of the Surface. Close-Packed Perpendicular Array and Same Distance from the Dipole to Surface are Assumed (53)

THE SIGNIFICANCE OF A SURFACE ELECTRIC FIELD

The substrate can cause perturbations of the lateral interaction potentials of adsorbed molecules. These perturbations are reflected in the operative values of the two-dimensional van der Waals' constants, α and β. Since the constants α and β describe the series of theoretical adsorption isotherms with which the experimental isotherms are compared, it is important to know the operative values of α and β for each substrate-adsorbate adsorption system.

For the ideal situation, the interaction of adsorbed molecules is identical with that in the gas phase. In this particular case, the operative values of α and β are calculated from the three-dimensional van der Waals' constants, a and b.

$$\alpha = a\left(\frac{9\pi}{256b}\right)^{1/3} \tag{20}$$

$$\beta = 2b\left(\frac{9\pi}{256b}\right)^{1/3} \tag{21}$$

$$\alpha/\beta = a/2b \tag{22}$$

However, the values of α and β from Equations (20) and (21) do not apply if the adsorbate is either polarized or oriented by the substrate. The ideal values of α and β must be corrected for orientation and polarization perturbations of the adsorbate.

The calculations in Appendix III show that the polarization of argon and nitrogen by the cellulose electrostatic field is very small. The dipole moments induced in argon and nitrogen are 0.0217 debye and 0.0317 debye, respectively. The changes in α due to these small polarizations are 0.11% for argon and 0.21% for nitrogen. A correction of this magnitude can be ignored. Considering only

polarization effects, a series of theoretical isotherms generated from the operating values of α and β cannot be distinguished from a series generated from the ideal values of α and β. Figure 11 illustrates this point; a correction of α of nearly 3% is required to cause a significant change in the shape and position of the theoretical isotherms.

The argon molecule is spherical, and as an adsorbed molecule, it is incapable of orientation. The ideal values of α and β calculated in Equations (20) and (21) are used to determine a series of theoretical isotherms with which the experimental argon adsorption isotherms are compared. The nitrogen molecule is capable of orientation in two positions – flat and upright – in which the plane of the molecular axis of symmetry is parallel and perpendicular to the substrate surface, respectively. As discussed, orientation of the adsorbate affects the lateral interaction potential as reflected by a change in α. The orientation of nitrogen also affects β – the surface area covered per molecule. More area of the substrate surface is covered per molecule when the orientation is flat. The influence of the molecular orientation of nitrogen on the average operating values of α and β is shown in Fig. 12. Also shown in Fig. 12 is the influence of orientation on the average molecular diameter.

EXPERIMENTAL ISOTHERM TO MODEL ISOTHERM COMPARISON AND VERIFICATION OF THE CURVE MATCHING

EXPERIMENTAL ISOTHERM TO MODEL ISOTHERM COMPARISON

Ross and Olivier (12) have indicated that a unique match can be found for the experimental to model isotherm comparison if the operative values of α and β are known. However, in practice, several curve matches can be found in a series of model isotherms calculated for one value of α/β, and a verification is required for the experimental to model isotherm match selected.

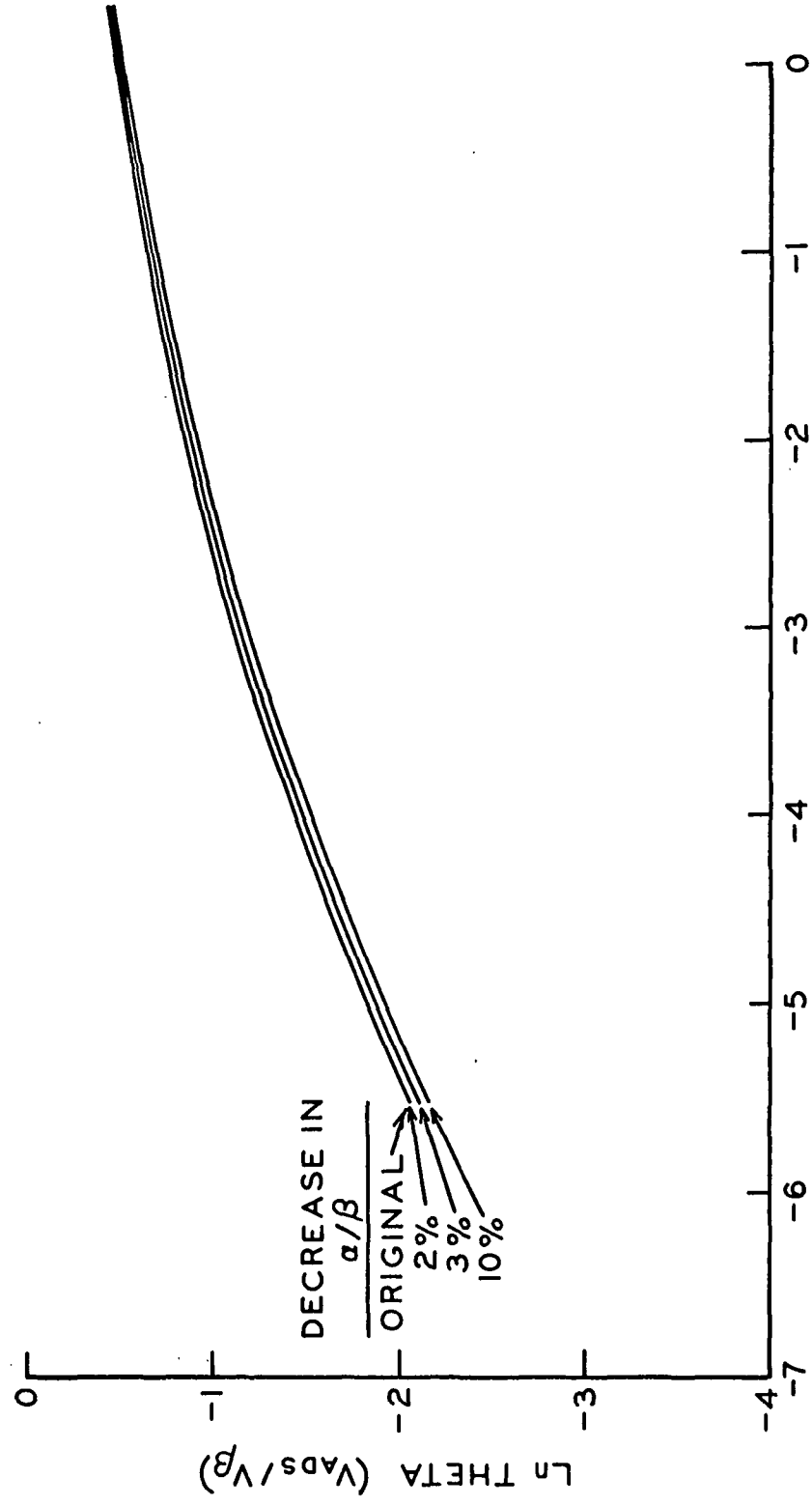

Figure 11. The Influence of a Change in α/β in Computed Model Isotherms (54)

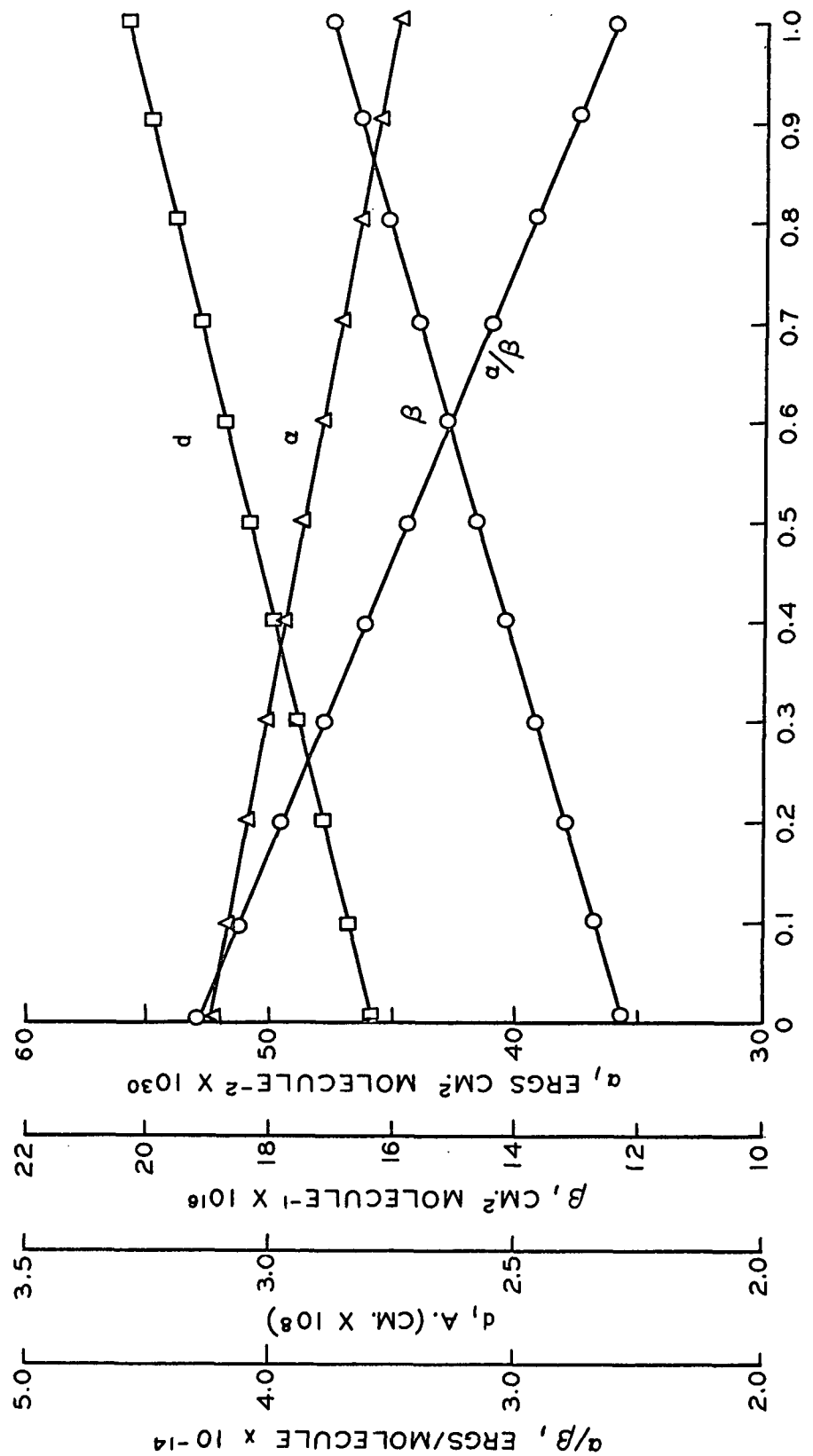

Figure 12. The Influence of the Orientation of Adsorbed Nitrogen on the Molecular Diameter and the Van der Waals' Constants, α and β, Diameter Values (d) are from Reference (8)

As reported by Barber, the following convention for isotherm matching was used:

> The experimental ln-ln plot was matched with the theoretical ln-ln plot with the position of the experimental plot as far to the right as possible. Use of this convention resulted in minimum values of $\underline{V}_\beta$ and maximum values of $\underline{U'}_o$. Since multilayer adsorption was observed at low monolayer completions resulting in an inflection in the ln-ln plots, this convention allowed for making use of the greatest part of the monolayer part of the ln-ln curve possible (55).

Because γ_o $\underline{U'}_o$, and $\underline{V}_\beta$ are temperature invariant, the number of possible isotherm matches can be reduced. For a given substrate-adsorbate system, an equivalent set of these parameters must result from a comparison of the 77.4°K experimental and model isotherms and from a comparison of the 90.2°K isotherms. Model curves for argon adsorption were generated at 0.1 intervals in the heterogeneity parameter, γ; for nitrogen adsorption, model curves were generated at 0.2 intervals in γ. The 0.2 interval was used to generate model curves for values of γ less than 2.0 because intervals of 0.1 resulted in isotherms that were similar.

Comparisons of the observed and calculated mean adsorptive potentials and the experimental and theoretical isosteric heats were used to verify the selected experimental to model isotherm match.

VERIFICATION OF ISOTHERM MATCH BY A COMPARISON OF EXPERIMENTAL AND THEORETICAL ISOSTERIC HEATS OF ADSORPTION

Theoretical or model isosteric heat curves are determined by extending the procedure for developing model adsorption isotherms as outlined in pages 14-19. In the model isotherm development, Θ was determined as a function of $\underline{P}/\underline{K}'$,

$$\Theta = \sum_{i=1}^{n} \Delta\delta_i\theta_i = \Delta\delta_1\theta_1 + \Delta\delta_2\theta_2 + \ldots + \Delta\delta_n\theta_n \qquad (14)$$

For the model isosteric heat development, Equation (14) was expanded to include the mean adsorptive potential of each homotattic patch:

$$U_o^{int} = \sum_{i=1}^{n} \Delta\delta_i\theta_i U_{o_i} = \Delta\delta_1\theta_1 U_{o_1} + \Delta\delta_2\theta_2 U_{o_2} + \ldots + \Delta\delta_n\theta_n U_{o_n} \qquad (23)$$

The integral potential of each patch, $\underline{U}_o^{int}$, is the product of the area covered and the adsorptive potential per unit area. The differential adsorptive potential, $\underline{U}_o^{diff}$, was determined on the computer as $\Delta\underline{U}_o^{int}/\Delta\Theta$. The differential heat of adsorption, $\underline{q}^{diff}$, was determined as,

$$q^{diff} = U_o^{diff} - \Delta E^{kin} + aP^{ia} \qquad (24)$$

where

$$aP^{ia} = 2\alpha\Theta/\beta \qquad (25)$$

and is the overall adsorbate-adsorbate interaction potential on a heterogeneous surface. The isosteric heat was determined from $\underline{q}^{diff}$,

$$q^{st} = q^{diff} + RT \qquad (26)$$

A series of model isosteric heat curves is presented in Fig. 13. The shape of the model curves depends upon the values of α, β, γ, and $\underline{K}'$. By selecting the operating values of α and β for the adsorption system and the values of $\underline{K}'$ and γ from the curve match, one can generate a model isosteric heat curve corresponding to that experimental to model isotherm match. The isotherm match can be verified by comparison of this model isosteric heat curve with one calculated from experimental

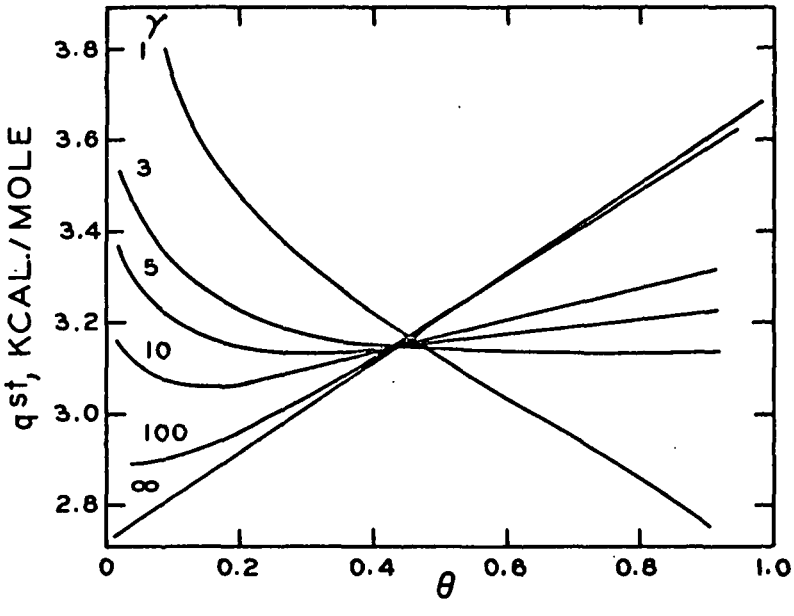

Figure 13. Model Isosteric Heat Curves as a Function of Θ, Based on the Model of a Mobile Adsorbed Film on the Series of Heterogeneous Substrates (56)

adsorption data. If experimental adsorption isotherms are measured at two temperatures not too far apart, isosteric heats of adsorption can be determined by the Clausius-Clapeyron equation:

$$q^{st} = R\left(\frac{T_1 T_2}{T_2 - T_1}\right) \ln P_2/P_1 \qquad (27)$$

VERIFICATION OF ISOTHERM MATCH BY A COMPARISON OF OBSERVED AND CALCULATED MEAN ADSORPTIVE POTENTIALS

Ross and Olivier (56) showed that at $\Theta = 0.4$, $\underline{U}_o^{diff} = \underline{U}'_o$, so that,

$$U'_o = q^{st}_{\Theta=0.4} - 3R\left(\frac{T_1 T_2}{T_1 + T_2}\right) - 0.8\ \alpha/\beta \qquad (28)$$

assuming the adsorbed molecules are in the ground state of vibration with respect to the surface and no change occurs in the rotational energy on adsorption. The isosteric heat of adsorption at $\Theta = 0.4$ (designated as $\underline{q}^{st}_{\Theta=0.4}$) is determined by the Clausius-Clapeyron equation, Equation (27), if experimental isotherms have been measured at two temperatures.

The approximate values of $\underline{U}'_o$ calculated in Equation (28) are denoted as $\underline{U}'_o$ (observed). The values of $\underline{U}'_o$ determined in the curve matching procedure are designated as $\underline{U}'_o$ (calculated). A comparison of calculated and observed values was presented by Ross and Olivier for numerous substrate-adsorbate systems (57). Agreement generally was within 6%. For cotton cellulose-argon, Barber (29) obtained a 3% agreement.

THE CELLULOSE – ARGON ADSORPTION SYSTEM

THE ANALYSIS OF THE ADSORPTION PARAMETER K'

For the Ross-Olivier model the mean adsorptive potential, $\underline{U'}_o$, of a substrate is calculated by Equation (29).

$$K' = A^o \exp(-U'_o/RT) \tag{29}$$

The adsorption parameter $\underline{K'}$ is determined in the experimental to model isotherm match, and for the mobile adsorbed film, $\underline{A}^o$ is calculated by:

$$\ln A^o = -\left[\frac{\Delta S_s^{tr} + \Delta S^{rot}}{R}\right] + \frac{a F^{vib} - a E_o^{vib}}{RT} + \frac{\Delta E^{kin}}{RT} - \ln \frac{\theta_s}{1-\theta_s} + \ln 760 \tag{30}$$

where

$-\Delta \underline{S}_{\underline{s}}^{tr}$ = the change in translational entropy per mole in the standard state on adsorption

$\Delta \underline{S}^{rot}$ = the change in rotational entropy on adsorption

$\underline{a}F^{vib}$ = the additional Gibbs free energy of the adsorbed phase due to molecular vibrations with respect to the surface

$\underline{a}E_o^{vib}$ = the average vibrational energy of an adsorbed molecule at 0°K

$\Delta \underline{E}^{kin}$ = the change in the kinetic energy per molecule on adsorption from the total kinetic energy in the gas phase to the kinetic energy of translation and rotation in the adsorbed phase

$\theta_{\underline{s}}$ = fraction of the surface covered at the standard state of the adsorbed phase.

The calculation of $\underline{U'}_o$ and the analysis of $\underline{K'}$ increases in difficulty with more complex adsorbate molecules. However, for a monatomic gas adsorbed at low temperatures, the analysis of $\underline{K'}$ is not difficult. For argon adsorption at a low temperature, the adsorbed molecules are assumed to be confined in the ground state of vibration with respect to the surface. Thus,

$$ {}_aF^{vib} - {}_aE_o^{vib} = RT \ln(1 - \exp(-h\nu/kT)) \simeq 0. \tag{31} $$

Also,

$$ \Delta E^{kin} = -1/2RT \tag{32} $$

$$ -\Delta S_s^{tr} = (R/2)(\ln M + \ln T) + 2.30 \tag{33} $$

where

$\underline{M}$ = adsorbate molecular weight

ν = vibrational frequency with respect to the surface

$\underline{k}$ = Boltzmann constant

$\underline{h}$ = Planck's constant

The argon molecule has no rotational energy or rotational entropy in either phase so that $\Delta\underline{S}^{rot} = 0$. With these conditions, Equation (30) is reduced to a manageable form,

$$ \ln A^o = -\Delta S_s^{tr}/R - 1/2 - \ln\frac{\theta_s}{1-\theta_s} + \ln 760 \tag{34} $$

These simplifications are assumed to be correct if a plot of the logarithmic form of Equation (29),

$$ \ln K' - \ln A^o = -U'_o/RT, \tag{35} $$

is a straight line with intercept at the origin. If the line does not pass through the origin, the assumption that the temperature of the experiment was low enough to confine the adsorbed molecules to the ground state of vibration is not valid. The validity of this assumption with respect to argon adsorption at 77.4°K and 90.2°K is shown in Fig. 14. The plot of Equation (35) is in the form ($\ln\underline{K}' - \ln A^{o}$) vs. $1/\underline{T}$.

ADSORPTION PARAMETERS

The Ross-Olivier parameters for argon adsorption on cotton cellulose at 77.4°K and 90.2°K are presented in Table III. The adsorption parameters for samples used in the heat of wetting study are presented in Table IV. The operative values of α and β were calculated from Equations (20) and (21). The ideal values and the operative values of α and β were the same because the small electrostatic field of cellulose had induced an insignificant polarization of the adsorbed argon molecules.

A range of values for acceptable curve matches is reported for γ. The values of γ used in generating a series of model curves were chosen arbitrarily. The experimental isotherm was bracketed by model isotherms to emphasize that the experimental curve may not match one of the chosen models but might match better a curve within that range.

The adsorption isotherms, experimental to model isotherm matches, and comparisons of isosteric heat curves for the cellulose-argon adsorption system are presented in Appendix III. The experimental and theoretical isosteric heat curves were within 5-7% agreement. A comparison of observed and calculated values of $\underline{U}'_{o}$ is presented in Tables V and VI; these values were within 3% agreement except Sample SV-2B-8HW. For a representative sample, these curves are presented in Fig. 15-18.

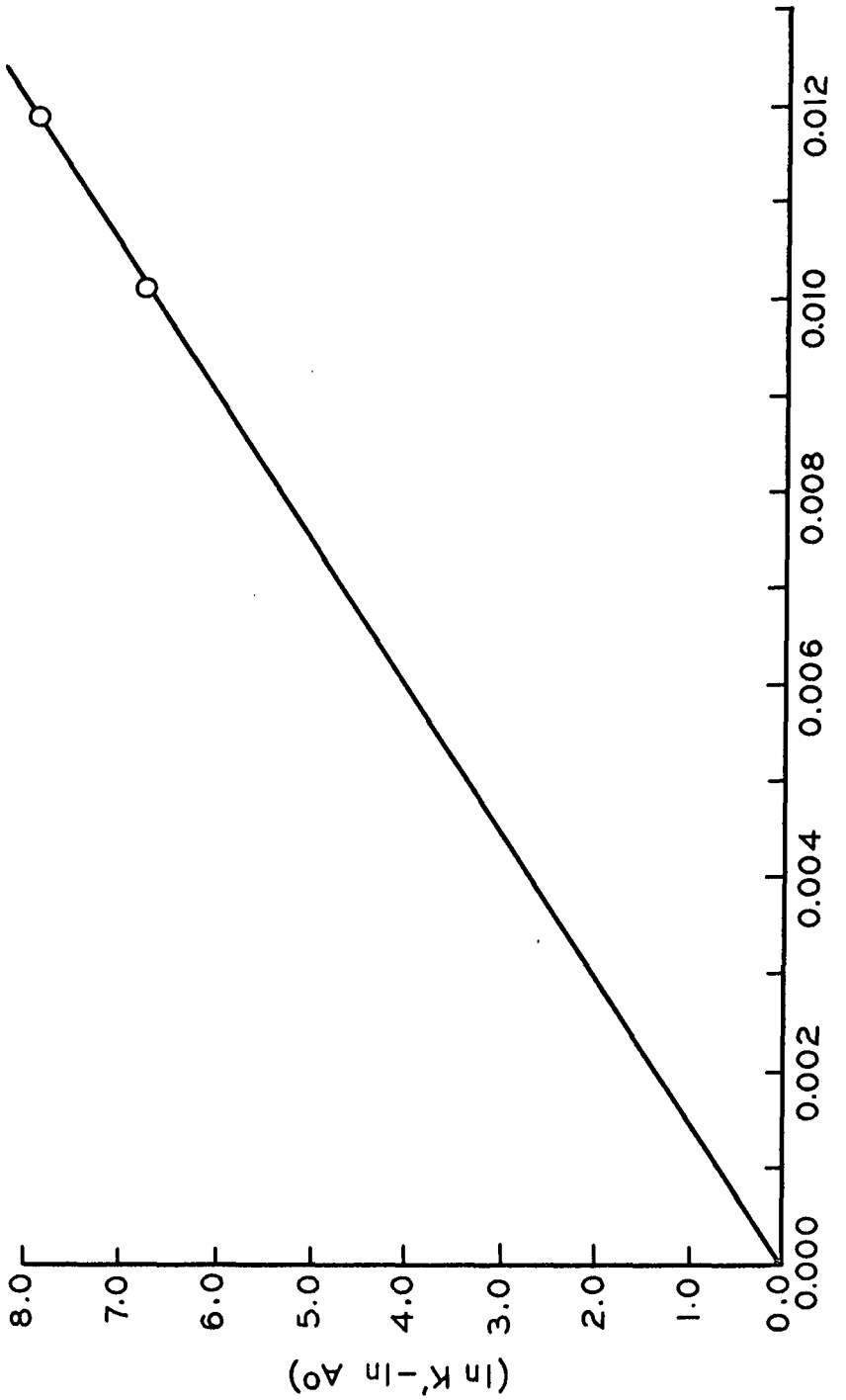

Figure 14. Plot of (ln $\underline{K}'$ - ln $\underline{A}^{o}$) vs. $1/\underline{T}$ for Argon Adsorption at 77.4°K and 90.2°K

TABLE III

ADSORPTION PARAMETERS FOR COTTON CELLULOSE – ARGON
AT 77.4°K AND 90.2°K

Sample	At 77.4°K				At 90.2°K			
	γ	$\underline{V}_{\beta}$	$\underline{V}_{m}$	$\underline{U'}_{o}$	$\gamma_{(77.4°K)}$	$\underline{V}_{\beta}$	$\underline{V}_{m}$	$\underline{U'}_{o}$
SV-2B-1	2.4-2.5	16.02	5.98	1.29	2.4-2.5	16.02	6.40	1.28
SV-2B-2	2.2-2.3	17.50	6.39	1.29	2.2-2.3	17.50	6.79	1.30
SV-2B-3	2.4-2.5	16.66	7.37	1.35	2.4-2.5	16.66	7.70	1.35
SV-2B-4	2.4-2.5	15.39	6.54	1.35	2.4-2.5	15.39	7.29	1.33
SV-2B-5	2.4-2.5	13.28	3.97	1.32	2.4-2.5	13.28	4.35	1.33
SV-2B-6	2.4-2.5	11.18	3.35	1.21	2.4-2.5	11.18	3.59	1.21

γ = heterogeneity parameter

$\underline{V}_{\beta}$ = Ross-Olivier monolayer capacity, cc.(STP)/g.

$\underline{V}_{m}$ = BET monolayer capacity, cc.(STP)/g.

$\underline{U'}_{o}$ = mean adsorptive potential, kcal./mole

TABLE IV

ADSORPTION PARAMETERS FOR COTTON CELLULOSE – ARGON
(HEAT OF WETTING SAMPLES) AT 77.4°K AND 90.2°K

Sample	At 77.4°K				At 90.2°K			
	γ	$\underline{V}_{\beta}$, cc./g.	$\underline{V}_{m}$, cc./g.	$\underline{U'}_{o}$, kcal./mole	$\gamma_{(77.4°K)}$	$\underline{V}_{\beta}$, cc./g.	$\underline{V}_{m}$, cc./g.	$\underline{U'}_{o}$, kcal./mole
SV-2B-7HW	2.0-2.2	16.89	5.50	1.25	2.0-2.2	16.89	5.93	1.25
SV-2B-8HW	2.4-2.5	9.97	2.89	1.19	2.4-2.5	9.97	2.87	1.19
SV-2B-9HW	2.4-2.5	14.73	5.30	1.29	2.4-2.5	14.73	5.77	1.29
SV-2B-10HW	2.4-2.5	14.88	5.50	1.25	2.4-2.5	14.88	5.68	1.27
SV-2B-11HW	2.4-2.5	15.01	5.89	1.33	2.4-2.5	15.01	6.17	1.33
SV-2B-12HW	2.4-2.5	12.45	4.77	1.30	2.4-2.5	12.45	4.93	1.30
SV-2B-13HW	2.4-2.5	18.65	5.53	1.21	2.4-2.5	18.65	6.19	1.22

TABLE V

COMPARISON OF OBSERVED AND CALCULATED VALUES OF $\underline{U}'_o$
CELLULOSE – ARGON

Sample	$\underline{U}'_o$ (Observed), kcal./mole	$\underline{U}'_o$ (Calculated), kcal./mole
SV-2B-1	1.31	1.29
SV-2B-2	1.32	1.29
SV-2B-3	1.36	1.35
SV-2B-4	1.35	1.32
SV-2B-5	1.27	1.25
SV-2B-6	1.23	1.21

TABLE VI

COMPARISON OF OBSERVED AND CALCULATED VALUES OF $\underline{U}'_o$
HEAT OF WETTING SAMPLES
CELLULOSE – ARGON

Sample	$\underline{U}'_o$ (Observed), kcal./mole	$\underline{U}'_o$ (Calculated), kcal./mole
SV-2B-7HW	1.28	1.25
SV-2B-8HW	1.35	1.19
SV-2B-9HW	1.30	1.29
SV-2B-10HW	1.26	1.25
SV-2B-11HW	1.35	1.33
SV-2B-12HW	1.37	1.35
SV-2B-13HW	1.24	1.21

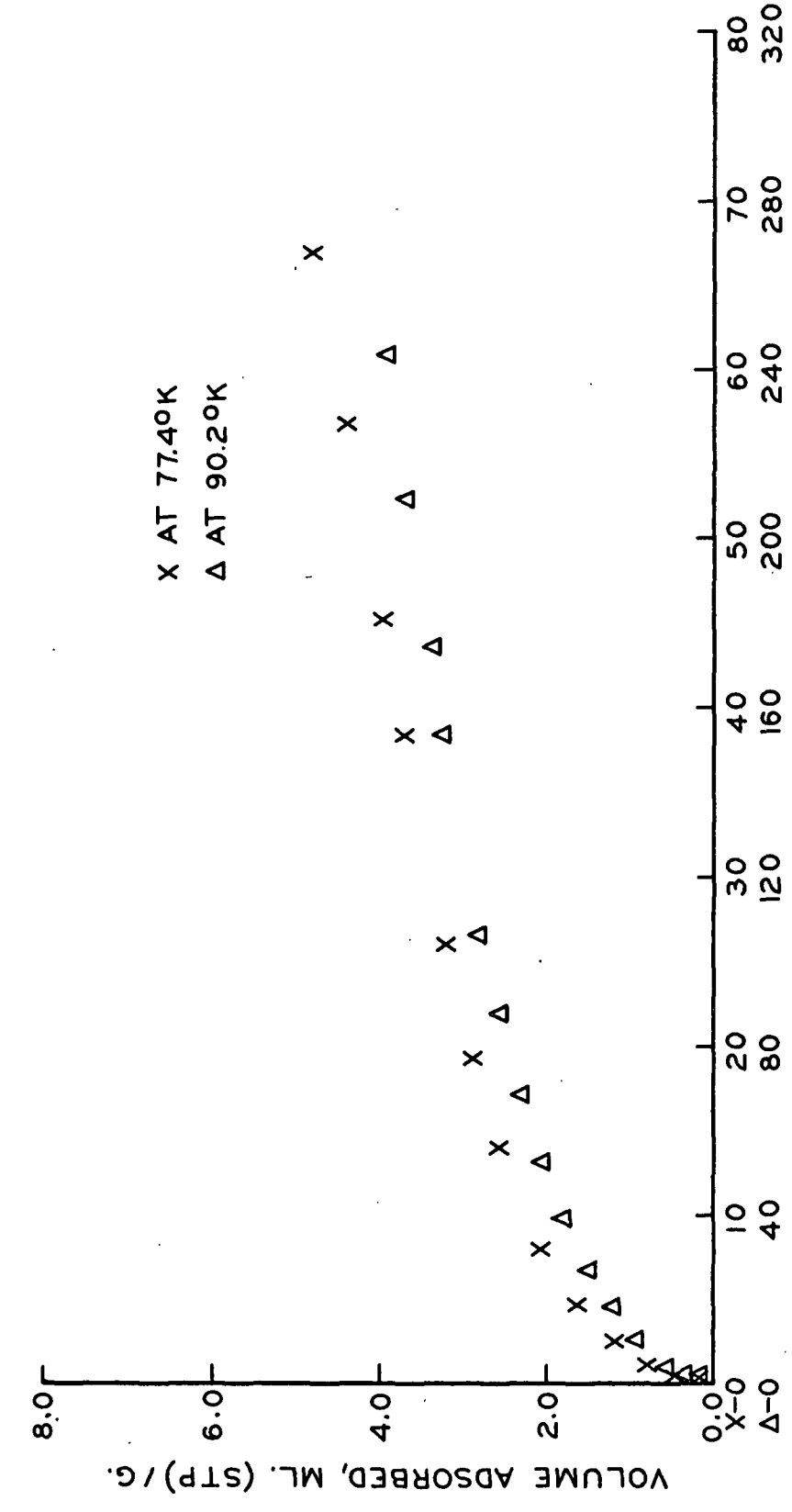

Figure 15. Argon Adsorption Isotherms at 77.4°K and 90.2°K for Sample SV-2B-6

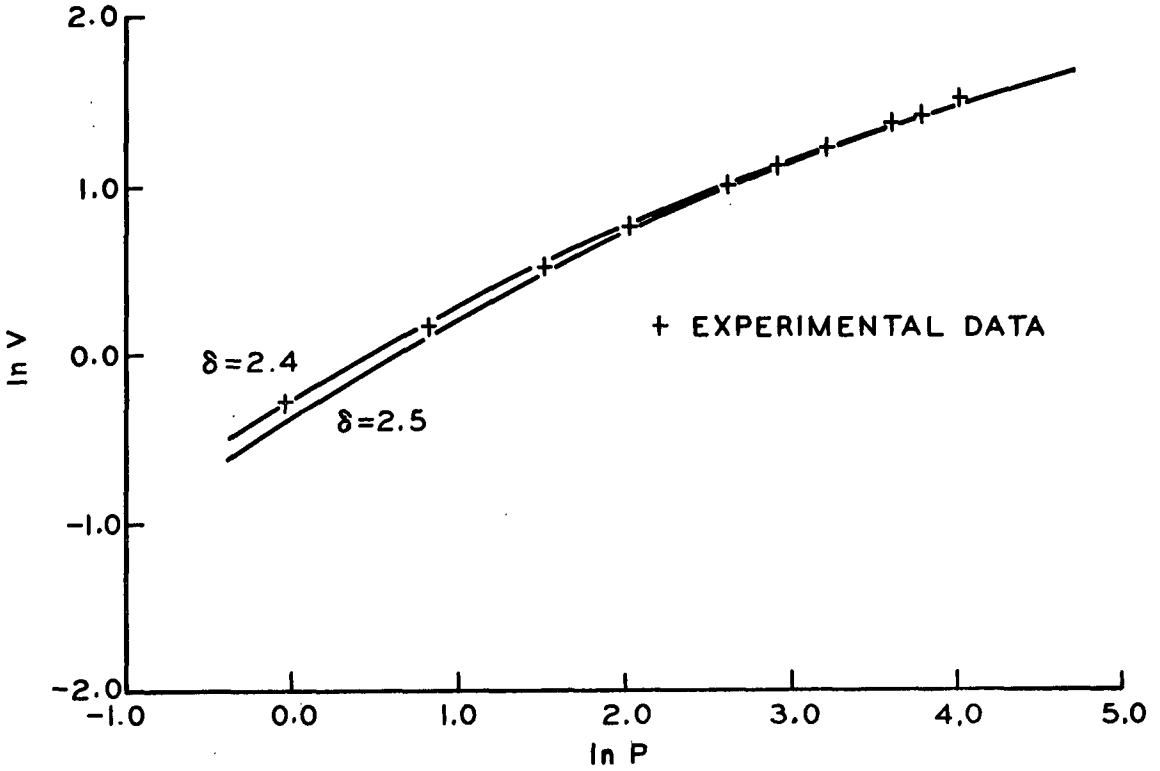

Figure 16. Comparison of Experimental to Model Adsorption Isotherms for Argon Adsorption on Sample SV-2B-6 at 77.4°K

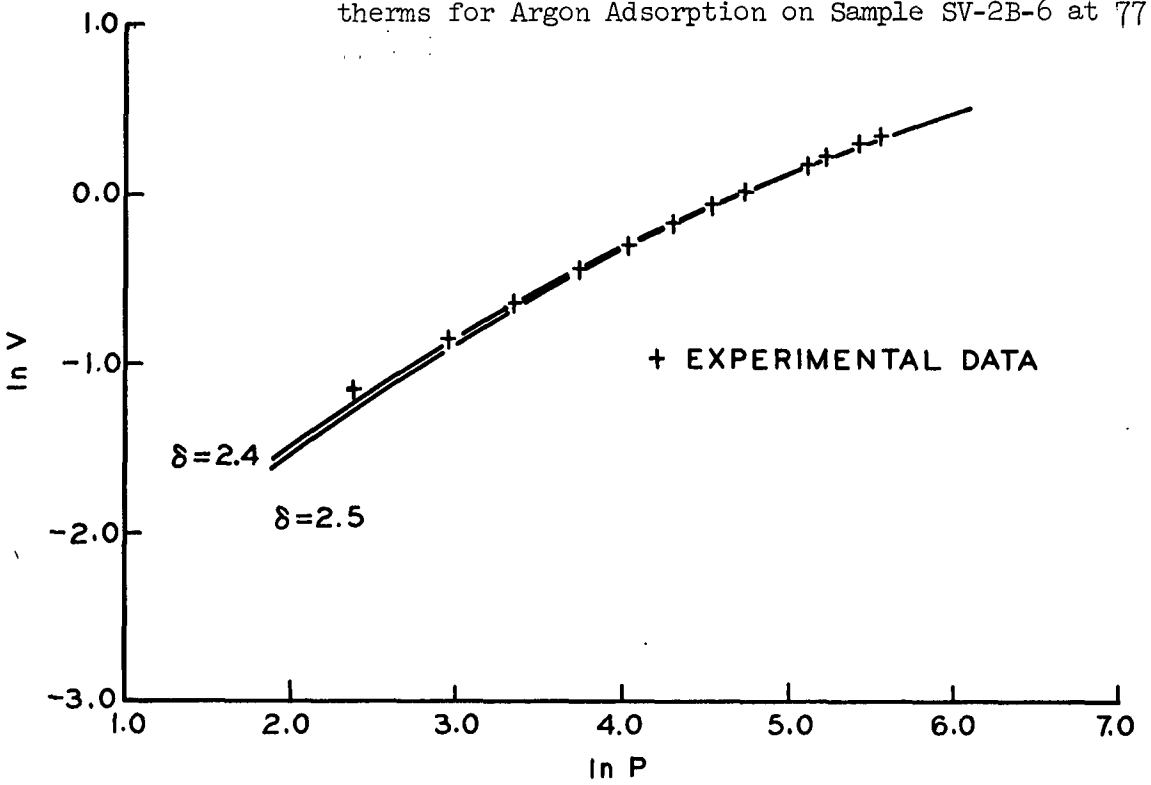

Figure 17. Comparison of Experimental to Model Adsorption Isotherms for Argon Adsorption on Sample SV-2B-6 at 90.2°K

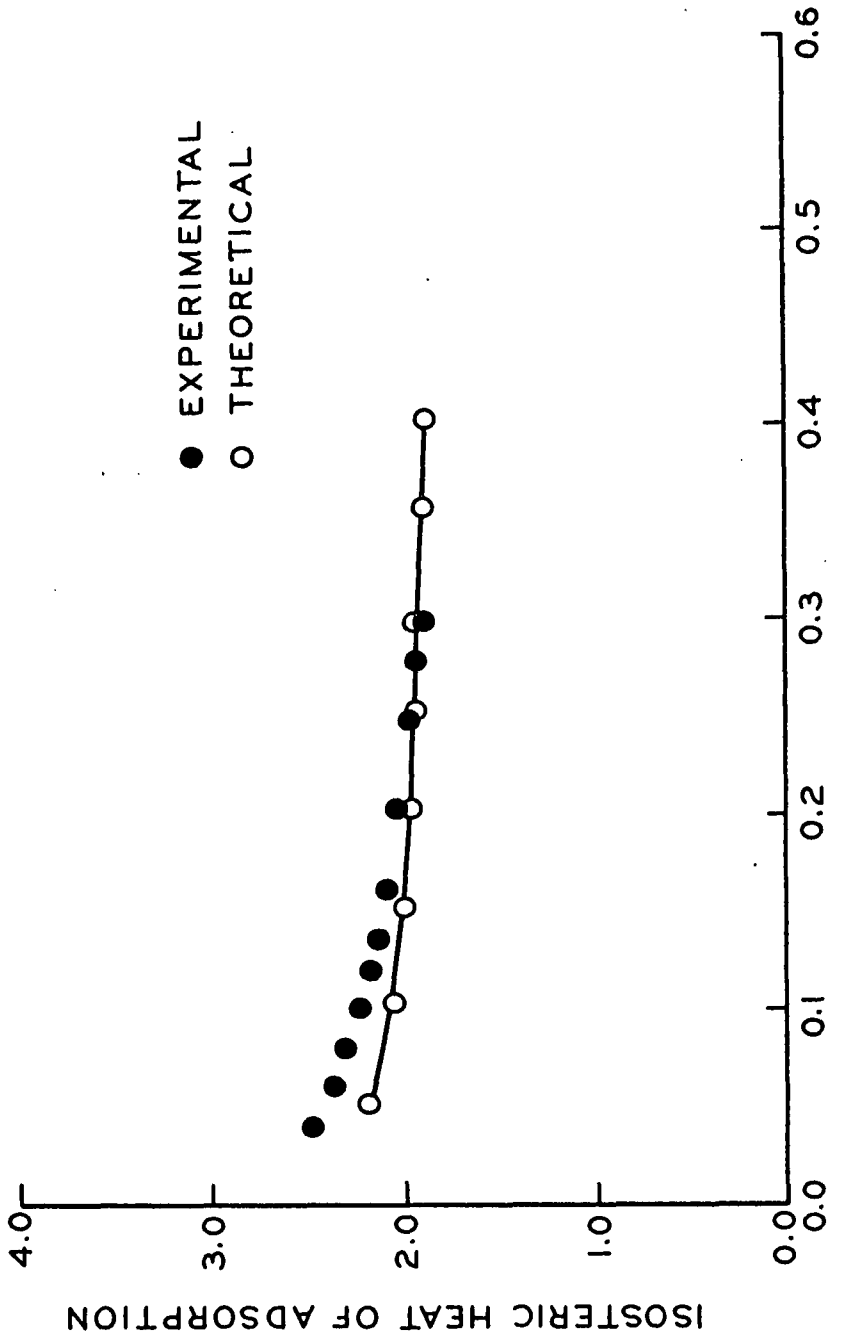

Figure 18. Experimental and Theoretical Isosteric Heat Curves for Argon Adsorption on Sample SV-2B-6

THE CELLULOSE-NITROGEN ADSORPTION SYSTEM

THE ANALYSIS OF THE ADSORPTION PARAMETER $\underline{K}'$

A diatomic adsorbate molecule makes the analysis of $\underline{K}'$ and the calculation of $\underline{U}'_o$ more complex. As with adsorbed argon, the adsorbed nitrogen molecules are assumed to be confined in the ground state of vibration with respect to the surface so that

$$ {}_aF^{vib} - {}_aE_o^{vib} \simeq 0. \tag{31} $$

The validity of this assumption for nitrogen adsorption is shown in Fig. 19, as a plot of Equation (35) intercepts at the origin. As before, $\Delta\underline{S}_{\underline{s}}^{tr}$ was calculated by Equation (33); no change in the rotational energy on adsorption was assumed (12), so that

$$ \Delta E^{kin} = -1/2RT. \tag{32} $$

The rotational entropy of nitrogen in the gas and adsorbed phases was calculated by the following equations (assuming that the nitrogen molecule acts as a rigid rotor).

$$ S^{rot} = R\ln Q^{rot} + RT\frac{d(Q^{rot})}{dT} \tag{36} $$

$$ Q^{rot} = \sum_{I=o}^{\infty} (2J+1)\exp(-J)(J+1)\rho \tag{37} $$

where

$$ \rho = h^2/(8\pi^2 IkT) \tag{38} $$

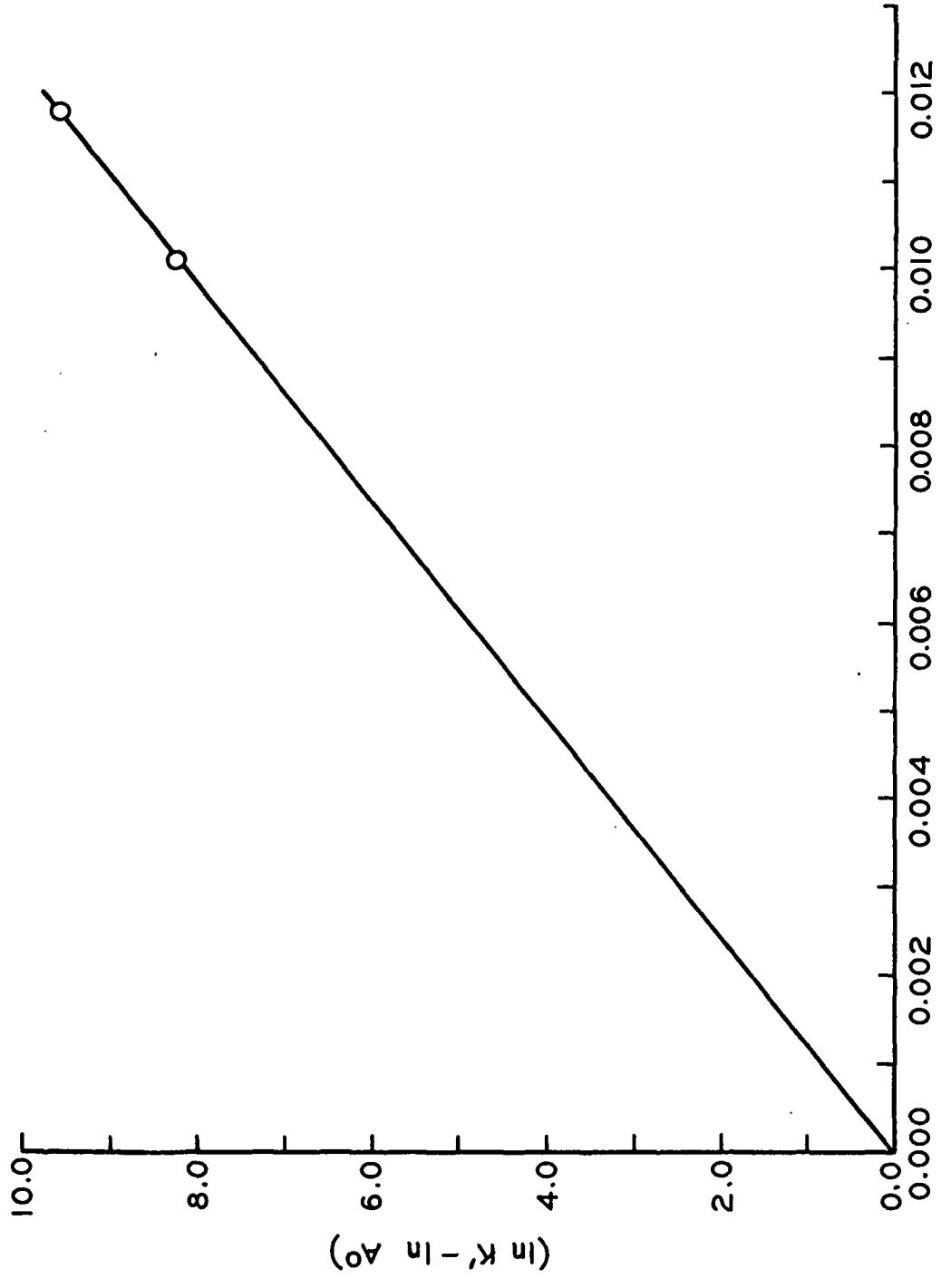

Figure 19. Plot of (ln K' - ln $\underline{A}^{o}$) vs. $1/\underline{T}$ for Nitrogen Adsorption at 77.4°K and $\underline{90.2°K}$

$\underline{Q}^{rot}$ = rotational partition function

$\underline{S}^{rot}$ = rotational entropy

$\underline{I}$ = moment of inertia

$$I = \sum_i m_i r_i^2 \qquad (39)$$

where $\underline{m}$ = atomic mass

$\underline{r}$ = covalent radius

The partition function was determined by the Euler-Maclaurin series, which is a good approximation to Equation (37).

$$Q^{rot} = \frac{1}{\sigma\rho}\left[1 + \rho/3 + \rho^2/15 + 4\rho^3/315 + \ldots\right] \qquad (40)$$

where σ = the symmetry number.

Assuming that adsorbed nitrogen molecules were oriented in the flat position, the change in rotational entropy for adsorption was calculated for the loss of one degree of freedom,

$$\Delta S^{rot} = -1.29 \times 10^{-3} \text{ kcal./mole°K.}$$

The mean adsorptive potential was determined from Equation (29) and from a more general form of Equation (30),

$$\ln A^{o} = -\left[\frac{\Delta S_s^{tr} - \Delta S^{rot}}{R}\right] - 1/2 - \ln\frac{\theta_s}{1-\theta_s} + \ln 760. \qquad (41)$$

ADSORPTION PARAMETERS

The values of α and β as calculated from Equations (20) and (21) must be corrected to reflect any orientation of the adsorbed nitrogen. The influence of nitrogen orientation on α and β has been discussed and presented in Fig. 12. The ratio α/β was determined for several orientation factors, x (cf. Fig. 12). The orientation factor is the fraction of the adsorbed nitrogen molecules that are in a flat or lateral position. A series of model adsorption isotherms were calculated for each value of α/β, and an experimental to model isotherm match was attempted for each series of model curves. Comparison of experimental to theoretical isosteric heat curves and comparison of calculated and observed values of U'_o were used to verify the isotherm match.

The Ross-Olivier parameters for nitrogen adsorption on cotton cellulose at 77.4°K and 90.2°K are presented in Table VII. The adsorption isotherms, experimental to model isotherm match, and comparisons of isosteric heat curves are presented in Appendix III. The experimental and theoretical isosteric heat curves were within 5-7% agreement. For a representative sample these curves are presented in Fig. 20-23. A comparison of observed and calculated values of U'_o is presented in Table VIII; these values were within 2% agreement.

DISCUSSION AND COMPARISON OF THE RESULTS OF ARGON AND NITROGEN ADSORPTION

The cotton cellulose presents a low potential surface which is extremely energetically heterogeneous (low value of γ, cf. p. 15); this is apparent from the adsorption parameters presented in Tables III, IV, and VII. A consideration of these characteristics of the cellulose surface, relative to what has been found for other surfaces, is given in Table IX. The other surfaces were investigated by Ross and Olivier (57).

TABLE VII

ADSORPTION PARAMETERS FOR COTTON CELLULOSE – NITROGEN
AT 77.4°K AND 90.2°K

Sample	At 77.4°K					At 90.2°K			
	$\underline{x}$	γ	$\underline{V}_\beta$	$\underline{V}_m$	$\underline{U'}_o$	$\gamma_{(77.4°K)}$	$\underline{V}_\beta$	$\underline{V}_m$	$\underline{U'}_o$
SV-2B-1	83	1.7-1.9	9.74	5.59	1.54	1.7-1.9	9.74	4.39	1.48
SV-2B-2	78	1.7-1.9	12.45	6.29	1.42	1.7-1.9	12.45	6.26	1.42
SV-2B-3	83	1.7-1.9	11.39	6.69	1.55	1.7-1.9	11.39	6.27	1.54
SV-2B-4	83	1.7-1.9	9.92	6.07	1.54	1.7-1.9	9.92	5.41	1.55
SV-2B-5	78	1.7-1.9	7.61	3.79	1.43	1.7-1.9	7.61	3.43	1.43
SV-2B-6	83	1.7-1.9	5.98	3.10	1.52	1.7-1.9	5.98	2.89	1.52

$\underline{x}$ = orientation factor, fraction of adsorbed molecules in the flat position

γ = heterogeneity parameter

$\underline{V}_\beta$ = Ross-Olivier monolayer capacity, cc.(STP)/g.

$\underline{V}_m$ = BET monolayer capacity, cc.(STP)/g.

$\underline{U'}_o$ = mean adsorptive potential, kcal./mole

TABLE VIII

COMPARISON OF OBSERVED AND CALCULATED VALUES OF $\underline{U'}_o$
CELLULOSE – NITROGEN

Sample	$\underline{U'}_o$ (Observed), kcal./mole	$\underline{U'}_o$ (Calculated), kcal./mole
SV-2B-1	1.53	1.54
SV-2B-2	1.37	1.42
SV-2B-3	1.54	1.55
SV-2B-4	1.53	1.54
SV-2B-5	1.40	1.43
SV-2B-6	1.50	1.52

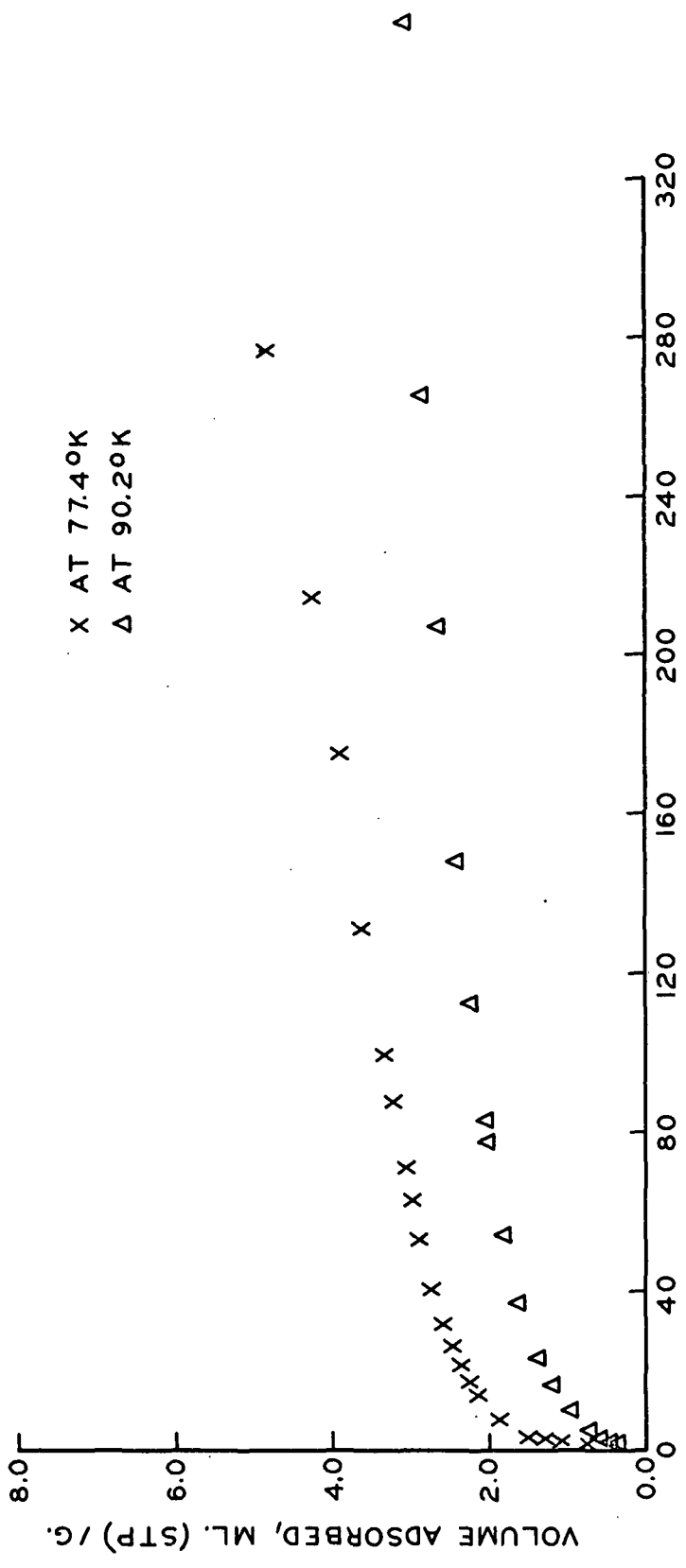

Figure 20. Nitrogen Adsorption Isotherms at 77.4°K and 90.2°K for Sample SV-2B-6

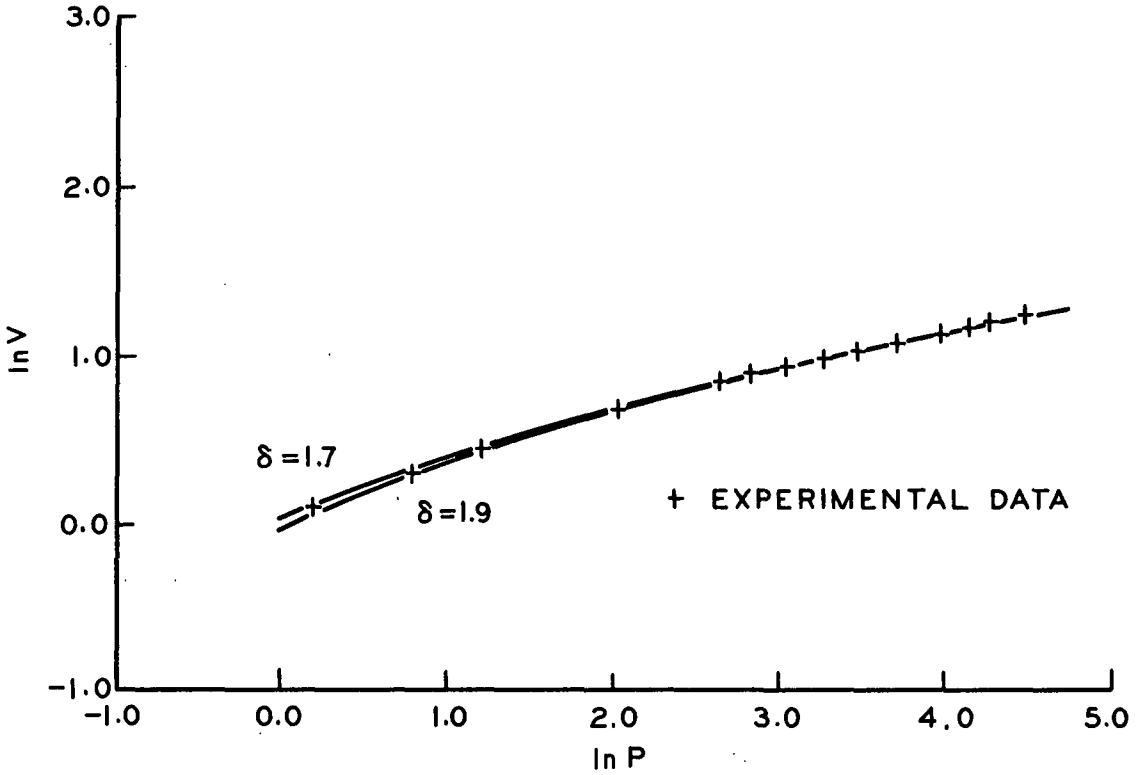

Figure 21. Comparison of Experimental to Model Adsorption Isotherms for Nitrogen Adsorption on SV-2B-6 at 77.4°K

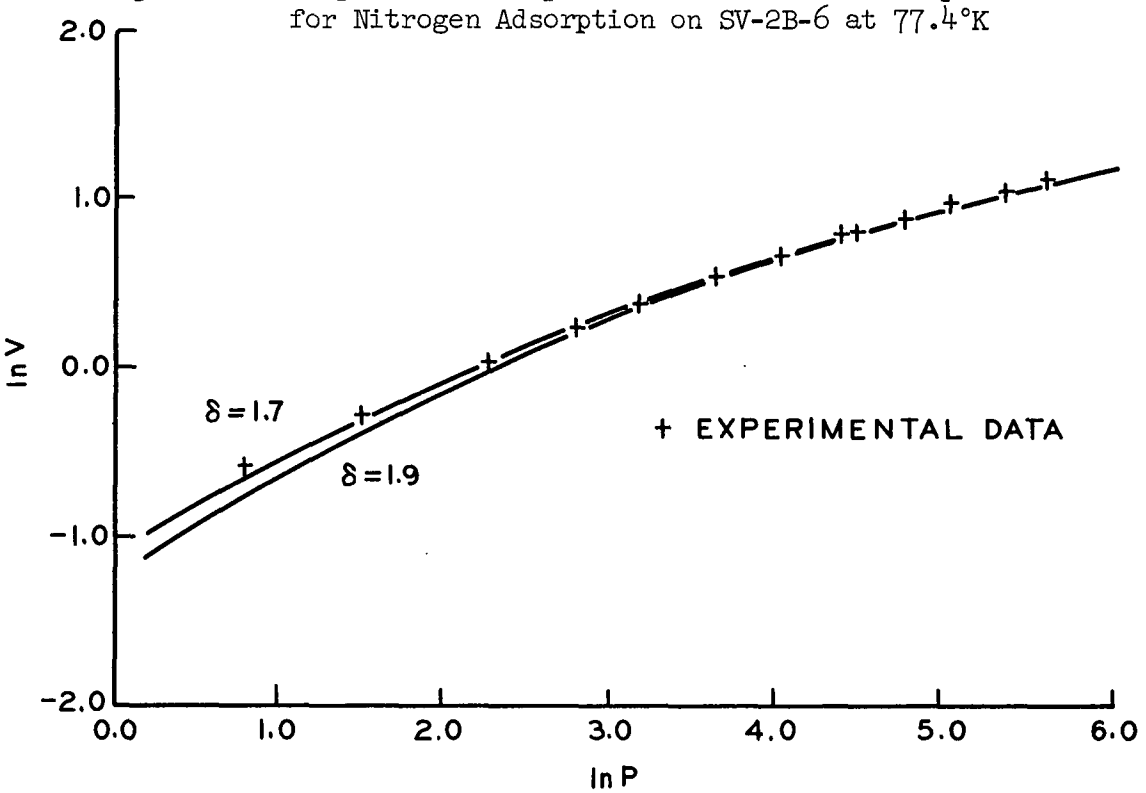

Figure 22. Comparison of Experimental to Model Adsorption Isotherms for Nitrogen Adsorption on SV-2B-6 at 90.2°K

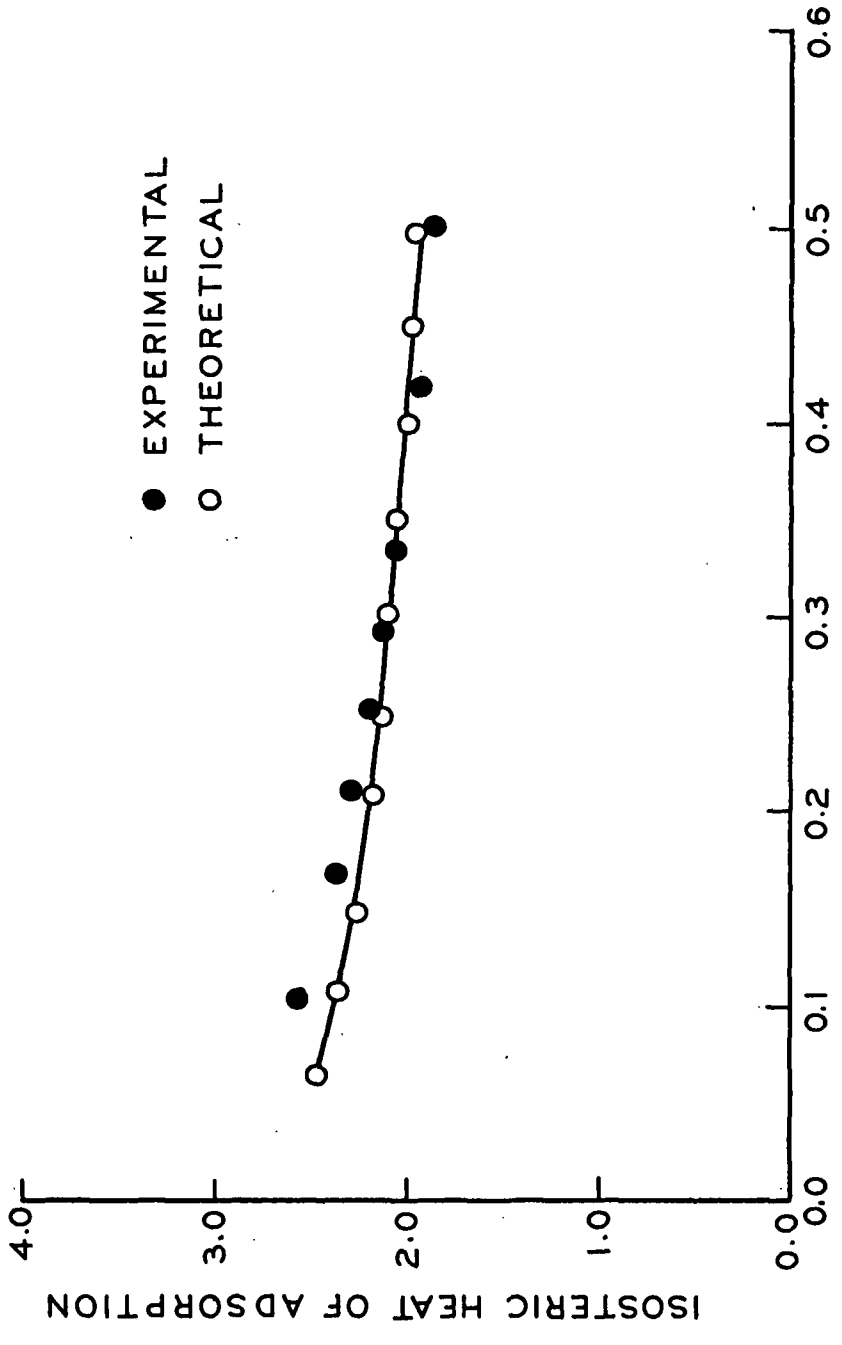

Figure 23. Experimental and Theoretical Isosteric Heat Curves for Nitrogen Adsorption on Sample SV-2B-6

TABLE IX

THE MEAN ADSORPTIVE POTENTIAL AND HETEROGENEITY PARAMETER FOR VARIOUS SURFACES[a]

		γ	$\overline{U'_o}$ kcal./mole
Graphitized carbon black			
MT(3100)	Argon	240	2.02
P-33(2700)	Argon	170	2.01
	Nitrogen	120	2.03
P-33(2000)	Argon	100	2.13
	Nitrogen	70	2.09
P-33(1500)	Argon	30	2.05
	Nitrogen	20	2.07
P-33(1000)	Argon	8.5	2.13
	Nitrogen	6.0	2.12
Boron nitride	Argon	310	1.85
	Nitrogen	220	1.84
Linde 13x sieve	Argon	22	2.24
Diamond	Argon	3	1.32
	Nitrogen	2	1.21
Rutile	Argon	2	1.72
Anatase	Argon	2	1.68
Cotton cellulose	Argon	2.4	1.30
	Nitrogen	1.8	1.50

[a] All data except cotton cellulose from Reference (57).

The cellulose surface shows a greater energy heterogeneity in the adsorption of nitrogen than in the adsorption of argon. However, within the range of γ values to infinity ($\gamma = \infty$ represents a homogeneous surface of uniform adsorptive potential), the difference between γ = 1.7-1.9 and γ = 2.3-2.5 for nitrogen and argon adsorption, respectively, is insignificant. Nitrogen is more strongly adsorbed by the cellulose surface than is argon. Since the electrostatic

field is incapable of inducing a significant dipole moment in adsorbed nitrogen, polar forces are negligible; the increase in the adsorptive potential for nitrogen is a result of an increase in the strength of the nonpolar dispersion forces.

There are several reasons for the increase in adsorptive potential for nitrogen. As a consequence of the additivity of the van der Waals' forces, the adsorption energy will be higher as there are more direct contacts between adsorbent and adsorbate atoms. Adsorbed nitrogen in the flat position presents two atoms for interaction with the surface whereas argon presents one. Due to the multiple bond, the electron density of the nitrogen molecule is such that interaction with the electron cloud of the surface atoms is more favorable than in the argon molecule, where the electron cloud is spherical.

Nitrogen is expected to be oriented in the flat position in the absence of a strong average electrostatic field. According to the results in Table VII about 80% of the adsorbed nitrogen molecules were oriented in the flat position. It must be mentioned, however, that if all adsorbed molecules were rotating freely, two-thirds of the molecules would be found in the flat position at any point in time. An orientation of 80% in the flat position represents a slight preference for that position. Molecules that are standing on end are not in the upright position because the electrostatic field presents an energy barrier to the rotation of the molecular axis out of the upright alignment. Calculation of this energy barrier by the following equations,

$$P^{rot} = F^2/2\ (\xi_1 - \xi_2) \tag{42}$$

$$\bar{x} = \exp(-P^{rot}/RT) \tag{43}$$

where $\underline{P}^{rot}$ = energy barrier to rotation

$\underline{F}$ = surface electric field

$\xi_1 \xi_2$ = molecular polarizability in the upright and flat orientations, respectively

$\underline{\bar{x}}$ = fraction of molecules with energy greater than $\underline{P}^{rot}$

indicates that more than 99.99% of the adsorbed molecules have enough energy to overcome the barrier to rotation provided by the surface electric field. The 20% that are standing on end are probably in that position because nearly 60% of all adsorbed molecules are rotating freely. For freely rotating nitrogen molecules, the probability of a molecule lying flat on the surface is twice the probability of a molecule standing on end; if 60% of all adsorbed molecules are freely rotating, 20% of all adsorbed molecules are upright. Therefore, the adsorbed film appears to be a mixture of freely rotating molecules and molecules lying flat on the surface.

No trend in $\underline{U'}_o$ and γ with increasing argon and nitrogen surface areas is indicated. It is reasonable to conclude that the additional surface developed in the samples with higher surface area had the same adsorption characteristics (similar values of $\underline{U'}_o$ and γ) as the accessible surface in the samples with low surface area. Barber (29) observed values of $\underline{U'}_o$ and γ that were similar for a water-dried sample and a solvent exchange, dried sample. The former sample exhibited 1% of the surface area of the latter. The surface area of these samples was determined by argon adsorption.

The ratio of surface area as found by argon to that found by nitrogen adsorption ($\Sigma_{\underline{A}}/\Sigma_{\underline{N}_2}$) versus the surface area by argon adsorption ($\Sigma_{\underline{A}}$) is shown in Fig. 24. An increase in $\Sigma_{\underline{A}}/\Sigma_{\underline{N}_2}$ with a decrease in $\Sigma_{\underline{A}}$ is noted. Since no trend in $\underline{U'}_o$ and γ with increasing argon and nitrogen surface areas was found, the plot shows

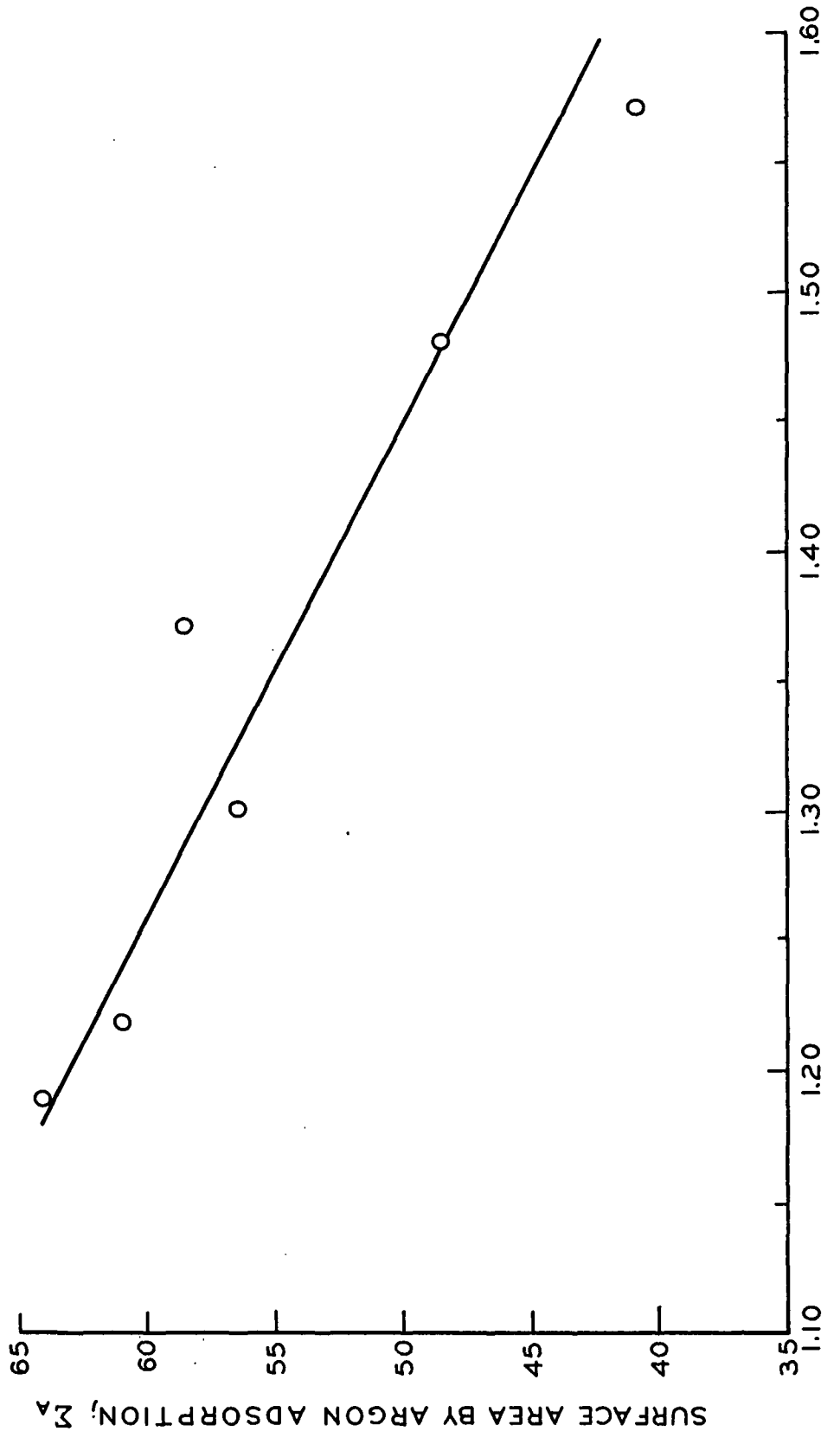

Figure 24. A Plot of the Ratio of Argon to Nitrogen Surface Areas vs. Argon Surface Area

that less surface became available or accessible to the nitrogen molecule as compared to the argon molecule as the surface area for argon adsorption decreased.

The Ross-Olivier theory predicts monolayer capacities, V_β, that are several times greater than the monolayer capacities, V_m, predicted by BET theory. The discrepancy between these two values for argon adsorption increases with decreasing substrate adsorptive potentials (12, 29). Barber (29) estimated the surface area of rayon samples from measurements of fiber cross-section perimeters. The estimate by Barber is expected to be low because of an inability to determine the roughness of the surface on a molecular scale. However, the geometric area was nearly twice as large as the surface area calculated from the BET monolayer capacity for argon adsorption. The surface area calculated from V_β was greater than the geometric area.

A discrepancy between the monolayer capacities and the surface areas determined from Ross-Olivier and BET theories is noted also for nitrogen adsorption. A comparison of surface areas (Σ_{R-O} and Σ_{BET}) is presented in Table X. All BET plots exhibited a linear region from which the slope and intercept of the straight line was easily determined. Calculation of R-O and BET surface areas at both temperatures were made with the value of β as the estimate of molecular area,

$$\Sigma(m.^2/g.) = 0.269\ \beta\ V_\beta\ (cc./g.) \qquad (44)$$

or

$$\Sigma(m.^2/g.) = 0.269\ \beta\ V_m\ (cc./g.) \qquad (45)$$

where

$$\beta = 13.6 \times 10^{-16}\ cm.^2/\text{molecule for argon}$$

TABLE X

A COMPARISON OF SURFACE AREAS (R-O AND BET) AND FRACTIONAL SURFACE COVERAGE AT WHICH MULTILAYER BUILDUP APPEARS

Sample	Σ_{R-O}, $m.^2/g.$	Σ_{BET}, $m.^2/g.$		Ratio $\Sigma_{R-O}/\Sigma_{BET}$		Apparent Θ at Multilayer Buildup	$\Theta \times \Sigma_{R-O}$, $m.^2/g.$
		77.4°K	90.2°K	77.4°K	90.2°K		
Argon							
SV-2B-1	58.61	21.87	23.41	2.68	2.50	0.38	22.3
SV-2B-2	64.02	22.37	24.84	2.74	2.58	--	--
SV-2B-3	60.95	26.96	28.17	2.26	2.16	0.38	23.2
SV-2B-4	56.30	23.92	26.67	2.35	2.11	0.39	22.0
SV-2B-5	48.58	14.52	15.91	3.35	3.05	0.34	16.5
SV-2B-6	40.90	12.25	13.13	3.24	3.11	0.36	14.7
Nitrogen							
SV-2B-1	42.65	24.51	19.25	1.74	2.22	0.57	24.3
SV-2B-2	53.75	27.07	26.94	1.98	1.99	0.51	27.4
SV-2B-3	49.88	29.33	27.49	1.70	1.82	0.58	28.9
SV-2B-4	43.44	26.62	23.72	1.63	1.83	0.56	24.3
SV-2B-5	32.86	16.31	14.76	2.01	2.22	0.57	18.7
SV-2B-6	26.22	13.59	12.67	1.93	2.07	0.57	14.9

$$\beta = 16.0 \times 10^{-16} \text{ cm.}^2\text{/molecule} \quad \text{for nitrogen - 78\% flat}$$

$$\beta = 16.3 \times 10^{-16} \text{ cm.}^2\text{/molecule} \quad \text{for nitrogen - 83\% flat}$$

As determined from Table X, the ratio $\Sigma_{R\text{-}O}/\Sigma_{BET}$ is less for nitrogen than for argon adsorption on the same sample. A comparison of this ratio with $\underline{U}'_o$ for argon and nitrogen adsorption is presented in Fig. 25. In this manner, the ratio $\Sigma_{R\text{-}O}/\Sigma_{BET}$ for nitrogen adsorption can be correlated with the ratio for argon adsorption. Figure 25 illustrates the increasing discrepancy between $\Sigma_{R\text{-}O}$ and Σ_{BET} estimates with decreasing mean adsorptive potential.

Ross and Olivier (30) have suggested that the value of Σ_{BET} is an estimate of the surface area having an adsorptive potential greater than that of the adsorbate film. Those portions of the surface with an adsorptive potential less than the adsorbate film remain sparsely occupied even as multilayers build up on the more energetic portions. During multilayer buildup on the more energetic regions, portions of the surface with low adsorptive potential remain uncovered because adsorption on the adsorbate film is favored. Therefore, when a surface is characterized by a low mean adsorptive potential and a broad distribution (small value of γ), it is reasonable to expect a significant part of the total surface not to be covered with adsorbate.

Cellulose is a low potential surface with a broad distribution of adsorptive potentials, and a significant portion of the total surface remains uncovered as multilayer buildup occurs. An estimate of the fraction of monolayer coverage that is achieved before the occurrence of significant multilayer build-up can be made from the experimental to model isotherm comparisons. The experimental to theoretical comparisons are presented in Appendix IV, between Fig. 34-108. In these comparisons a discrepancy occurs in the higher pressure region.

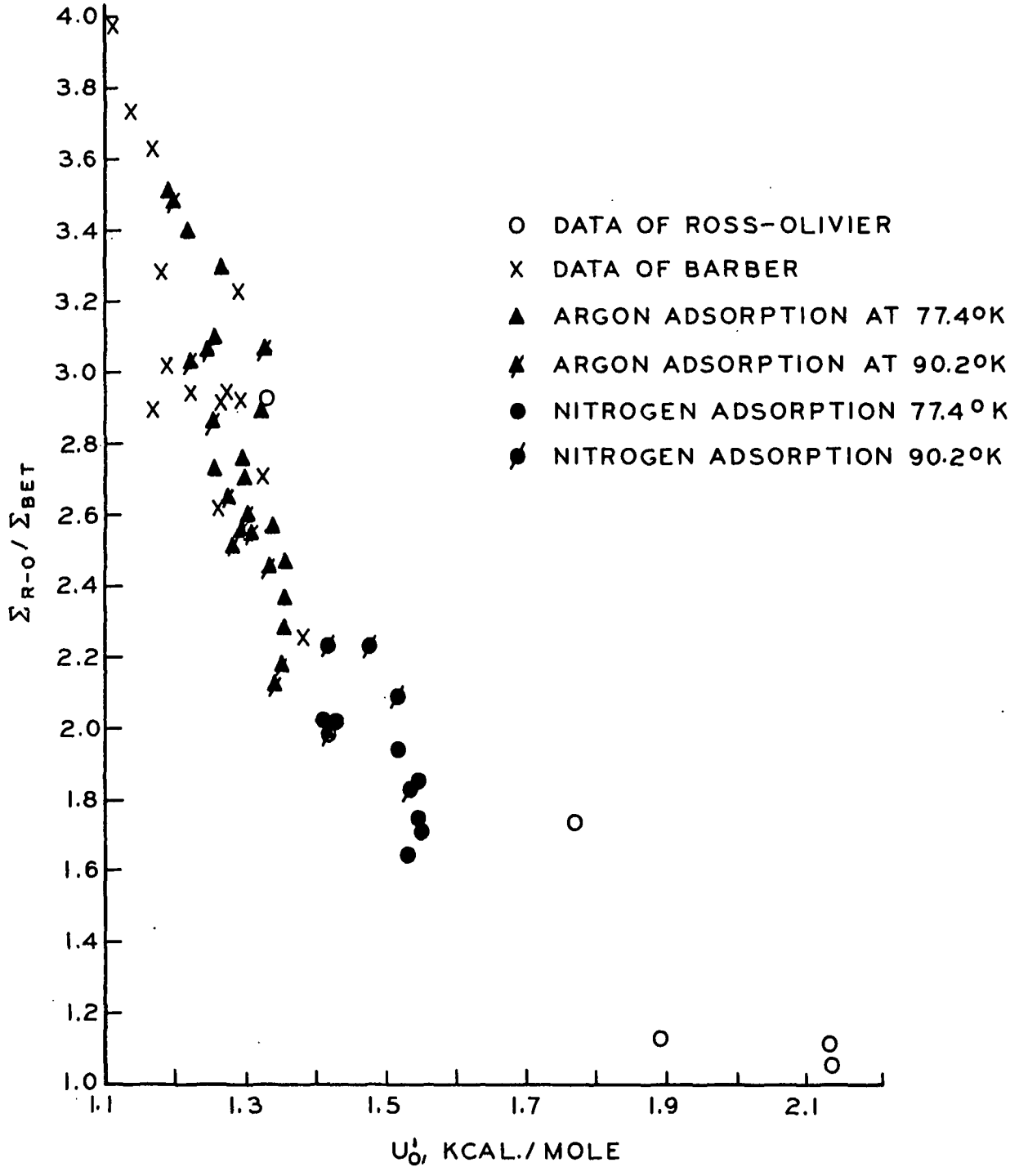

Figure 25. Variation of the Ratio $\Sigma_{R-O}/\Sigma_{BET}$ with Mean Adsorptive Potential

The rise in the experimental isotherm is interpreted as multilayer adsorption. The fraction of monolayer completion, Θ, is estimated by dividing the volume adsorbed by $\underline{V}_\beta$. These values are estimates since a judgment is required to determine the exact point at which the experimental and model isotherms deviate. The estimates of Θ are presented in Table X; for argon adsorption, $\Theta = 0.37$ and for nitrogen, $\Theta = 0.56$ as an average.

A consideration of clustering of the adsorbate suggests that these values of Θ are good approximations for the fraction of monolayer coverage where multilayer buildup occurs. The clustering function as used here was developed by Brown (54) from the work of McMillan and Mayer (58), Zimm (59), and Zimm and Lundberg (60). Using previously presented notation (60) the clustering function is given by $\emptyset_1 \underline{G}_{11}/\underline{V}_1$,

where

$\underline{G}_{11}$ = the clustering integral

$\emptyset_1$ = volume fraction

$\underline{V}_1$ = molecular volume of the adsorbate

The clustering function is equal to the mean number of adsorbate molecules near a given adsorbate molecule in excess of the random expectation. At monolayer completion, the clustering function is a minimum; the function increases during multilayer formation (61, 62).

From gas adsorption data, the adsorbate volume ($\underline{V}_1$) as a function of adsorbate pressure and mass is known. The clustering function is computed by

$$\emptyset_1 \, G_{11}/V_1 = -\emptyset_2 \emptyset_1 \, [\partial(z_1/\emptyset_1)/\partial z_1]_{T,P} - \emptyset_1 \qquad (46)$$

The volume fraction ($\emptyset$) is calculated from adsorbent density and mass assuming additivity of volumes.

The activity ($\underline{z}$) is computed from a relationship derived from the Berthelot equation. The derivative $[\partial(\underline{z}_1/\underline{\phi}_1)/\partial\underline{z}_1]$ is computed from the best polynomial fit to the $\underline{z}_1/\underline{\phi}_1$ versus $\underline{z}_1$ data. After determination of the derivative, the clustering value in Equation (46) is computed using appropriate volume fractions (54).

The clustering functions for argon and nitrogen adsorption on representative samples are presented in Fig. 26-27. It is seen that the minimums in the clustering functions occur at $\Theta = 0.39$ for argon and $\Theta = 0.65$ for nitrogen adsorption, suggesting multilayer buildup at these points. An error of 10-15% is expected in these values of Θ since the clustering function includes a differentiation of point values on a curve.

The product of Σ_{R-O} and the fraction of monolayer completion, Θ, is the surface area covered before significant multilayer buildup occurs. These areas are presented in Table X, and are similar to the BET estimate of the surface area. For the low potential, cellulose surface, the BET estimate of the surface area is a good representation of the surface portions covered with adsorbate. However, the Ross-Olivier estimate of the surface area is a more reasonable estimate of the total surface area accessible to the adsorbate molecules.

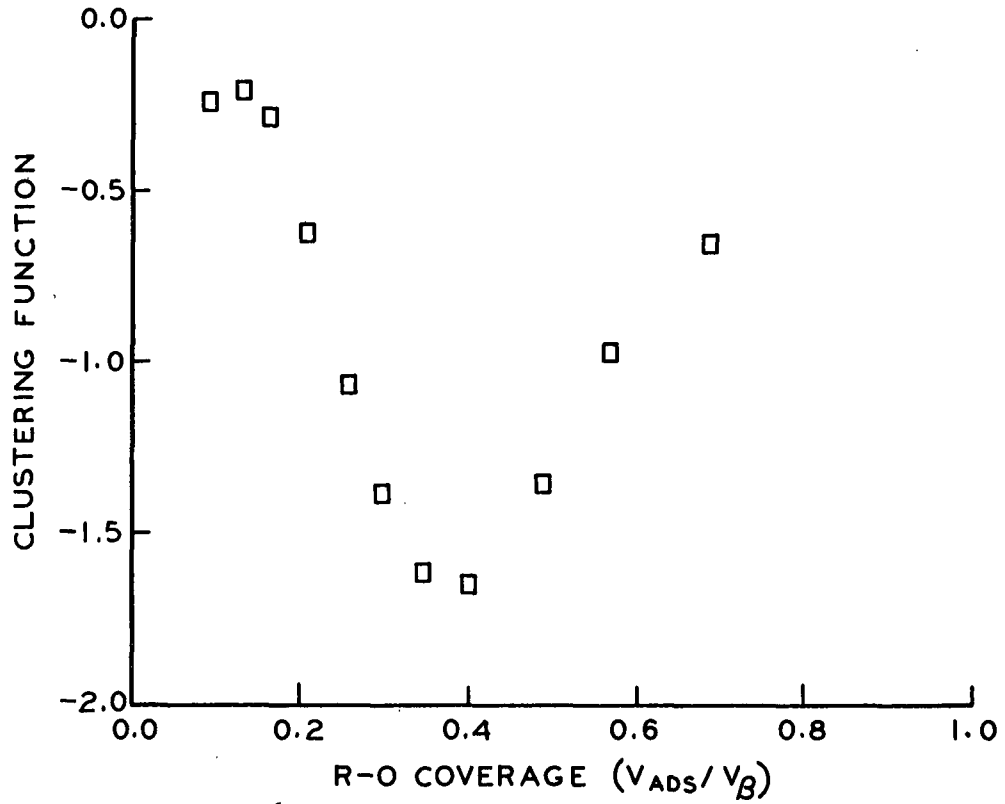

Figure 26. Clustering Value vs. R-O Coverage for Argon Adsorption on Sample SV-2B-5

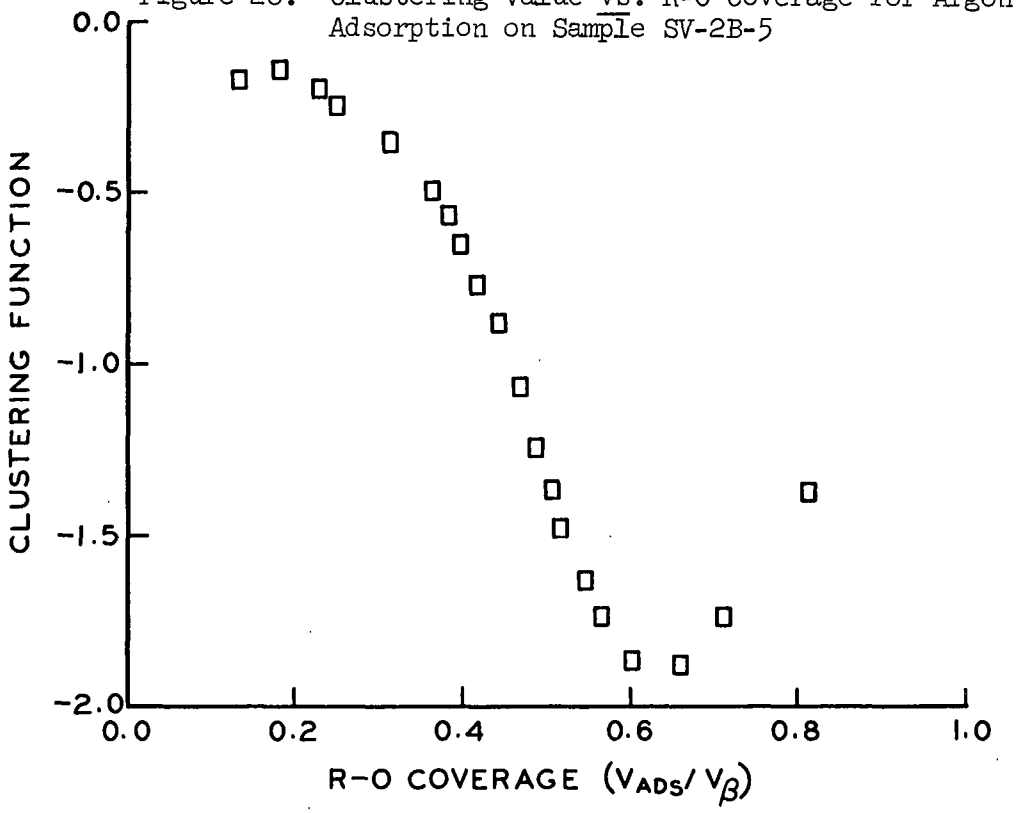

Figure 27. Clustering Value vs. R-O Coverage for Nitrogen Adsorption on Sample SV-2B-6

CONCLUSIONS

The surface electric field of cellulose was calculated from the results of a heat of wetting study. The average cellulose surface electric field is 0.13 x 10^5 esu/cm.^{2}. At this strength the electrostatic field induces an insignificant dipole moment in the adsorbed nitrogen molecules (μ = 0.0317 debyes). This dipole moment is insignificant because the resulting perturbations in the lateral interaction potentials of the adsorbed molecules are very small (the change in α is 0.21%). A 3% change in α is necessary to significantly change the shape of the model isotherms of Ross-Olivier.

A reasonable description of the adsorbed nitrogen film is a mixture of molecules freely rotating (about 60%) and molecules lying flat on the surface (about 40%). By calculation, it was demonstrated that 99.99% of the adsorbed molecules have the energy to overcome the barrier to rotation provided by the average electrostatic field.

For argon and nitrogen adsorption, the cellulose surface is characterized by a low mean adsorptive potential, $\underline{U}'_o$ and a broad distribution of potentials, γ. The portions of the cellulose surface accessible to the adsorbates are characterized by similar values of $\underline{U}'_o$ and γ regardless of the location of that surface within the fiber structure.

The potential for nitrogen adsorption is greater than for argon adsorption because the nonpolar, dispersion forces are greater for nitrogen. Argon surface areas were greater than nitrogen areas but the ratio of $\Sigma_{\underline{A}}/\Sigma_{\underline{N}_2}$ was shown to decrease as the surface area by argon adsorption increased. The correlation between $\Sigma_{\underline{A}}/\Sigma_{\underline{N}_2}$ and $\Sigma_{\underline{A}}$ was a result of a difference in accessibility of the surface to argon and nitrogen molecules.

Marked differences in Ross-Olivier and BET estimates of surface area were observed. The discrepancy between Ross-Olivier and BET surface areas increases for surfaces of decreasing $\underline{U}'_o$. Thus, the ratio $\Sigma_{R-O}/\Sigma_{BET}$ was greater for argon than for nitrogen adsorption since $\underline{U}'_o$ for the adsorption of argon was less.

Ross and Olivier (12) suggested that multilayer buildup occurs at $\Theta < 1.0$ for low potential surfaces because the adsorbed film is a more favorable site for adsorption than the lower potential portions of the surface. The present study showed the fraction of monolayer coverage where multilayer buildup occurred was about $\Theta = 0.37$ for argon and $\Theta = 0.56$ for nitrogen adsorption. Because the product of the Ross-Olivier estimate of surface area, Σ_{R-O}, and the fraction of monolayer completion, Θ, was nearly equal to the BET estimate of surface area, the BET estimate appears to be a good approximation of the surface area covered before multilayer buildup occurred. The Ross-Olivier estimate is a more reasonable approximation of the total surface area accessible to the adsorbate molecule.

FUTURE WORK

The adsorption by cellulose of selected adsorbates such as xenon and krypton should be studied. Since the adsorption of a polar molecule by cellulose presently is being investigated, the study of krypton and xenon adsorption would be a logical continuation. Such an investigation and analysis by Ross-Olivier theory would be uncomplicated. Xenon and krypton molecules are of different size, and the adsorptive potential of the adsorbed layer of each adsorbate is probably different from argon or nitrogen. An adsorption study of these spherical molecules should result in additional verification of the Ross-Olivier estimate of surface area as a more reasonable value than that provided by BET theory.

This study would require a more sensitive adsorption apparatus than used in the present investigation. If isotherms at temperatures other than 77.4°K and 90.2°K are needed, a cryostat is required for temperature control. Additional information about the changes in energy and entropy on adsorption can be obtained from the study of adsorption at several temperatures.

An adsorption study in conjunction with a thermodynamic study will provide a more complete description of the adsorption system. A thermodynamic study of a cellulose-adsorbate system can be made by calorimetrically determining the heat of adsorption as a function of the adsorbed volume. Either the integral or differential heat of adsorption is determined. The isosteric heat of adsorption is calculated from the integral or differential heat. The entropy change accompanying adsorption may be obtained as the function of the volume adsorbed, when the adsorption isotherm and the heat of adsorption are known. These thermodynamic quantities may be complemented by a calorimetric determination of the heat capacity of the adsorbed film.

ACKNOWLEDGMENTS

The author gratefully acknowledges the constructive criticism of this work by his Thesis Advisory Committee: Chairman J. W. Swanson, G. F. Richards and R. A. Holm.

The continued financial support of The Institute of Paper Chemistry during this work and the help of fellow students P. F. Brown and G. W. Brown and M. Filz and P. Van Rossum of the Institute Machine Shop were appreciated.

Finally, I wish to thank my wife Sue for typing the original manuscript of this dissertation and for her encouragement throughout this work, and son John to whom all other things are relative.

NOMENCLATURE

(A Summary of the More Important Symbols)

$\underline{a}$	Van der Waals' constant of a nonideal gas
$\underline{A}^{o}$	Constant defined by Equation (30)
$\underline{b}$	Van der Waals' constant of a nonideal gas
$\underline{C}$	Constant in Equation (2)
$\underline{E}_{\underline{A}}$	Energy of adsorption per molecule
$\underline{E}_{\underline{L}}$	Energy of removing a molecule from the bulk liquid
$\underline{E}_{\underline{W}}$	Energy contribution from the nonpolar Van der Waals forces
$\underline{E}_{\alpha}$	Energy contribution due to the induction of a dipole moment in the adsorbate
$\underline{E}_{\mu}$	Energy contribution arising from the interaction of the permanent dipole of the adsorbate and the surface electric field of the substrate
$\Delta\underline{E}^{kin}$	The change in the kinetic energy of the molecule on adsorption from the total kinetic energy in the gas phase to the kinetic energy of translation and rotation in the adsorbed phase
$\underline{a}\underline{E}_{o}^{vib}$	The average vibrational energy of an adsorbed molecule at 0°K
$\underline{f}$	Exponential distribution function of Halsey and Taylor, Equation (2)
$\underline{f}_{\underline{i}}$	Frequency of occurrence of particular surface patches per unit energy interval
$\underline{F}$	Surface electric field
$\underline{a}\underline{F}^{vib}$	The additional Gibb's free energy of the adsorbed phase due to molecular vibrations with respect to the surface
$\underline{h}$	Planck's constant (6.626×10^{-27} ergs/sec.)
$\underline{h}_{\underline{I}(\underline{SL})}$	The heat of immersion of the clean solid surface
$\underline{h}_{\underline{L}}$	The heat of immersing a unit area of the liquid surface
$\underline{H}_{\underline{I}}$	The heat of immersion
$\underline{H}_{\underline{BB}}$	The heat of bulb breaking
$\underline{H}$	The heat of wetting
$\underline{I}$	The moment of inertia

I_C	Electric current
k	Boltzmann constant (1.38×10^{-16} ergs/degrees)
K'	Particular constant associated with the mean adsorptive potential according to Equation (29)
K_i	A constant related to the adsorptive potential of each patch according to Equation (6)
M	Molecular mass
n	Normalizing factor of the Gaussian distribution
N	Avogadro's number (6.023×10^{23} molecules/mole)
N_A	The number of molecules adsorbed per area in the monolayer
p	System equilibrium pressure
$_aP^{ia}$	Potential energy of interaction of the adsorbate
P_o	Saturation vapor pressure
P^{rot}	Energy barrier to rotation
q^{st}	Isosteric heat of adsorption
q^{diff}	Differential heat of adsorption
Q^{rot}	Rotational partition function
R	Gas constant (1.987 cal./mole degree); Resistance
S^{rot}	Rotational entropy
ΔS_s^{tr}	The change in translational entropy per mole in the standard state of adsorption
ΔS^{rot}	The change in rotational entropy on adsorption
t	Time
T	Absolute temperature
Δt_A, Δt_C	Temperature deflection
U'_o	Mean adsorptive potential
U_o	Adsorptive potential of a homottatic surface
U_{oi}	Adsorptive potential of the ith patch
U_o^{diff}	Differential adsorptive potential

$\underline{U}_o^{int}$	Integral adsorptive potential
$\underline{V}_\beta$	Ross-Olivier theory predicted monolayer capacity
$\underline{V}_{BET}$	BET theory predicted monolayer capacity
$\underline{W}$	Sample weight
$\underline{x}$	Fraction of adsorbed molecules lying flat on the surface
α,β	Two-dimensional van der Waals constants
γ	Heterogeneity parameter
$\Delta\delta_{\underline{i}}$	Fraction of the surface having adsorptive potentials between $\underline{U}_{o\underline{i}}$ and $\underline{U}_{o\underline{i}} + \underline{U}_o$
Θ	Overall monolayer completion fraction
$\Theta(\underline{p},\underline{T})$	Experimentally observed adsorption function
$\phi_1 G_{11}/V_1$	Clustering function
$\theta_{\underline{i}}$	Fraction of the $\underline{i}$th patch of the adsorbent surface covered by the adsorbate
$\theta_{\underline{s}}$	Standard state of the surface phase, taken so that the average intermolecular separation would be the same in the gas and adsorbed phases at 0°C.
$\phi(\underline{U}_o)$	Energy of adsorption distribution function
$\psi(\underline{p},\underline{T},\underline{U}_o)$	Local adsorption isotherm function
λ	Polarization factor
μ	Dipole moment
ν	Vibrational frequency
ξ	Electron polarizability of the molecule
σ	Symmetry factor
Σ	Surface area in $m.^2/g.$

LITERATURE CITED

1. Ross, S. In Burke, Reed, and Weiss' Surfaces and interfaces, I, pp. 169-96. Syracuse, New York, Syracuse University Press, 1967.

2. Young, D. M., and Crowell, A. D. Physical adsorption of gases. London, Butterworth, 1962. 426 p.

3. Langmuir, I., J. Am. Chem. Soc. 40:1361-1403(1918).

4. Polanyi, M., Trans. Faraday Soc. 28:316-33(1932).

5. Brunauer, S., Emmett, P. H., and Teller, E. J., J. Am. Chem. Soc. 60:309-19 (1938).

6. Hill, T. L. In Gomer and Smith's Structure and properties of the solid surface. pp. 384-99. Chicago, Illinois, University of Chicago Press, 1953.

7. Hill, T. L., J. Chem. Phys. 14:263-7(April, 1946); 14:441-53(July, 1946); 15:767-77(Nov., 1947); 16:181-9(March, 1948); 17:762-71(Sept., 1949).

8. deBoer, J. H. The dynamical character of adsorption. Oxford, Clarendon Press, 1953. 239 p.

9. Halsey, G. D., and Taylor, H. S., J. Chem. Phys. 15:624-30(Sept., 1947).

10. Sips, R., J. Chem. Phys. 16:490-5(May, 1948); 18:1024-6(Aug., 1950).

11. Drain, L. E., and Morrison, J. A., Trans. Faraday Soc. 48:840-7(1952); 49:654-73(1953).

12. Ross, S., and Olivier, J. P. On physical adsorption. New York, Interscience, 1964. 401 p.

13. Morrison, J. A., Los, J. M., and Drain, L. E., Trans. Faraday Soc. 47: 1023-30(1951).

14. Chessick, J. J., and Zettlemoyer, A. C., J. Phys. Chem. 62:1217-19(Oct., 1958).

15. Young, G. J., and Healey, F. H., J. Phys. Chem. 58:885-6(Oct., 1954).

16. Harkins, W. D., and Stearns, R. S., J. Phys. Chem. 58:292-8(April, 1954).

17. Tompkins, F. C., Trans. Faraday Soc. 46:569-80, 580-6(1950).

18. Everett, D. H., Trans. Faraday Soc. 46:952-7(1950).

19. Reference 12, p. 129.

20. Adamson, A. W., and Ling, I. In Advances in chemistry series. No. 33. pp. 51-61. Washington, D. C., Am. Chem. Soc., 1961; J. Colloid Sci. 21: 445-57(April, 1966).

21. Honig, J. M., and Reyerson, L. H., J. Phys. Chem. 56:140-4(Jan., 1952).

22. Joyner, L. G., and Emmett, P. H., J. Am. Chem. Soc. 70:2353-9(July, 1948).

23. Hsieh, P. Y., J. Phys. Chem. 68:1068-71(May, 1964).

24. Hobson, J. P., Can. J. Phys. 43:1934-40, 1940-50(Nov., 1965).

25. Ross, S., and Clark, H., J. Am. Chem. Soc. 76:4291-7, 4297-300(Sept., 1954).

26. Ross, S., and Winkler, W., J. Colloid Sci. 10:319-29, 330-7(Aug., 1955); J. Am. Chem. Soc. 76:2637-40(May, 1954).

27. Ross, S., and Pultz, W. W., J. Colloid Sci. 13:397-406(Aug., 1958).

28. Gregg, S. J., and Sing, K. S. W. Adsorption, surface area, and porosity. pp. 241-50. New York, Academic Press, 1967.

29. Barber, H. A. The determination of the energy site distribution of the surface of cellulose fibers by gas adsorption methods. Doctor's Dissertation. Appleton, Wis., The Institute of Paper Chemistry, 1969. 104 p.

30. Reference 12. pp. 204-5.

31. Reference 12. p. 224.

32. Chessick, J. J., Zettlemoyer, A. C., Healey, F. H., and Young, G. J., Can. J. Chem. 33:251-8(Feb., 1955); Healey, F. H., Chessick, J. J., Zettlemoyer, A. C. and Young, G. J., J. Phys. Chem. 58:887-90(Oct., 1954); Zettlemoyer, A. C., and Narayan, K. S. In Flood's The solid-gas interface. I. pp. 145-74. New York, Marcel Dekker, 1967.

33. Cochrane, H., Walker, P. L., Diethorn, W. S., and Friedman, H. C. Xenon adsorption on graphitized carbon blacks over a wide coverage range. pp. 119-29. 41st National Colloid Symposium, Buffalo, New York, June, 1967.

34. Gomer, R., J. Chem. Phys. 29:441-2(Aug., 1958); J. Phys. Chem. 63:468-72 (April, 1959).

35. Ehrlich, G., Hickmott, T. W., and Hudda, F. G., J. Chem. Phys. 28:977-8 (May, 1958); Ehrlich, G., and Hudda, F. G., J. Chem. Phys. 30:493-512 (Feb., 1959).

36. Hobson, J. P. In Flood's The solid-gas interface. I. pp. 447-89. New York, Marcel Dekker, June, 1967.

37. Sommers, R. A. A surface-area study of cotton dried from liquid carbon dioxide at zero surface tension. Doctor's Dissertation. Appleton, Wis., The Institute of Paper Chemistry, 1963. 157 p.

38. Conrad, C. M. Chemical properties of cotton cellulose. In Ward's Chemistry and chemical technology of cotton. New York, Interscience, 1955. 782 p.

39. Lund, H., and Bjerrum, J., Ber. 64B:210-13(1931); C.A. 25:3310.

40. Haselton, W. R. An investigation of the adsorption of gases by wood and its components and of gas adsorption techniques as a means of studying the area and structure of pulp and paper. Doctor's Dissertation. Appleton, Wis., The Institute of Paper Chemistry, 1957. 172 p.

41. Merchant, M. V. A study of certain phenomena of the liquid exchange of water-swollen cellulose fibers and their subsequent drying from hydrocarbons. Doctor's Dissertation. Appleton, Wis., The Institute of Paper Chemistry, 1957. 124 p.

42. Robertson, A. A., Pulp Paper Mag. Can. 65:T171-8(April, 1964).

43. Kraus, G. In Adhesions and adhesives, fundamentals and practice. pp. 45-9. New York, John Wiley and Sons, 1954.

44. Berghausen, P. E. In Adhesions and adhesives, fundamentals and practice. pp. 225-7. New York, John Wiley and Sons, 1954.

45. Brown, P. F. Unpublished work, 1970.

46. Hunt, C. M., Blaine, R. L., and Rowen, J. W., J. Res. Nat'l. Bur. Stds. 43:547-54(Dec., 1949).

47. Zettlemoyer, A. C., and Narayan, K. S. In Flood's The solid-gas interface. I. p. 171. New York, Marcel Dekker, 1967.

48. Romo, L. A., J. Colloid Sci. 16:139-49(April, 1961).

49. Dear, D. J. A., Eley, D. D., and Johnson, B. C., Trans. Faraday Soc. 59: 713-20(1963).

50. Zettlemoyer, A. C., Chessick, J. J., and Hollabaugh, C. M., J. Phys. Chem. 62:489-90(April, 1958).

51. Young, G. J., Chessick, J. J., Healey, F. H., and Zettlemoyer, A. C., J. Phys. Chem. 58:313-15(April, 1964).

52. Chessick, J. J., Healey, F. H., and Zettlemoyer, A. C., J. Phys. Chem. 60:1345-7(Oct., 1956).

53. Reference 47, p. 170.

54. Brown, G. Unpublished work, 1970.

55. Reference 29, p. 170.

56. Reference 12, p. 147, 200.

57. Reference 12, p. 187.

58. McMillan, W., and Mayer, J., J. Chem. Phys. 13:276-305(July, 1945).

59. Zimm, B. H., J. Chem. Phys. 21:934-5(May, 1953).

60. Zimm, B. H., and Lundberg, J. L., J. Phys. Chem. 60:425-8(April, 1956).

61. Lohr, J. E., and Scholz, J. J., J. Colloid Sci. 20:846-56(Oct., 1965).

62. Hoburg, R. F., Handler, G. S., and Scholz, J. J., J. Colloid Sci. 27:642-8 (Aug., 1968).

APPENDIX I

PREPARATION OF CELLULOSE SUBSTRATE

PURIFICATION TREATMENT

1. Initially the cotton was sorted and extraneous visible material was removed.

2. About 15 grams of the sorted material was extracted in 95% ethanol (1500 cc.) for 10 hours in a Soxhlet extractor.

3. Followed by a wash in three portions of distilled water (about 1500 cc. each).

A basket arrangement of glass rods was used to hold the cellulose below the liquid surface and above the bottom of the container in all subsequent boiling operations.

4. The cotton was boiled in 1500 cc. of distilled water for 20 minutes.

5. The boiling water was siphoned off and simultaneously replaced with 1500 cc. of boiling 1% caustic.

6. During a period of 1 hour, 6000 cc. of boiling caustic was passed through the sample. The final stage was in contact with the cotton for one additional hour.

7. Boiling water (6000 cc.) was passed through the sample in 2 hours.

8. The cotton was treated with 0.5% acetic acid (1700 cc.) for 45 minutes.

9. The acid was displaced with at least 9000 cc. distilled water for at least 1 hour and until the wash tested neutral with litmus paper.

SOLVENT EXCHANGE SCHEDULE

Exchange Number	Solvent	Volume Each Exchange, ml.	Time Each Exchange, min.
1 to 10	Reagent Methanol	40	10
11 to 15	Dried Methanol	40	10
16 to 20	Reagent Pentane	40	10
21 to 25	Dried Pentane	40	10

APPENDIX II

THE CALORIMETER AND LINEAR QUARTZ THERMOMETER (Fig. 28-32)

QUARTZ CRYSTALS AS TEMPERATURE SENSORS

The angle from the crystalline axis at which a quartz crystal is cut determines its temperature coefficient. A crystal can be prepared to exhibit a negative or positive coefficient or a zero temperature coefficient at a selected temperature. A crystal of zero coefficient is used in the thermometer to provide a stable reference frequency. The performance of the reference crystal is maintained in a temperature-controlled oven.

The temperature sensing crystal exhibits the most linear possible change of frequency with changing temperature. However, the response curve is not a perfectly straight line over the range of temperatures to which the crystal can be exposed (-80 to 250°C.); a constant ratio of frequency to temperature is not maintained. At any given point on the response curve, compensation can be made by changing the sampling period. This compensation is made electronically by setting numerical thumbwheel switches in the thermometer. The effect of the change in timing brings the slope of the curve up to the ideal of 1.0 at some preselected temperature.

Hysteresis causes the crystal to resonate at different frequencies for the same temperature depending on the span and direction from which the temperature is approached. The width of the hysteresis decreases as the total span of temperature is made smaller.

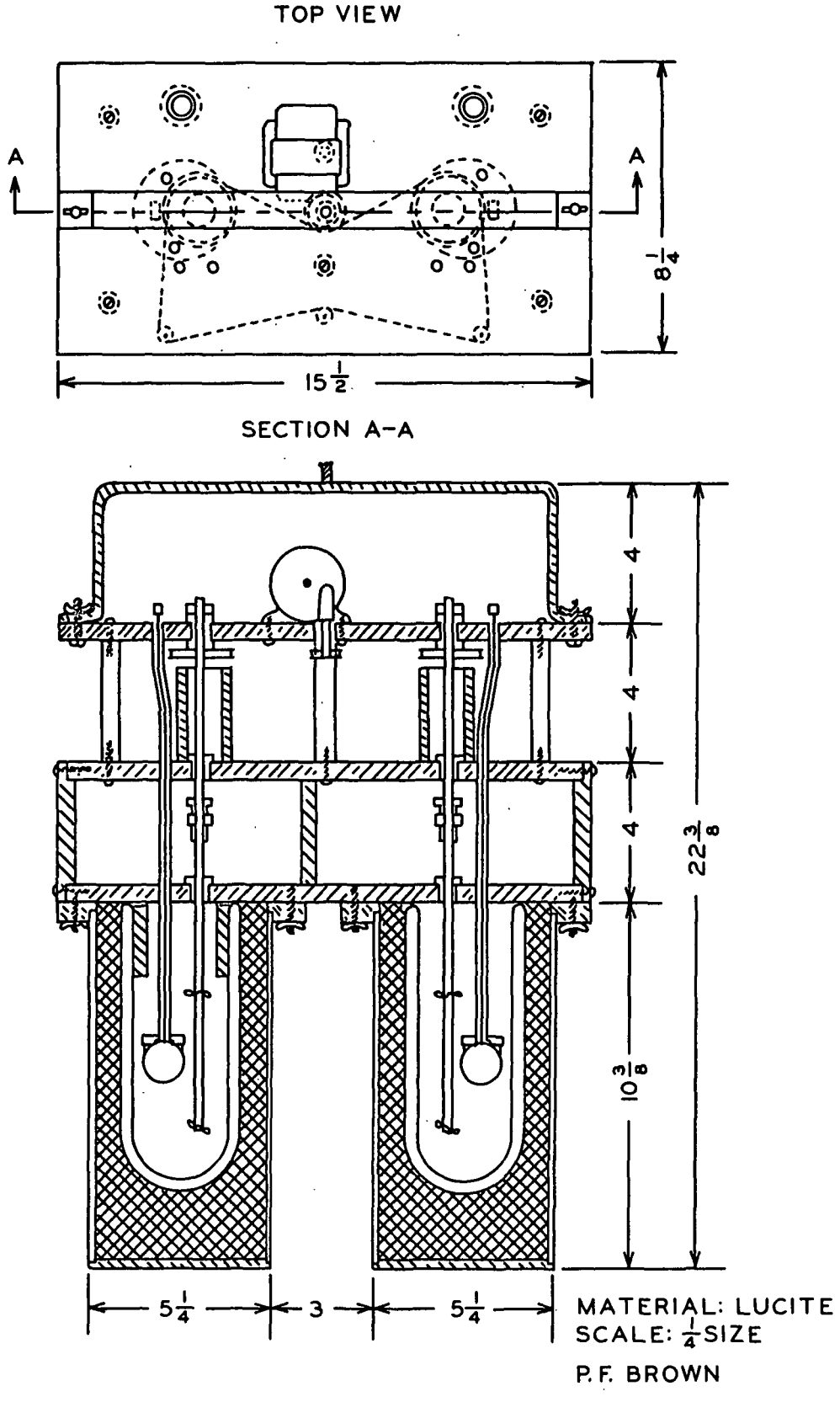

Figure 28. Calorimeter Assembly (45)

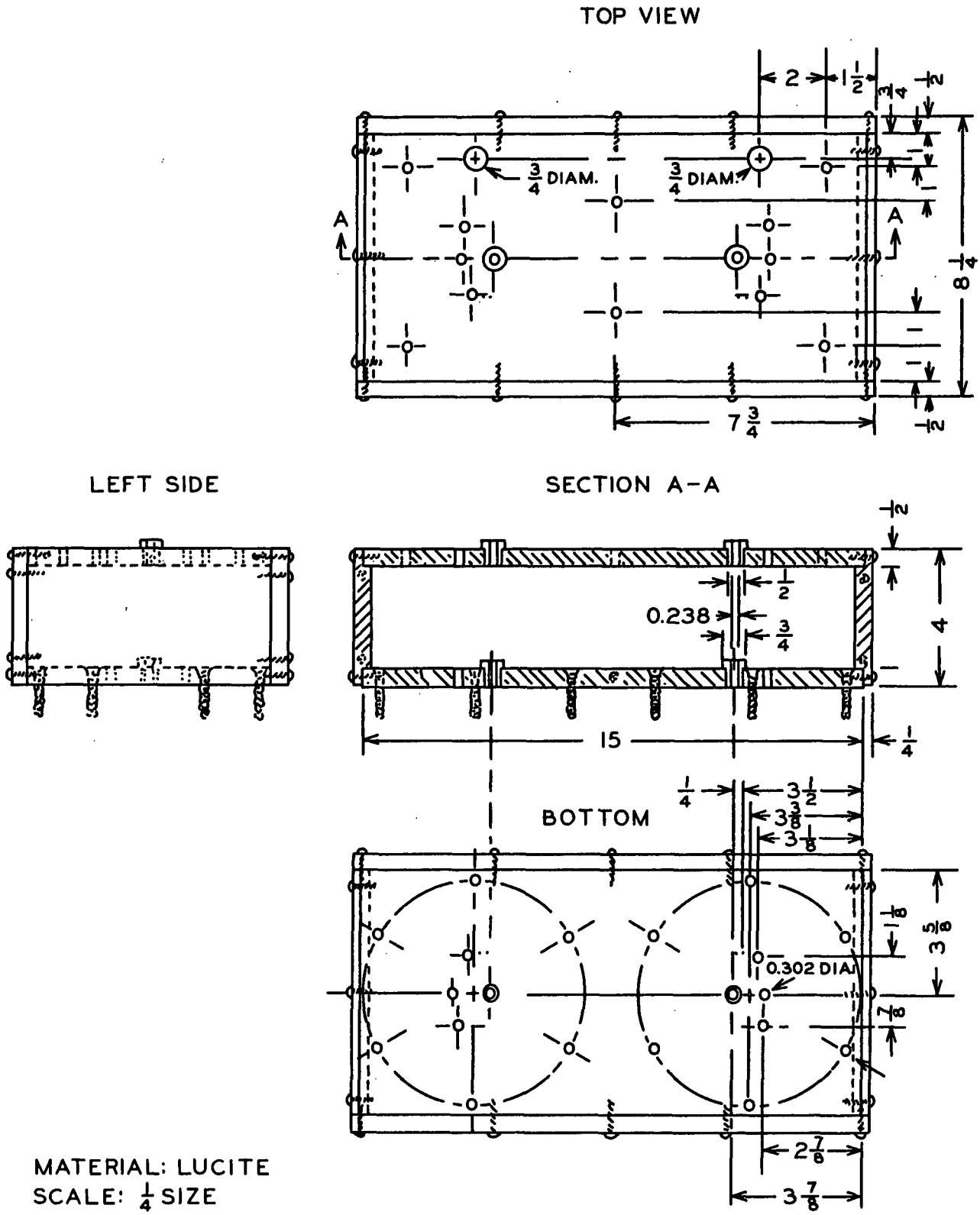

Figure 29. Submarine Jacket (45)

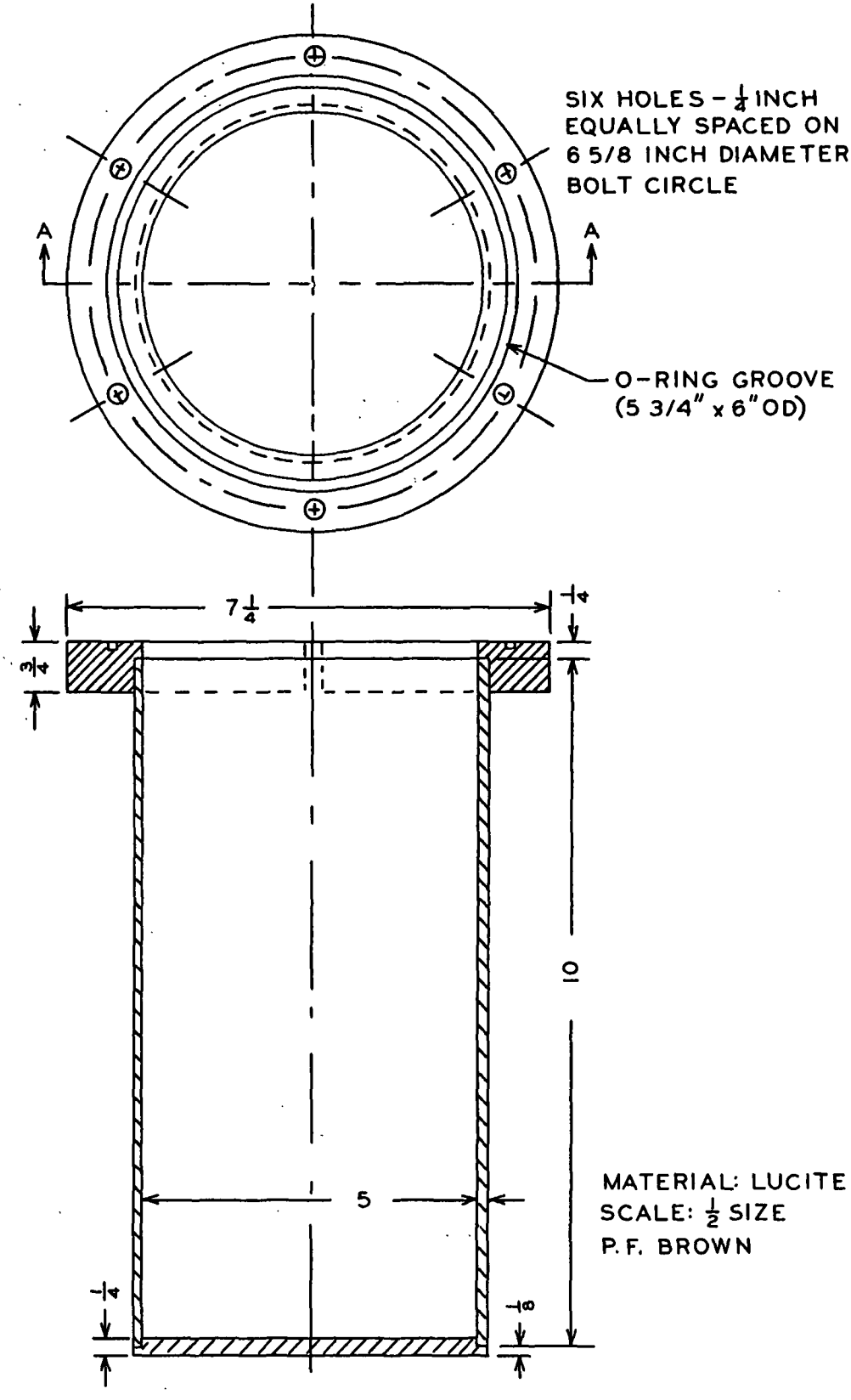

Figure 30. Dewar Case (45)

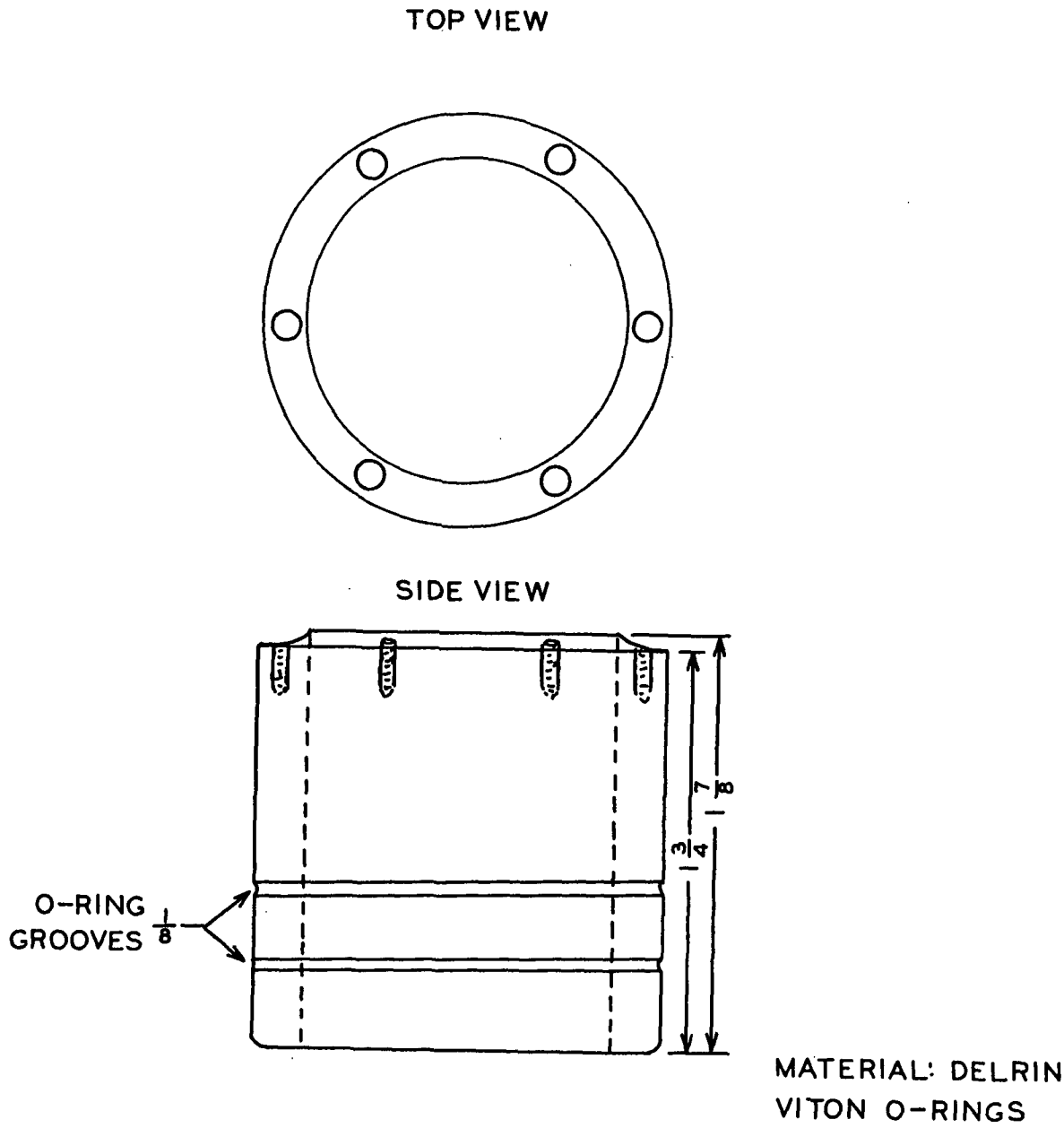

Figure 31. Hollow Plug

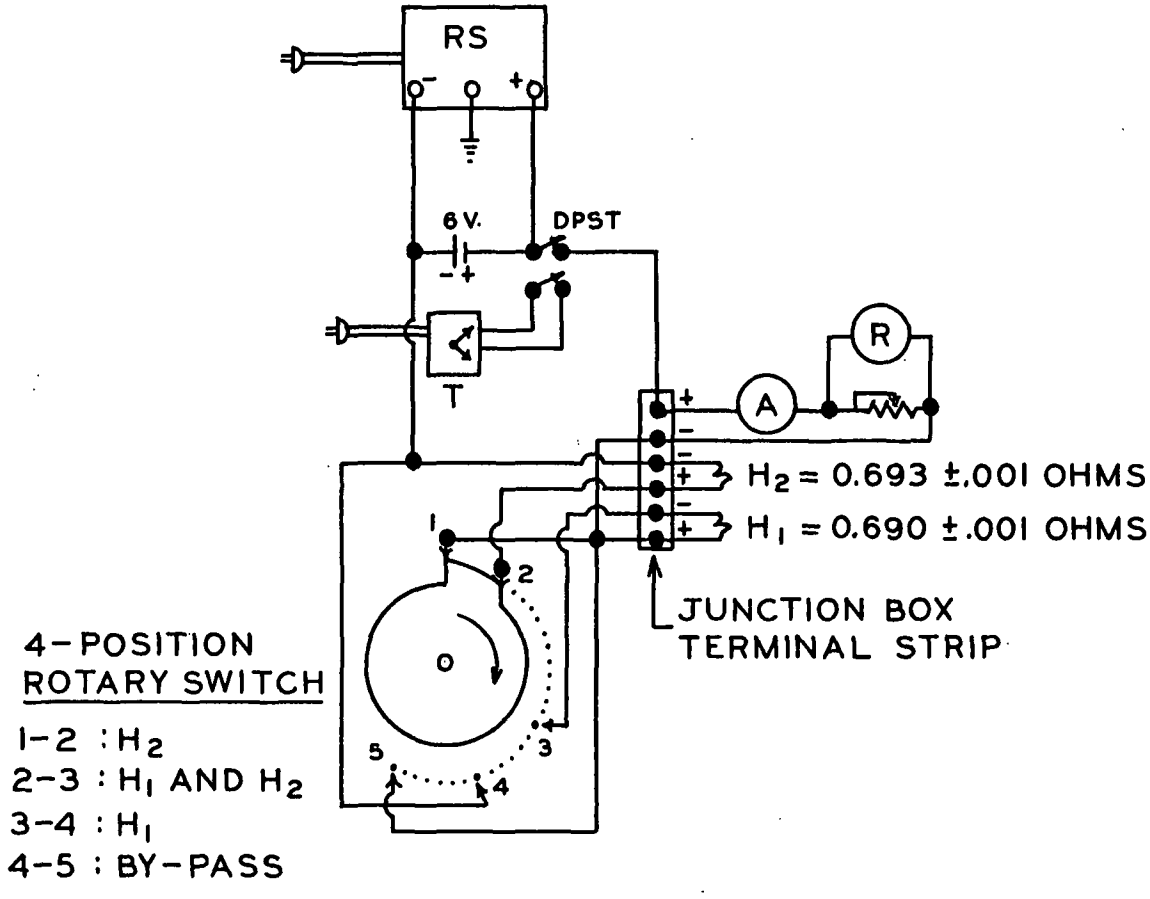

RS REGULATED DC POWER SUPPLY
KEPCO MODEL ABC (0 - 0.5 AMP, 0 - 18. VOLTS)

A DC POLYRANGER AMMETER (0 - 1 AMP)

T TIMER STANDARD TYPE S-1

R BECKMAN RECORDING POTENTIOMETER (TYPE RS)

Figure 32. Heater Circuit

PURIFICATION OF WETTING LIQUIDS

BENZENE

B.p. 80.1°C., f.p. 5.5°C., n_D^{25} 1.4979. Dried with sodium, fractionally distilled and stored over 4A molecular sieve and CaH_2.

CHLOROBENZENE

B.p. 131.7°C., n_D^{20} 1.5248. Washed several times with concd. H_2SO_4, then aq. $NaHCO_3$, and water, dried with 4A molecular sieve followed by drying with calcium hydride.

NITROBENZENE

F.p. 5.8°C., b.p. 84-86.5°C./6.5-8 mm. Extraction from aq. 2M NaOH, water, dil. HCl, water, followed by drying with $MgSO_4$, and fractionally distilled under reduced pressure, stored in a colored glass bottle over CaH_2.

DETERMINATION OF WATER CONTENT OF THE WETTING LIQUIDS

The amount of water in each wetting liquid was determined with the aid of a gas chromatograph equipped with a thermal conductivity sensor. A Por-Pak Q column was used for liquid separation. The water concentration was determined by measuring the area under the water peak and comparing this area to that of several standards. The standards were prepared by adding 0, 1, 3, and 5 p.p.m. water to 1 liter of reagent-grade benzene. The change in area of the water peak was determined and plotted against the amount of water added. The correlation was fairly linear, as shown in Fig. 33.

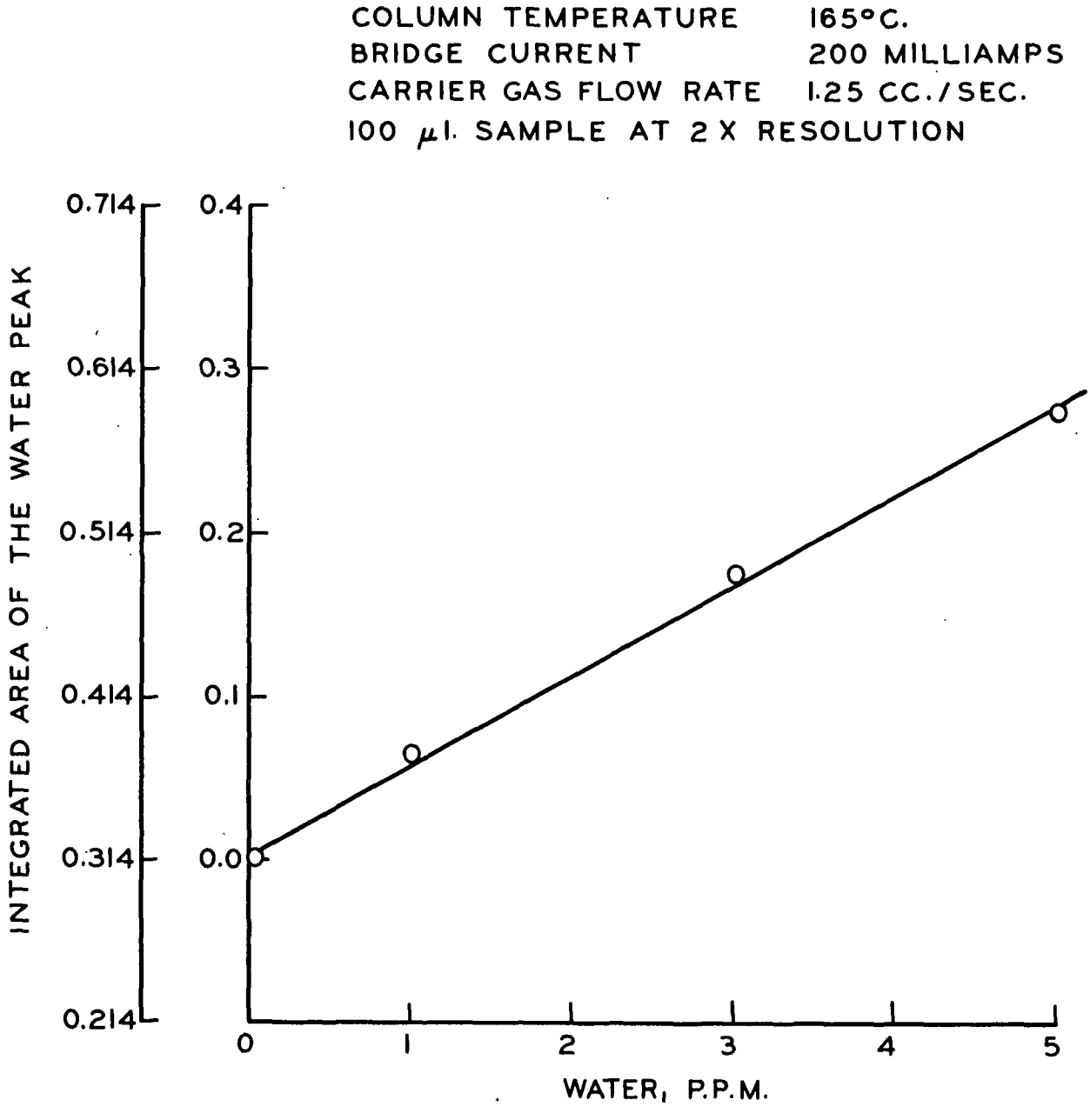

Figure 33. Integrated Area of the Water Peak vs. Water Concentration in p.p.m.

APPENDIX III

CALCULATIONS – THE EFFECT OF THE SURFACE ELECTRIC FIELD ON α

1. "Best fit" slope = $(77.7 - 61.7)/3.93 = 4.07$ ergs/cm.^{2} debye.

   Maximum slope = $(78.7 - 60.7)/3.93 = 4.58$ ergs/cm.^{2} debye.

2. Average electrostatic field strength.

   surface concn. of adsorbed molecules = $1/\beta_{\phi H}$

   $1/\beta_{\phi H} = 0.0306 \times 10^{16}$ molecules/cm.^{2}

   electrostatic field strength, $\underline{F} = (4.07 \times 10^{18})/3.06 \times 10^{14}$

   $= 0.133 \times 10^5$ esu/cm.^{2}

3. Induced dipole in nitrogen molecule

   $\mu = \underline{F}\xi = (0.133 \times 10^5)(2.38 \times 10^{-24}) = 0.317 \times 10^{-19}$ esu cm.

   $\mu = 0.0317$ debye Note: $\xi = 2.38 \times 10^{-24}$ for the upright orientation (12)

4. Correction factor to be applied to α.

   $\lambda = -\mu^2(\pi/d)$

   where $\underline{d} = 3.20 \times 10^{-8}$ cm.

   $\lambda = -(3.17 \times 10^{-2})^2 (\pi/3.20 \times 10^{-8}) 10^{-36}$

   $\lambda = -0.0982 \times 10^{-30}$ ergs cm.^{2}/molecule^2.

5. Using the maximum slope

   $\underline{F} = 4.58/3.06 = 0.15 \times 10^5$ esu/cm.^{2}

   $\mu = 0.0357 \times 10^{-18} = 0.0357$ debye.

   $\lambda = -0.124 \times 10^{-30}$ ergs cm.^{2}/molecule^2.

6. The effect of these corrections on the ideal value of α

   $0.124/45.7 \times 100 = 0.27\%$.

   $0.098/45.7 \times 100 = 0.21\%$.

APPENDIX IV

ADSORPTION ISOTHERMS, COMPARISONS OF EXPERIMENTAL TO MODEL ISOTHERMS, AND COMPARISONS OF EXPERIMENTAL AND THEORETICAL ISOSTERIC HEAT CURVES

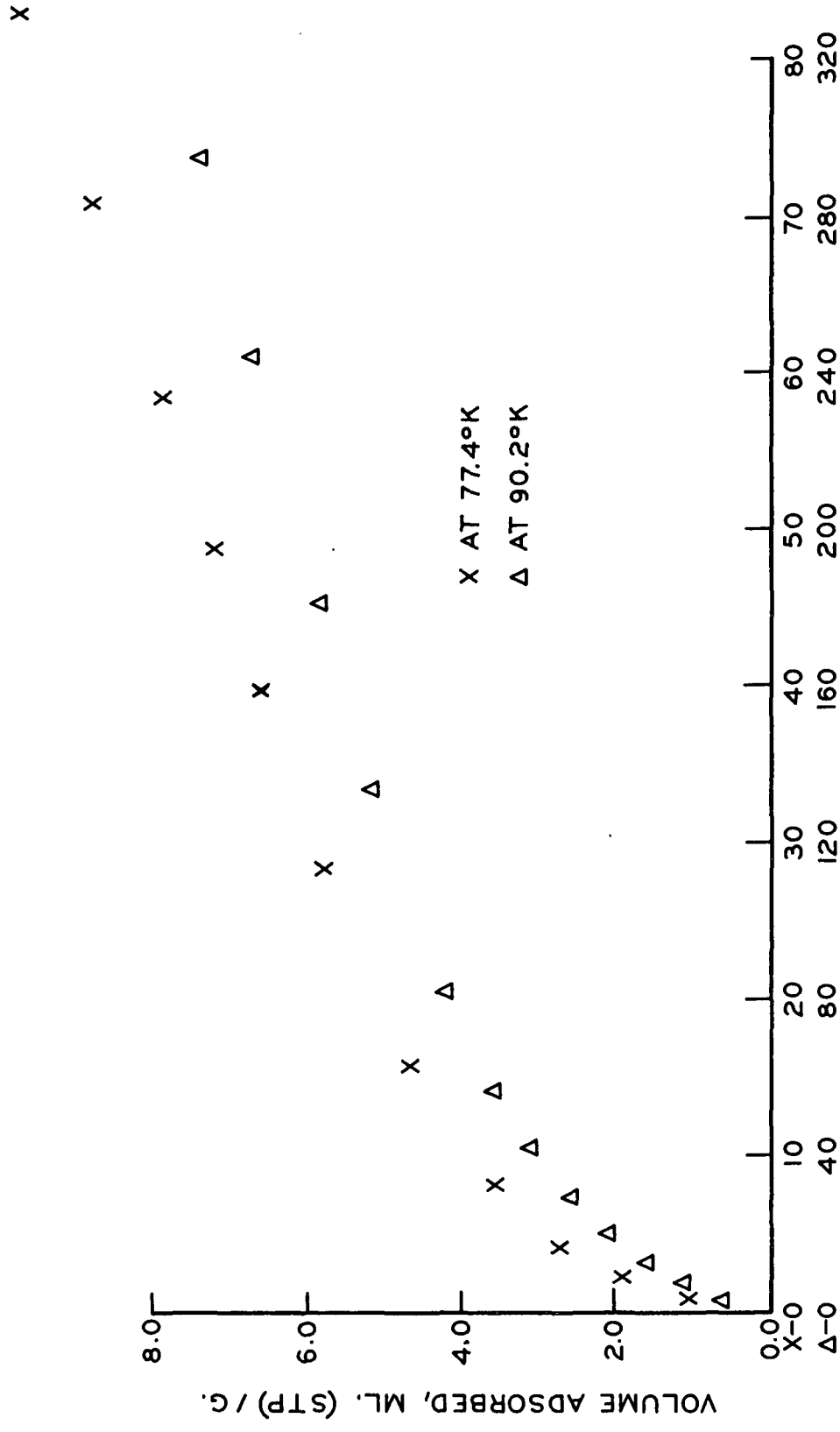

Figure 34. Argon Adsorption Isotherms at 77.4°K and 90.2°K for Sample SV-2B-1

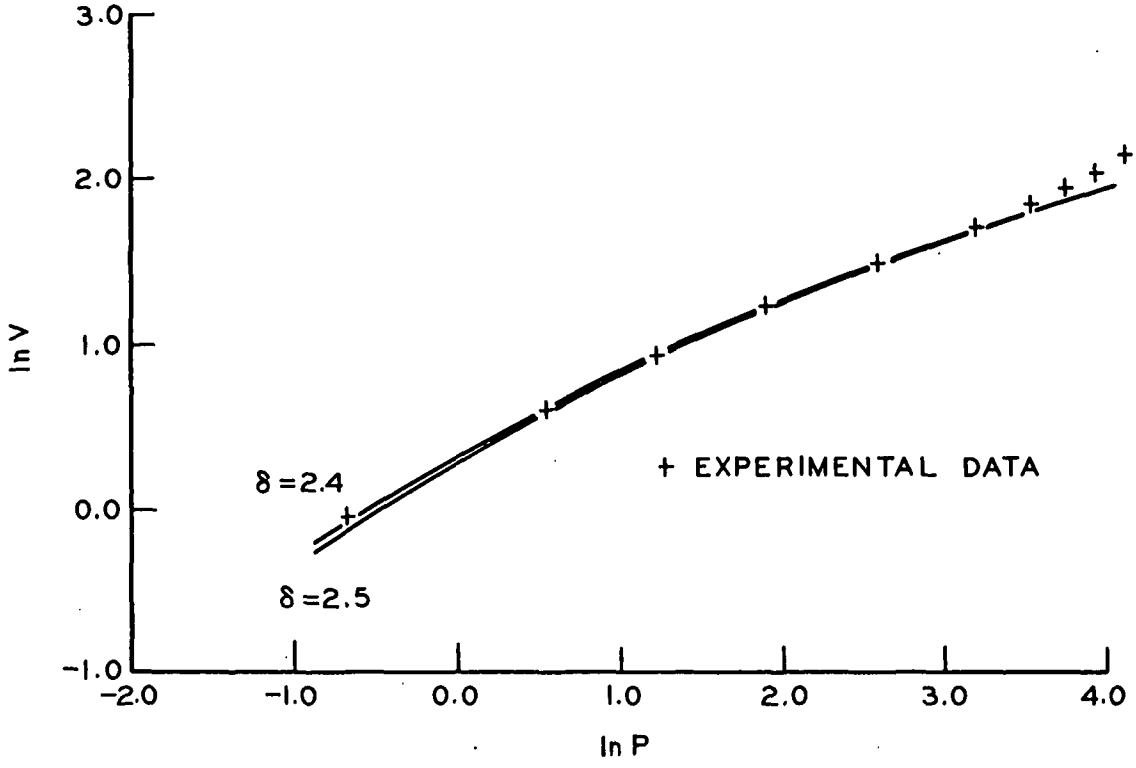

Figure 35. Comparison of Experimental to Model Adsorption Isotherms for Argon Adsorption on SV-2B-1 at 77.4°K

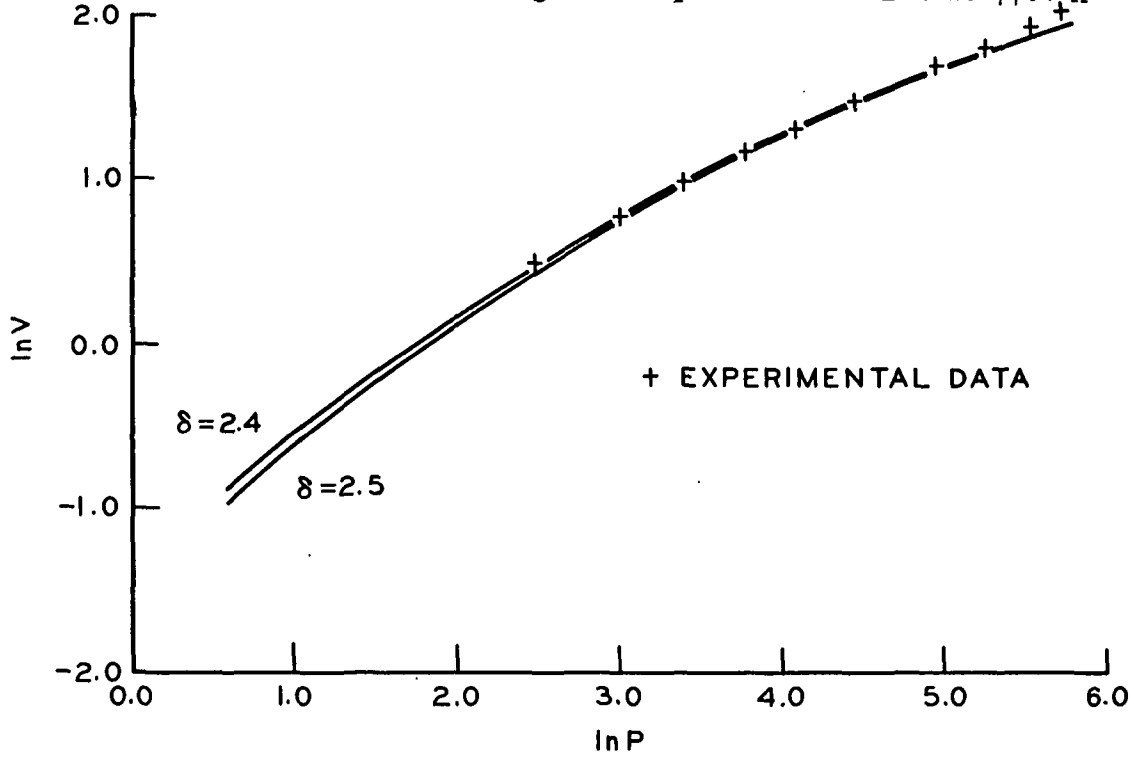

Figure 36. Comparison of Experimental to Model Adsorption Isotherms for Argon Adsorption on SV-2B-1 at 90.2°K

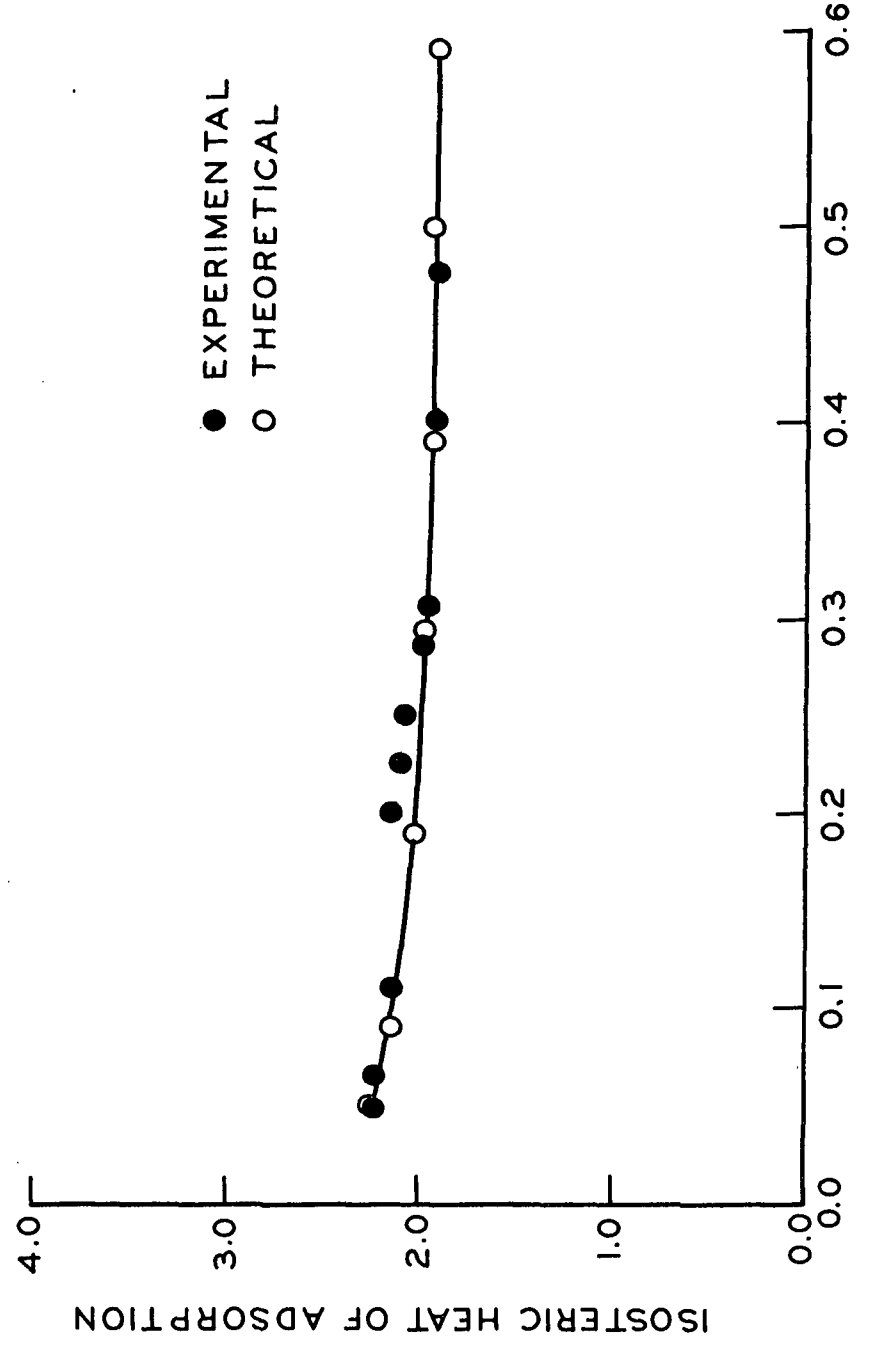

Figure 37. Experimental and Theoretical Isosteric Heat Curves for Argon Adsorption on SV-2B-1

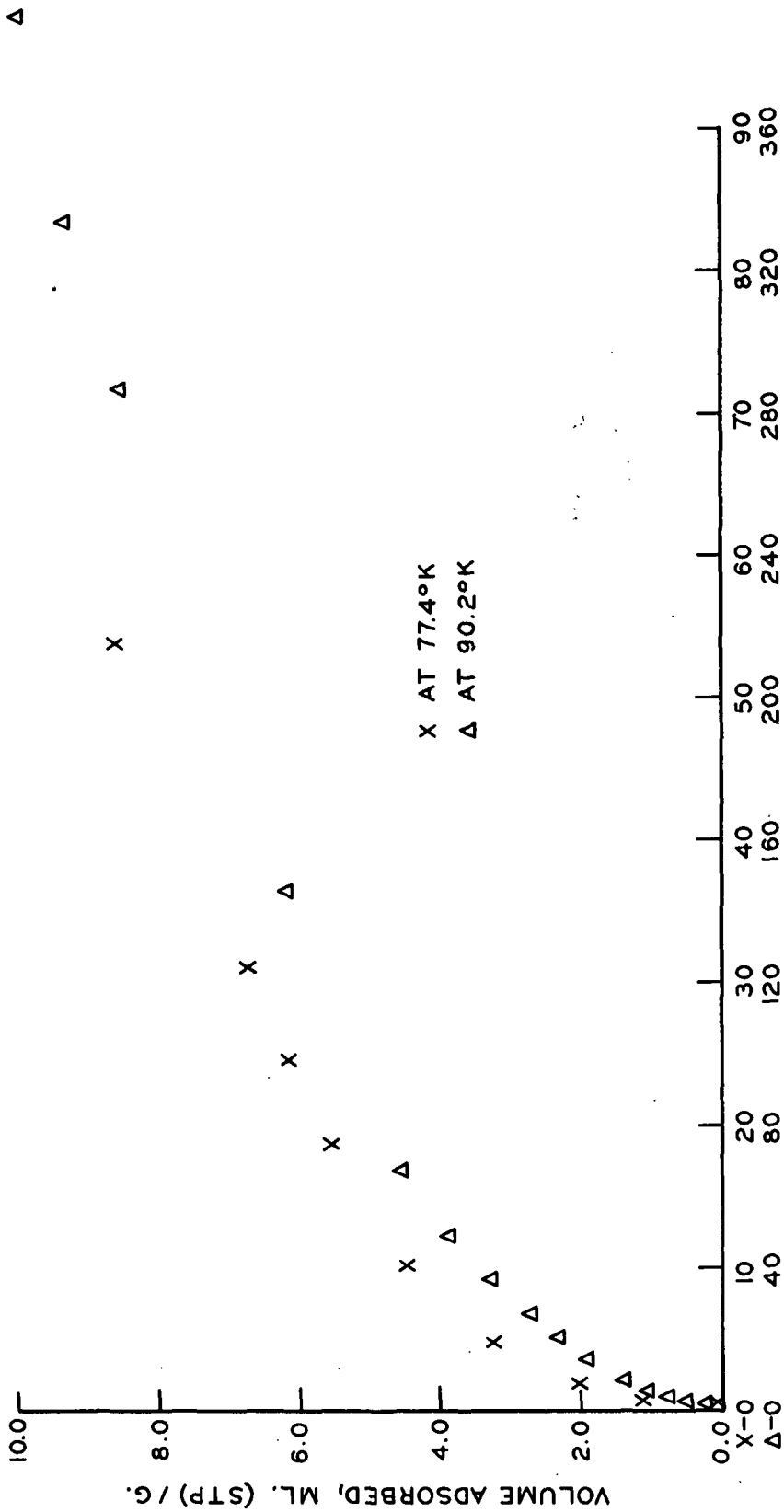

Figure 38. Argon Adsorption Isotherms at 77.4°K and 90.2°K for Sample SV-2B-2

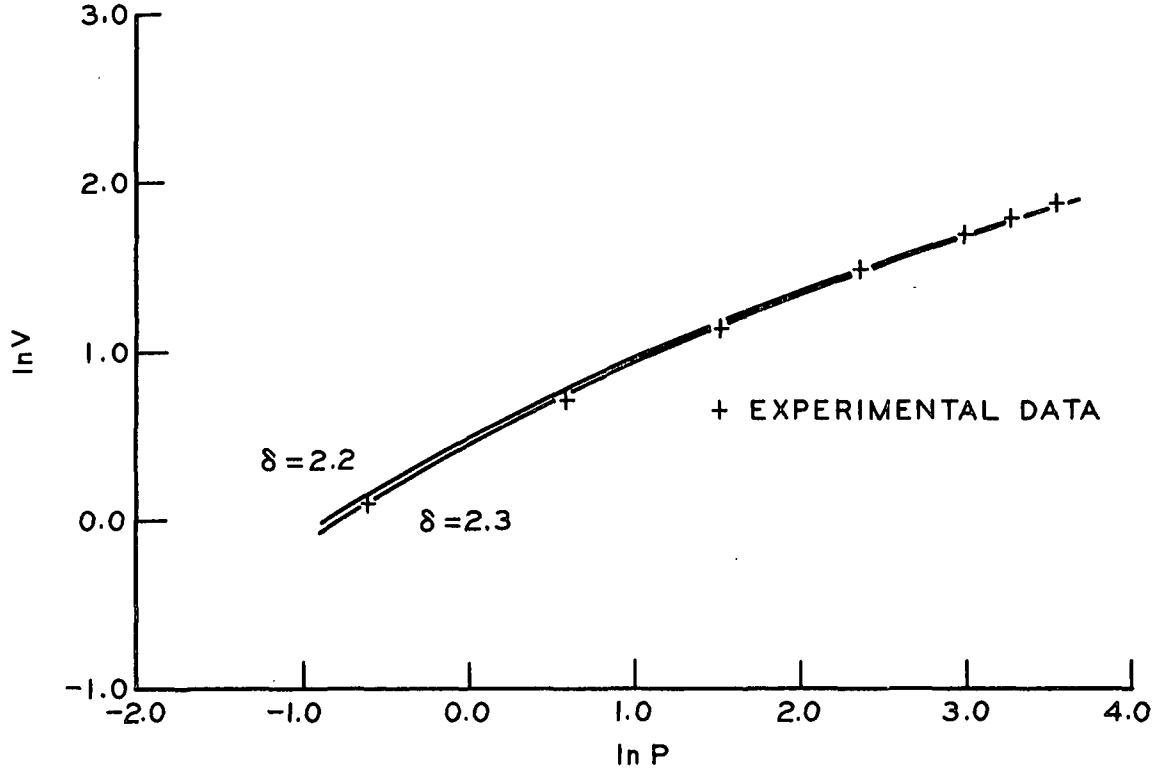

Figure 39. Comparison of Experimental to Model Adsorption Isotherms for Argon Adsorption on SV-2B-2 at 77.4°K

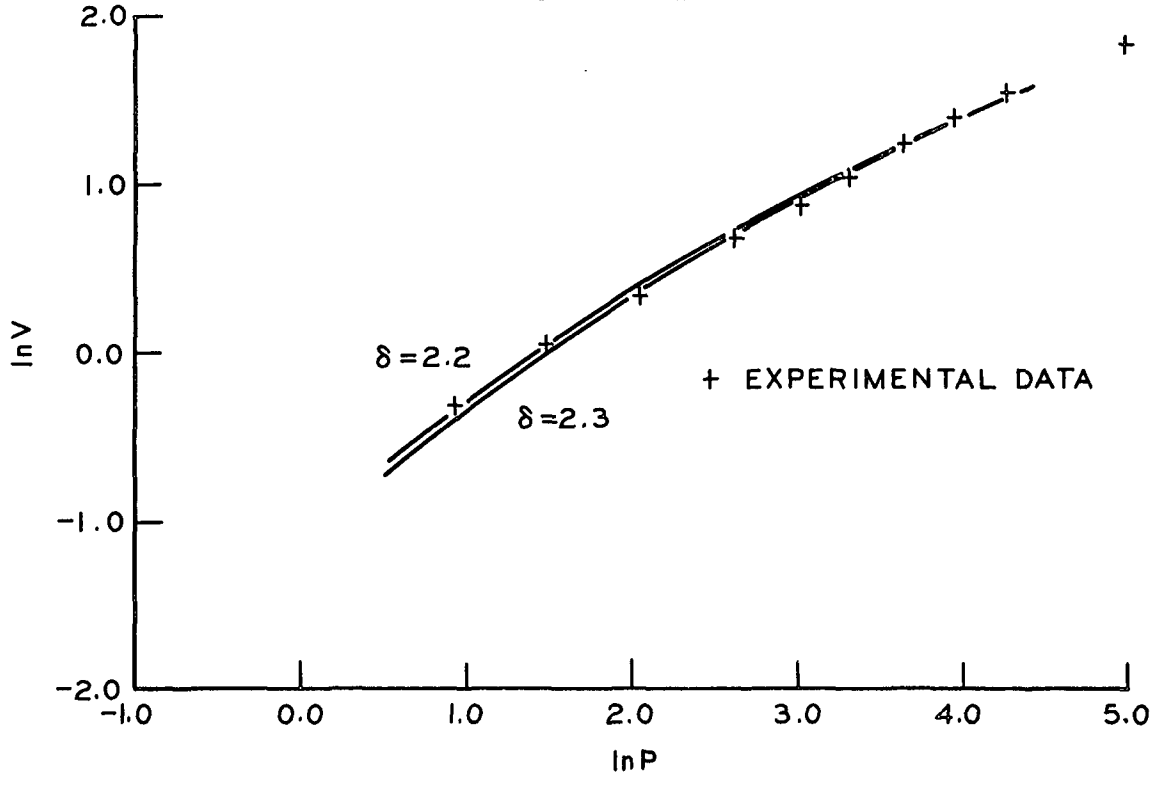

Figure 40. Comparison of Experimental to Model Adsorption Isotherms for Argon Adsorption on SV-2B-2 at 90.2°K

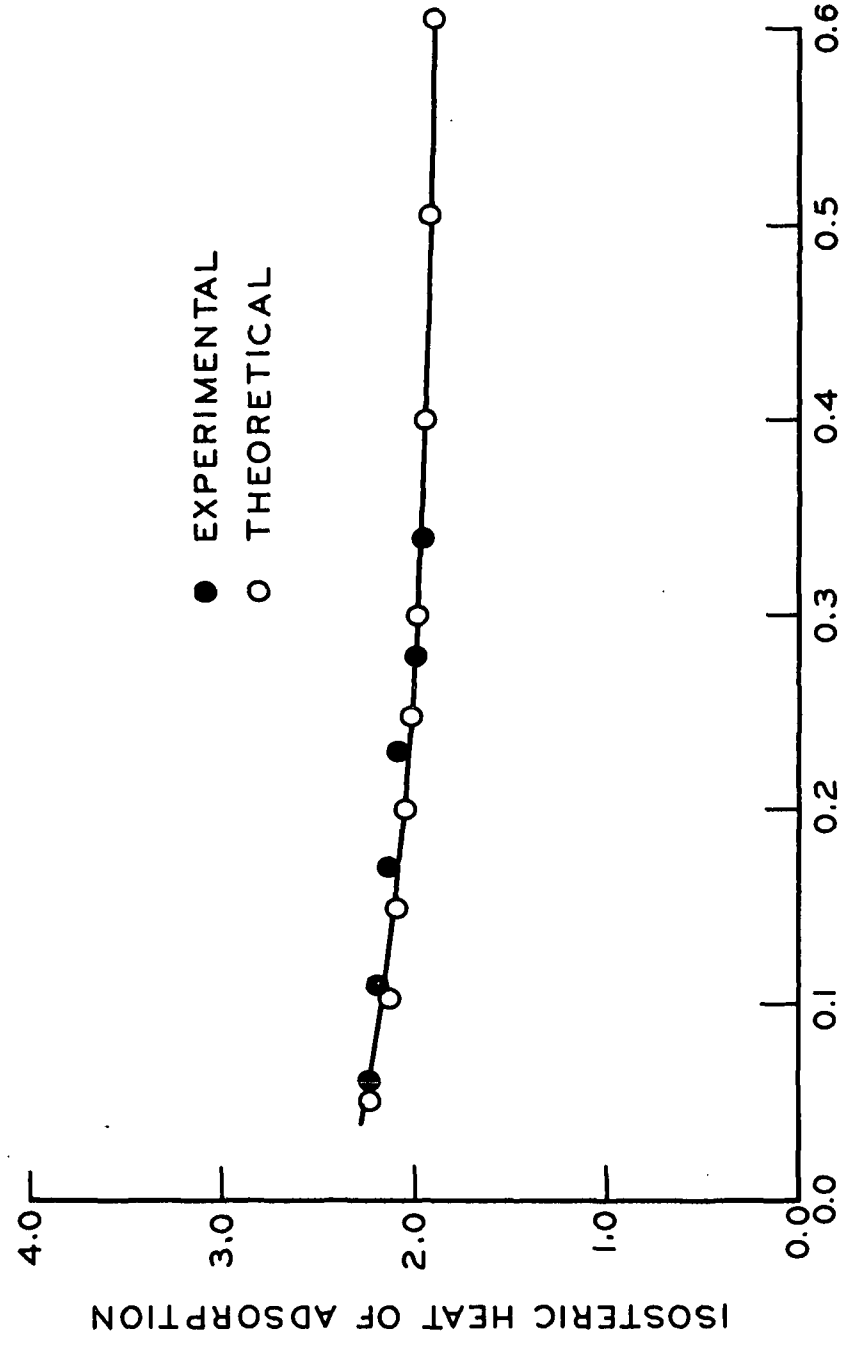

Figure 41. Experimental and Theoretical Isosteric Heat Curves for Argon Adsorption on SV-2B-2

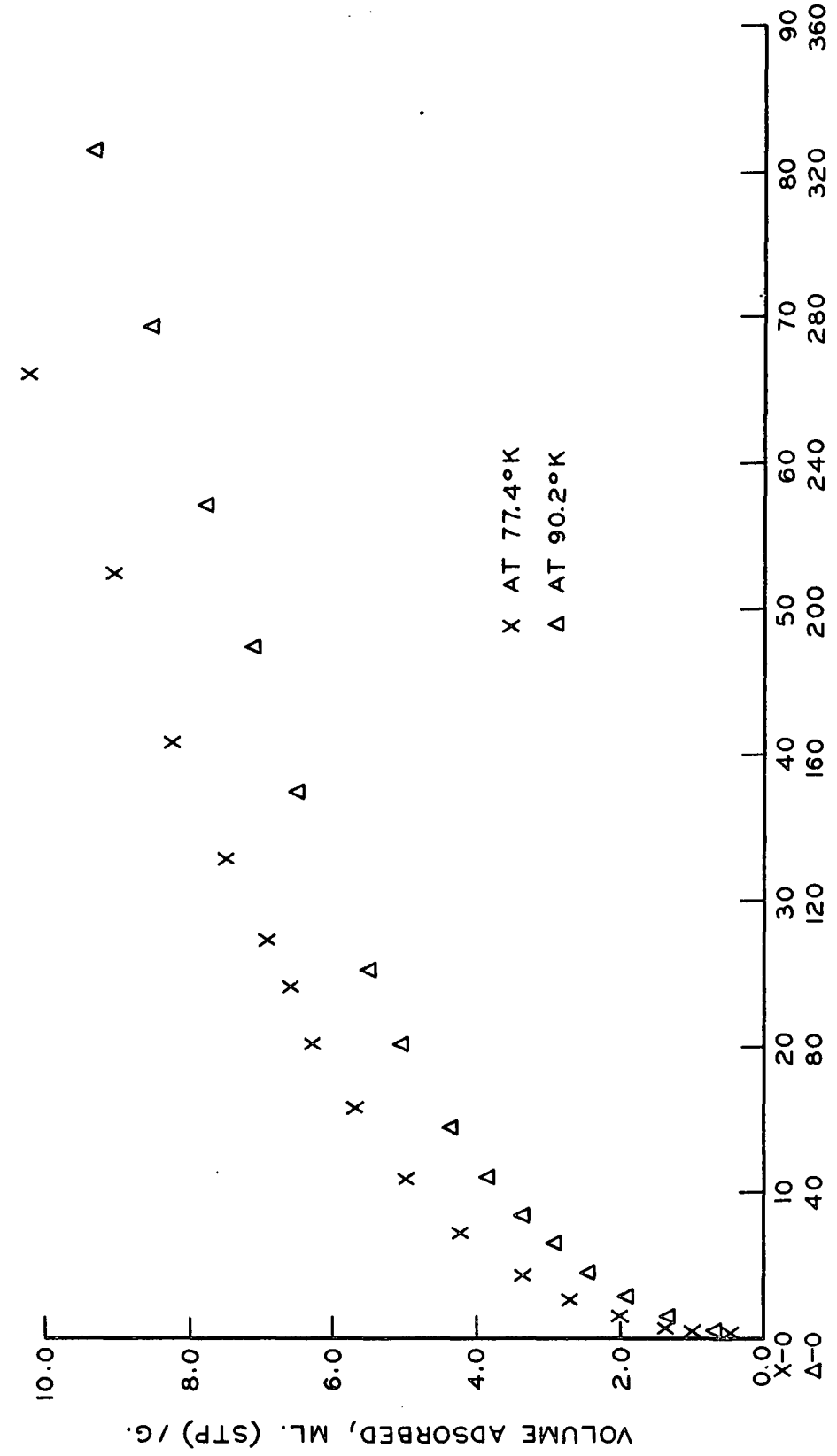

Figure 42. Argon Adsorption Isotherms at 77.4°K and 90.2°K for Sample SV-2B-3

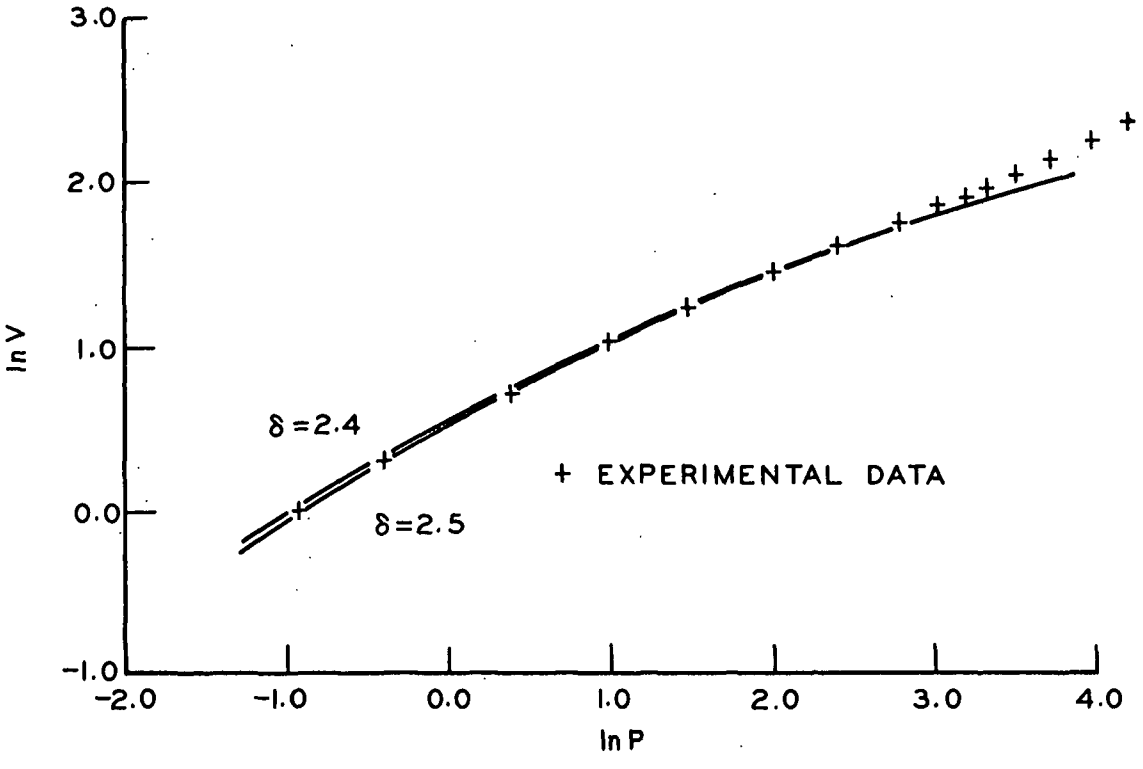

Figure 43. Comparison of Experimental to Model Adsorption Isotherms for Argon Adsorption on SV-2B-3 at 77.4°K

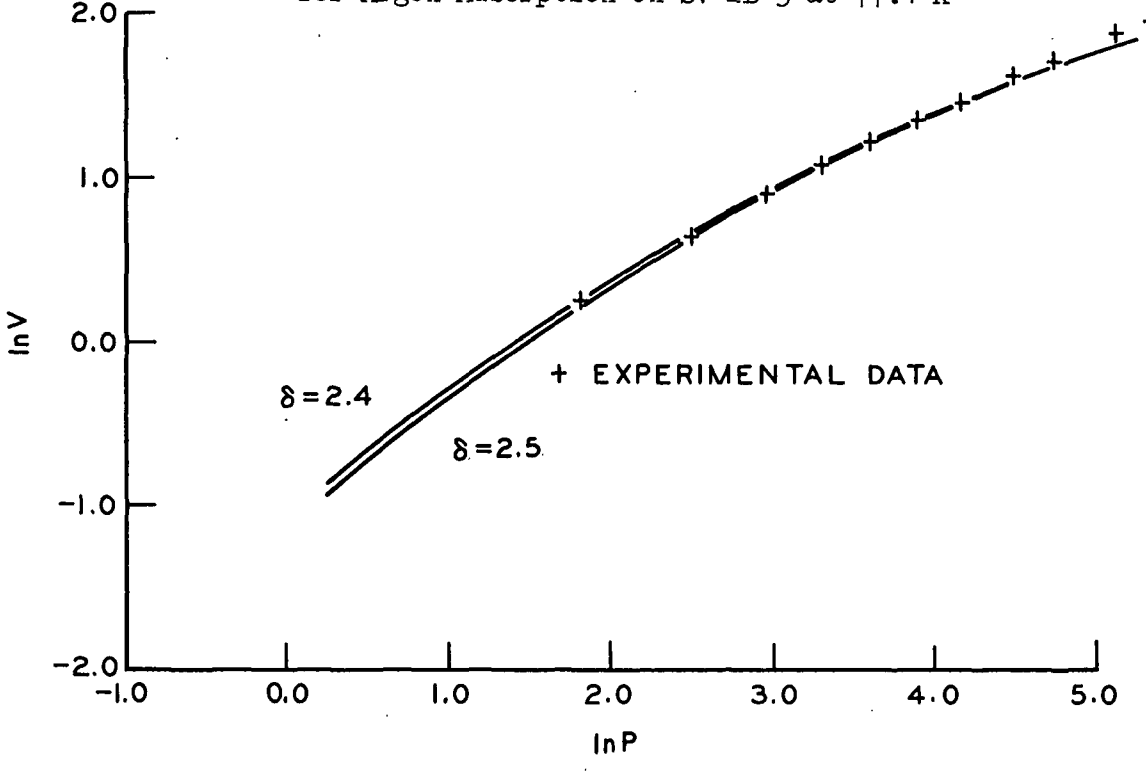

Figure 44. Comparison of Experimental to Model Adsorption Isotherms for Argon Adsorption on SV-2B-3 at 90.2°K

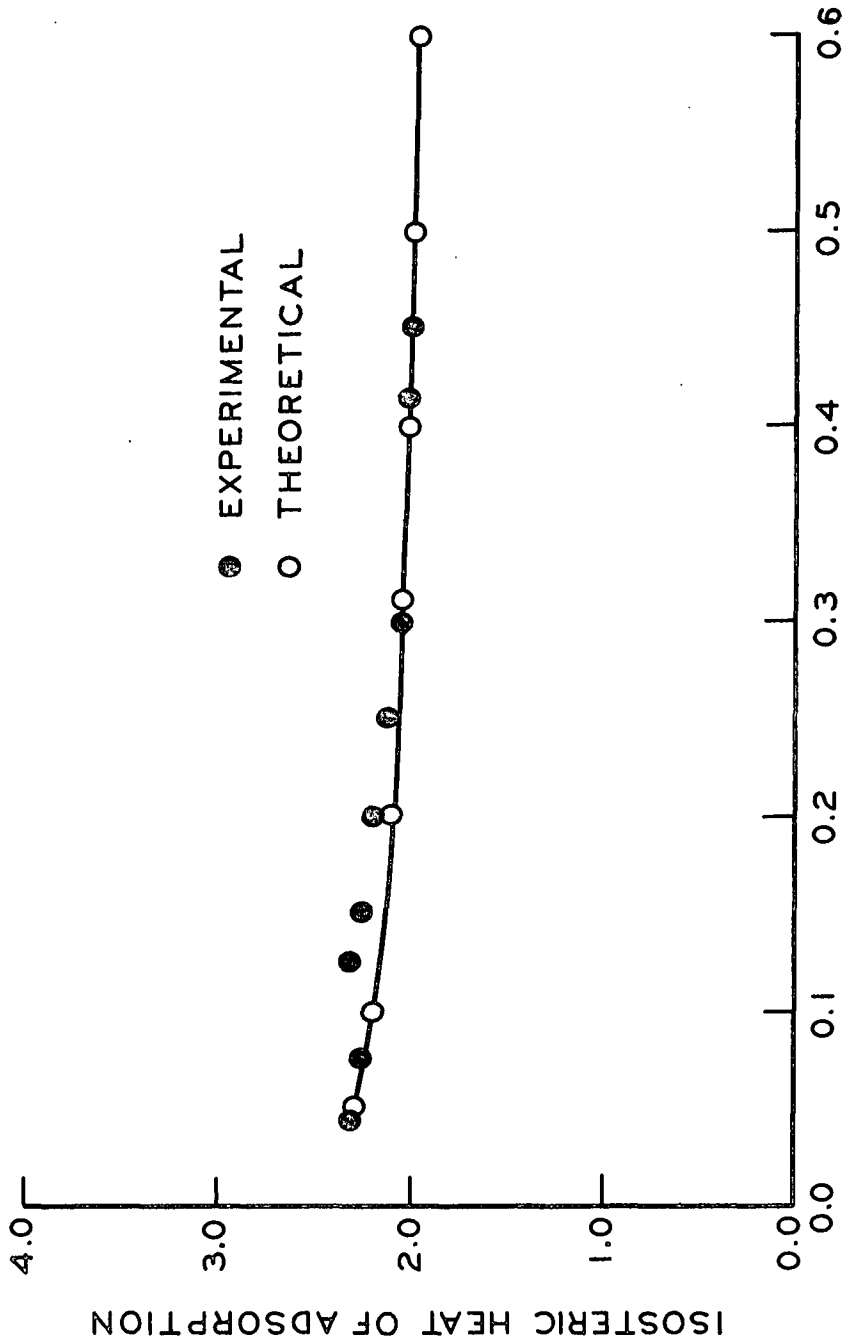

Figure 45. Experimental and Theoretical Isosteric Heat Curves for Argon Adsorption on SV-2B-3

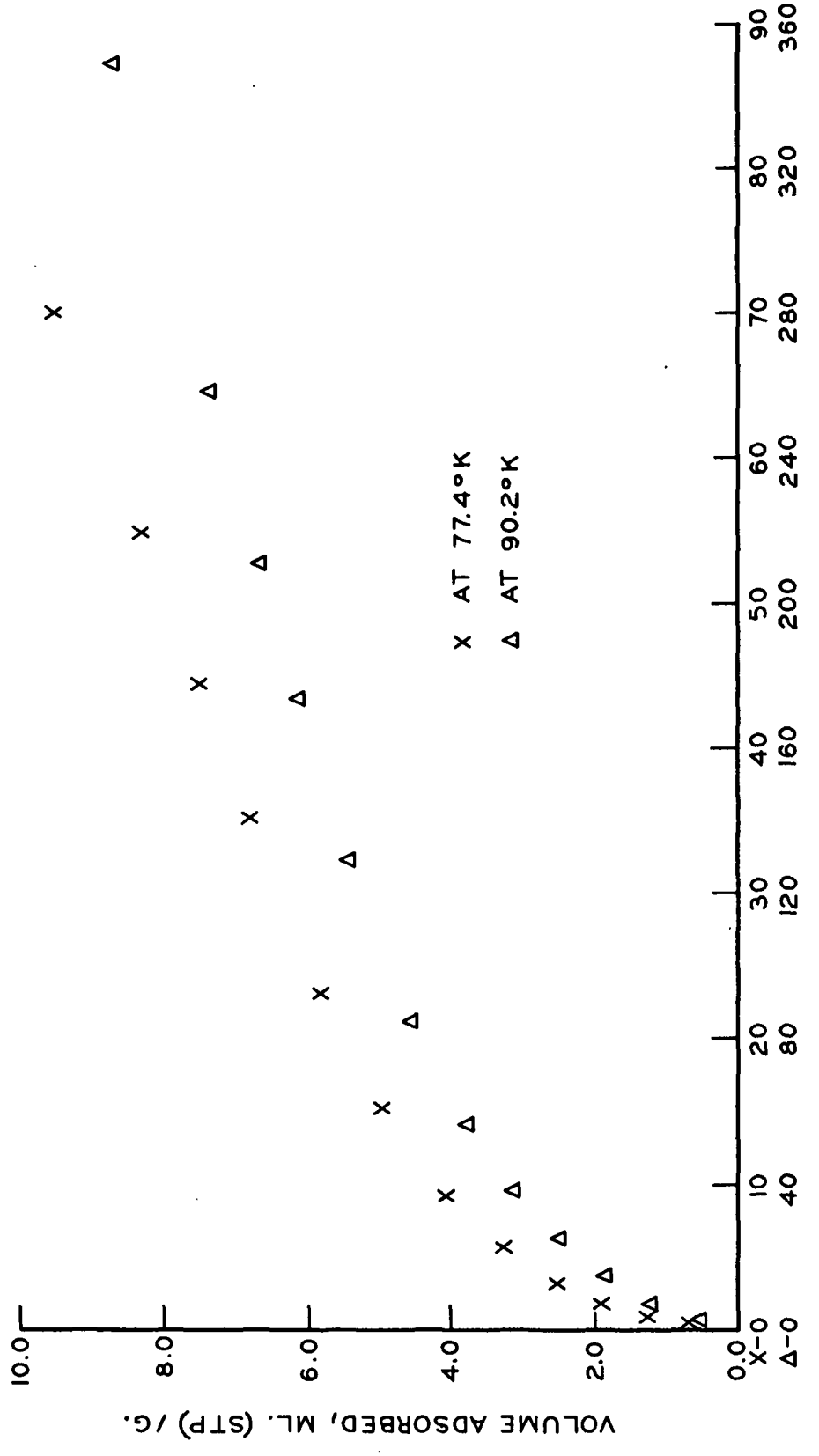

Figure 46. Argon Adsorption Isotherms at 77.4°K and 90.2°K for Sample SV-2B-4

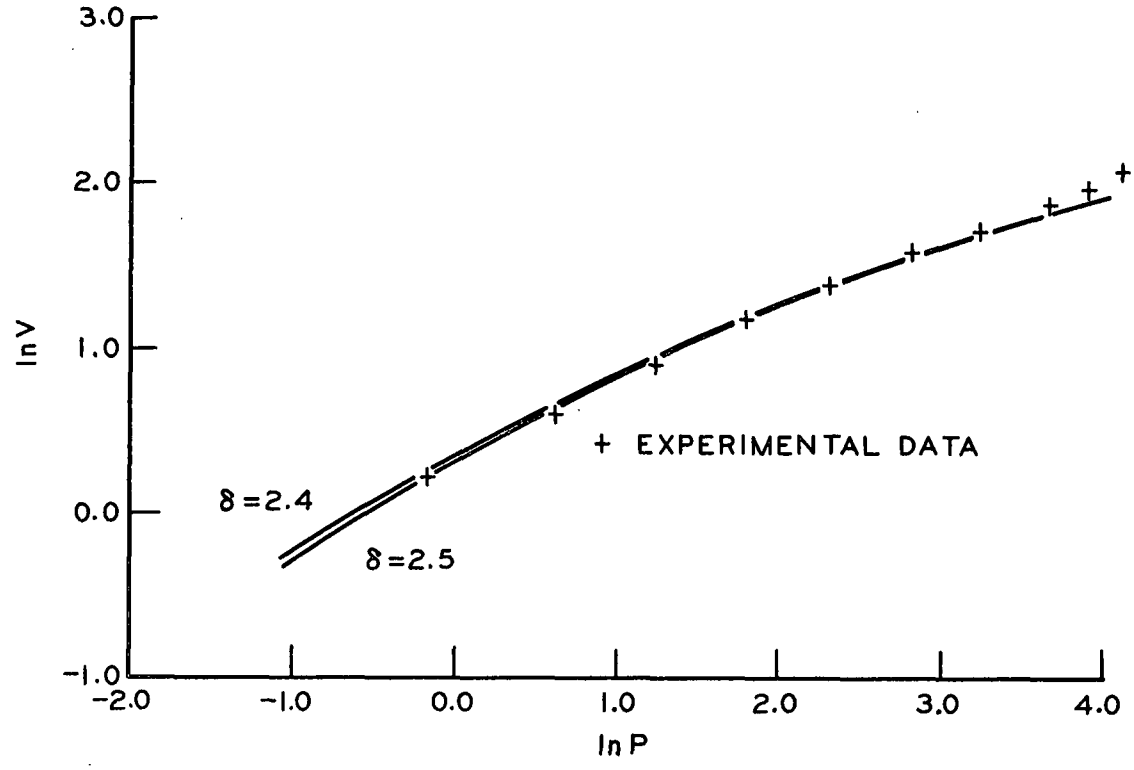

Figure 47. Comparison of Experimental to Model Adsorption Isotherms for Argon Adsorption on SV-2B-4 at 77.4°K

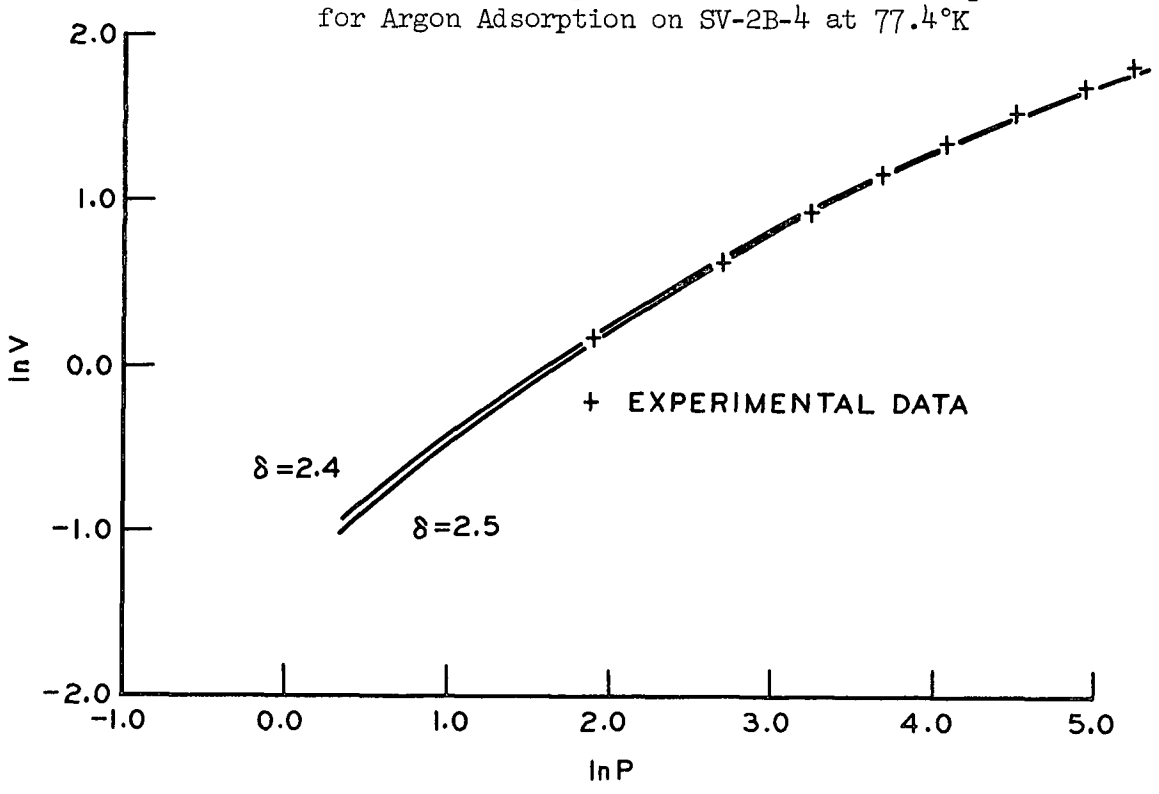

Figure 48. Comparison of Experimental to Model Adsorption Isotherms for Argon Adsorption on SV-2B-4 at 90.2°K

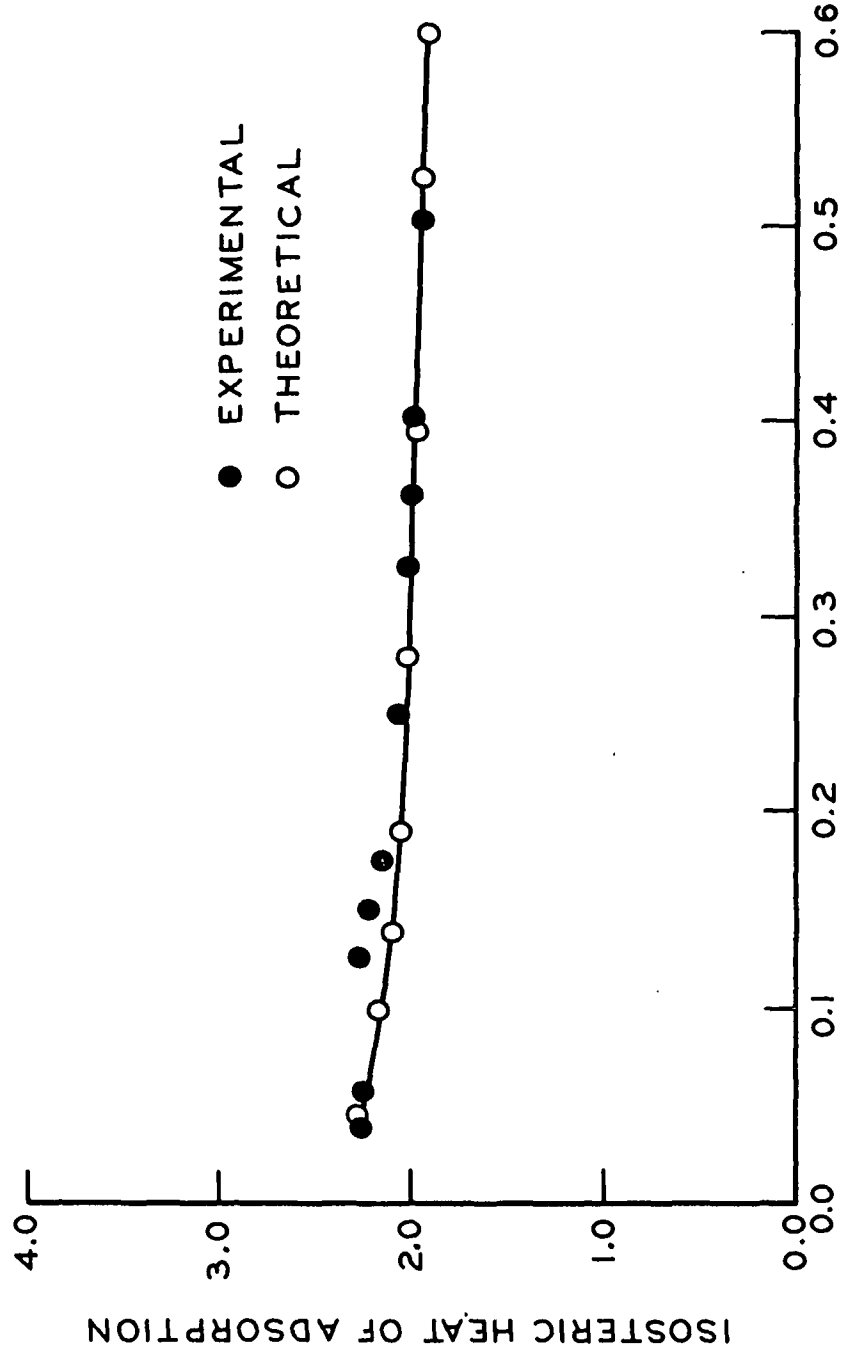

Figure 49. Experimental and Theoretical Isosteric Heat Curves for Argon Adsorption on SV-2B-4

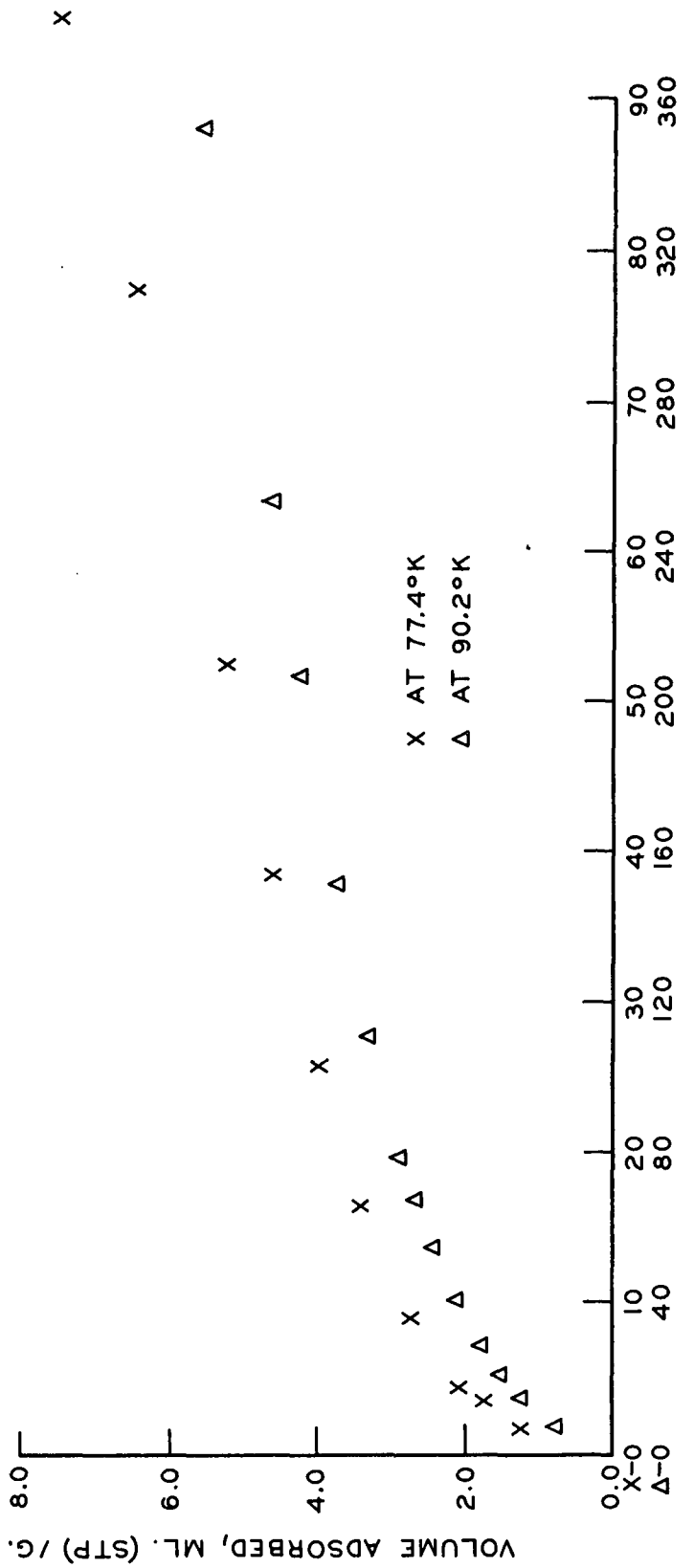

Figure 50. Argon Adsorption Isotherms at 77.4°K and 90.2°K for Sample SV-2B-5

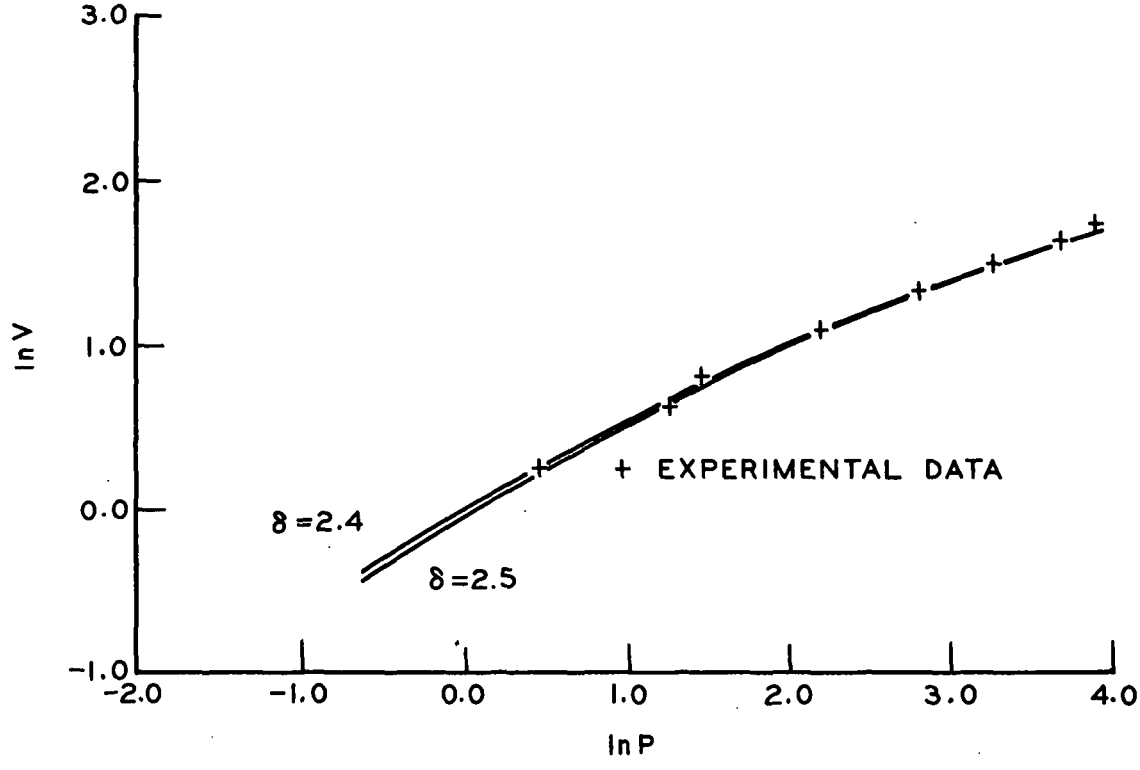

Figure 51. Comparison of Experimental to Model Adsorption Isotherms for Argon Adsorption on SV-2B-5 at 77.4°K

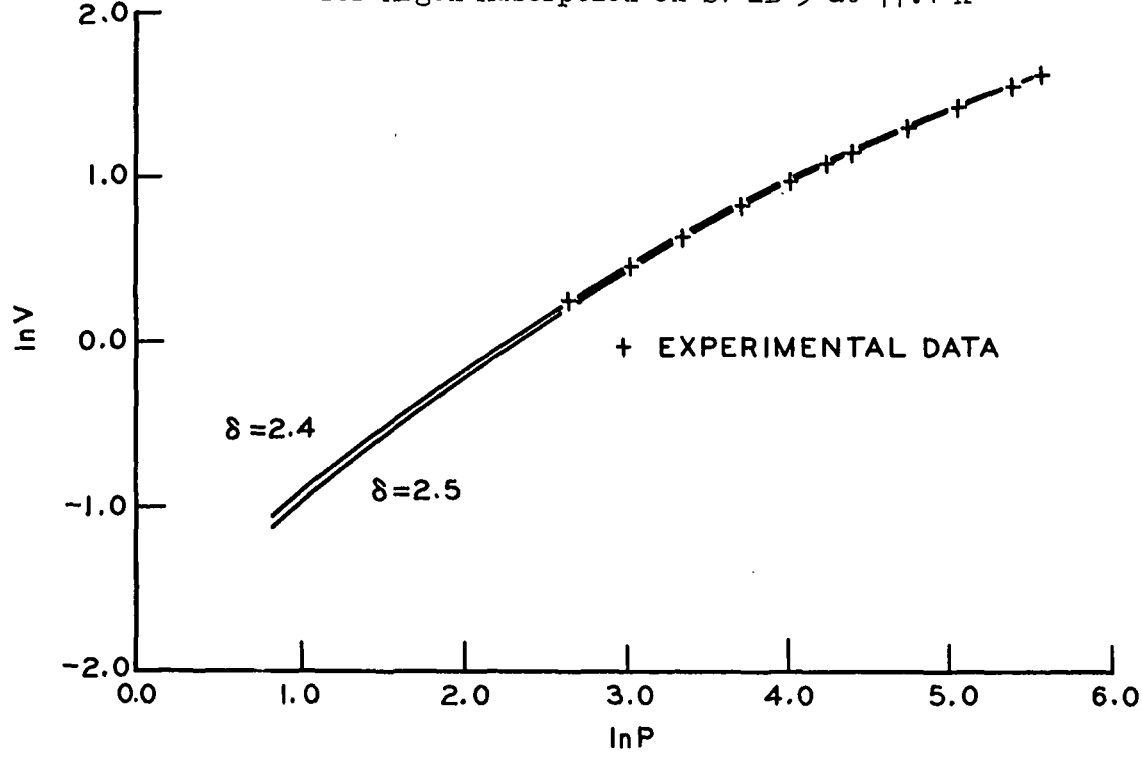

Figure 52. Comparison of Experimental to Model Adsorption Isotherms for Argon Adsorption on SV-2B-5 at 90.2°K

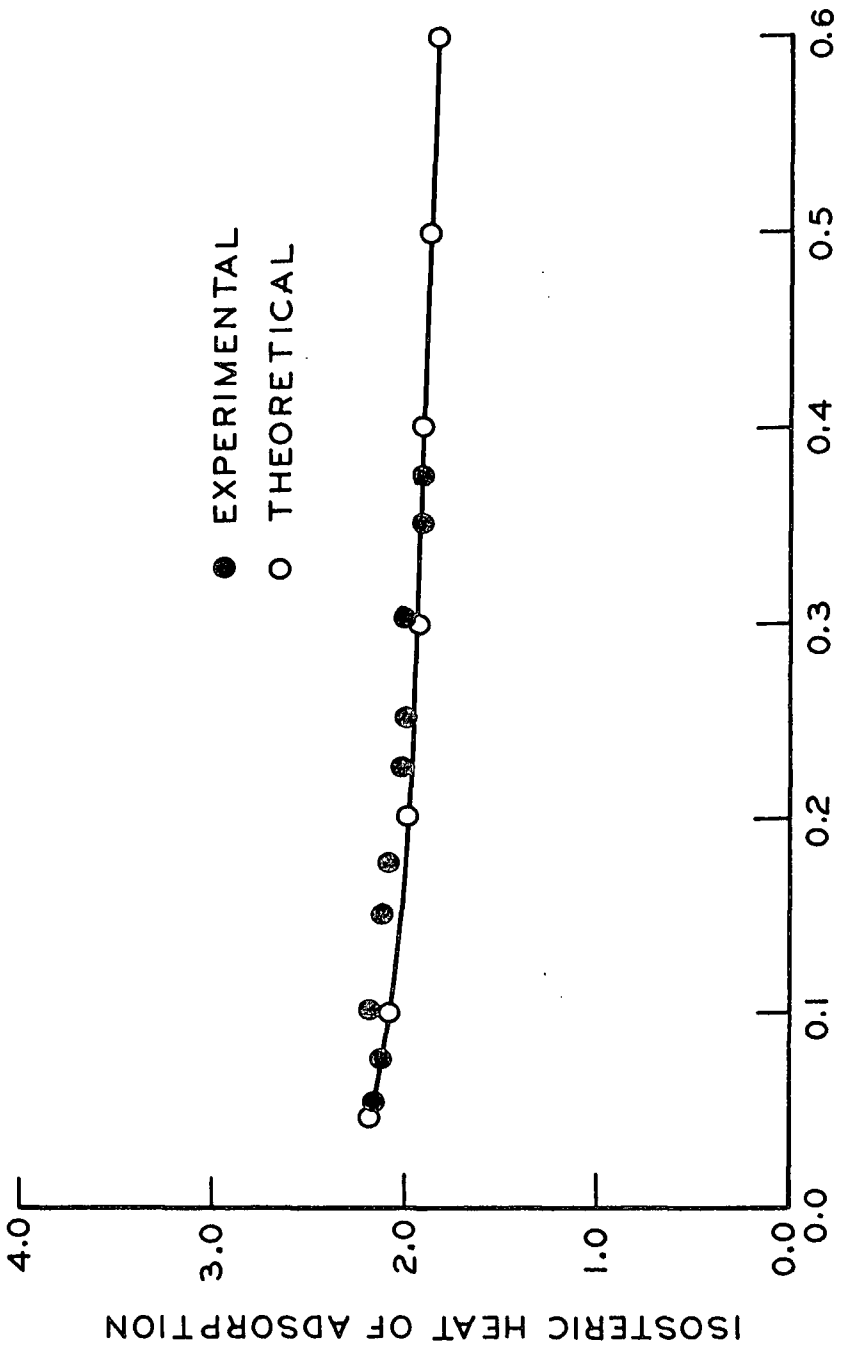

Figure 53. Experimental and Theoretical Isosteric Heat Curves for Argon Adsorption on Sample SV-2B-5

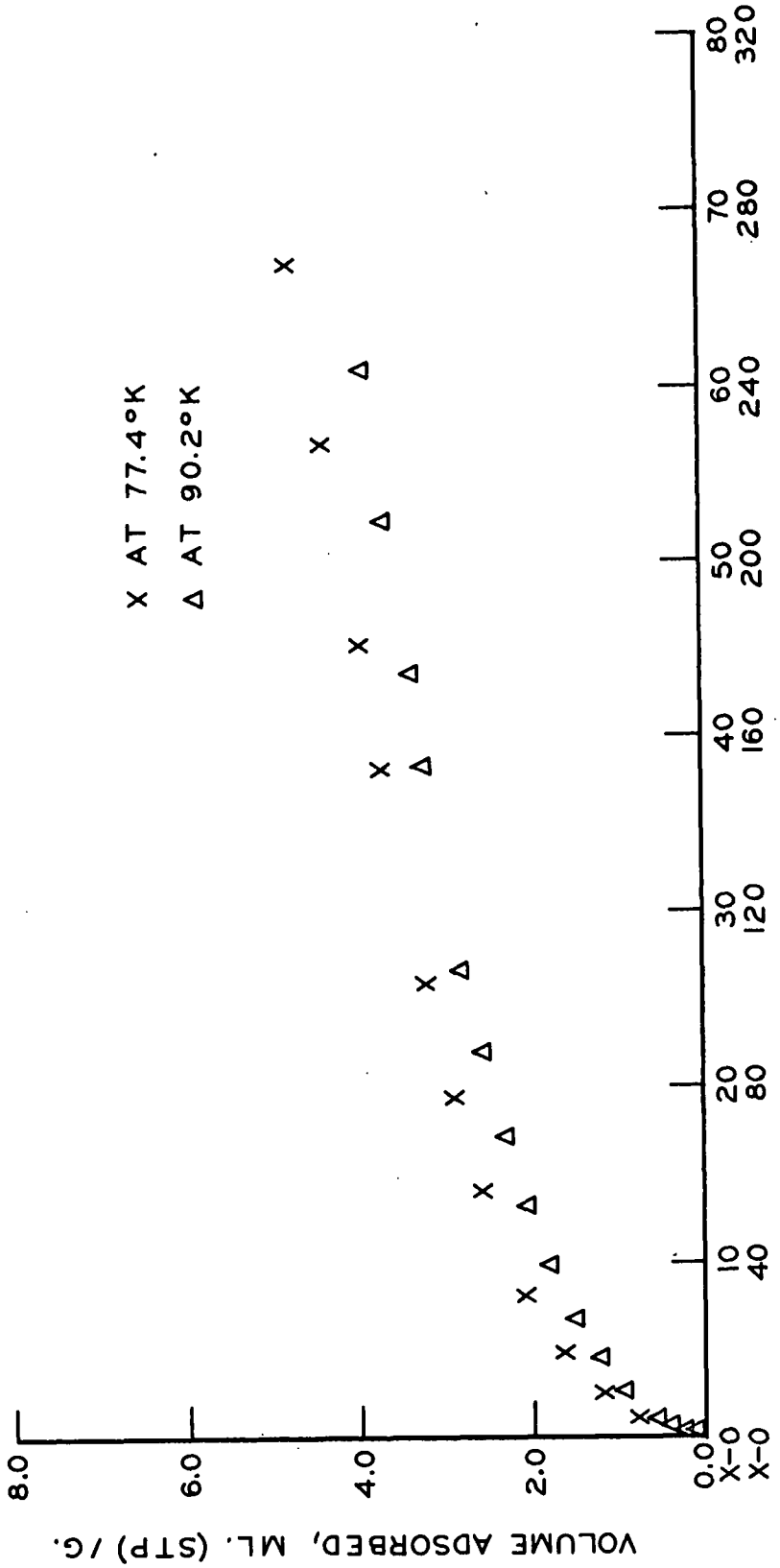

Figure 54. Argon Adsorption Isotherms at 77.4°K and 90.2°K for Sample SV-2B-6

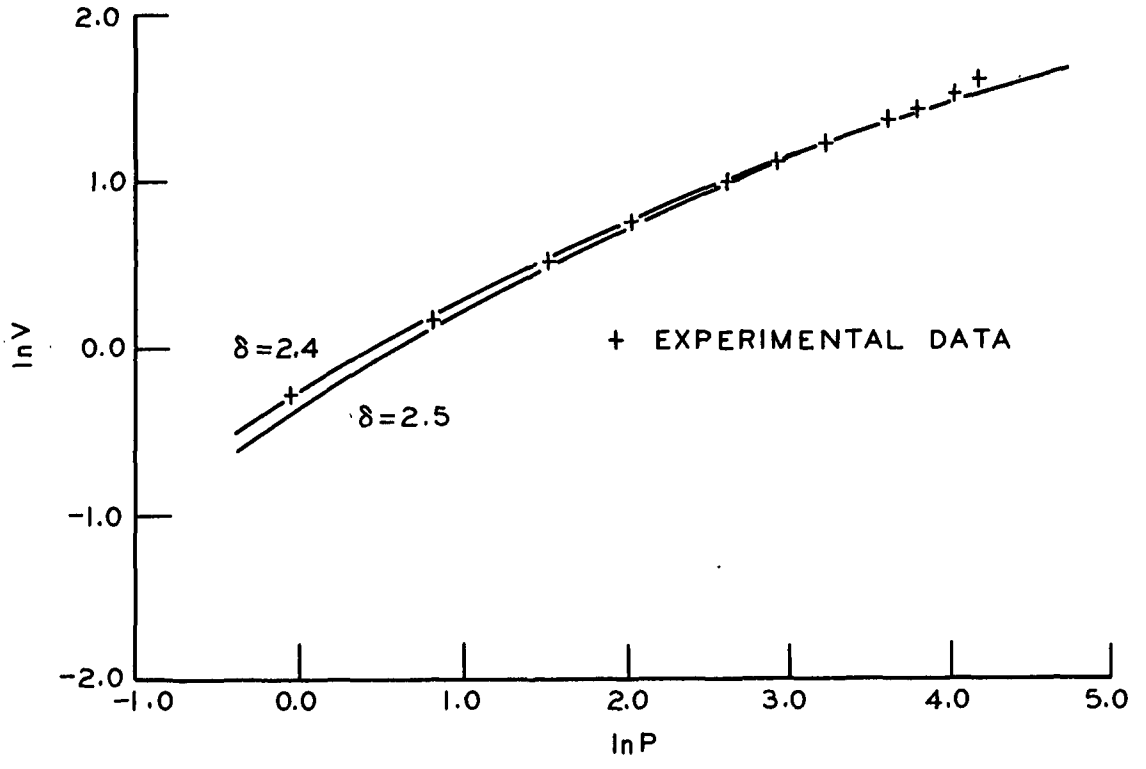

Figure 55. Comparison of Experimental to Model Adsorption Isotherms for Argon Adsorption on SV-2B-6 at 77.4°K

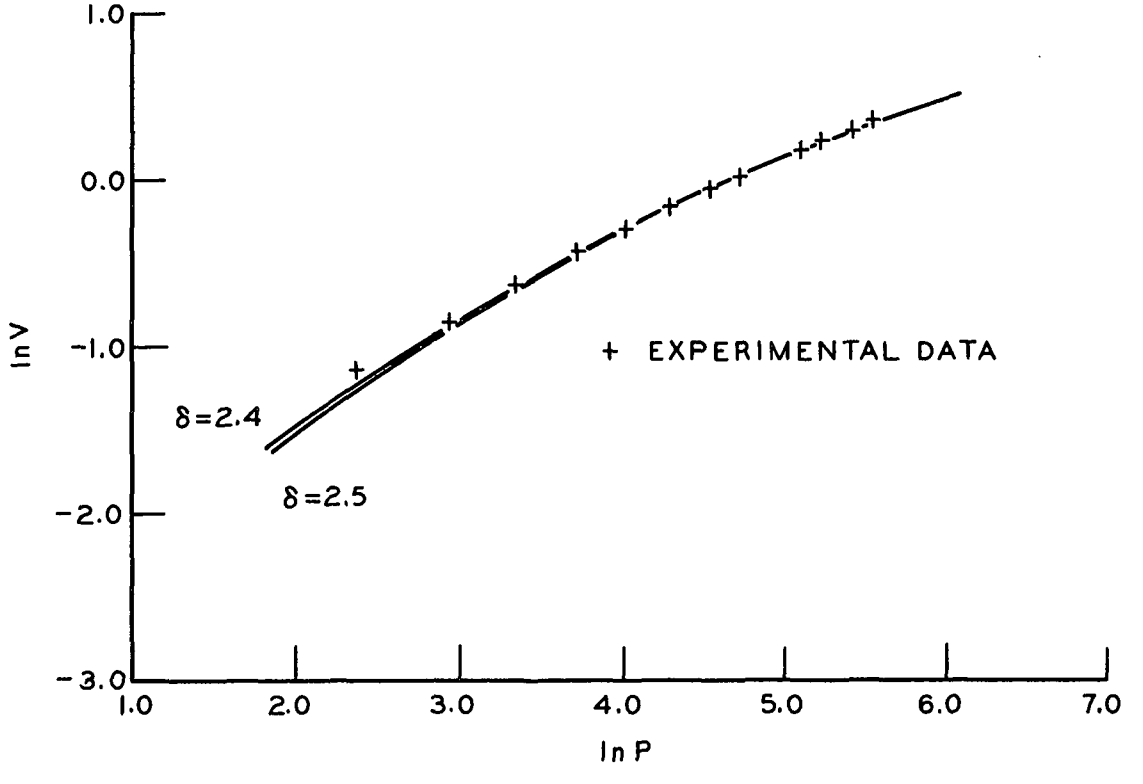

Figure 56. Comparison of Experimental to Model Adsorption Isotherms for Argon Adsorption on SV-2B-6 at 90.2°K

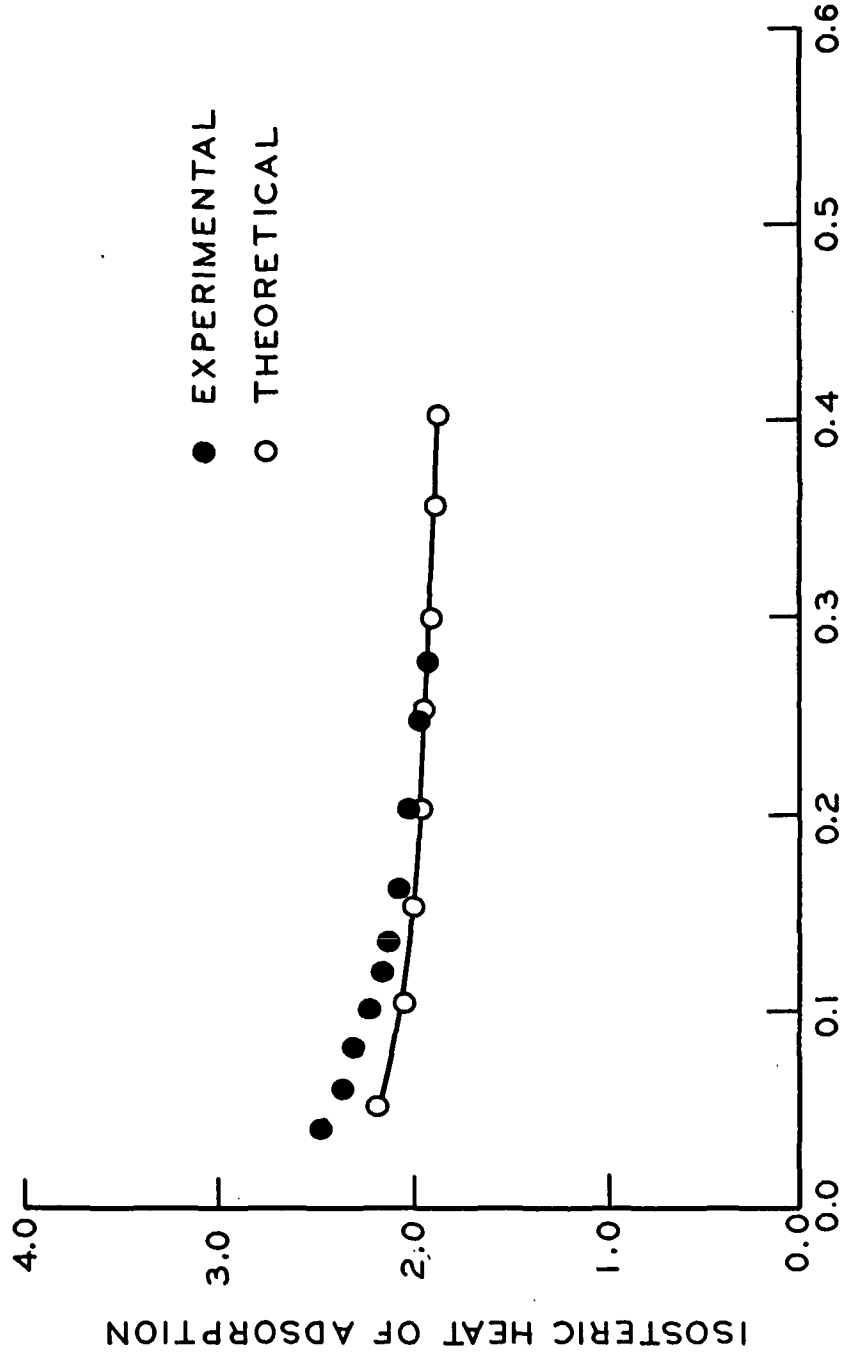

Figure 57. Experimental and Theoretical Isosteric Heat Curves for Argon Adsorption on Sample SV-2B-6

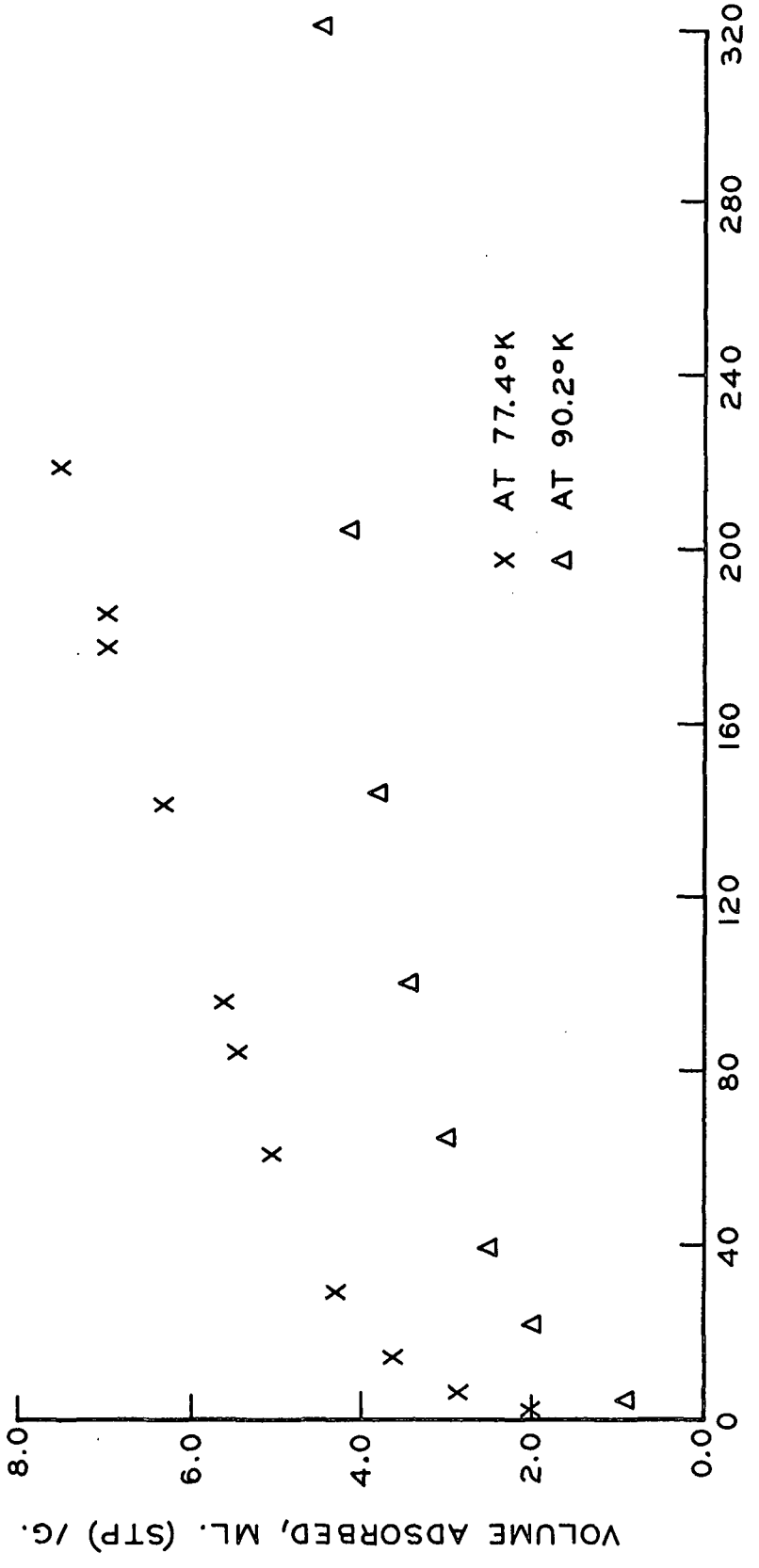

Figure 58. Nitrogen Adsorption Isotherms at 77.4°K and 90.2°K for Sample SV-2B-1

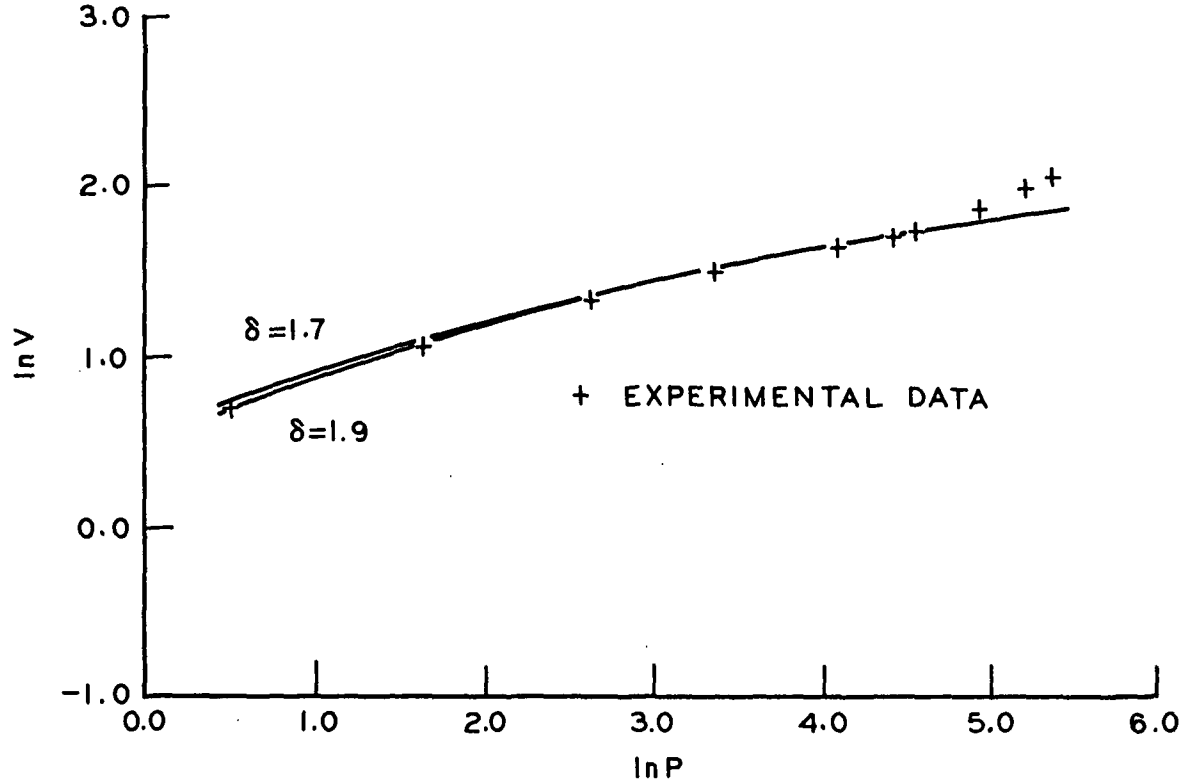

Figure 59. Comparison of Experimental to Model Adsorption Isotherms for Nitrogen Adsorption on SV-2B-1 at 77.4°K

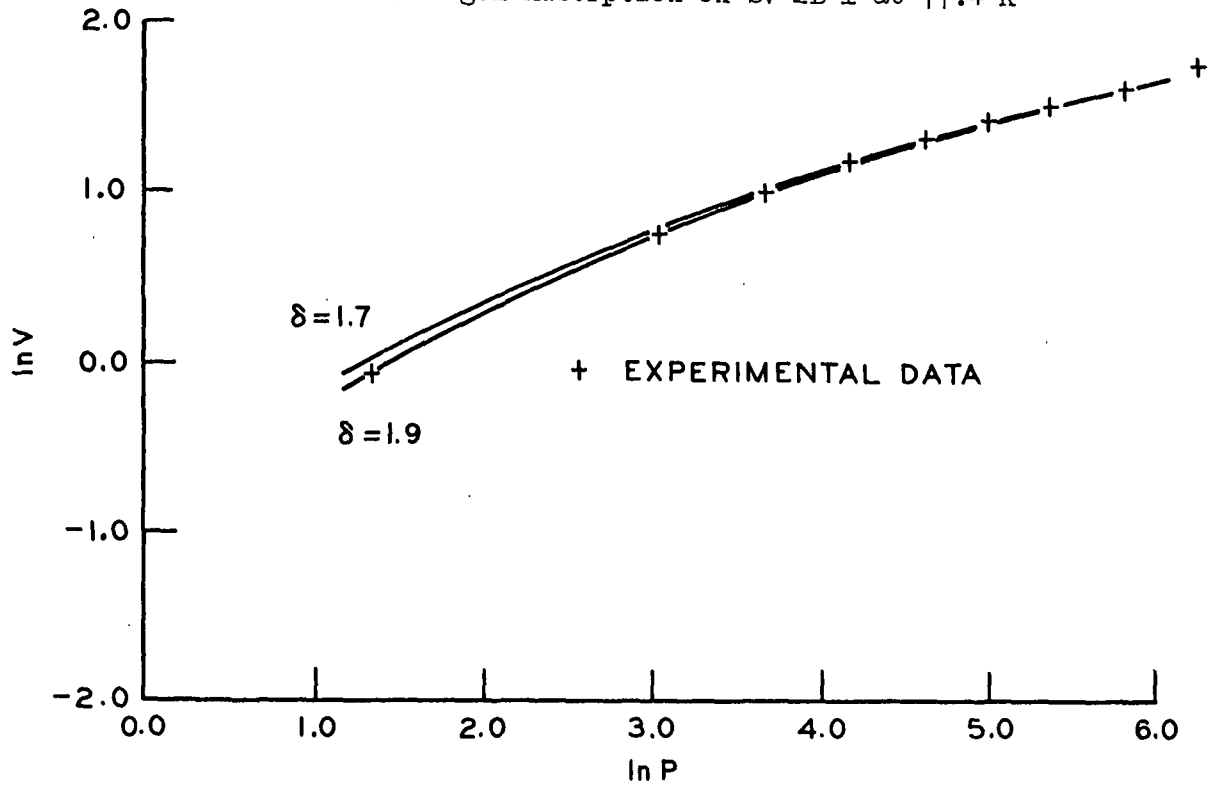

Figure 60. Comparison of Experimental to Model Adsorption Isotherms for Nitrogen Adsorption on SV-2B-1 at 90.2°K

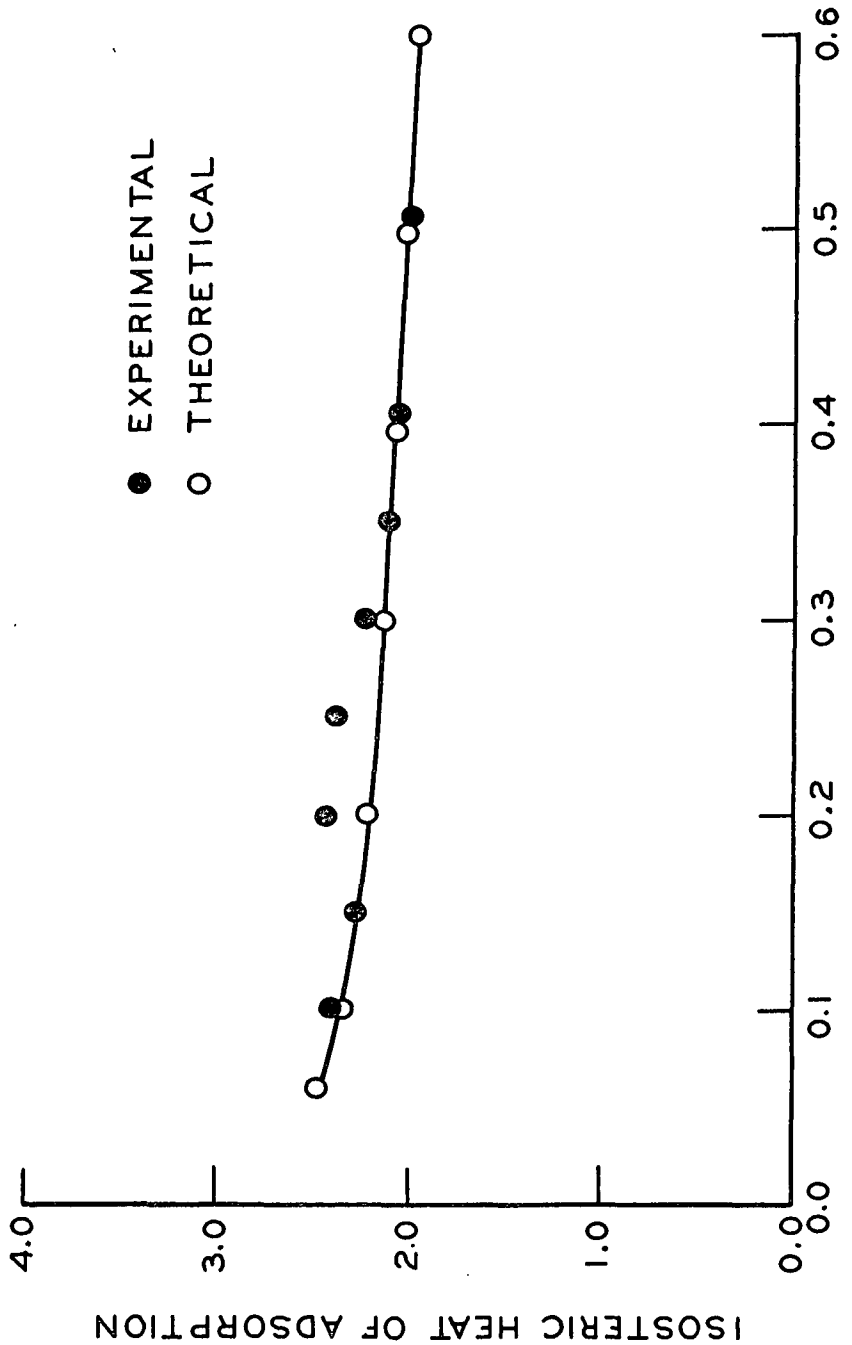

Figure 61. Experimental and Theoretical Isosteric Heat Curves for Nitrogen Adsorption on SV-2B-1

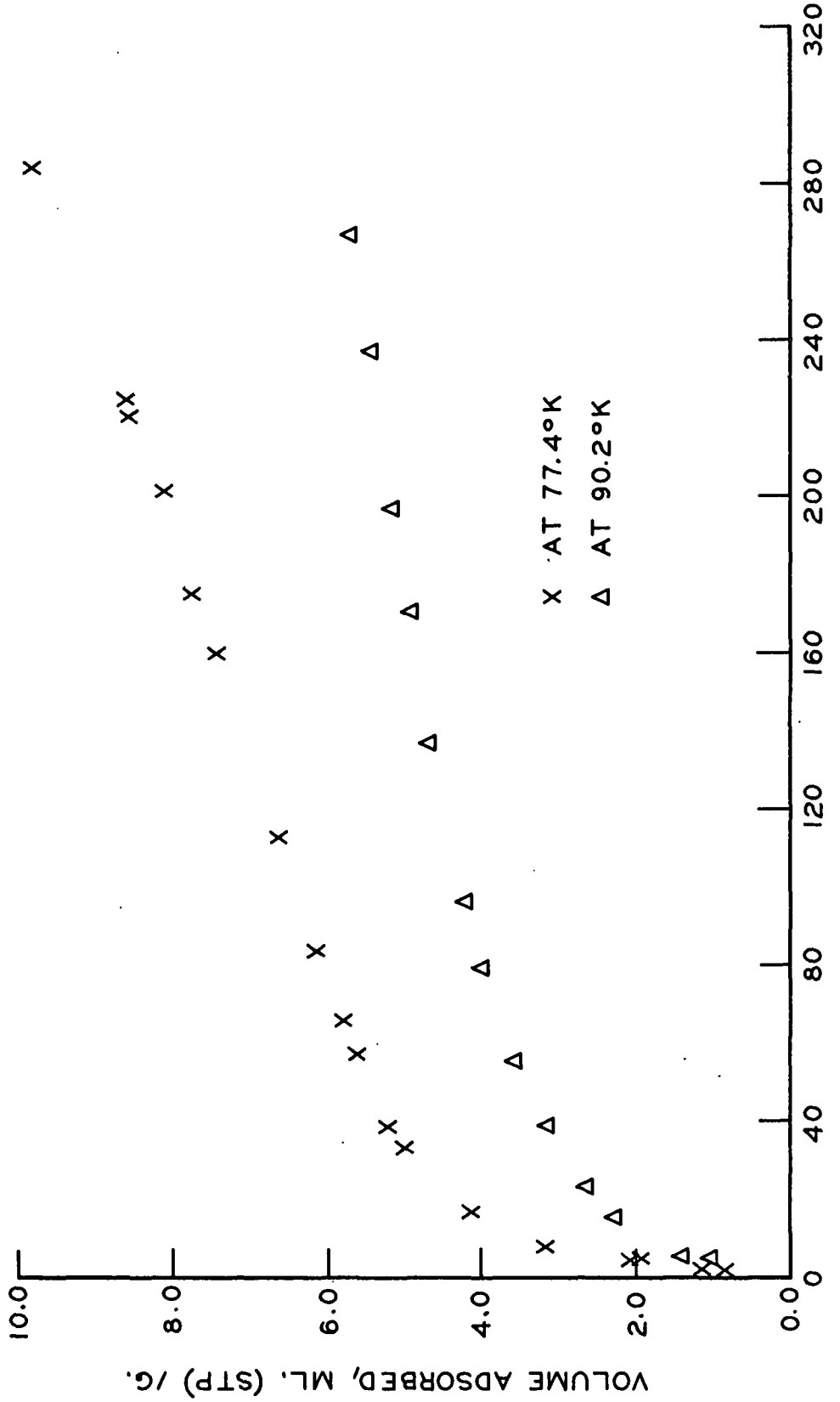

Figure 62. Nitrogen Adsorption Isotherms at 77.4°K and 90.2°K for Sample SV-2B-2

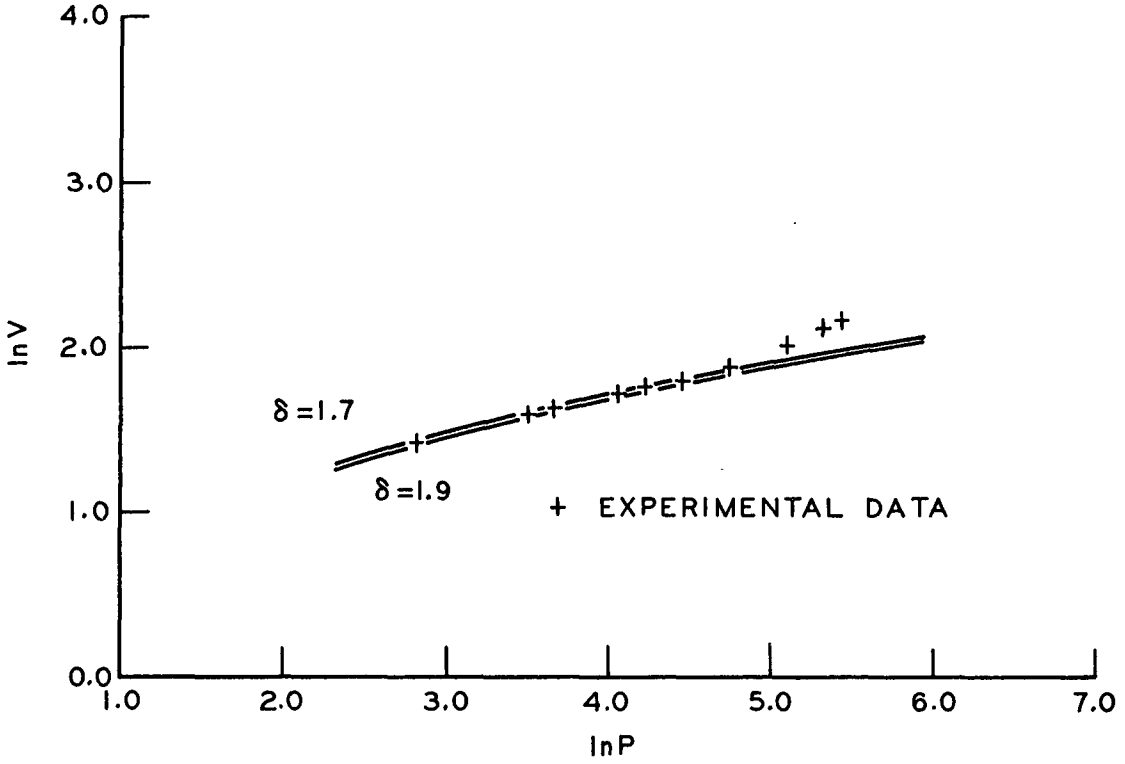

Figure 63. Comparison of Experimental to Model Adsorption Isotherms for Nitrogen Adsorption on SV-2B-2 at 77.4°K

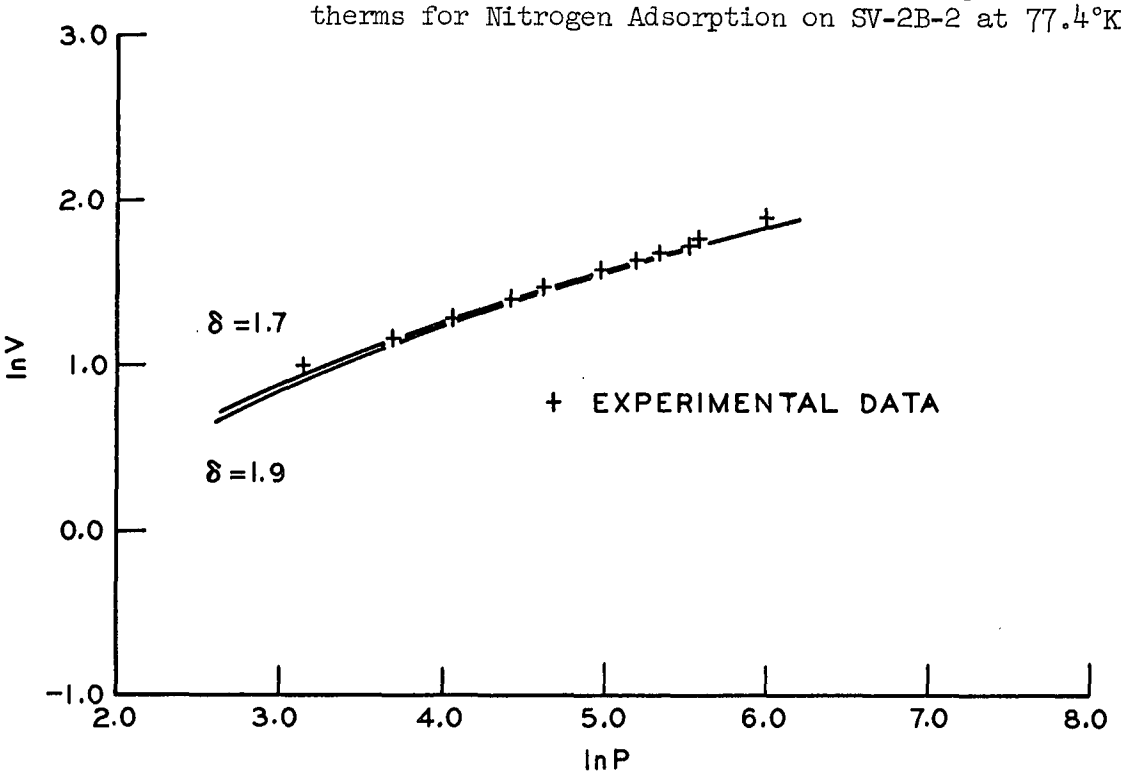

Figure 64. Comparison of Experimental to Model Adsorption Isotherms for Nitrogen Adsorption on SV-2B-2 at 90.2°K

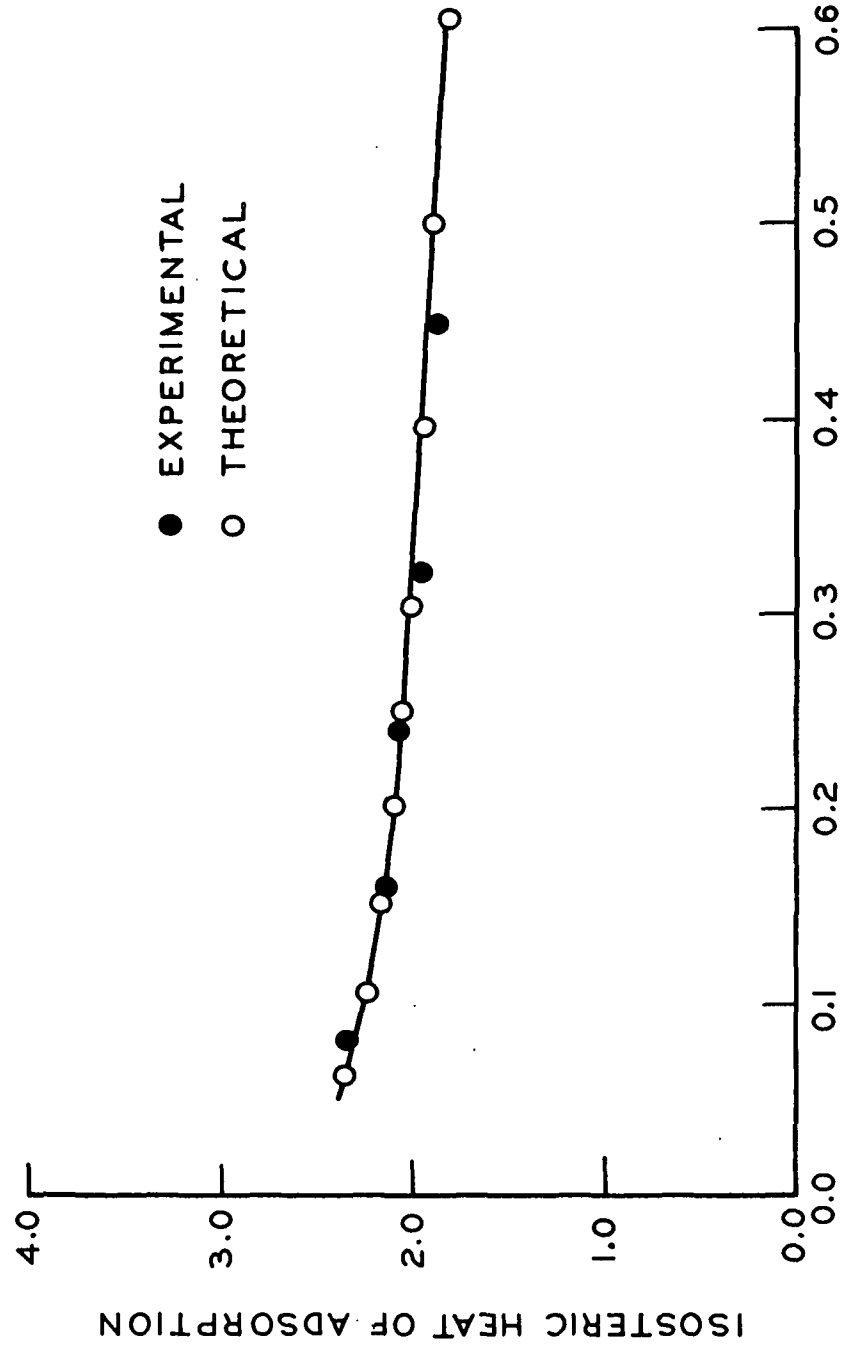

Figure 65. Experimental and Theoretical Isosteric Heat Curves for Nitrogen Adsorption on SV-2B-2

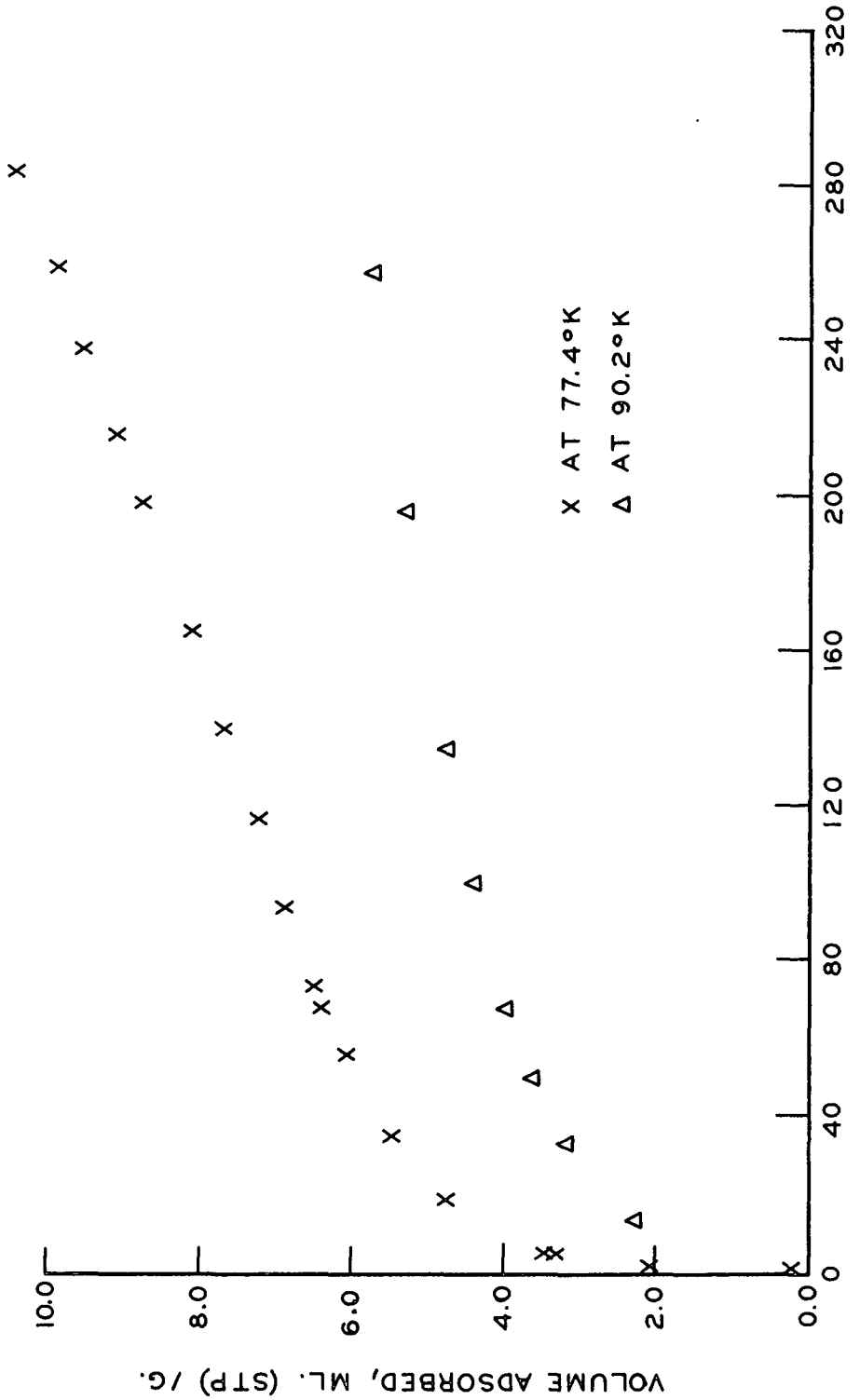

Figure 66. Nitrogen Adsorption Isotherms at 77.4°K and 90.2°K for Sample SV-2B-3

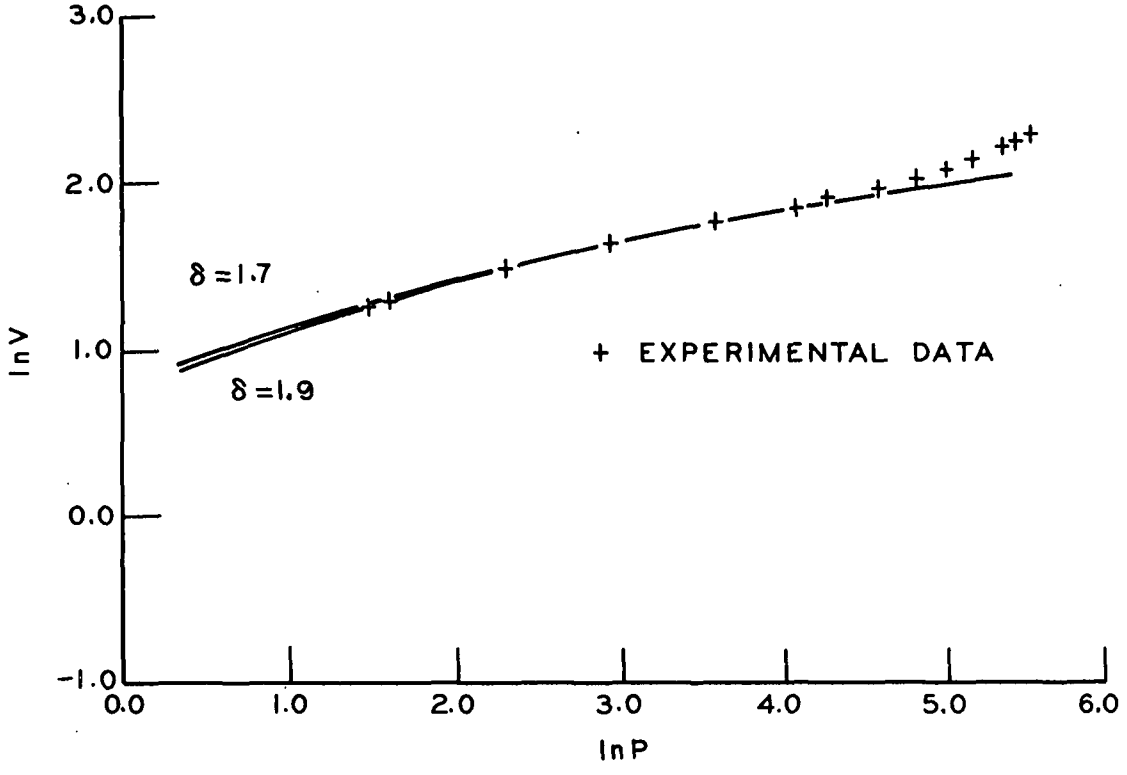

Figure 67. Comparison of Experimental to Model Adsorption Isotherms for Nitrogen Adsorption on SV-2B-3 at 77.4°K

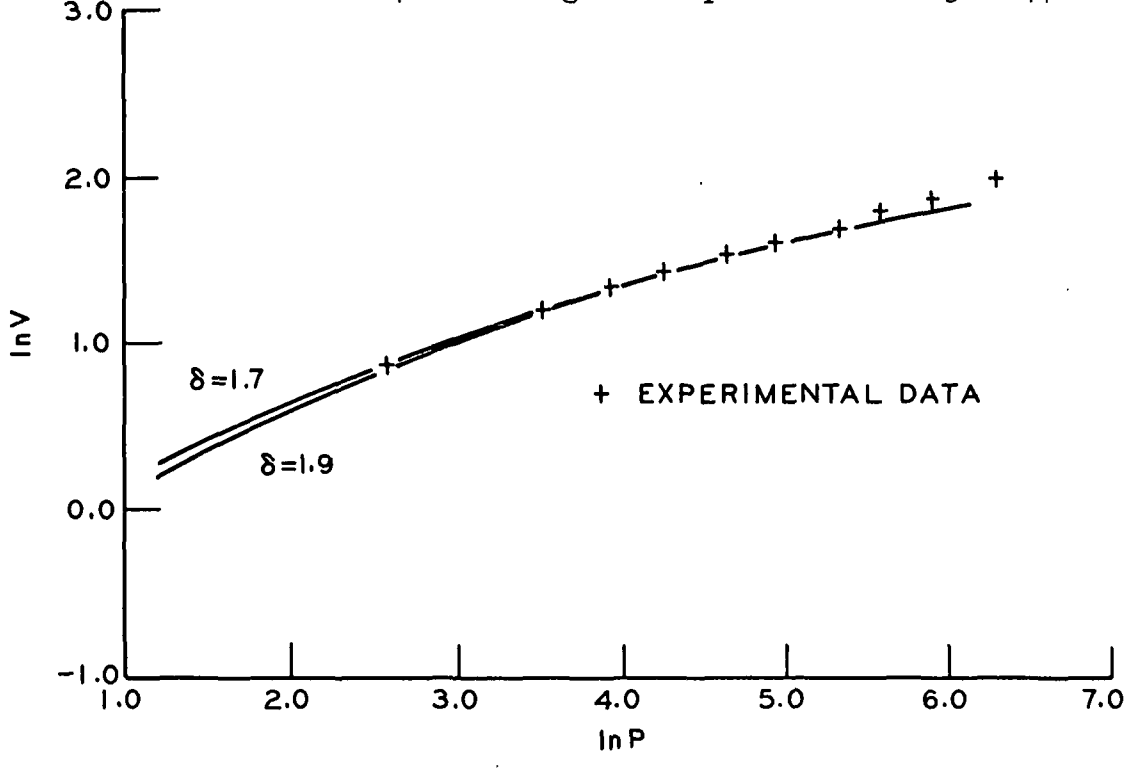

Figure 68. Comparison of Experimental to Model Adsorption Isotherms for Nitrogen Adsorption on SV-2B-3 at 90.2°K

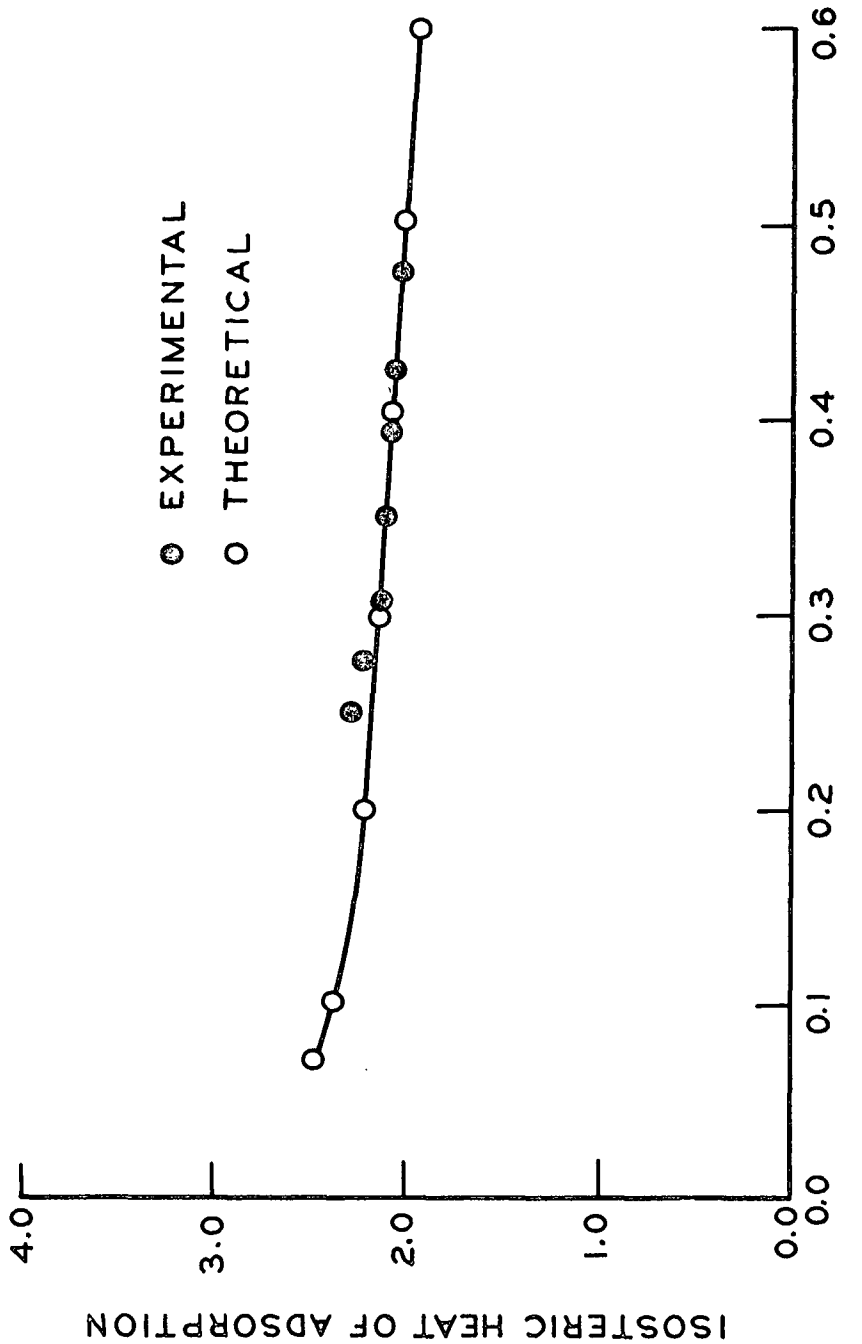

Figure 69. Experimental and Theoretical Isosteric Heat Curves for Nitrogen Adsorption on SV-2B-3

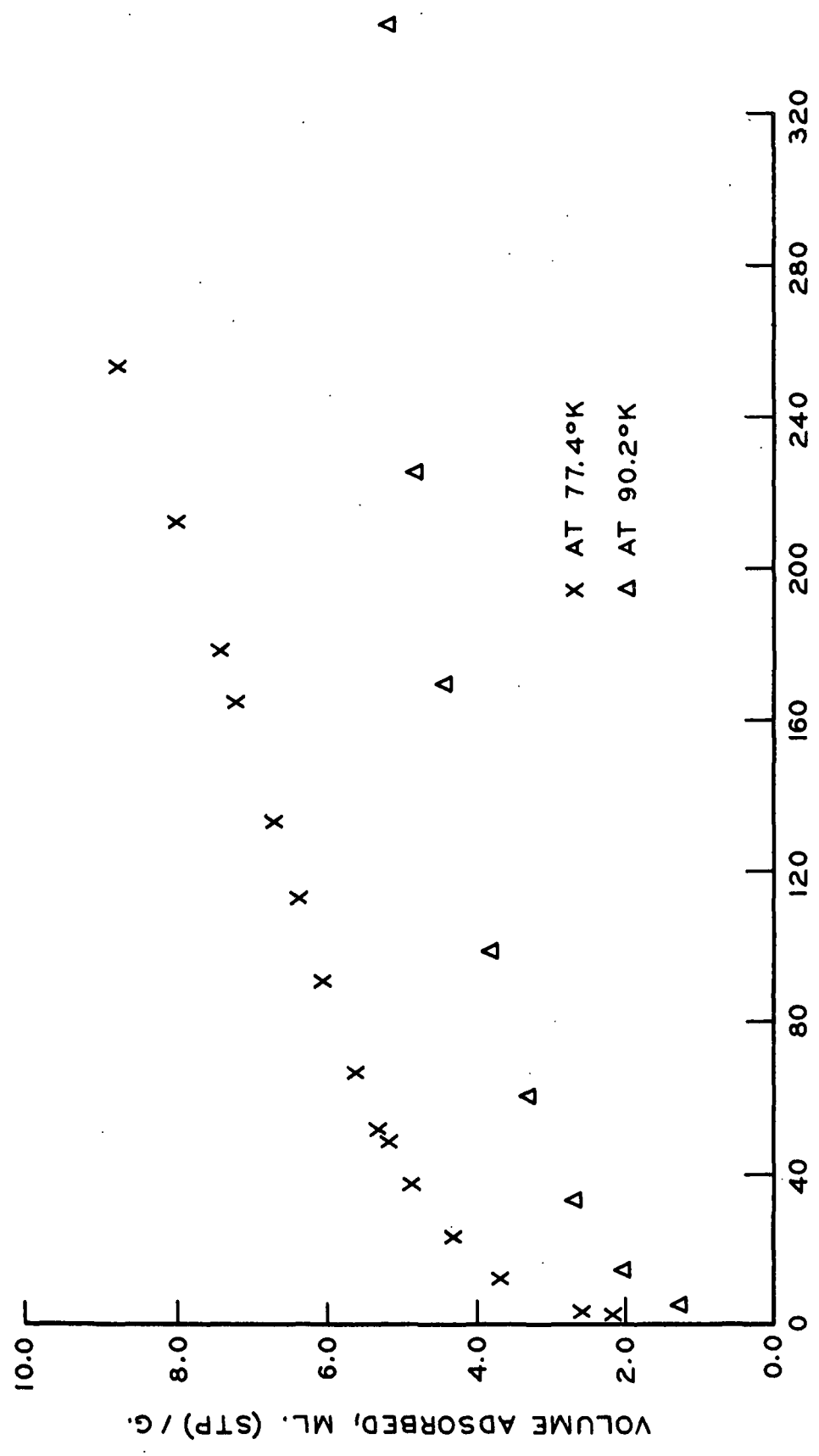

Figure 70. Nitrogen Adsorption Isotherms at 77.4°K and 90.2°K for Sample SV-2B-4

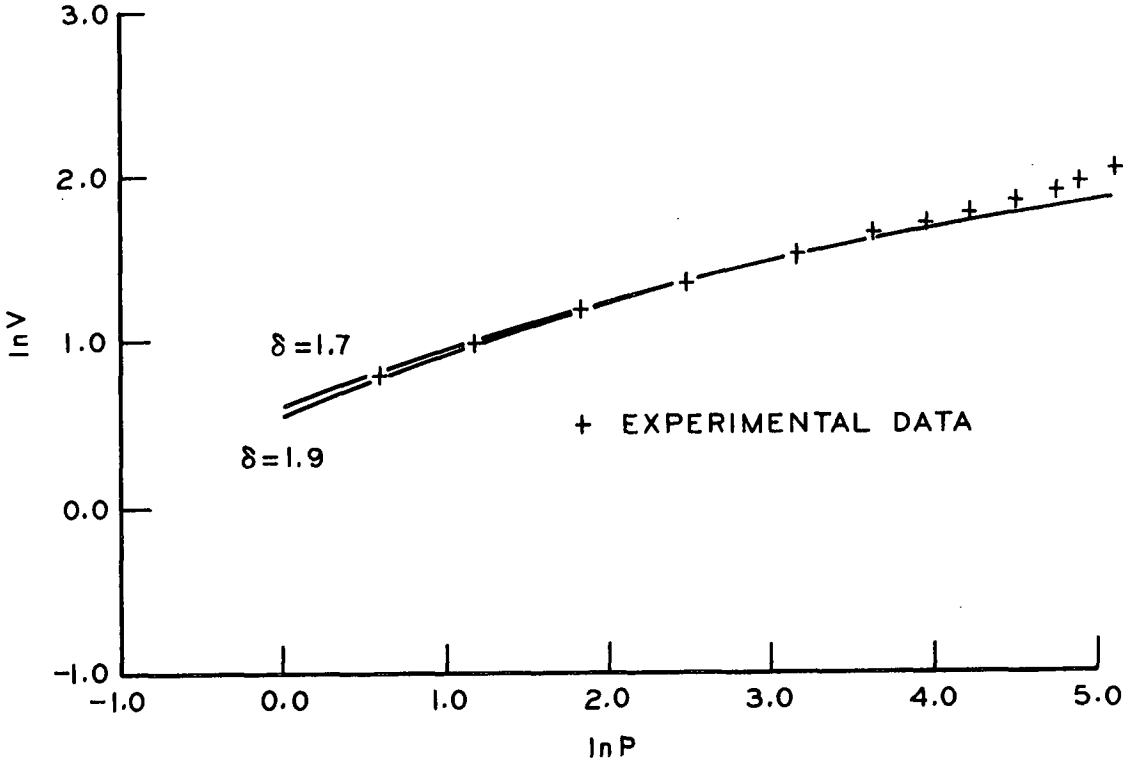

Figure 71. Comparison of Experimental to Model Adsorption Isotherms for Nitrogen Adsorption on SV-2B-4 at 77.4°K

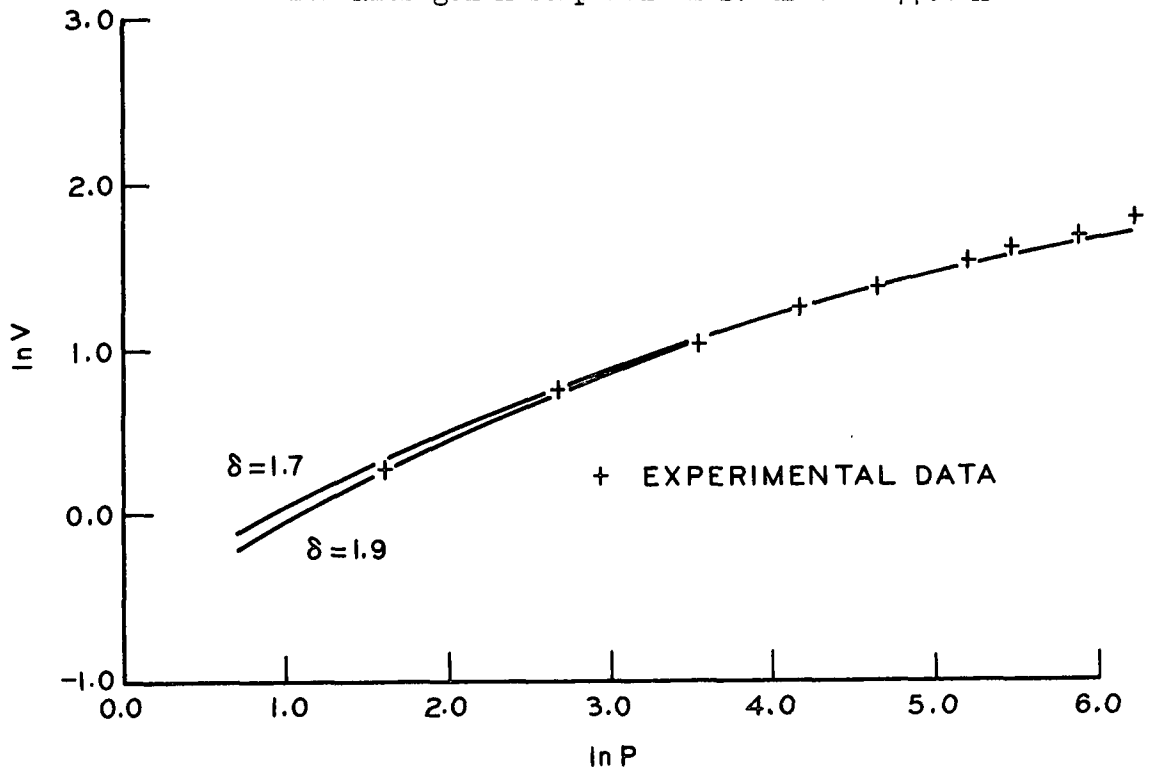

Figure 72. Comparison of Experimental to Model Adsorption Isotherms for Nitrogen Adsorption on SV-2B-4 at 90.2°K

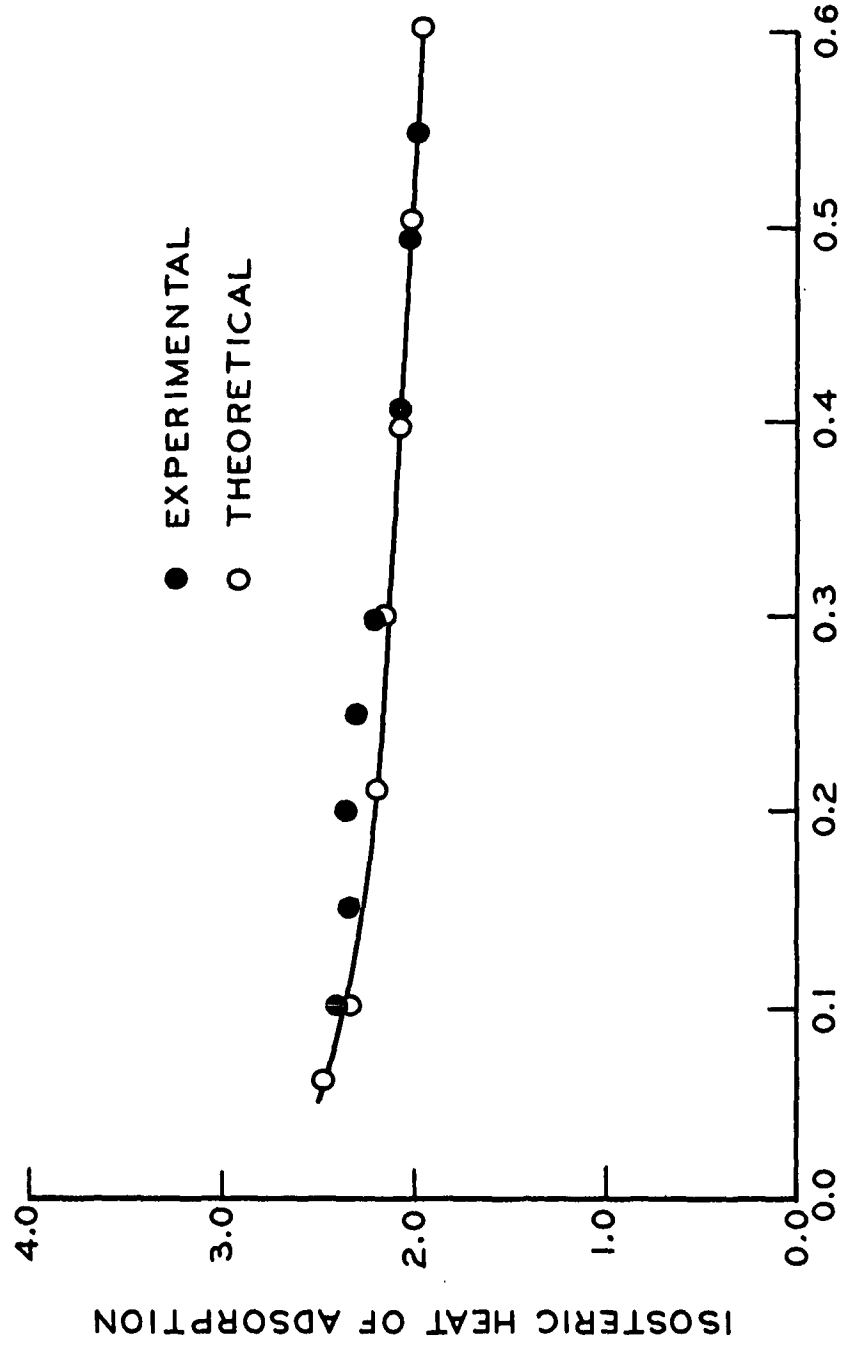

Figure 73. Experimental and Theoretical Isosteric Heat Curves for Nitrogen Adsorption on SV-2B-4

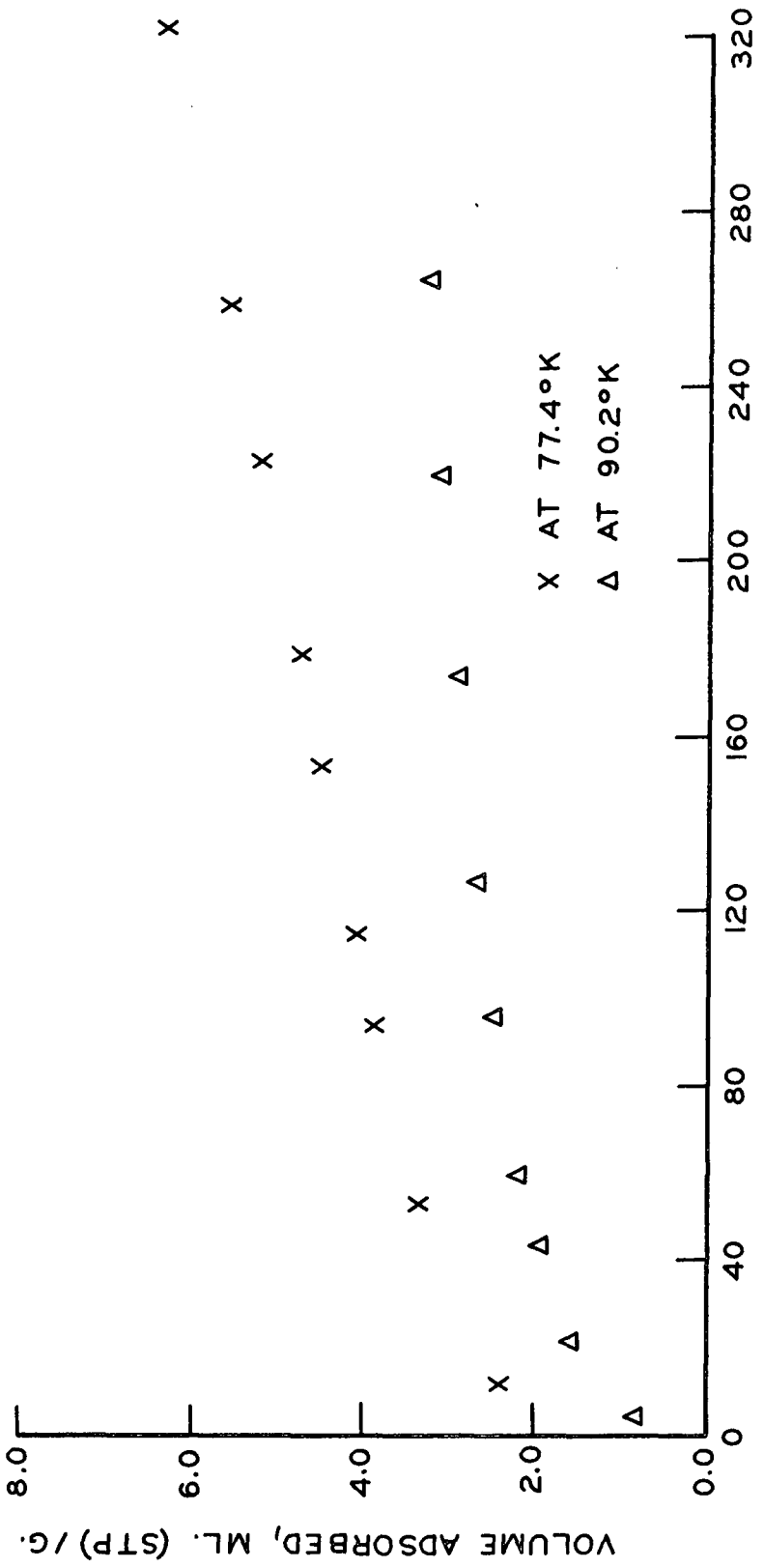

Figure 74. Nitrogen Adsorption Isotherms at 77.4°K and 90.2°K for Sample SV-2B-5

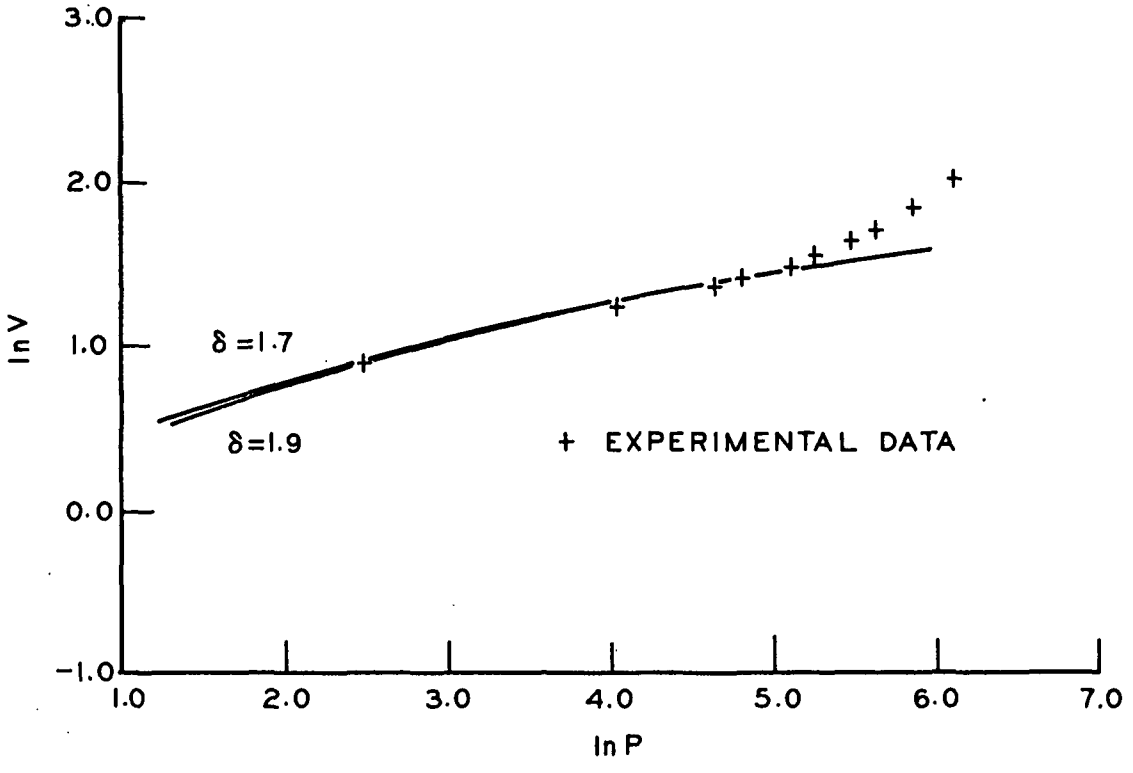

Figure 75. Comparison of Experimental to Model Adsorption Isotherms for Nitrogen Adsorption on SV-2B-5 at 77.4°K

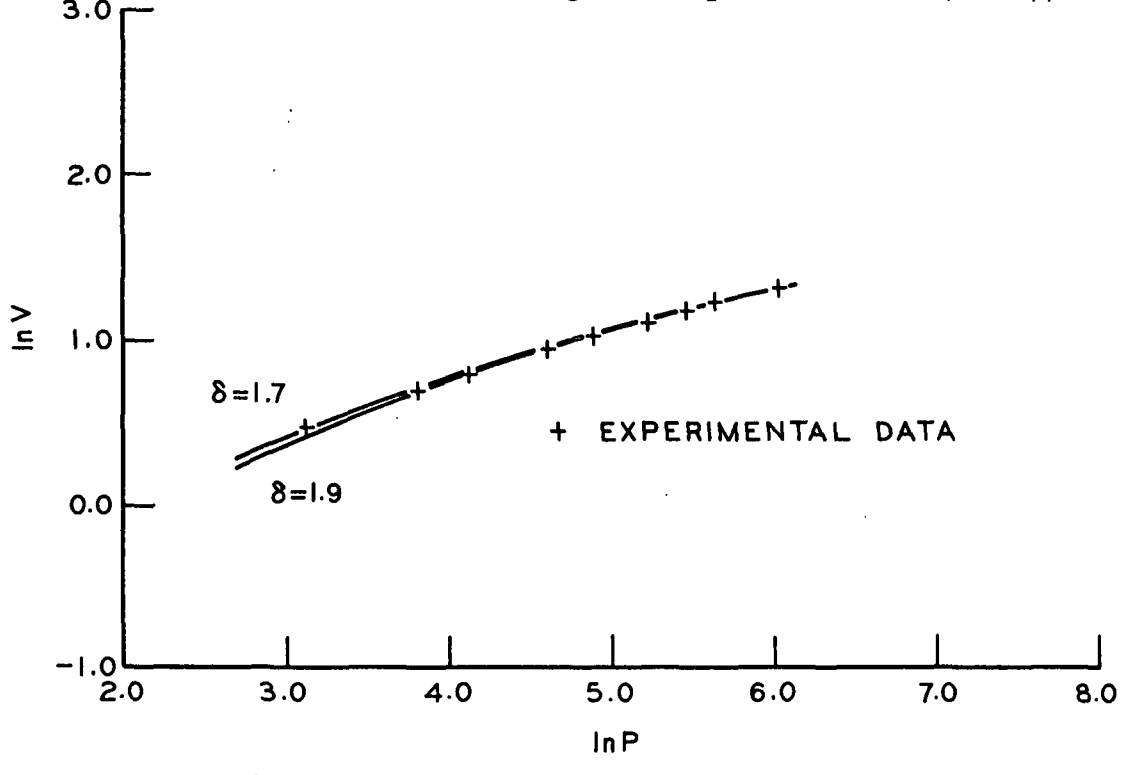

Figure 76. Comparison of Experimental to Model Adsorption Isotherms for Nitrogen Adsorption on SV-2B-5 at 90.2°K

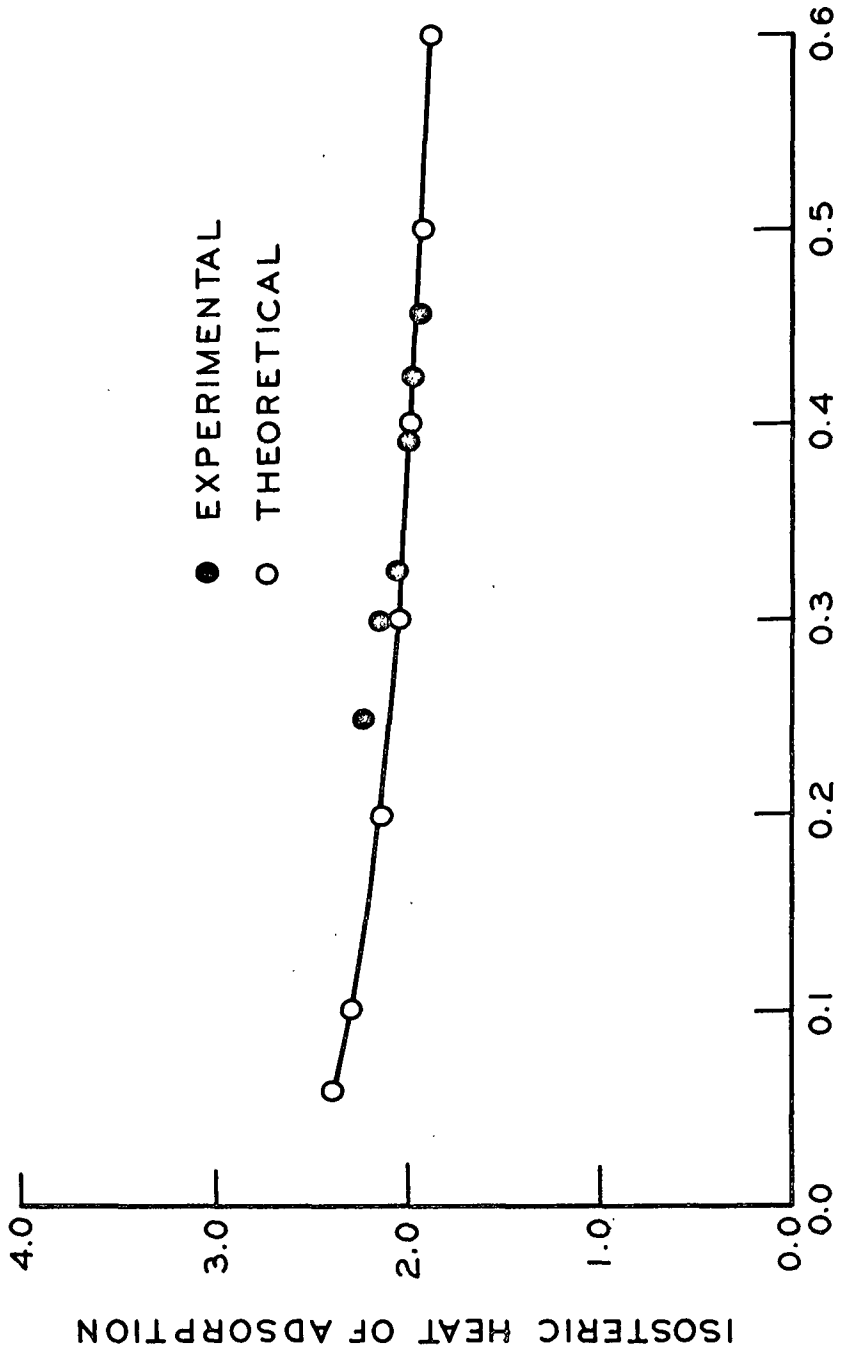

Figure 77. Experimental and Theoretical Isosteric Heat Curves for Nitrogen Adsorption on SV-2B-5

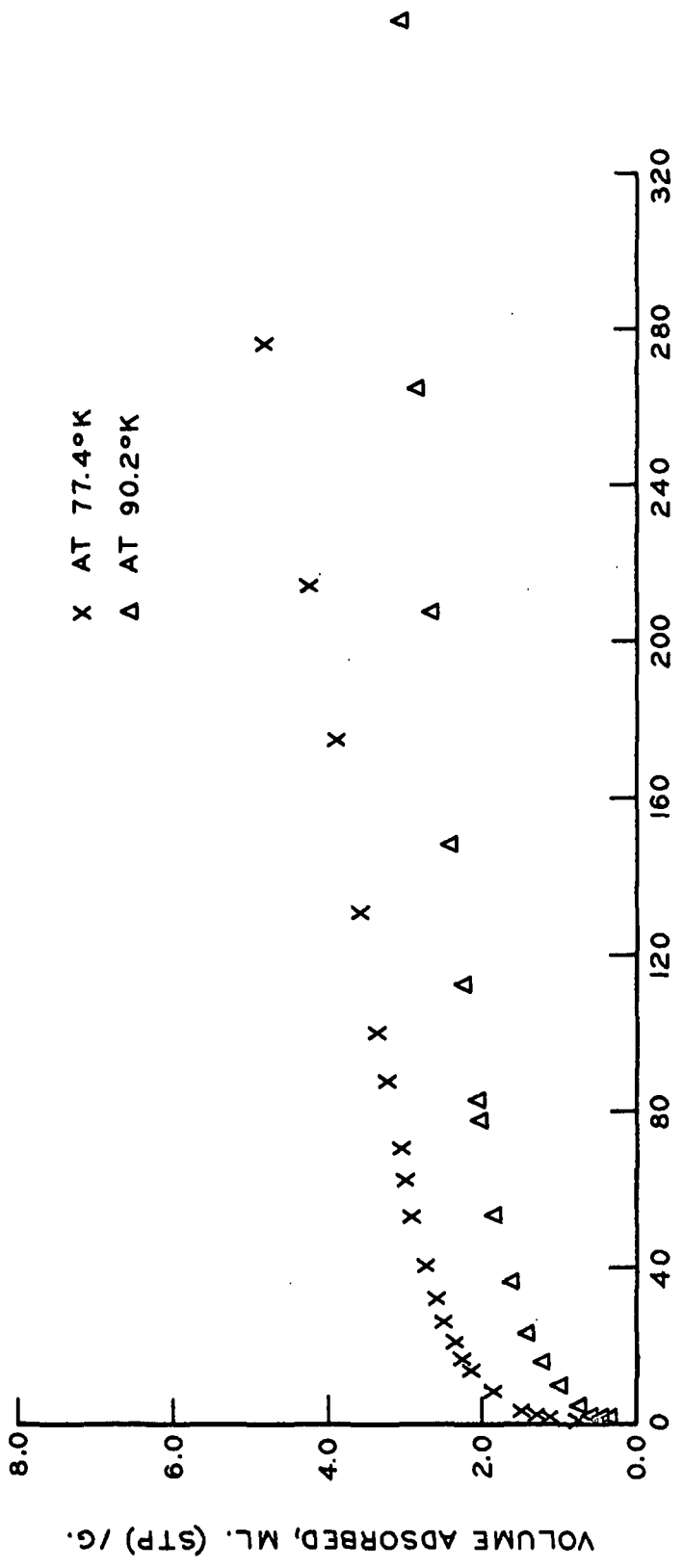

Figure 78. Nitrogen Adsorption Isotherms at 77.4°K and 90.2°K for Sample: SV-2B-6

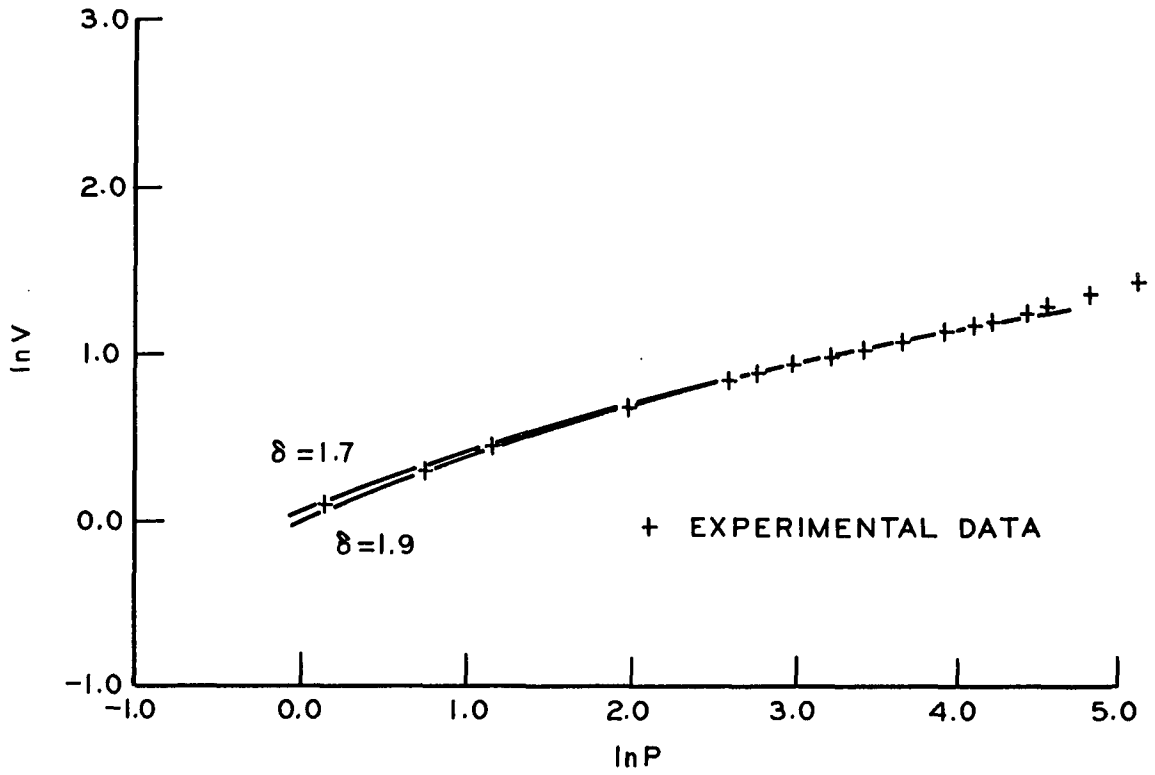

Figure 79. Comparison of Experimental to Model Adsorption Isotherms for Nitrogen Adsorption on SV-2B-6 at 77.4°K

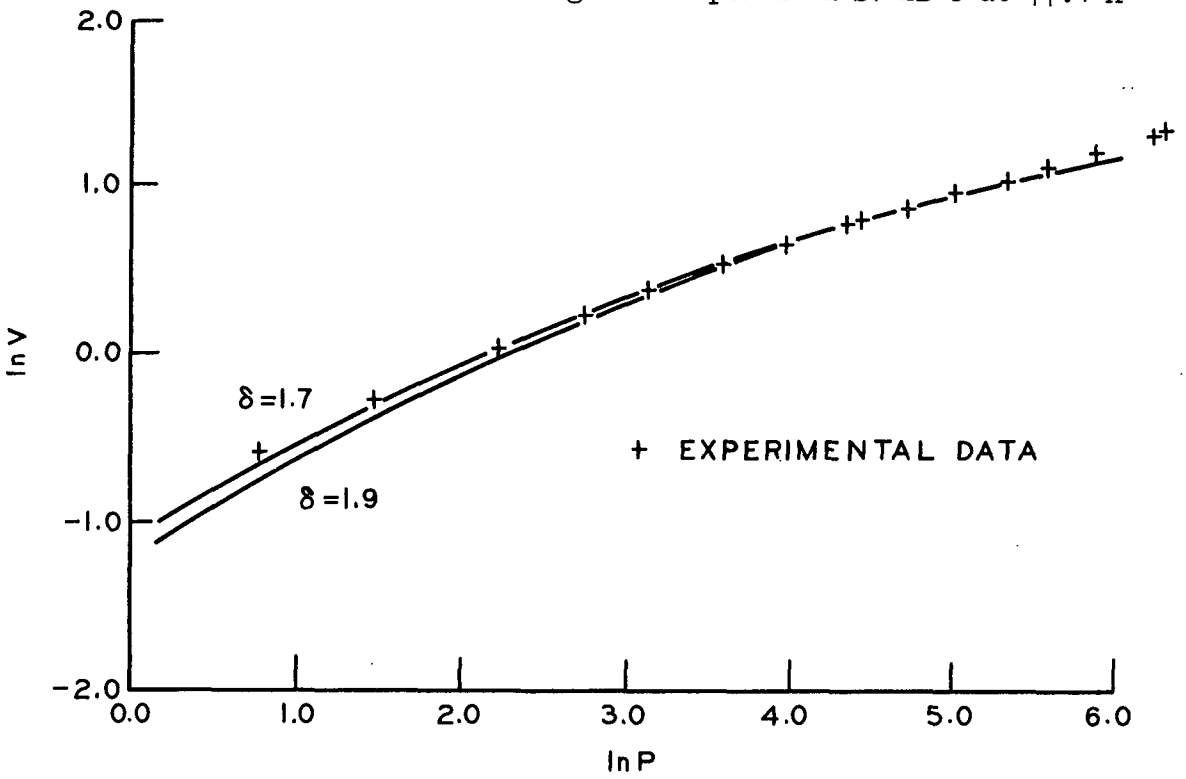

Figure 80. Comparison of Experimental to Model Adsorption Isotherms for Nitrogen Adsorption on SV-2B-6 at 90.2°K

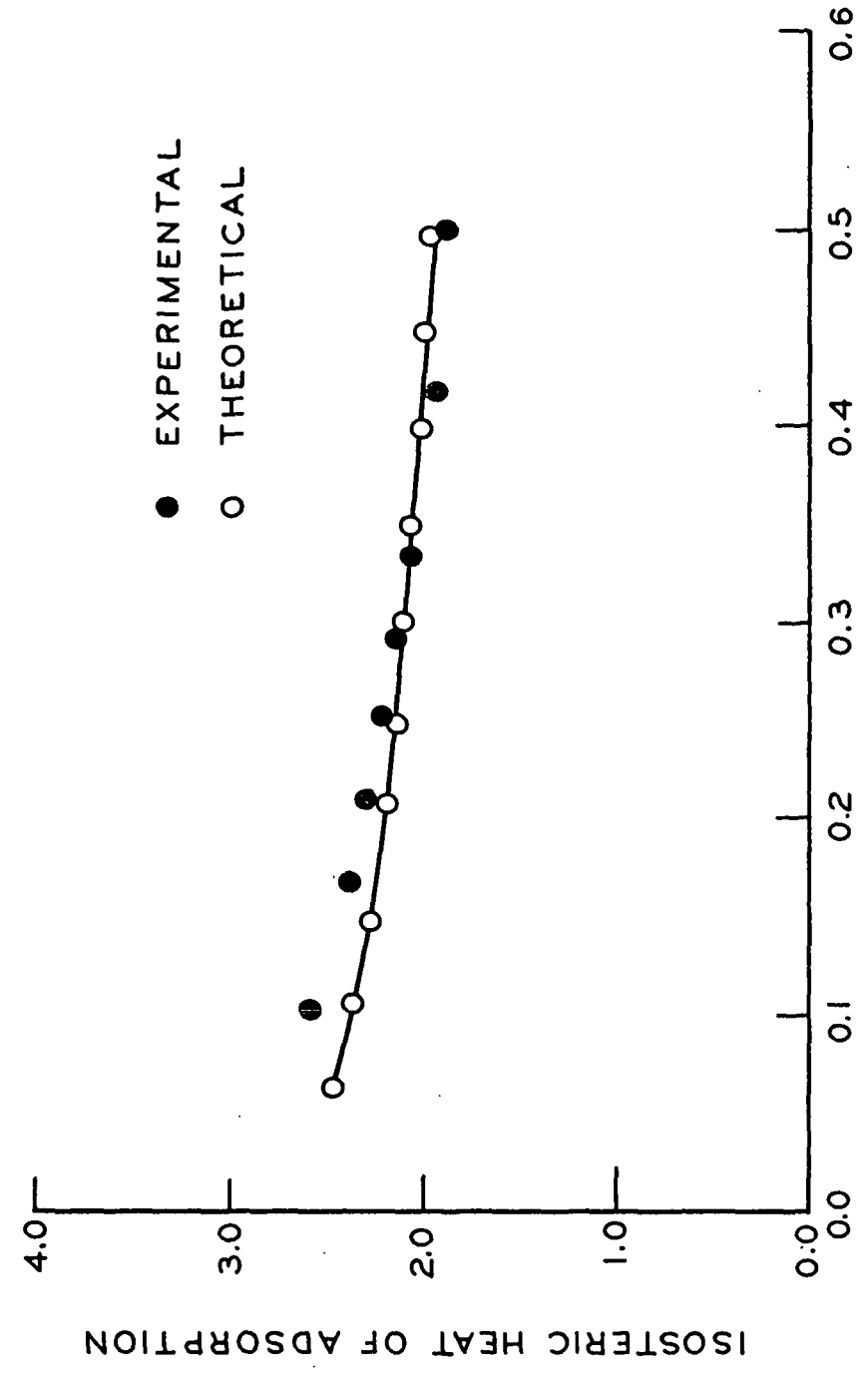

Figure 81. Experimental and Theoretical Isosteric Heat Curves for Nitrogen Adsorption on Sample SV-2B-6

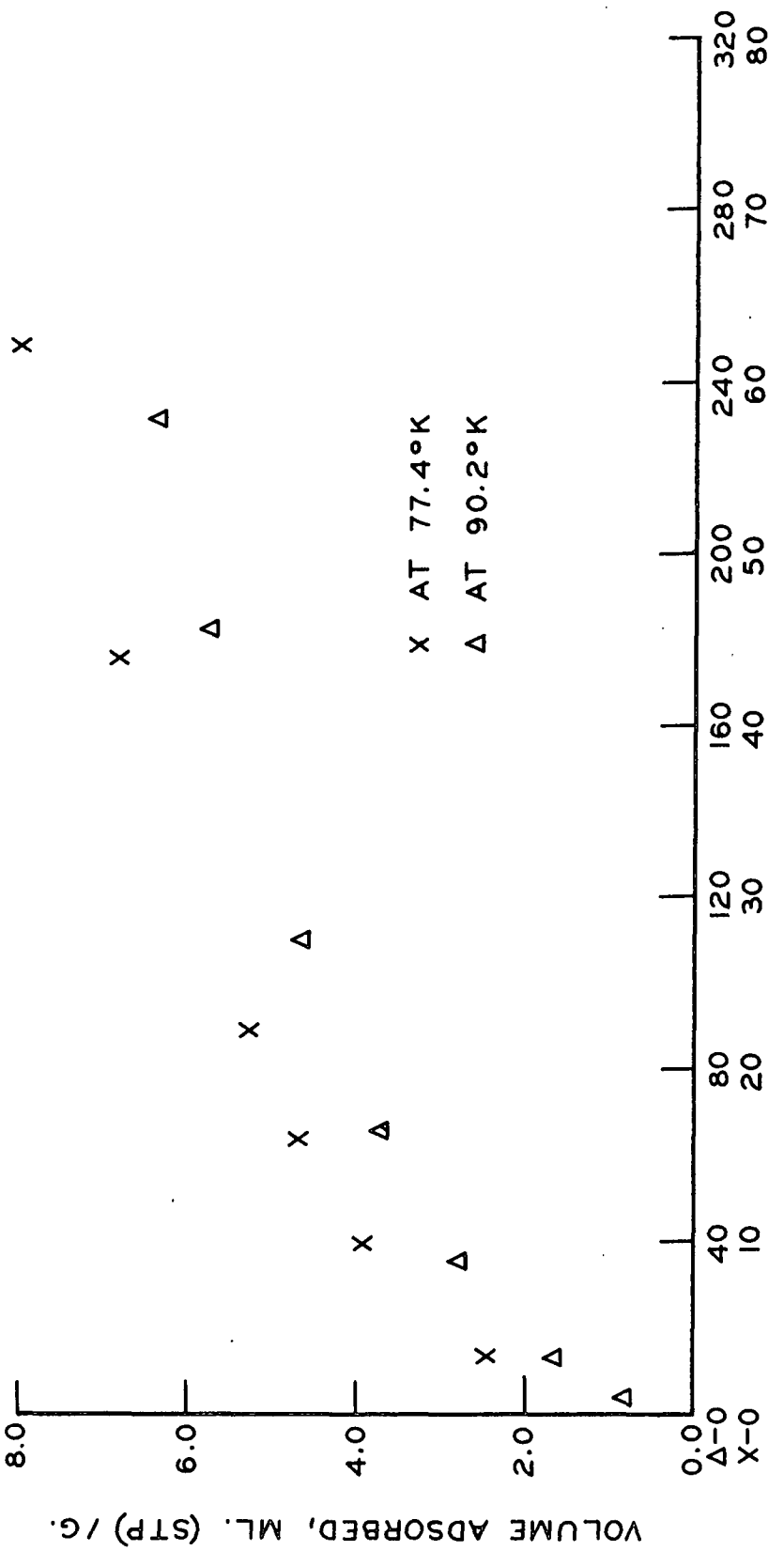

Figure 82. Argon Adsorption Isotherms at 77.4°K and 90.2°K for Sample SV-2B-7HW

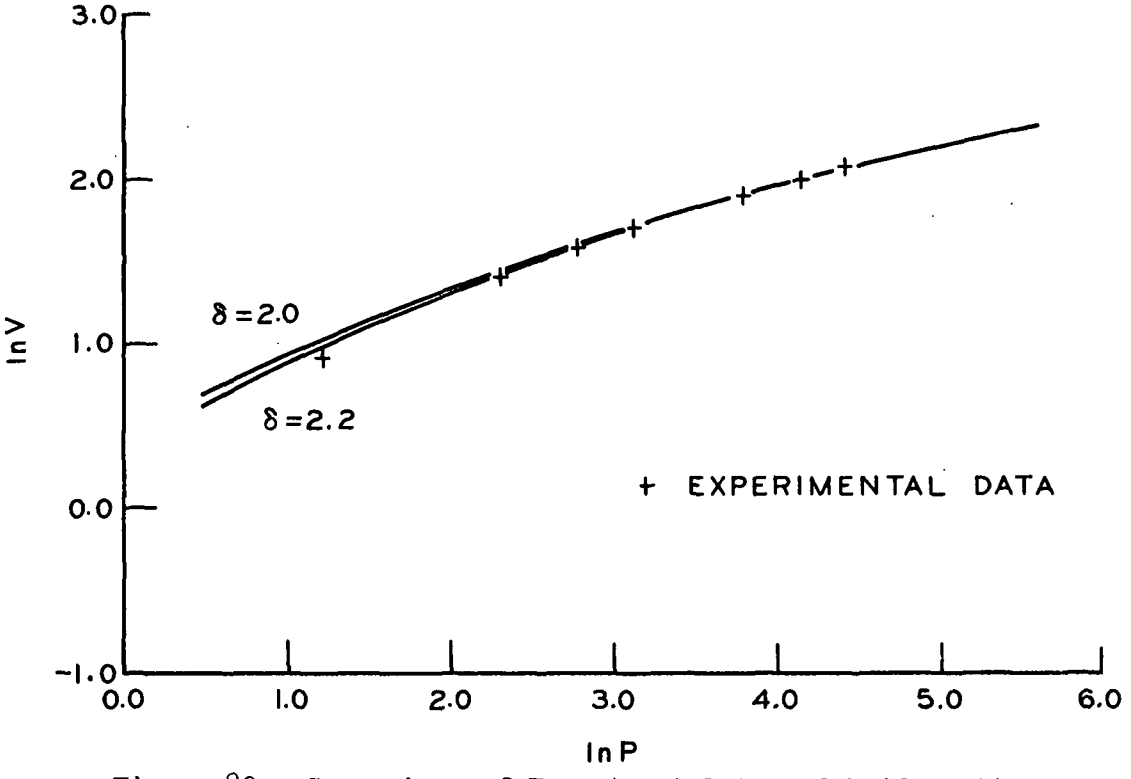

Figure 83. Comparison of Experimental to Model Adsorption Isotherms for Argon Adsorption on SV-2B-7HW at 77.4°K

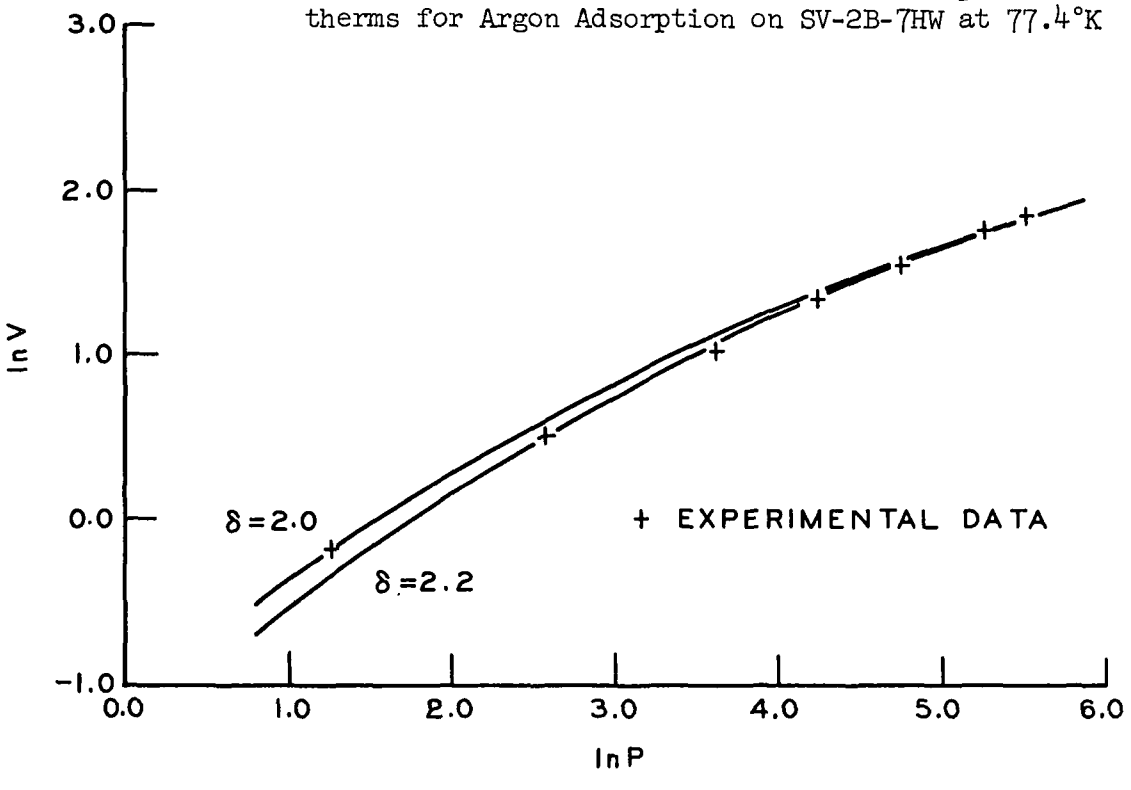

Figure 84. Comparison of Experimental to Model Adsorption Isotherms for Argon Adsorption on SV-2B-7HW at 90.2°K

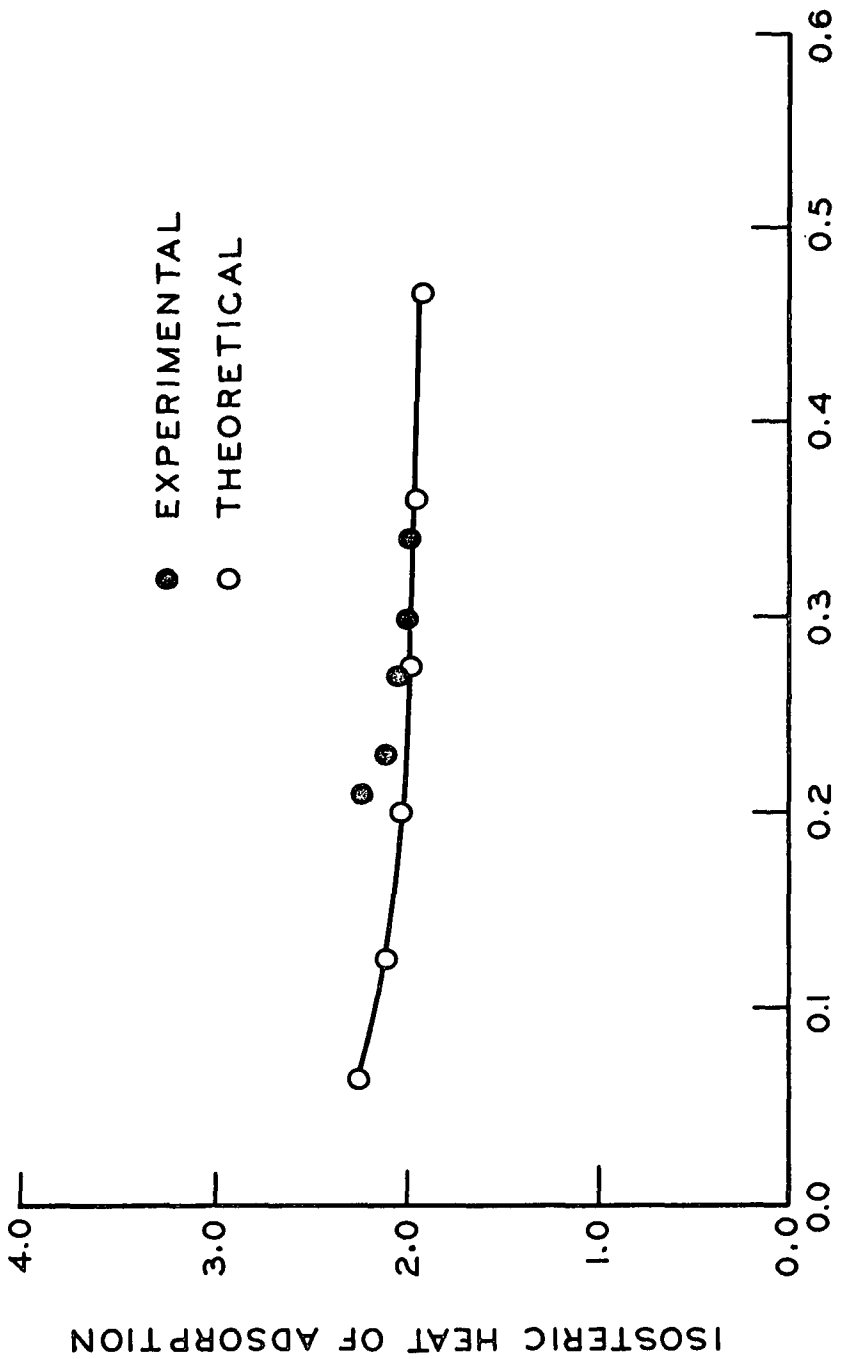

Figure 85. Experimental and Theoretical Isosteric Heat Curves for Argon Adsorption on Sample SV-2B-7HW

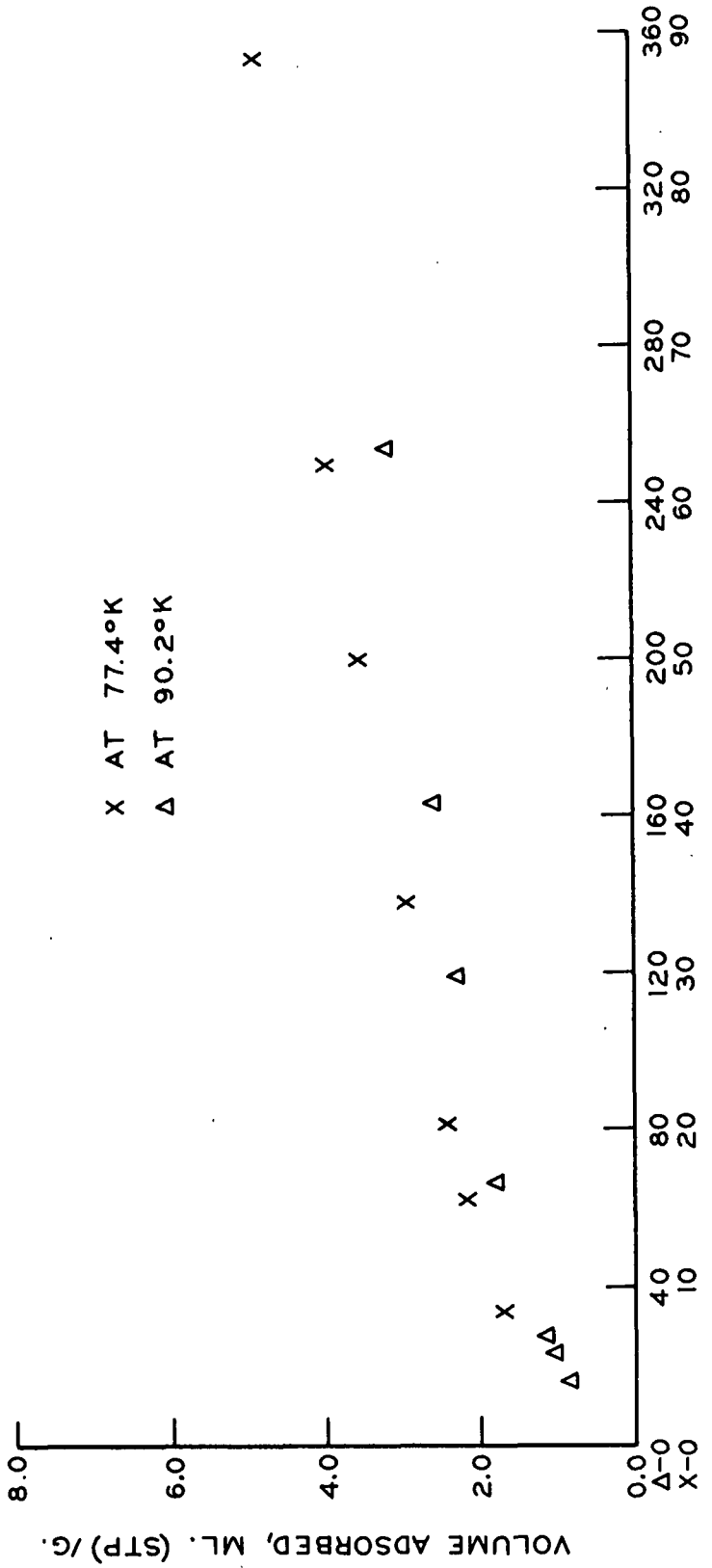

Figure 86. Argon Adsorption Isotherms at 77.4°K and 90.2°K for Sample SV-2B-8HW

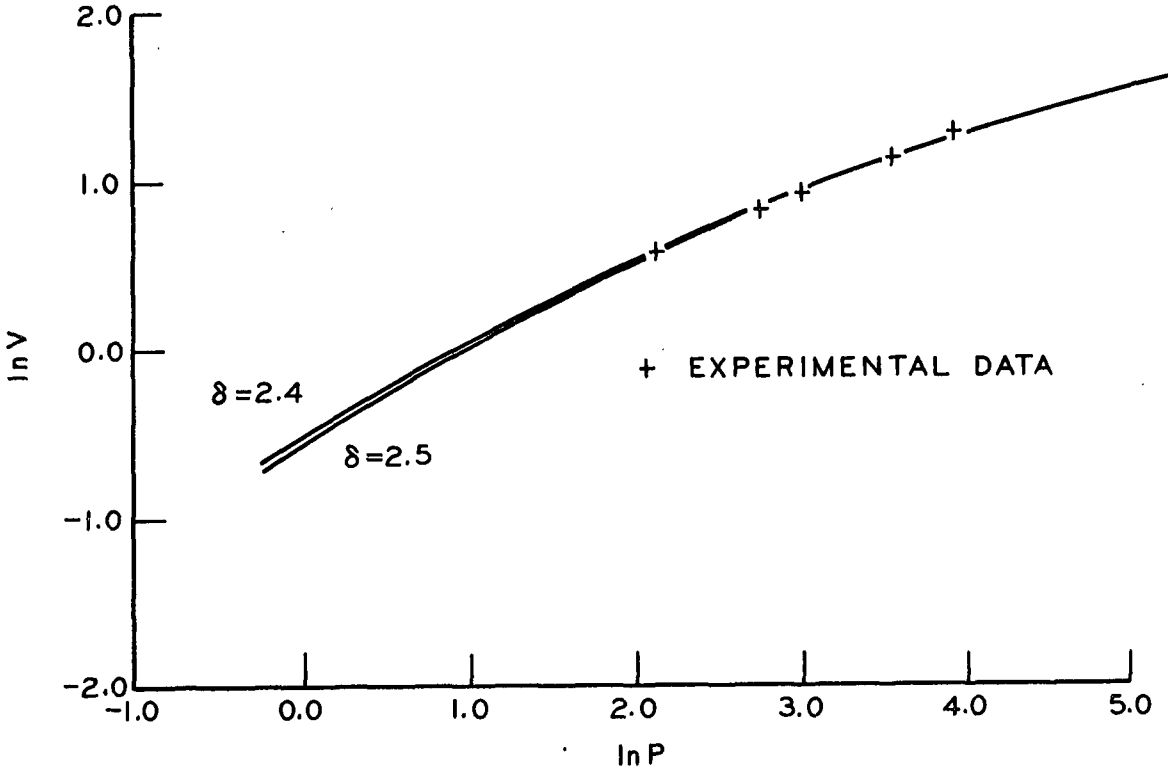

Figure 87. Comparison of Experimental to Model Adsorption Isotherms for Argon Adsorption on SV-2B-8HW at 77.4°K

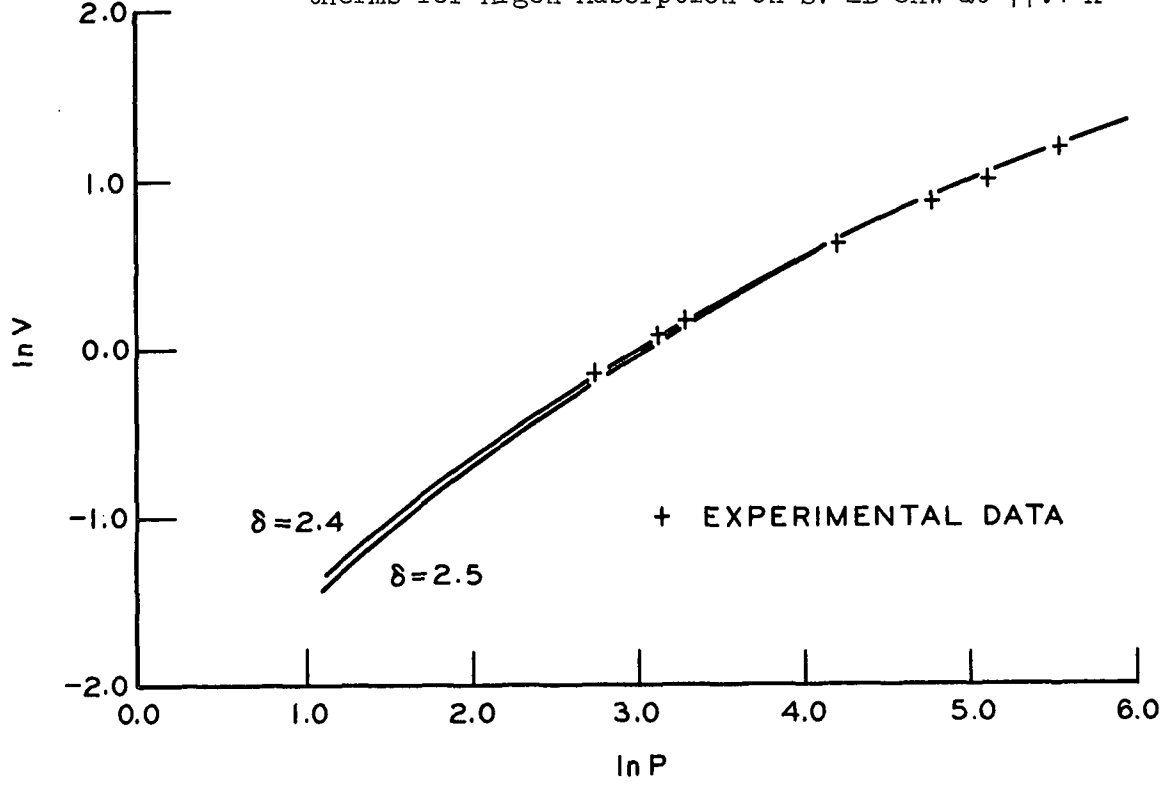

Figure 88. Comparison of Experimental to Model Adsorption Isotherms for Argon Adsorption on SV-2B-8HW at 90.2°K

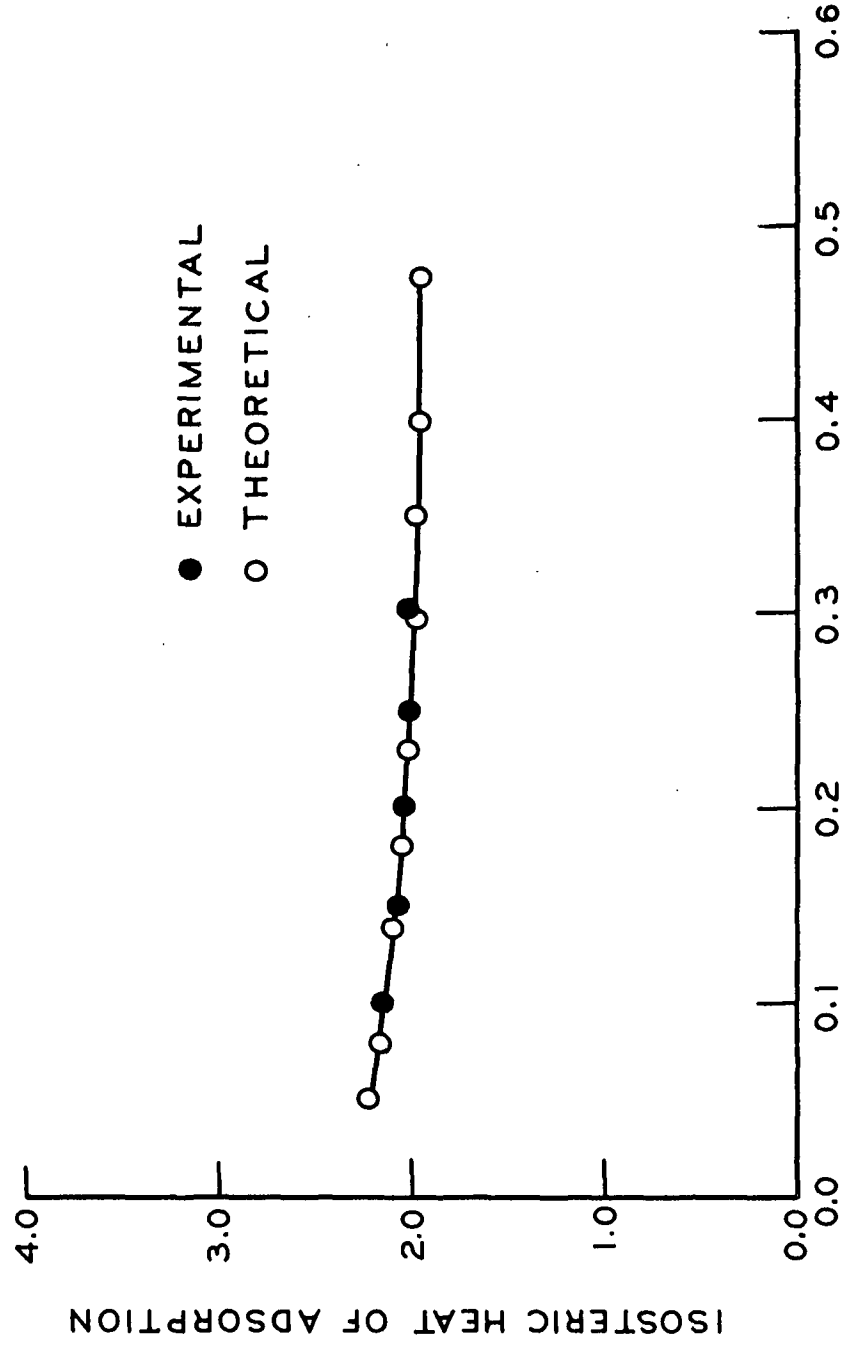

Figure 89. Experimental and Theoretical Isosteric Heat Curves for Argon Adsorption on Sample SV-2B-8HW

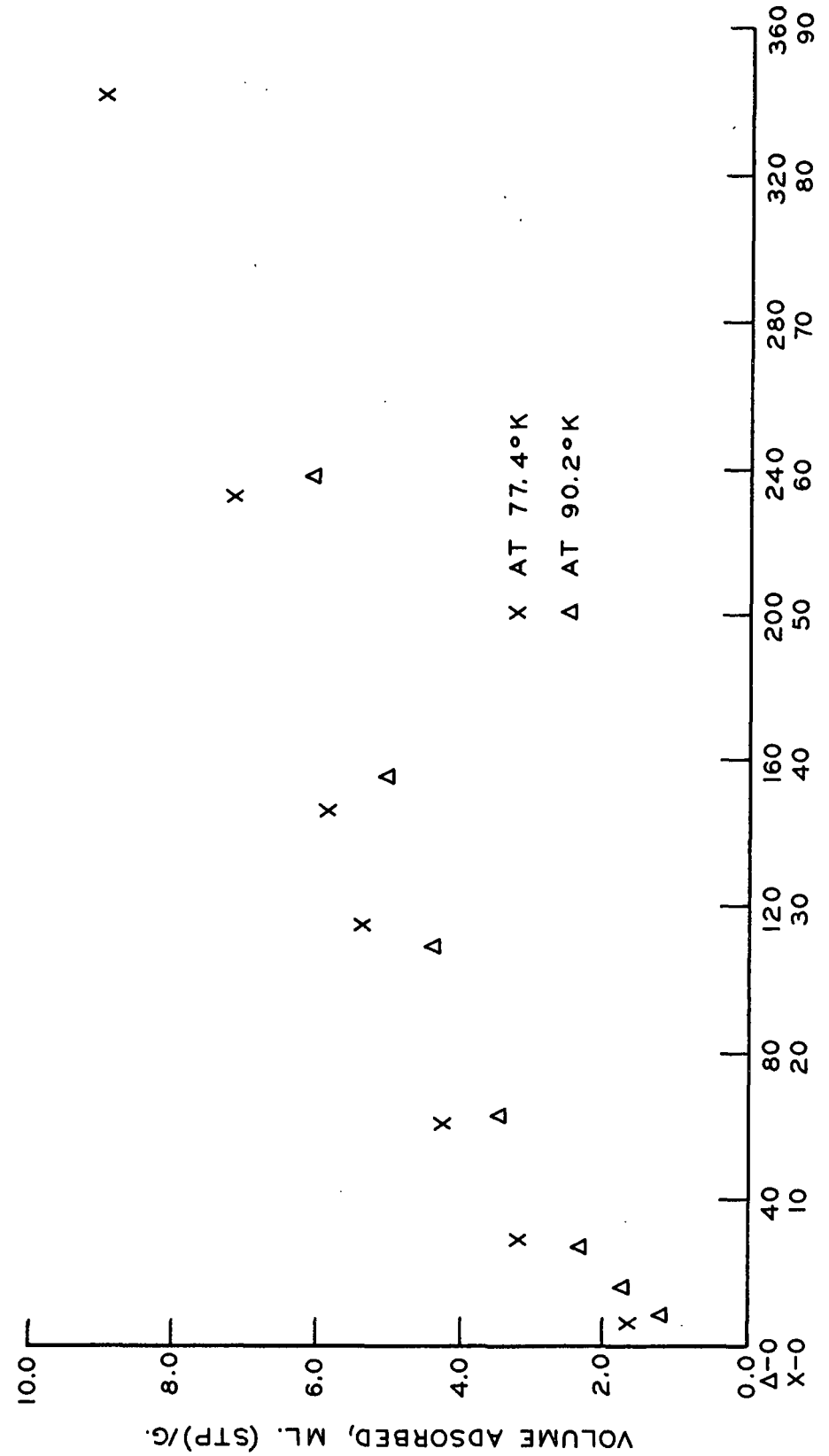

Figure 90. Argon Adsorption Isotherms at 77.4°K and 90.2°K for Sample SV-2B-9HW

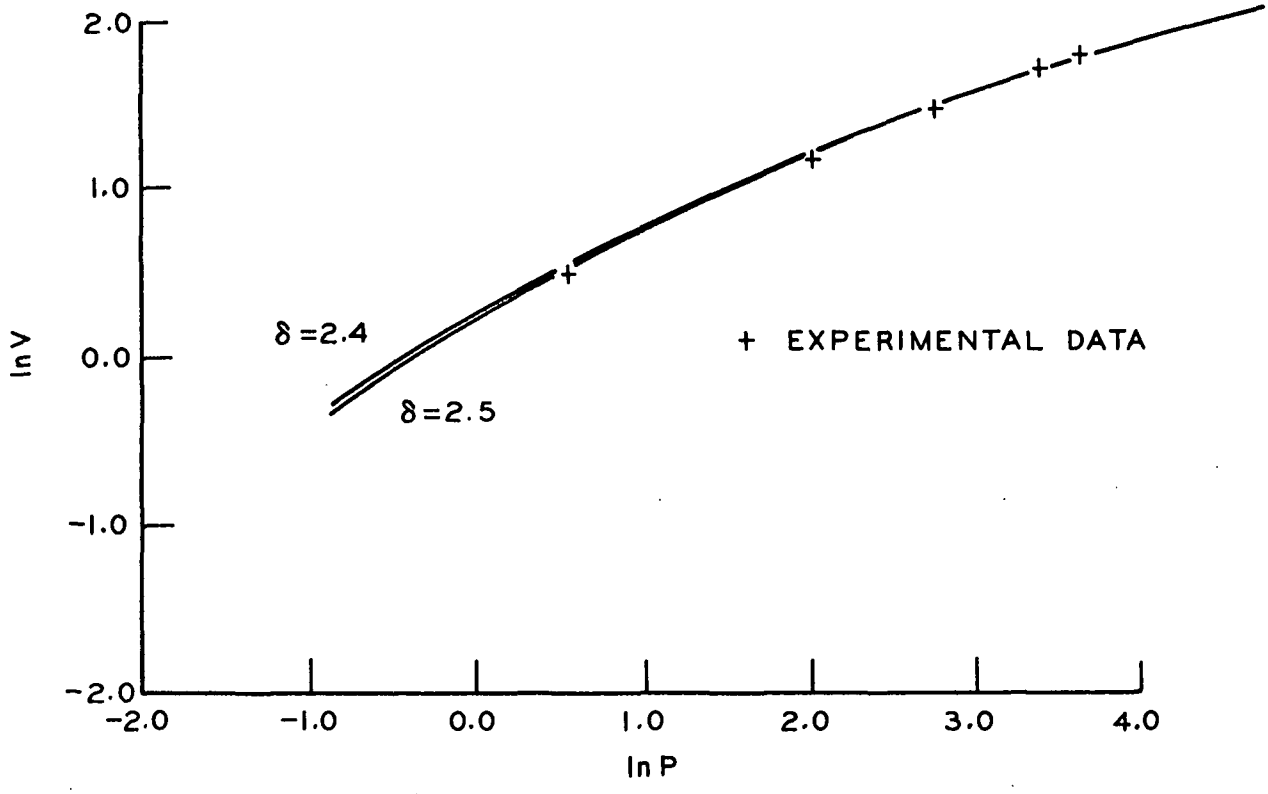

Figure 91. Comparison of Experimental to Model Adsorption Isotherms for Argon Adsorption on SV-2B-9HW at 77.4°K

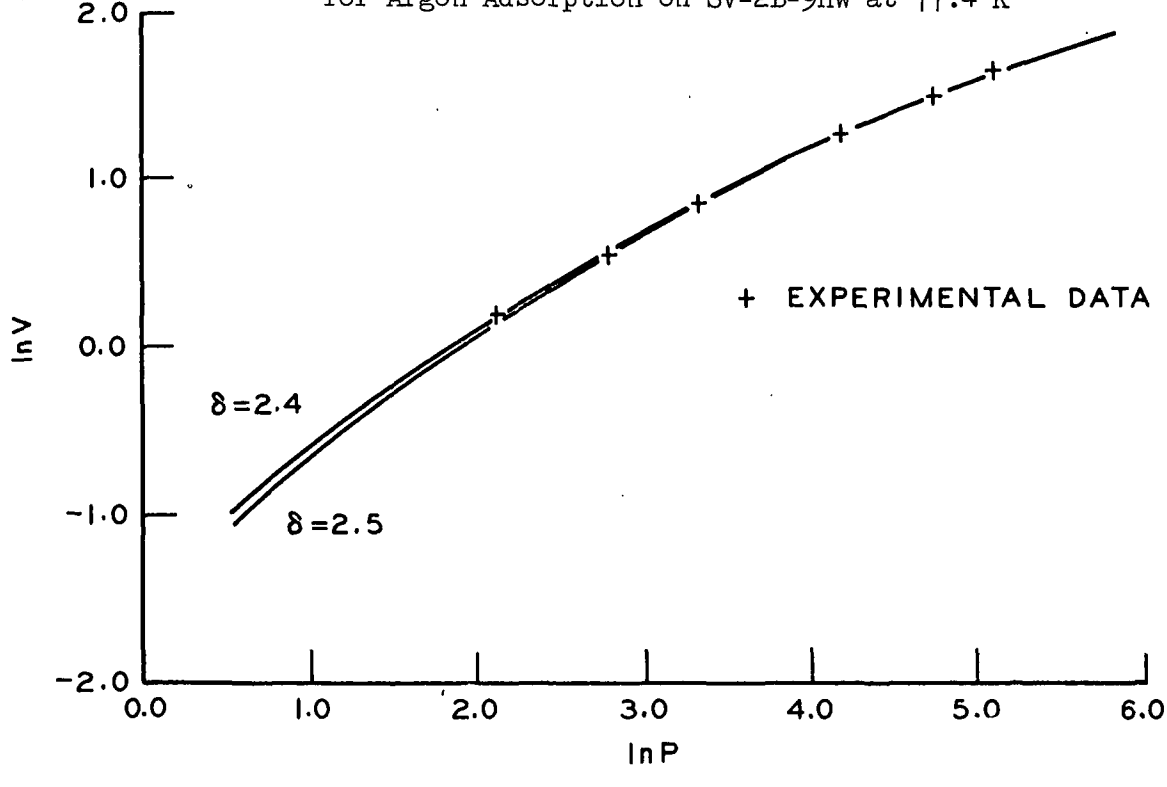

Figure 92. Comparison of Experimental to Model Adsorption Isotherms for Argon Adsorption on SV-2B-9HW at 90.2°K

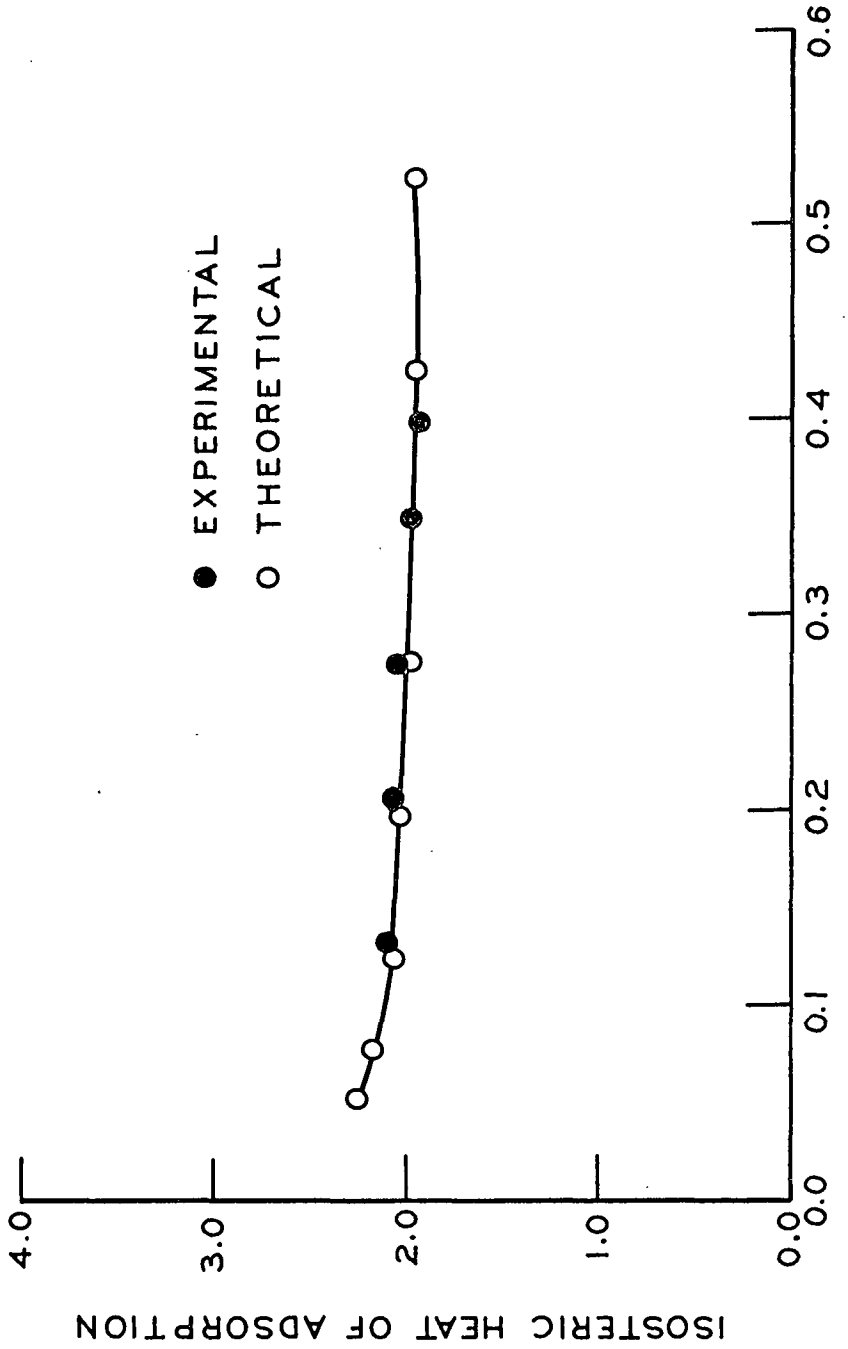

Figure 93. Experimental and Theoretical Isosteric Heat Curves for Argon Adsorption on SV-2B-9HW

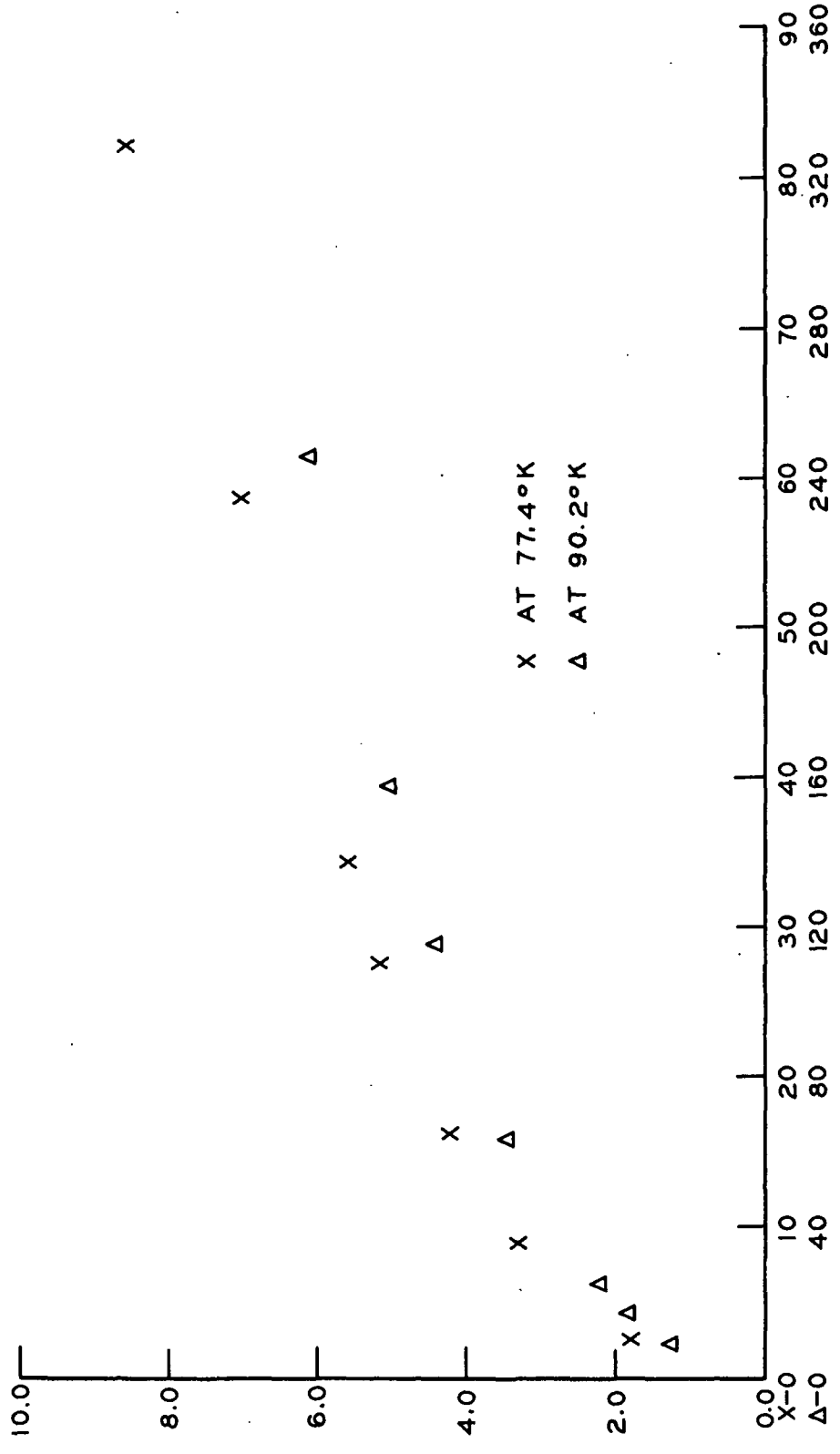

Figure 94. Argon Adsorption Isotherms at 77.4°K and 90.2°K for Sample SV-2B-10HW

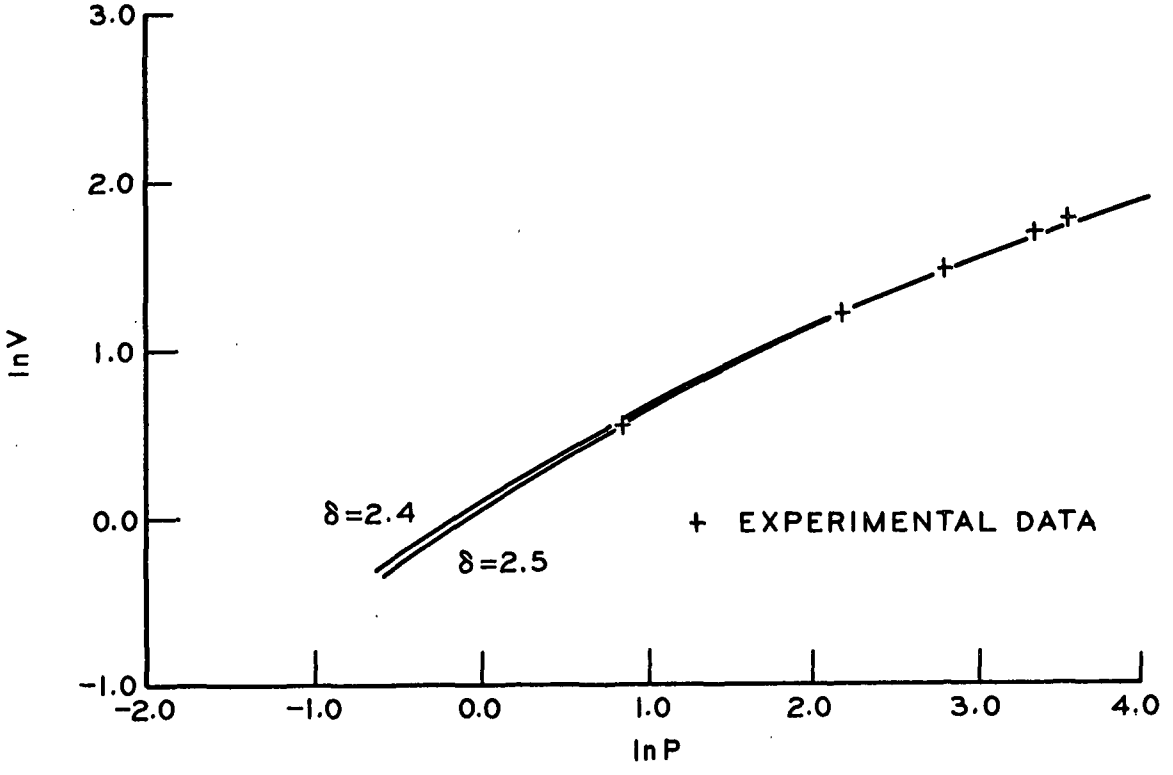

Figure 95. Comparison of Experimental to Model Adsorption Isotherms for Argon Adsorption on SV-2B-10HW at 77.4°K

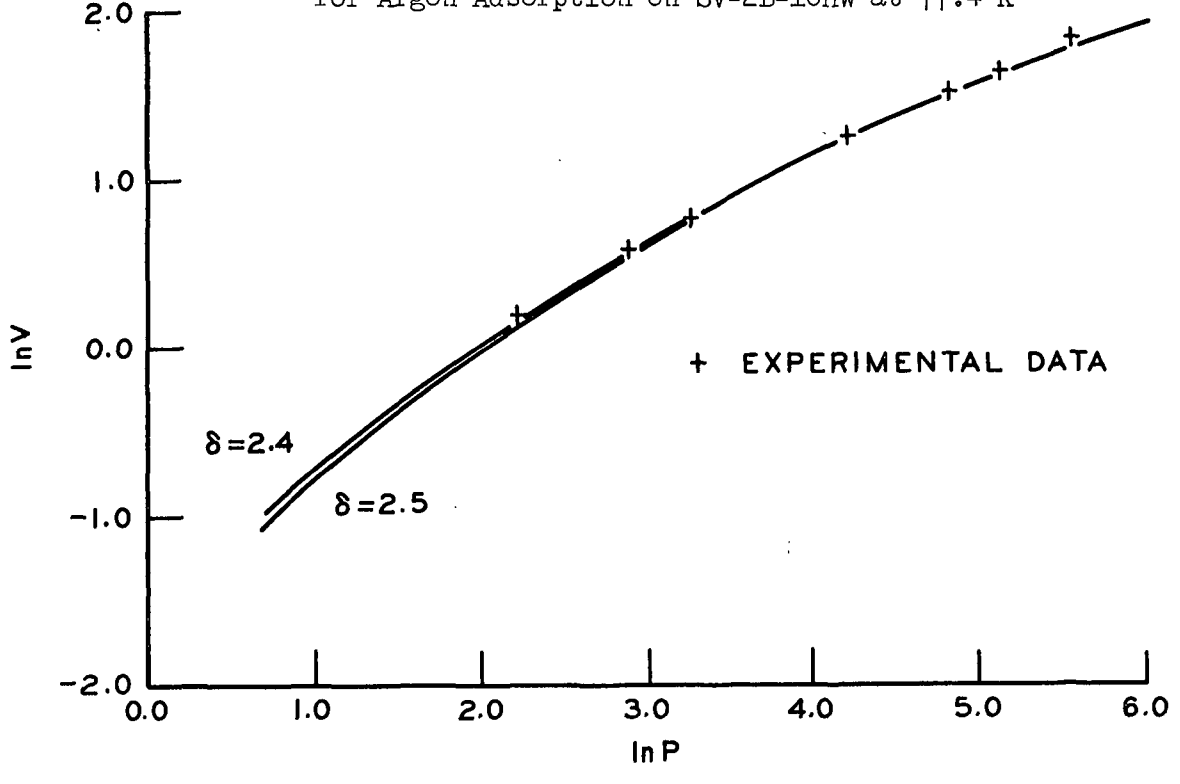

Figure 96. Comparison of Experimental to Model Adsorption Isotherms for Argon Adsorption on SV-2B-10HW at 90.2°K

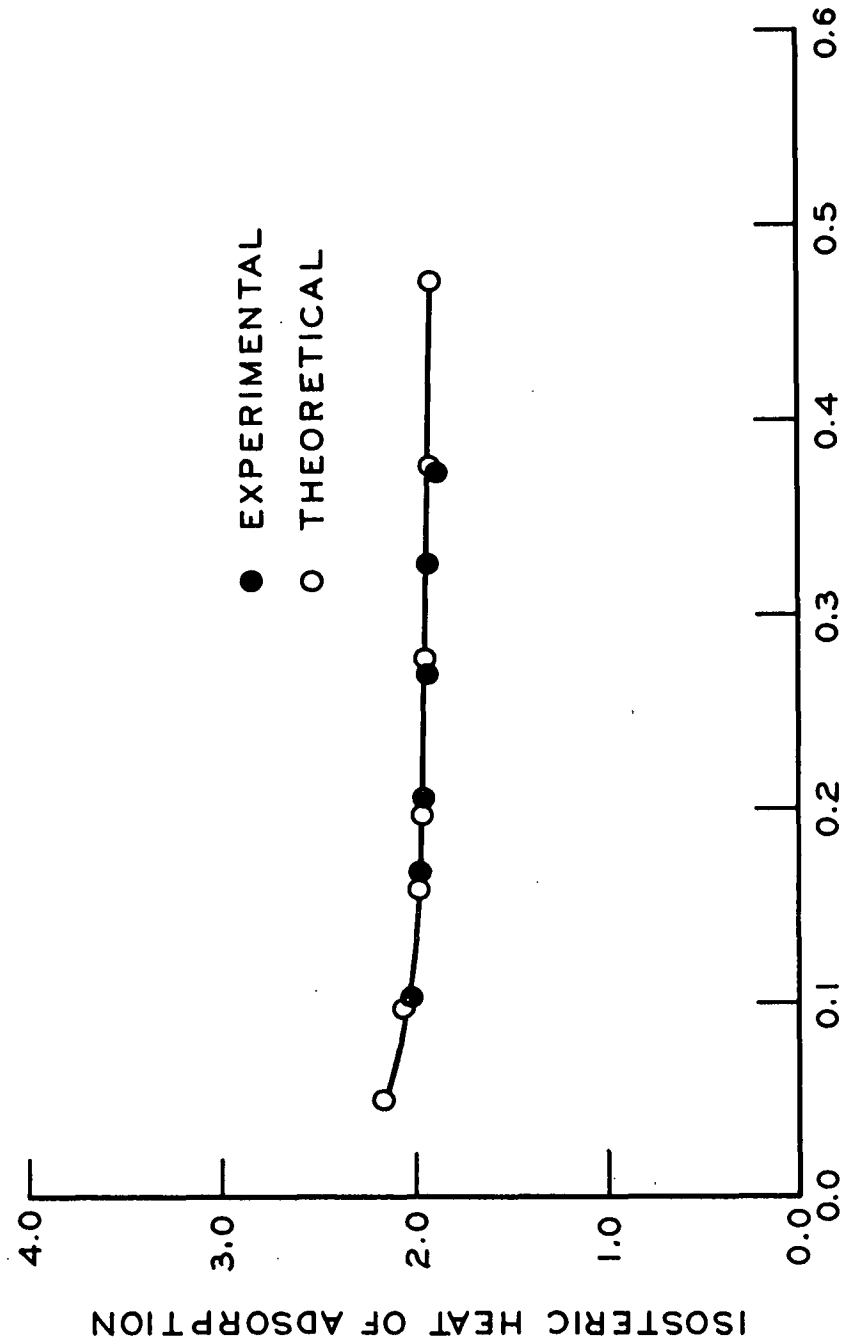

Figure 97. Experimental and Theoretical Isosteric Heat Curves for Argon Adsorption on SV-2B-10HW

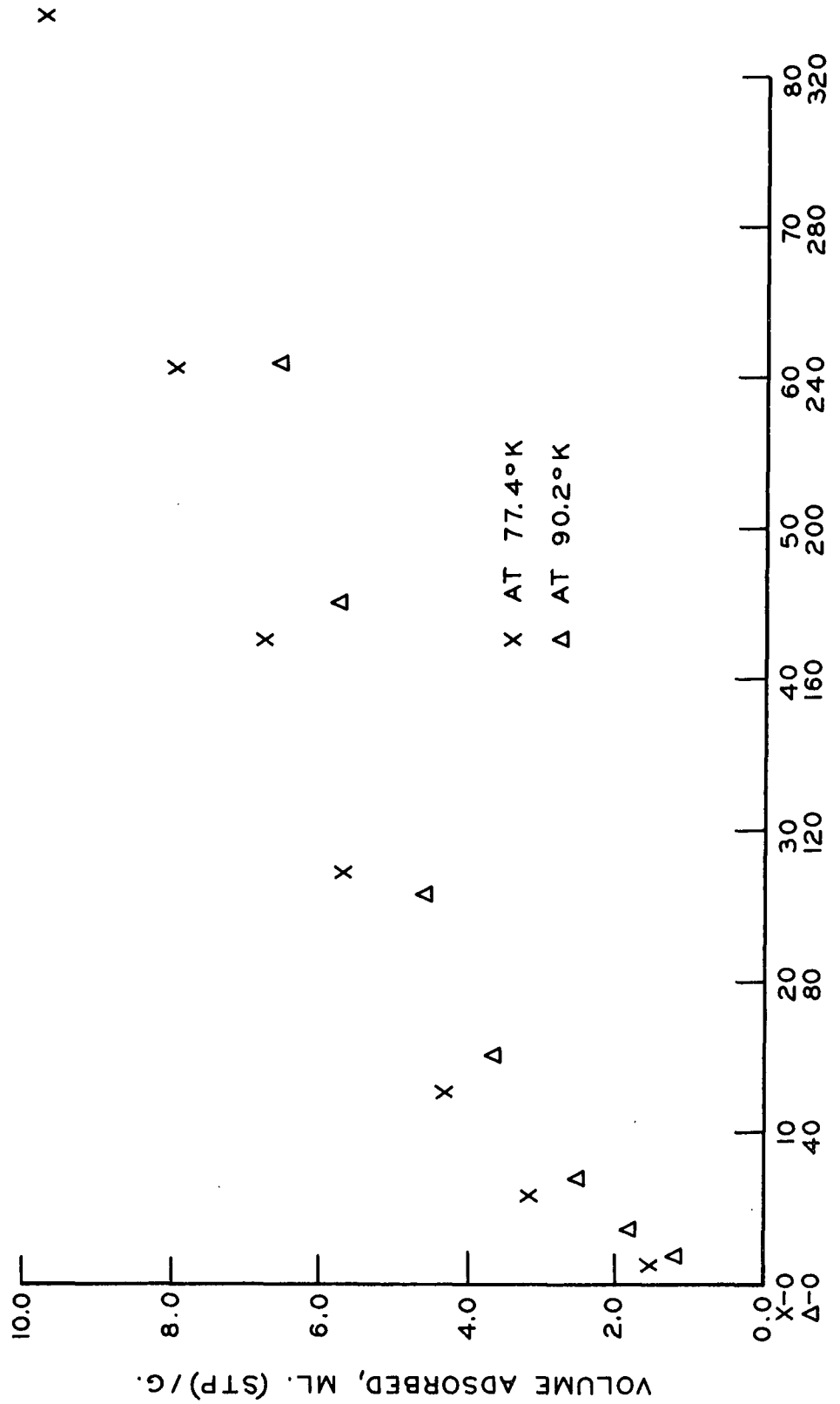

Figure 98. Argon Adsorption Isotherms at 77.4°K and 90.2°K for Sample SV-2B-11HW

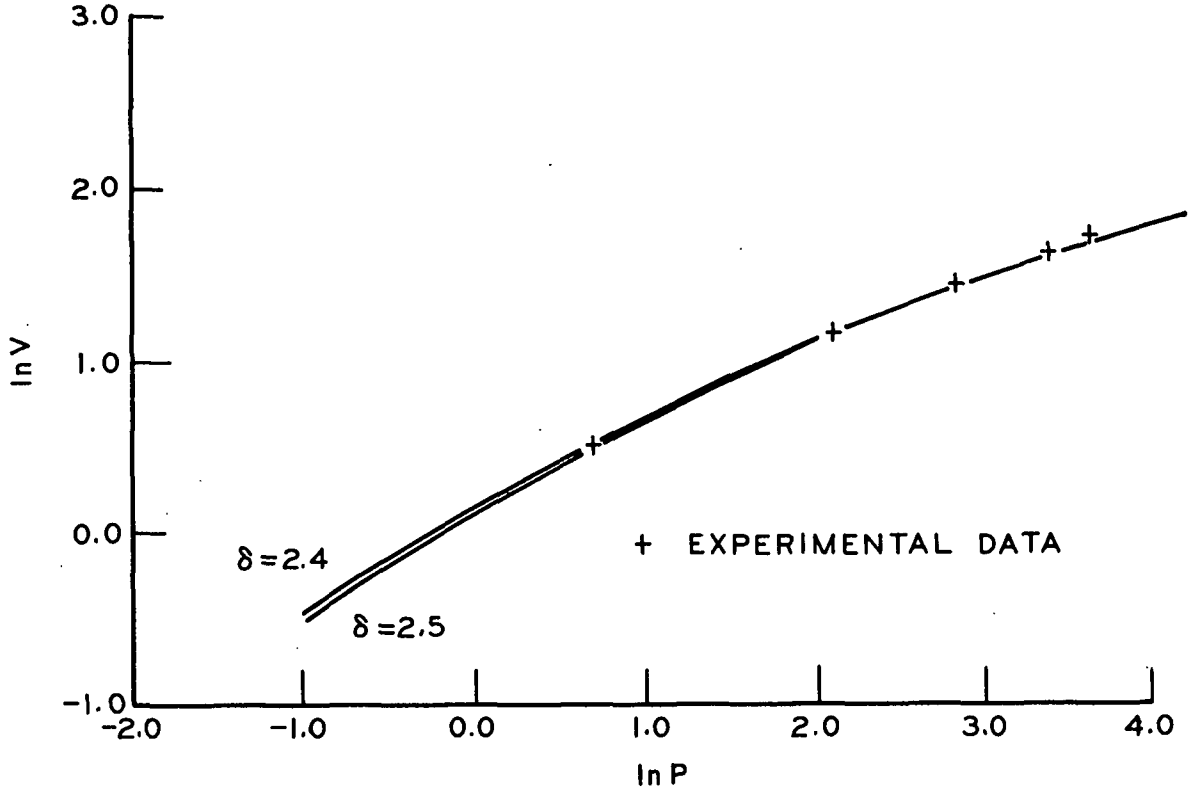

Figure 99. Comparison of Experimental to Model Adsorption Isotherms for Argon Adsorption on SV-2B-11HW at 77.4°K

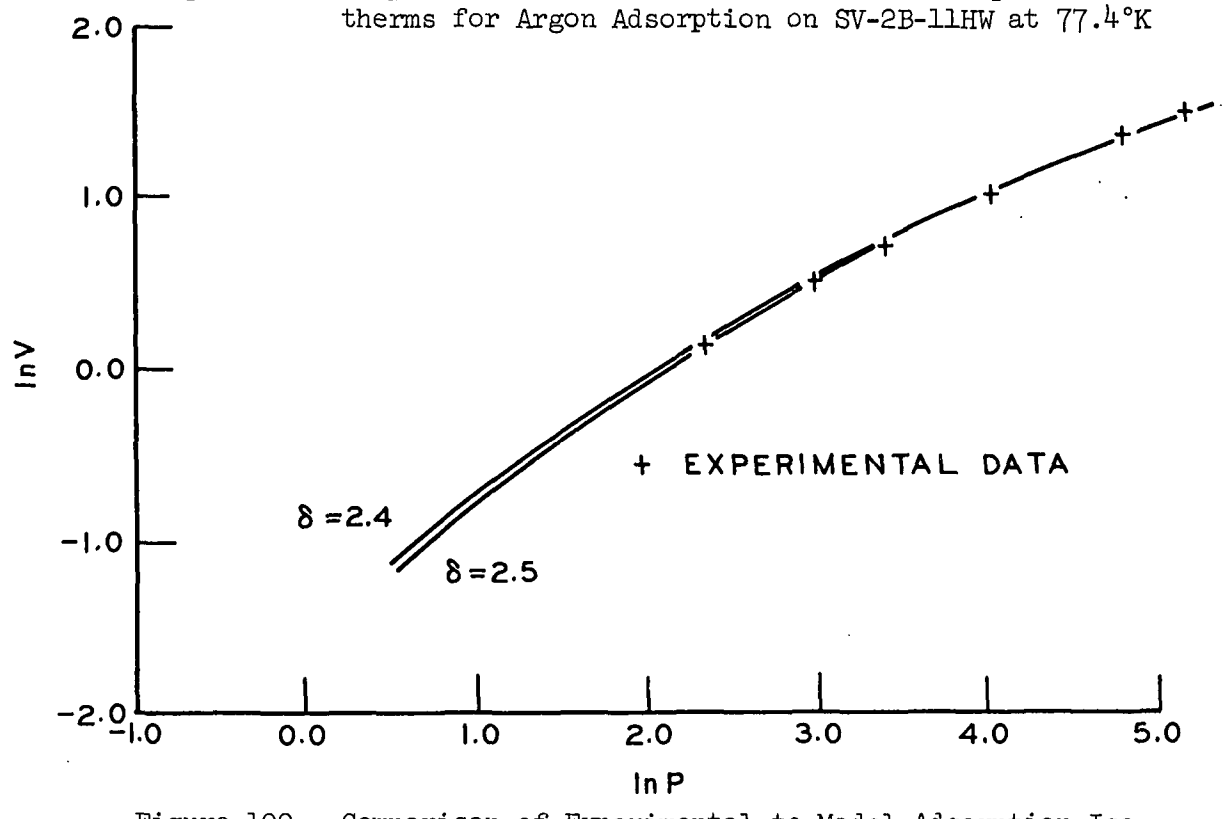

Figure 100. Comparison of Experimental to Model Adsorption Isotherms for Argon Adsorption on SV-2B-11HW at 90.2°K

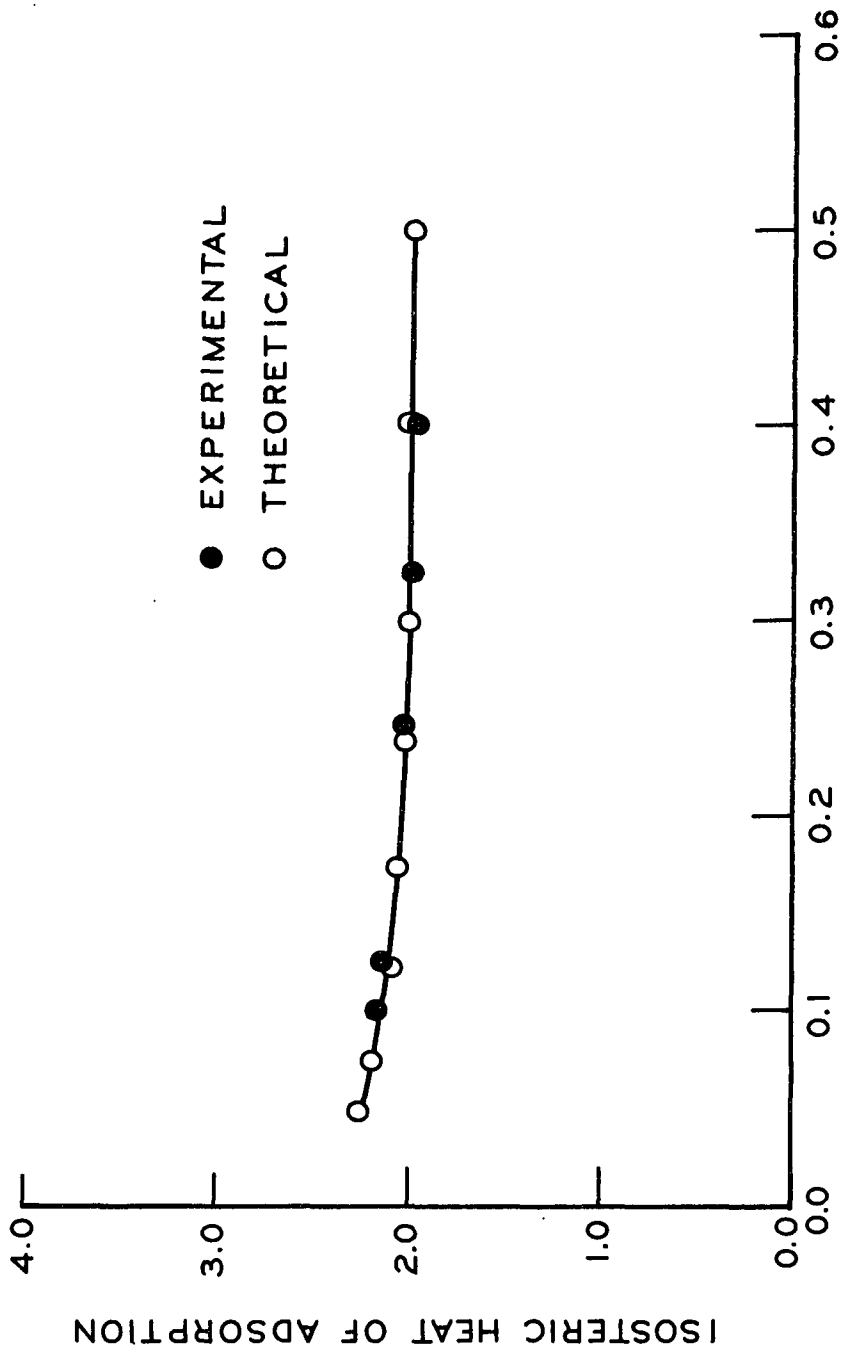

Figure 101. Experimental and Theoretical Isosteric Heat Curves for Argon Adsorption on SV-2B-11HW

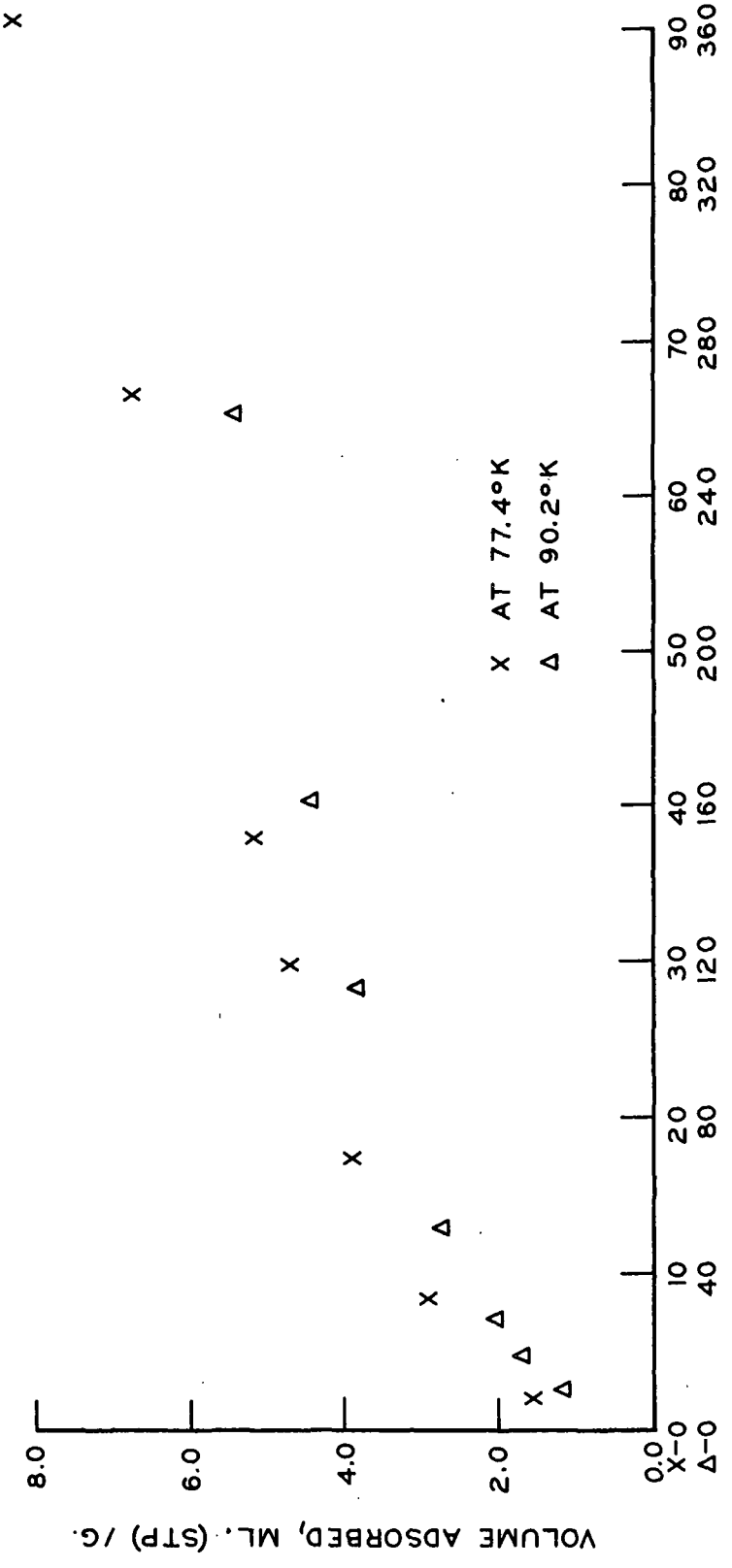

Figure 102. Argon Adsorption Isotherms at 77.4°K and 90.2°K for Sample SV-2B-12HW

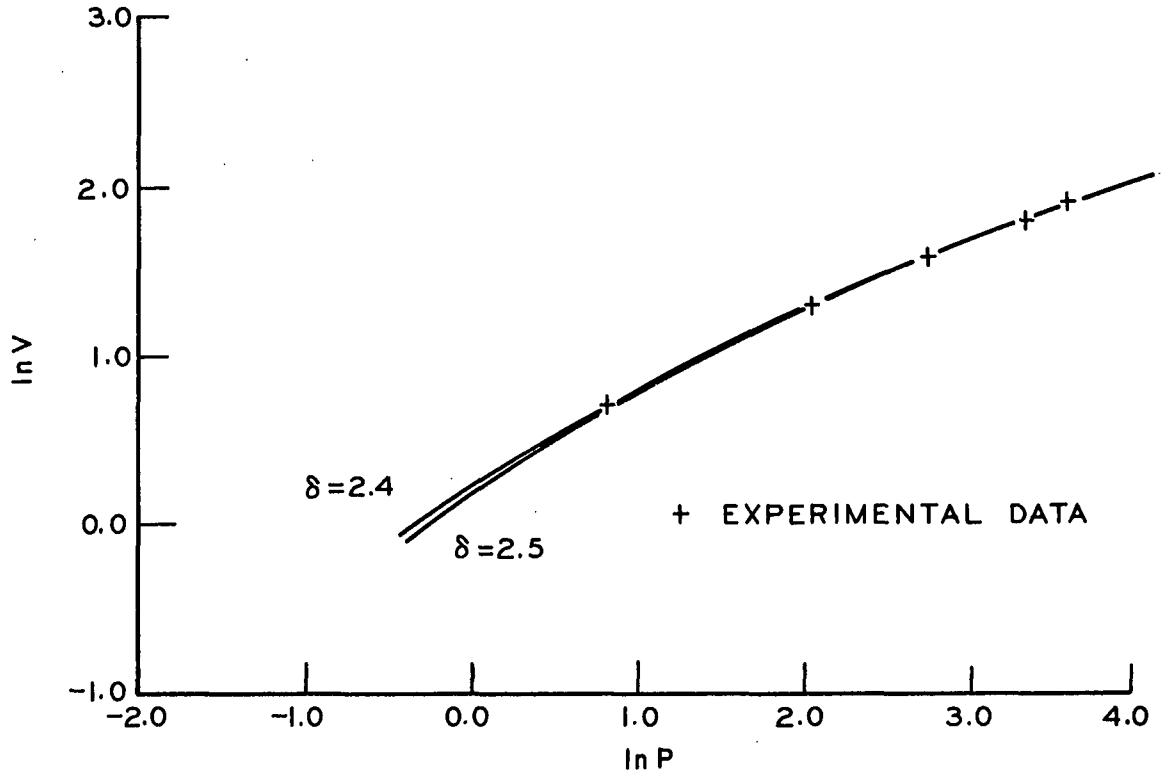

Figure 103. Comparison of Experimental to Model Adsorption Isotherms for Argon Adsorption on SV-2B-12HW at 77.4°K

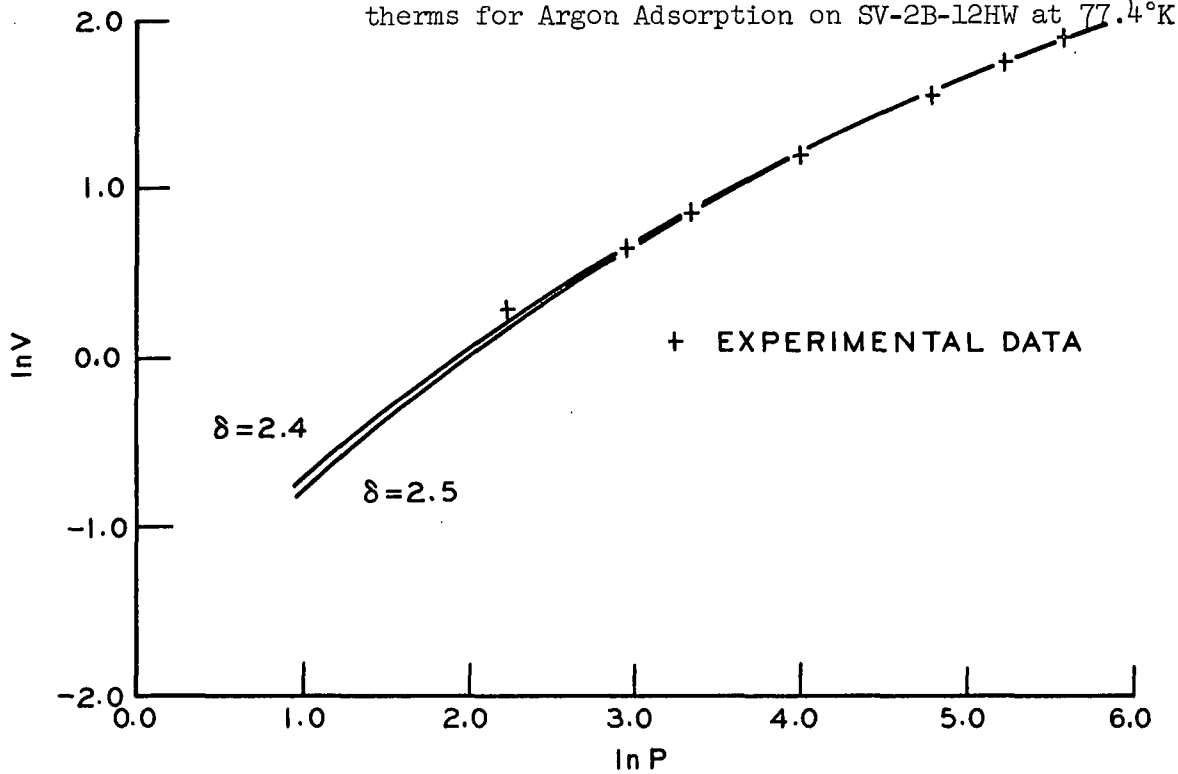

Figure 104. Comparison of Experimental to Model Adsorption Isotherms for Argon Adsorption on SV-2B-12HW at 90.2°K

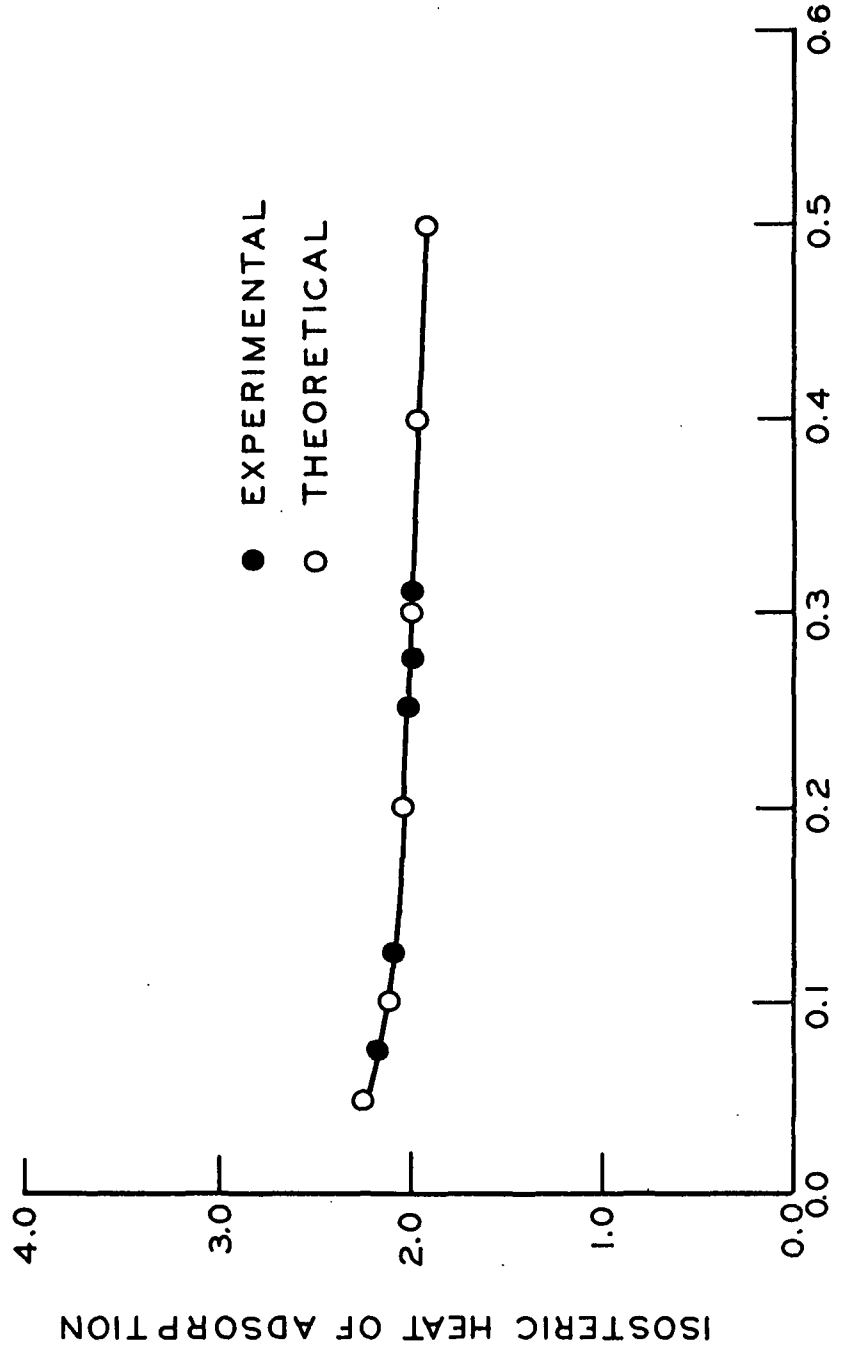

Figure 105. Experimental and Theoretical Isosteric Heat Curves for Argon Adsorption on SV-2B-12HW

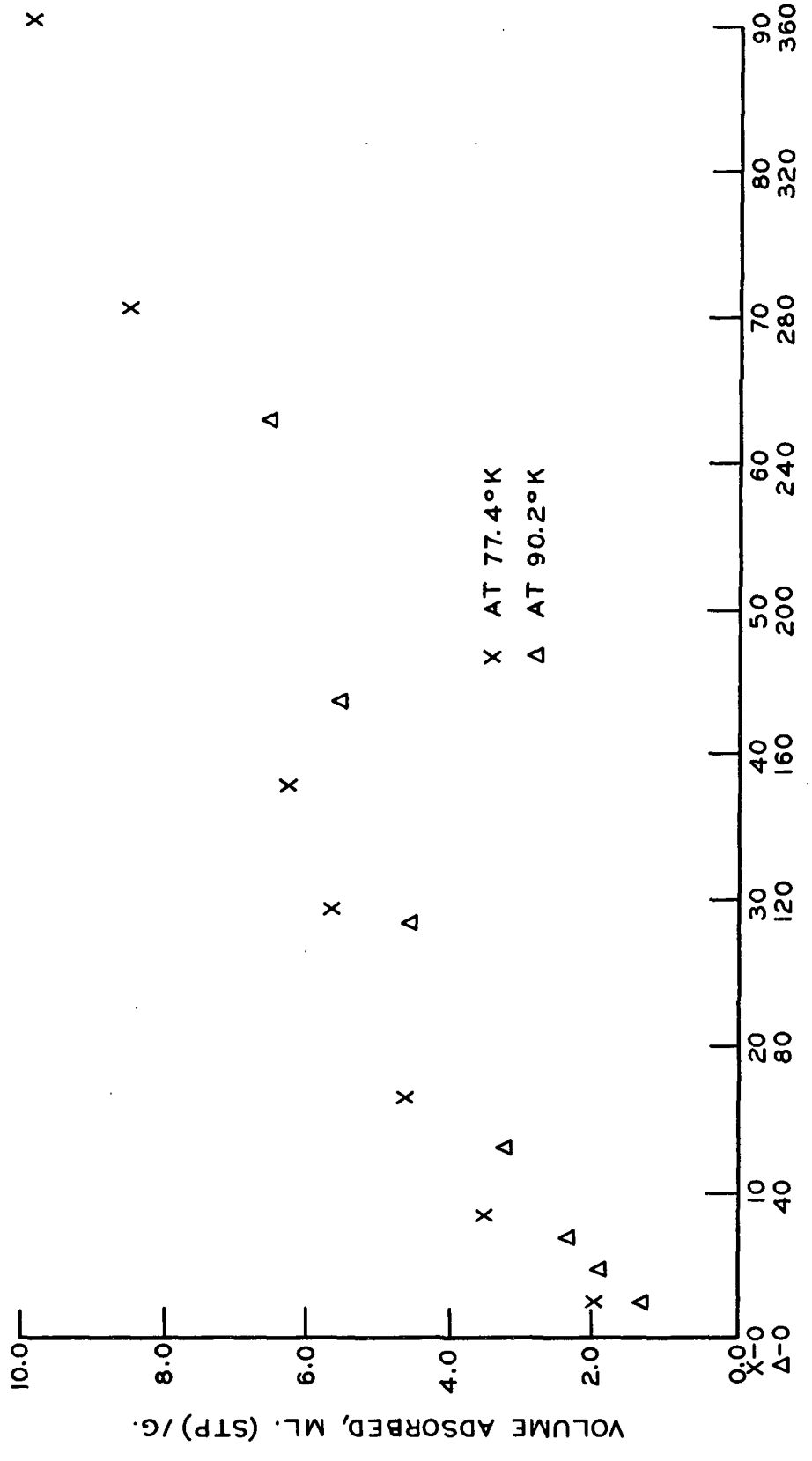

Figure 106. Argon Adsorption Isotherms at 77.4°K and 90.2°K for Sample SV-2B-13HW

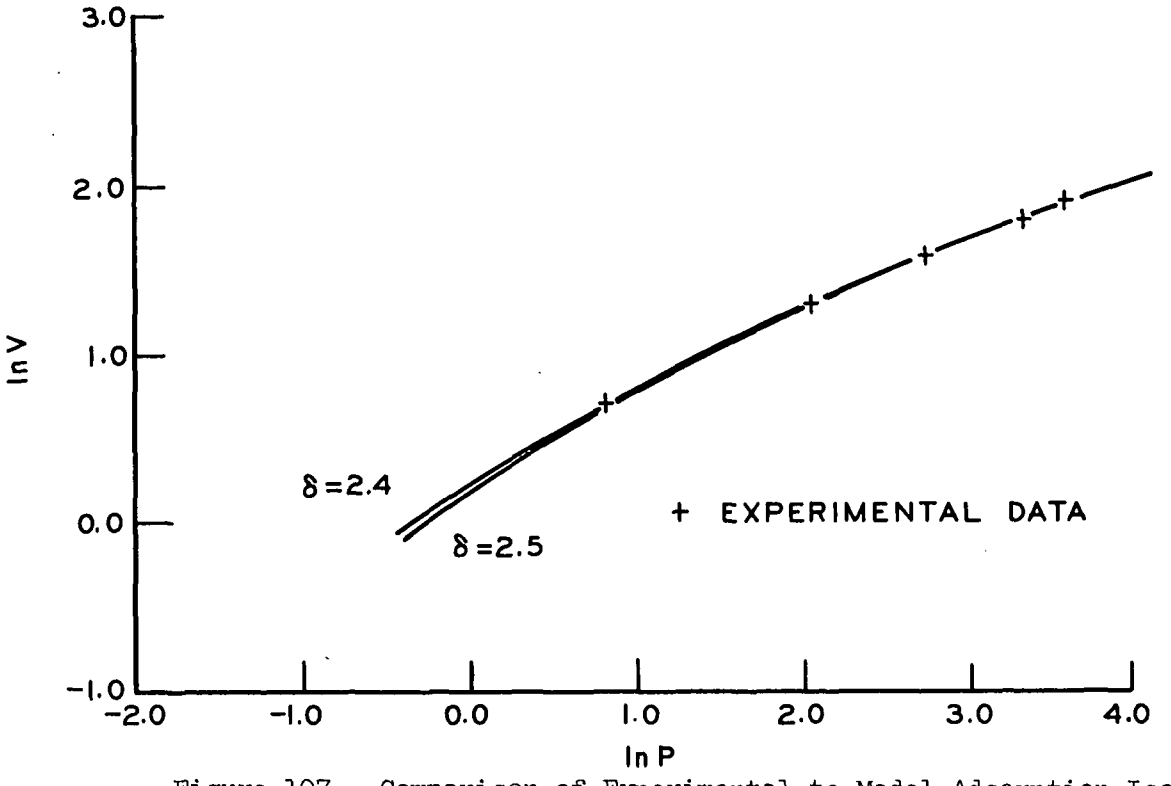

Figure 107. Comparison of Experimental to Model Adsorption Isotherms for Argon Adsorption on SV-2B-13HW at 77.4°K

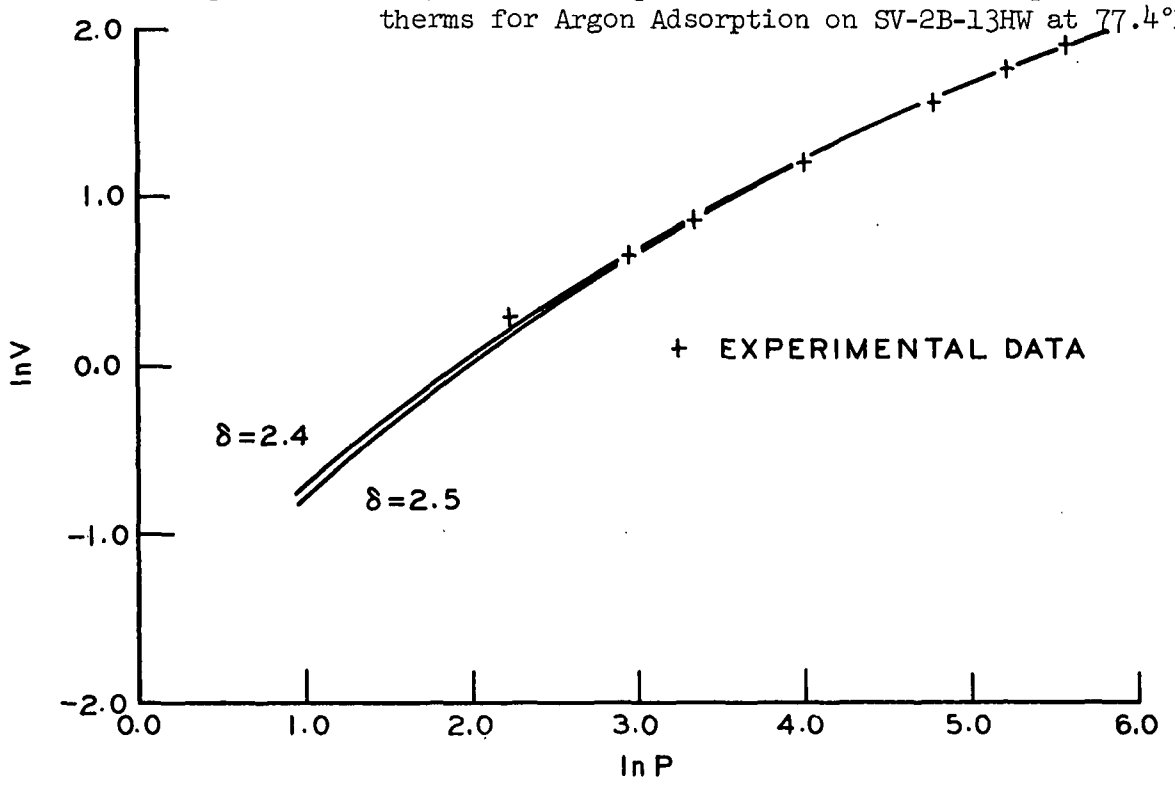

Figure 108. Comparison of Experimental to Model Adsorption Isotherms for Argon Adsorption on SV-2B-13HW at 90.2°K

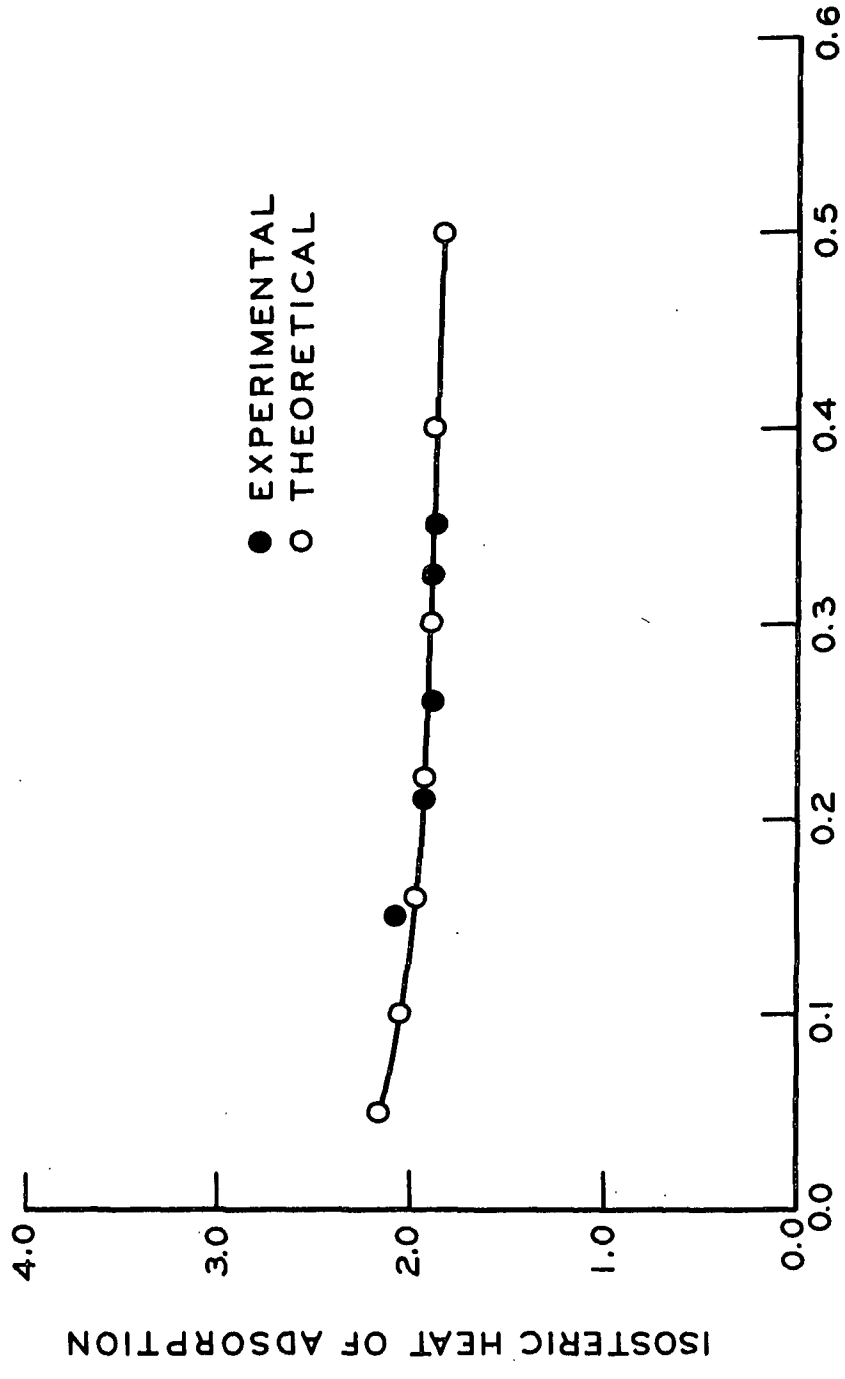

Figure 109. Experimental and Theoretical Isosteric Heat Curves for Argon Adsorption on SV-2B-13HW

APPENDIX V

ARGON ADSORPTION DATA

TABLE XI

ARGON ADSORPTION DATA FOR
SAMPLE SV-2B-1 AT 77.4°K

Deadspace 0.1245 ml./mm.
Sample weight 7.8201 g.

Equilibrium Pressure, mm. Hg	Volume Adsorbed, ml. (STP)/g.	Volume Adsorbed Error
0.584	1.034	0.00
2.048	1.919	0.00
4.070	2.703	0.00
7.841	3.557	0.00
15.637	4.662	0.01
28.286	5.783	0.01
39.736	6.597	0.01
48.743	7.216	0.01
58.435	7.890	0.02
71.074	8.795	0.02
83.060	9.723	0.04

TABLE XII

ARGON ADSORPTION DATA FOR
SAMPLE SV-2B-2 AT 77.4°K

Deadspace 0.1184 ml./mm.
Sample weight 8.1856 g.

Equilibrium Pressure, mm. Hg	Volume Adsorbed, ml. (STP)/g.	Volume Adsorbed Error
0.022	0.091	0.00
0.154	0.600	0.00
0.535	1.135	0.00
1.758	2.038	0.00
4.583	3.244	0.01
10.004	4.456	0.01
18.708	5.523	0.01
24.614	6.143	0.01
	--	--
6.396	3.000	0.00
32.309	6.721	0.00
53.707	8.528	0.01
	--	--
4.304	3.077	0.00

TABLE XIII

ARGON ADSORPTION DATA FOR
SAMPLE SV-2B-3 AT 77.4°K

Deadspace	0.1407 ml./mm.
Sample weight	7.2766 g.

Equilibrium Pressure, mm. Hg	Volume Adsorbed, ml. (STP)/g.	Volume Adsorbed Error
0.174	0.484	0.00
0.393	0.996	0.00
0.669	1.351	0.00
1.443	1.988	0.00
2.628	2.672	0.01
4.286	3.356	0.01
7.210	4.219	0.01
10.827	4.977	0.01
15.896	5.685	0.01
20.222	6.291	0.01
24.151	6.555	0.02
27.401	6.935	0.02
32.946	7.516	0.02
40.823	8.243	0.02
52.453	9.088	0.03
66.203	10.257	0.03
85.555	12.294	0.04
106.180	14.421	0.05
123.060	16.505	0.06
132.067	17.606	0.09

TABLE XIV

ARGON ADSORPTION DATA FOR
SAMPLE SV-2B-4 AT 77.4°K

Deadspace 0.1407 ml./mm.
Sample weight 7.2766 g.

Equilibrium Pressure, mm. Hg	Volume Adsorbed, ml. (STP)/g.	Volume Adsorbed Error
0.245	0.691	0.00
0.813	1.276	0.00
1.771	1.886	0.00
3.209	2.224	0.00
5.589	3.271	0.01
9.273	4.074	0.01
15.252	4.968	0.01
23.173	5.808	0.01
35.278	6.822	0.01
44.432	7.500	0.02
55.012	8.301	0.02
70.142	9.530	0.02
82.186	10.594	0.04

TABLE XV

ARGON ADSORPTION DATA FOR
SAMPLE SV-2B-5 AT 77.4°K

Deadspace 0.1301 ml./mm.
Sample weight 7.0307 g.

Equilibrium Pressure, mm. Hg	Volume Adsorbed, ml. (STP)/g.	Volume Adsorbed Error
1.611	1.177	0.00
3.520	1.704	0.00
4.362	2.043	0.00
8.971	2.717	0.01
16.398	3.396	0.01
25.585	3.957	0.01
38.570	4.573	0.01
52.529	5.215	0.02
77.671	6.428	0.02
95.690	7.434	0.03
117.683	9.124	0.06

TABLE XVI

ARGON ADSORPTION DATA FOR
SAMPLE SV-2B-6 AT 77.4°K

Deadspace 0.06196 ml./mm.
Sample weight 2.9245 g.

Equilibrium Pressure, mm. Hg	Volume Adsorbed, ml. (STP)/g.	Volume Adsorbed Error
0.043	0.126	0.00
0.277	0.421	0.00
0.961	0.770	0.00
2.283	1.177	0.00
4.600	1.626	0.01
7.804	2.041	0.01
13.823	2.548	0.01
19.133	2.875	0.01
25.779	3.205	0.02
37.998	3.683	0.03
45.177	3.943	0.03
56.610	4.349	0.04
66.894	4.740	0.08

TABLE XVII

ARGON ADSORPTION DATA FOR
SAMPLE SV-2B-7HW AT 77.4°K

Deadspace 0.06325 ml./mm.
Sample weight 2.266 g.

Equilibrium Pressure, mm. Hg	Volume Adsorbed, ml. (STP)/g.	Volume Adsorbed Error
3.378	2.433	0.00
10.095	3.885	0.01
16.070	4.661	0.01
22.415	5.264	0.02
44.108	6.811	0.03
62.438	8.056	0.03
81.697	9.480	0.09

TABLE XVIII

ARGON ADSORPTION DATA FOR
SAMPLE SV-2B-8HW AT 77.4°K

Deadspace 0.06826 ml./mm.
Sample weight 2.236 g.

Equilibrium Pressure, mm. Hg	Volume Adsorbed, ml. (STP)/g.	Volume Adsorbed Error
8.453	1.675	0.00
15.587	2.154	0.00
20.340	2.398	0.00
34.629	2.897	0.01
50.126	3.498	0.01
62.621	3.900	0.01
88.610	4.817	0.02

TABLE XIX

ARGON ADSORPTION DATA FOR
SAMPLE SV-2B-9HW AT 77.4°K

Deadspace 0.07516 ml./mm.
Sample weight 2.608 g.

Equilibrium Pressure, mm. Hg	Volume Adsorbed, ml. (STP)/g.	Volume Adsorbed Error
1.736	1.623	0.00
7.414	3.174	0.01
15.286	4.224	0.01
28.802	5.368	0.02
36.662	5.835	0.02
58.358	7.153	0.04
85.601	8.974	0.08

TABLE XX

ARGON ADSORPTION DATA FOR
SAMPLE SV-2B-10HW AT 77.4°K

Deadspace	0.07033 ml./mm.
Sample weight	2.608 g.

Equilibrium Pressure, mm. Hg	Volume Adsorbed, ml. (STP)/g.	Volume Adsorbed Error
2.365	1.772	0.00
8.867	3.290	0.00
16.168	4.205	0.00
27.563	5.139	0.00
34.222	5.569	0.01
58.703	7.041	0.02
82.099	8.579	0.04

TABLE XXI

ARGON ADSORPTION DATA FOR
SAMPLE SV-2B-11HW AT 77.4°K

Deadspace	0.07803 ml./mm.
Sample weight	2.856 g.

Equilibrium Pressure, mm. Hg	Volume Adsorbed, ml. (STP)/g.	Volume Adsorbed Error
1.331	1.546	0.00
5.941	3.141	0.00
12.830	4.303	0.01
27.385	5.666	0.01
42.825	6.734	0.02
60.975	7.951	0.03
84.331	9.688	0.07

TABLE XXII

ARGON ADSORPTION DATA FOR
SAMPLE SV-2B-12HW AT 77.4°K

Deadspace 0.07359 ml./mm.
Sample weight 2.555 g.

Equilibrium Pressure, mm. Hg	Volume Adsorbed, ml. (STP)/g.	Volume Adsorbed Error
2.069	1.554	0.00
8.485	2.926	0.01
17.339	3.866	0.01
29.868	4.717	0.01
38.078	5.170	0.02
66.661	6.755	0.04
90.744	8.280	0.08

TABLE XXIII

ARGON ADSORPTION DATA FOR
SAMPLE SV-2B-13HW AT 77.4°K

Deadspace 0.06808 ml./mm.
Sample weight 2.331 g.

Equilibrium Pressure, mm. Hg	Volume Adsorbed, ml. (STP)/g.	Volume Adsorbed Error
2.415	1.985	0.00
8.242	3.488	0.01
16.341	4.596	0.01
29.260	5.662	0.02
37.829	6.253	0.03
70.674	8.513	0.04
90.619	9.893	0.09

TABLE XXIV

ARGON ADSORPTION DATA FOR
SAMPLE SV-2B-1 AT 90.2°K

Deadspace	0.1071 ml./mm.
Sample weight	7.8201 g.

Equilibrium Pressure, mm. Hg	Volume Adsorbed, ml. (STP)/g.	Volume Adsorbed Error
2.000	0.623	0.00
6.371	1.154	0.00
11.750	1.614	0.00
19.531	2.119	0.01
29.062	2.602	0.01
41.759	3.112	0.01
56.077	3.574	0.02
81.235	4.205	0.02
133.583	5.163	0.03
181.136	5.855	0.04
244.493	6.697	0.04
295.136	7.375	0.07

TABLE XXV

ARGON ADSORPTION DATA FOR
SAMPLE SV-2B-2 AT 90.2°K

Deadspace	0.09899 ml./mm.
Sample weight	8.1856 g.

Equilibrium Pressure, mm. Hg	Volume Adsorbed, ml. (STP)/g.	Volume Adsorbed Error
0.313	0.237	0.00
1.197	0.508	0.00
2.465	0.750	0.00
4.360	1.042	0.00
13.449	1.393	0.00
19.872	1.930	0.01
26.703	2.309	0.01
36.454	2.707	0.01
48.833	3.302	0.01
67.057	4.512	0.02
--	--	--
145.341	6.155	0.01
286.508	8.485	0.02
333.958	9.277	0.03
391.900	9.918	0.05
438.379	11.019	0.09

TABLE XXVI

ARGON ADSORPTION DATA FOR
SAMPLE SV-2B-3 AT 90.2°K

Deadspace 0.1205 ml./mm.
Sample weight 7.2766 g.

Equilibrium Pressure, mm. Hg	Volume Adsorbed, ml. (STP)/g.	Volume Adsorbed Error
1.566	0.649	0.00
5.870	1.299	0.00
11.441	1.897	0.01
18.056	2.426	0.01
25.352	2.904	0.01
33.812	3.349	0.01
44.077	3.845	0.01
57.812	4.355	0.02
80.669	5.040	0.02
100.982	5.513	0.03
150.012	6.480	0.04
189.536	7.112	0.04
228.439	7.752	0.05
277.508	8.543	0.06
326.016	9.351	0.11

TABLE XXVII

ARGON ADSORPTION DATA FOR
SAMPLE SV-2B-4 AT 90.2°K

Deadspace 0.1172 ml./mm.
Sample weight 7.2766 g.

Equilibrium Pressure, mm. Hg	Volume Adsorbed, ml. (STP)/g.	Volume Adsorbed Error
1.586	0.529	0.00
6.558	1.171	0.00
14.286	1.822	0.00
24.352	2.441	0.01
37.691	3.099	0.01
55.772	3.732	0.01
84.108	4.495	0.02
128.407	5.388	0.02
173.150	6.117	0.03
210.457	6.666	0.04
258.358	7.351	0.05
348.223	8.714	0.08
501.321	11.472	0.11

TABLE XXVIII

ARGON ADSORPTION DATA FOR
SAMPLE SV-2B-5 AT 90.2°K

Deadspace 0.1110 ml./mm.
Sample weight 7.0307 g.

Equilibrium Pressure, mm. Hg	Volume Adsorbed, ml. (STP)/g.	Volume Adsorbed Error
5.963	0.749	0.00
14.081	1.186	0.00
20.641	1.458	0.00
28.506	1.727	0.01
40.573	2.060	0.01
54.758	2.400	0.01
67.678	2.645	0.02
78.918	2.829	0.02
110.851	3.262	0.02
151.693	3.690	0.03
207.393	4.191	0.06
253.884	4.584	0.07
353.251	5.494	0.08

TABLE XXIX

ARGON ADSORPTION DATA FOR
SAMPLE SV-2B-6 AT 90.2°K

Deadspace 0.05240 ml./mm.
Sample weight 2.9245 g.

Equilibrium Pressure, mm. Hg	Volume Adsorbed, ml. (STP)/g.	Volume Adsorbed Error
3.677	0.499	0.00
10.111	0.869	0.00
17.755	1.168	0.01
26.648	1.453	0.01
38.711	1.763	0.02
52.355	2.026	0.02
68.507	2.289	0.03
87.589	2.550	0.04
105.563	2.760	0.07
152.574	3.216	0.09
208.456	3.679	0.16
--	--	--
0.189	0.095	0.00
0.434	0.159	0.00
2.034	0.363	0.01

TABLE XXX

ARGON ADSORPTION DATA FOR
SAMPLE SV-2B-7HW AT 90.2°K

Deadspace 0.05465 ml./mm.
Sample weight 2.266 g.

Equilibrium Pressure, mm. Hg	Volume Adsorbed, ml. (STP)/g.	Volume Adsorbed Error
3.482	0.817	0.00
12.723	1.630	0.01
35.187	2.775	0.01
65.597	3.714	0.03
110.319	4.735	0.04
183.057	5.713	0.07
232.192	6.343	0.17

TABLE XXXI

ARGON ADSORPTION DATA FOR
SAMPLE SV-2B-8HW AT 90.2°K

Deadspace 0.05870 ml./mm.
Sample weight 2.236 g.

Equilibrium Pressure, mm. Hg	Volume Adsorbed, ml. (STP)/g.	Volume Adsorbed Error
15.791	0.838	0.00
22.873	1.044	0.01
26.882	1.128	0.01
66.824	1.776	0.03
119.513	2.294	0.04
163.990	2.589	0.07
254.192	3.152	0.07

TABLE XXXII

ARGON ADSORPTION DATA FOR
SAMPLE SV-2B-9HW AT 90.2°K

Deadspace	0.06405 ml./mm.
Sample weight	2.688 g.

Equilibrium Pressure, mm. Hg	Volume Adsorbed, ml. (STP)/g.	Volume Adsorbed Error
8.135	1.183	0.00
15.788	1.712	0.01
26.918	2.285	0.01
62.866	3.444	0.02
109.195	4.354	0.03
155.430	5.006	0.06
238.004	6.064	0.13

TABLE XXXIII

ARGON ADSORPTION DATA FOR
SAMPLE SV-2B-10HW AT 90.2°K

Deadspace	0.06037 ml./mm.
Sample weight	2.608 g.

Equilibrium Pressure, mm. Hg	Volume Adsorbed, ml. (STP)/g.	Volume Adsorbed Error
8.725	1.230	0.00
17.314	1.787	0.01
25.031	2.184	0.01
63.570	3.439	0.02
115.483	4.427	0.03
157.943	5.056	0.06
245.451	6.139	0.14

TABLE XXXIV

ARGON ADSORPTION DATA FOR
SAMPLE SV-2B-11HW AT 90.2°K

Deadspace 0.06724 ml./mm.
Sample weight 2.856 g.

Equilibrium Pressure, mm. Hg	Volume Adsorbed, ml. (STP)/g.	Volume Adsorbed Error
6.773	1.168	0.00
14.582	1.790	0.00
27.670	2.497	0.01
60.449	3.634	0.02
103.566	4.566	0.04
180.332	5.729	0.06
244.416	6.586	0.14

TABLE XXXV

ARGON ADSORPTION DATA FOR
SAMPLE SV-2B-12HW AT 90.2°K

Deadspace 0.06380 ml./mm.
Sample weight 2.555 g.

Equilibrium Pressure, mm. Hg	Volume Adsorbed, ml. (STP)/g.	Volume Adsorbed Error
9.982	1.140	0.00
18.888	1.654	0.01
28.094	2.023	0.01
51.728	2.723	0.03
113.450	3.804	0.05
161.834	4.406	0.07
261.409	5.424	0.15

TABLE XXXVI

ARGON ADSORPTION DATA FOR
SAMPLE SV-2B-13HW AT 90.2°K

Deadspace	0.05231 ml./mm.
Sample weight	2.331 g.

Equilibrium Pressure, mm. Hg	Volume Adsorbed, ml. (STP)/g.	Volume Adsorbed Error
9.150	1.317	0.00
18.496	1.906	0.01
27.496	2.363	0.01
52.382	3.255	0.02
114.150	4.571	0.05
174.963	5.586	0.07
252.275	6.552	0.16

APPENDIX VI

NITROGEN ADSORPTION DATA

TABLE XXXVII

NITROGEN ADSORPTION DATA FOR SAMPLE SV-2B-1 at 77.4°K

Deadspace	0.1245 ml./mm.
Sample weight	7.8201 g.

Equilibrium Pressure, mm. Hg	Volume Adsorbed, ml. (STP)/g.	Volume Adsorbed Error
1.705	2.040	0.00
14.157	3.634	0.00
29.304	4.302	0.01
60.503	5.041	0.01
84.467	5.470	0.02
141.158	6.329	0.03
185.497	6.983	0.03
219.044	7.528	0.06
--	--	--
5.292	2.841	0.00
95.833	5.608	0.01
177.770	6.939	0.02
311.791	9.054	0.07

TABLE XXXVIII

NITROGEN ADSORPTION DATA FOR
SAMPLE SV-2B-2 AT 77.4°K

Deadspace 0.1184 ml./mm.
Sample weight 8.1856 g.

Equilibrium Pressure, mm. Hg	Volume Adsorbed, ml. (STP)/g.	Volume Adsorbed Error
3.738	1.999	0.00
7.373	3.141	0.00
16.870	4.145	0.00
33.104	4.986	0.01
65.781	5.786	0.01
83.788	6.142	0.02
112.329	6.630	0.02
160.078	7.432	0.03
201.340	8.128	0.04
224.680	8.568	0.06
--	--	--
2.349	1.106	0.00
3.775	2.085	0.00
56.560	5.593	0.01
--	--	--
0.860	0.817	0.00
38.390	5.191	0.01
175.091	7.767	0.02
220.640	8.562	0.03
283.881	9.800	0.04
367.983	11.612	0.09

TABLE XXXIX

NITROGEN ADSORPTION DATA FOR
SAMPLE SV-2B-3 AT 77.4°K

Deadspace 0.1407 ml./mm.
Sample weight 7.2766 g.

Equilibrium Pressure, mm. Hg	Volume Adsorbed, ml. (STP)/g.	Volume Adsorbed Error
0.000	0.175	0.00
0.282	2.016	0.00
4.345	3.267	0.01
18.721	4.731	0.01
34.665	5.415	0.01
56.357	6.049	0.02
68.454	6.344	0.02
94.296	6.851	0.02
116.942	7.199	0.03
140.859	7.645	0.03
165.795	8.104	0.04
198.955	8.727	0.05
216.435	9.060	0.06
238.866	9.507	0.07
258.964	9.741	0.08
284.384	10.390	0.10
--	--	--
4.914	3.403	0.00
35.016	5.455	0.01
74.274	6.475	0.02
138.939	7.696	0.04

TABLE XL

NITROGEN ADSORPTION DATA FOR
SAMPLE SV-2B-4 AT 77.4°K

Deadspace	0.1407 ml./mm.
Sample weight	7.2766 g.

Equilibrium Pressure, mm. Hg	Volume Adsorbed, ml. (STP)/g.	Volume Adsorbed Error
1.856	2.144	0.00
11.908	3.667	0.00
23.286	4.307	0.01
36.947	4.866	0.01
51.328	5.266	0.01
66.311	5.598	0.02
90.548	6.049	0.02
112.844	6.355	0.03
132.221	6.678	0.04
163.941	7.202	0.05
211.302	8.000	0.05
253.210	8.780	0.06
--	--	--
3.250	2.594	0.00
48.938	5.143	0.01
113.437	6.356	0.02
178.820	7.414	0.03

TABLE XLI

NITROGEN ADSORPTION DATA FOR
SAMPLE SV-2B-5 AT 77.4°K

Deadspace 0.1301 ml./mm.
Sample weight 7.0307 g.

Equilibrium Pressure, mm. Hg	Volume Adsorbed, ml. (STP)/g.	Volume Adsorbed Error
11.634	2.382	0.00
53.168	3.353	0.01
94.170	3.848	0.01
114.824	4.061	0.02
153.559	4.450	0.03
179.216	4.711	0.04
223.301	5.162	0.04
259.447	5.540	0.08
323.031	6.280	0.09
421.747	7.537	0.12

TABLE XLII

NITROGEN ADSORPTION DATA FOR
SAMPLE SV-2B-6 AT 77.4°K

Deadspace 0.06196 ml./mm.
Sample weight 2.9245 g.

Equilibrium Pressure, mm. Hg	Volume Adsorbed, ml. (STP)/g.	Volume Adsorbed Error
0.392	0.723	0.00
3.301	1.446	0.00
7.542	1.818	0.01
13.925	2.122	0.01
16.575	2.217	0.02
20.751	2.336	0.02
25.906	2.456	0.02
31.516	2.569	0.03
40.518	2.709	0.04
52.503	2.865	0.04
62.539	2.976	0.05
70.509	3.061	0.06
87.613	3.223	0.06
99.676	3.337	0.08
130.831	3.588	0.13
--	--	--
1.187	1.056	0.00
2.162	1.277	0.00
174.516	3.894	0.03
214.710	4.235	0.05
276.612	4.796	0.07
447.201	6.762	0.20

TABLE XLIII

NITROGEN ADSORPTION DATA FOR
SAMPLE SV-2B-1 AT 90.2°K

Deadspace 0.1071 ml./mm.
Sample weight 7.8201 g.

Equilibrium Pressure, mm. Hg	Volume Adsorbed, ml. (STP)/g.	Volume Adsorbed Error
3.768	0.899	0.00
20.554	1.979	0.00
38.907	2.503	0.01
63.722	2.989	0.01
99.494	3.429	0.02
143.598	3.810	0.02
204.284	4.174	0.03
314.488	4.773	0.05
501.337	5.547	0.09

TABLE XLIV

NITROGEN ADSORPTION DATA FOR
SAMPLE SV-2B-2 AT 90.2°K

Deadspace 0.09899 ml./mm.
Sample weight 8.1856 g.

Equilibrium Pressure, mm. Hg	Volume Adsorbed, ml. (STP)/g.	Volume Adsorbed Error
4.645	1.413	0.00
14.598	2.274	0.00
22.554	2.643	0.00
38.344	3.149	0.01
55.100	3.568	0.01
78.897	3.975	0.02
96.106	4.226	0.02
136.580	4.657	0.03
169.963	4.906	0.03
196.592	5.137	0.04
236.927	5.427	0.05
267.095	5.682	0.06
405.276	6.480	0.11
--	--	--
4.285	1.030	0.00

TABLE XLV

NITROGEN ADSORPTION DATA FOR
SAMPLE SV-2B-3 AT 90.2°K

Deadspace 0.1205 ml./mm.
Sample weight 7.2766 g.

Equilibrium Pressure, mm. Hg	Volume Adsorbed, ml. (STP)/g.	Volume Adsorbed Error
12.872	2.274	0.00
32.940	3.163	0.01
49.936	3.613	0.01
68.169	3.979	0.01
100.293	4.387	0.02
135.280	4.761	0.03
196.361	5.272	0.04
258.139	5.754	0.04
349.102	6.257	0.06
525.965	7.102	0.11

TABLE XLVI

NITROGEN ADSORPTION DATA FOR
SAMPLE SV-2B-4 AT 90.2°K

Deadspace 0.1172 ml./mm.
Sample weight 7.2766 g.

Equilibrium Pressure, mm. Hg	Volume Adsorbed, ml. (STP)/g.	Volume Adsorbed Error
5.004	1.250	0.00
13.995	2.009	0.00
33.213	2.666	0.01
61.055	3.296	0.01
98.715	3.799	0.02
169.905	4.400	0.03
226.031	4.796	0.03
339.855	5.367	0.05
481.151	5.954	0.09

TABLE XLVII

NITROGEN ADSORPTION DATA FOR
SAMPLE SV-2B-5 AT 90.2°K

Deadspace 0.1110 ml./mm.
Sample weight 7.0307 g.

Equilibrium Pressure, mm. Hg	Volume Adsorbed, ml. (STP)/g.	Volume Adsorbed Error
3.928	0.798	0.00
21.880	1.561	0.00
43.202	1.955	0.01
59.311	2.161	0.01
95.962	2.492	0.02
126.599	2.688	0.02
173.793	2.934	0.03
219.564	3.125	0.05
264.496	3.280	0.08
393.539	3.635	0.10

TABLE XLVIII

NITROGEN ADSORPTION DATA FOR
SAMPLE SV-2B-6 AT 90.2°K

Deadspace 0.05240 ml./mm.
Sample weight 2.9245 g.

Equilibrium Pressure, mm. Hg	Volume Adsorbed, ml. (STP)/g.	Volume Adsorbed Error
0.816	0.342	0.00
1.179	0.407	0.00
2.137	0.534	0.00
4.302	0.717	0.00
9.213	0.980	0.01
15.409	1.187	0.01
22.651	1.368	0.01
35.816	1.599	0.02
53.037	1.811	0.03
77.276	2.031	0.05
--	--	--
82.408	2.035	0.01
112.084	2.239	0.02
147.801	2.425	0.05
206.947	2.646	0.06
264.572	2.857	0.10
358.994	3.097	0.13
508.507	3.465	0.17
558.172	3.571	0.29